Republic of Iraq

Ministry of Higher Education and Scientific Research

Babylon University

College of Materials Engineering

Department of Metallurgical Engineering

Surfaces Modification of High Speed Steel Cutting Tools by $TiO_2/Al_2O_3/ZrO_2$ Multilayers Coatings Using Sol-gel Method

A Dissertation

Submitted to the Department of Metallurgical Engineering/ College of Materials Engineering/ University of Babylon in Partial Fulfillment of the Requirements for the Degree of Doctor of Philosophy in Materials Engineering /Metallurgical

By

Wurood Asaad Midab Abbas

Supervised by

Prof. Dr. Haydar Al-Ethari **Dr. Shaimaa Jaber Kareem**

2022 A.D 1443A.H

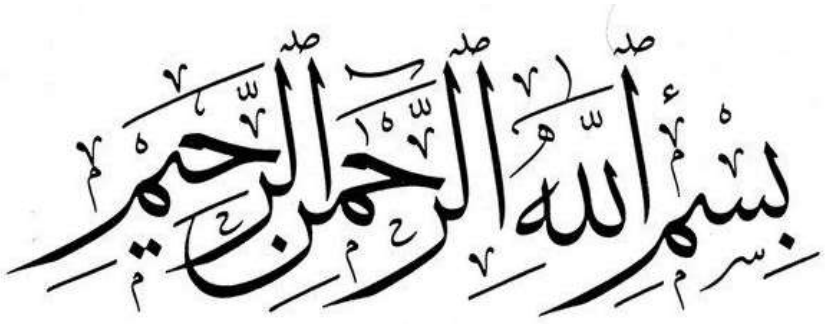

لَقَدْ أَرْسَلْنَا رُسُلَنَا بِالْبَيِّنَاتِ وَأَنزَلْنَا مَعَهُمُ الْكِتَابَ وَالْمِيزَانَ لِيَقُومَ النَّاسُ بِالْقِسْطِ ۖ وَأَنزَلْنَا الْحَدِيدَ فِيهِ بَأْسٌ شَدِيدٌ وَمَنَافِعُ لِلنَّاسِ وَلِيَعْلَمَ اللَّهُ مَن يَنصُرُهُ وَرُسُلَهُ بِالْغَيْبِ ۚ إِنَّ اللَّهَ قَوِيٌّ عَزِيز

سورة الحديد/ آية 25

Acknowledgments

I would like to express my gratitude and thanks

To God the Lord of the Worlds

To my Supervisors Prof. Dr. Haydar Al-Ethari and Dr. Shaimaa Jaber Kareem

To my College, Materials Engineering / University of Babylon and the Department of Metallurgical Engineering.

To the Ministry of Industry &Minerals State Company for Automotive & Equipment Industry.

To the University of Technology, special thanks are given to the Training and Workshop Center.

To Phi Nano -Science Center PNSC and Nano Lab, in Al-khora Company

To the Department of Chemical Science / College of Science / University of Baghdad

To the Department of Chemical Science / College of Science / University of Anbar

To the Ministry of Science and Technology, and General Company for Inspection and Engineering Rehabilitation-Baghdad.

To my family, special thanks are given to my lovely husband for standing beside me.

Abstract

In order to obtain better cutting tools performance, the coatings appear as an alternative in the machining process. The goal of the coating is to improve tribological conditions in the chip-tool and tool-workpiece interfaces. The current work offers a coating for high-speed steel (HSS) tools that is thinner and less expensive than commercial coatings. A single point AISI M3 high speed steel tool having a square cross section was used to prepare the cutting inserts for turning purpose.

The study investigates the thermal and tribological characteristics of the uncoated cutting insert and the coated with mono and multi- layers. The machining experiments were conducted on a work piece of ASTM A519- grade 1045 unalloyed medium carbon steel. The best conditions for coating the HSS insert with ceramic oxides using the sol-gel process were determined. These precursor conditions involved : viscosity, PH, dispersions materials, and the aging period. The depositions conditions were the number of coating cycles, the immersion time, the calcination temperature, and dry temperature which affects the layer thickness, adhesion, surface roughness, and homogeneity for coating layer.

Titanium tetra-isopropoxide (TTIP), a catalyst HCl, and a disperssion material (triethanolamine) were employed to prepare the precursor (titanium hydroxide). The PH, the viscosity, and the aging time, of the produced precursor were 6.46 and 8.74 cP, and 6 hours respectively. After the dip coating of the cutting inserts for 5 sec immersion time and 2 number of coating cycle in titania precursor, the inserts were dried at 355°C for one hour. The coating films were created by dipping the cutting inserts in the alumina hydroxide sol, which was made by

combining aluminum isopropoxide IPA, deionized water H_2O, and nitric acid (HNO_3). At 80°C, the solution mixture was whirled continuously for two hours. The produced precursor had a PH of 5.83, viscosity of 8.11 cP, with an aging time of 12 hours. The immersion time and number of coating cycle in alumina precursor were 10 sec, and two respectively. The inserts were dried at 355℃ for one hour.

Finally, these inserts were dipped in zirconia precursor, which was prepared from Zirconium 70 percent n-propoxide ($Zr(OC_3H_7)_4$), glacial acetic acid, ethylene glycol, and glycerol were used to prepare the mixture. The PH, the viscosity, and the aging time of precursor were 4.87, 7.9 cP, and 24-48 hours respectively. These inserts were dipped at 15 sec immersion time and 2-3 number of coating cycle, then dried at 290 ℃. To accomplish densification of the sol-gel layers, the inserts were calcination in a furnace for two hours at 500 ℃ with a 6°C/min heating rate. Douple and triplex layers of (TiO_2/ Al_2O_3)and (TiO_2/ Al_2O_3 ZrO_2) were deposited on the surface.

Metallurgical examination, physical and mechanical tests were performed on the best multilayer coating (douple and triplex layers) which have good adhesive strength (89.56, 93.60) MPa with acceptable thickness in machining (5-6)μm, less surface roughness, and good homogeneity. Furthermore, it was investigated the attributes of each monolayer coating: Al_2O_3 layer, ZrO_2 layer with highest adhesive strength (10.65,11.15) MPa. All of this is based on mentioned conditions of coating. Multilayer (triplex) coated HSS insert achieved the best results in mechanical, physical, and machining tests. For the triplex layers coated HSS insert comparing with the uncoated cutting insert: the friction coefficient was decreased by (80)%, the hardness was increased by 57%, the surface roughness was decreased by 63%, the thermal conductivity was decreased by 36%, and the wear rate was decreased by 71%. The average thermal expansion coefficient of the

titania ceramic coating is generally quite close to the thermal expansion coefficient of the bulk HSS ($11*10^{-6}$, $13*10^{-6}$ 1/K) .

The machining tests were based on turning conditions of three cutting velocity (56, 88, and 112 m/min), , three feeds (0.065,0.165, and 0.265 mm/rev), and three cutting depths (0.2, 0.5 and 0.7 mm). The results of the machining temperature at the tool–work piece interface, the surface roughness for work-piece at first minute machining, the flank wear width, and the tools life, indicated that the multi-layer coating significantly reduces the temperature and flank wear during cutting, while, the life time of coated insert is increased by about 85-183% compared to uncoated insert. Temperature at first minute was decreased by (11-13)% . In addition the surface roughness for work piece was decreased by (30- 96)%.

The effects of turning conditions on cutting performance were studied for each (uncoated, monolayer coated, douple layer coated , triplex layer coated) HSS cutting insert using analysis of variance (ANOVA). The greatest value of the grey relational grade for multilayer (triplex layer) coated HSS cutting insert, 56m/min, and 0.065 mm/rev, and 0.2 mm was found. Finally, as the same conditions of machining process and the same work piece, coated insert with triplex layers compared to carbide cutting inserts then machining output with coated HSS inserts were better, as its tool life was greater by (30-53)%.

Table of Content

List of Abbreviations and *Symbols*

Abbreviations	***Description***
AFM	*Atomic Force Microscope*
ASTM	*American Society for Testing and Materials*
ANOVA	*Analysis of Variances*
CVD	*Chemical Vapor Deposition*
DOE	*Design of Experiment*
EDS	*Electron dispersive Spectroscopy*
FE-SEM	*Field emission Scanning Electron Microscopy*
GRA	*Grey relational analysis*
GRG	*Grey relational Grade*
GRC	*Grey relational Coefficient*
HV	*Vickers hardness (kg/mm2)*
H.S.S.	*High speed steel*
Hs	*Scratch hardness*
IPA	*mixing aluminum isopropoxide*
IP	*Isopropanol*
Lc	*Critical Length*
PVD	*Physical Vapor Deposition*
Ra	*Surface Roughness*
R.W	*Rate of wear*
SST	*Total Sum of Squared Deviations*
TEOA	*Triethanolamine*
TTIP	*Titanium tetra-isopropoxide*
TPS	*Transient Plane Source*
VB	*Wear width*
XRD	*X-Ray diffraction*
Symbols	***Description***
q	*Quality factor*
w	*Newton's normal force*

d	*scratch width*
K	*thermal conductivity coefficient*
$\boldsymbol{C}$	*specific heat capacity*
γm	*the total mean of the grey relational grade*
γi	*the mean of the grey relational grade at the optimal level*
γ	*Flank angle*
$\boldsymbol{\alpha}$	*Rake angle*
$\boldsymbol{f}$	*Feed mm/rev*
v	*Cutting velocity m/min*
t	*Depth of cut mm*
T	*Temperature ℃*
F	*Tool life min*
$\boldsymbol{\xi i}$	*Grey Relational Coefficient*

CHAPTER ONE

Chapter One

Introduction

1.1.General Review

Machining is one of the most widely used metal manufacturing procedures [1]. Additional operations are frequently required after casting, forming, and other shaping procedures. To work properly and reliably over their specified service lives, parts must be interchangeable in many technological applications; thus, dimensional correctness and surface polish of the parts must be controlled during manufacture. Machining is the process of removing some material from a workpiece in order to produce a part of the designed geometry with the required level of precision and surface quality [2].

In comparison to other manufacturing processes, machining process can machine a wide range of geometric features and product shapes, as well as a wide range of work piece materials (metals, ceramics, plastics, and plastic composites), with a tighter surface finish (surface roughness around 1μm) and more accurate dimensions (machining tolerance less than 50μm). Traditional machining is the process of removing some material from a workpiece (machining allowance) in order to produce a given geometry with a high level of precision and surface quality. During this cold-working action, heat is invariably generated as mechanical energy, which is absorbed [3].

Cutting tool has is normally subjected to extremely severe wear, plastic deformation, fatigue crack, thermal crack, brittle crack, breakage, and built-up-edge due to metal-to-metal contact (between the tool and the work piece) under conditions of extremely high temperature, high stress, thermal shock in the cutting area, high pressure, and high sliding velocity.

Using the technology of hard coatings deposition on tools, the functional features of the equipment tool used can be improved. Deposited hard coatings used in order to provide a fully capable cutting tool to meet the growing demands for excellent manufacturing quality, fast machining times, and increased production rates in order to achieve the current machining idea in terms of cost. A thin film produced or deposited on the surface of a component made of another material that has good wear resistance and low friction is known as a coating [4, 5].

Tool wear is a significant occurrence in any metal cutting process, as it impacts machining outputs such as machining forces, temperature generation, machined surface integrity, tool life, and total production cost directly or indirectly [4]. Combating wear in machining is difficult due to the hostile environment of machine operations, particularly in dry machining [5].

In response to expanding demand for wear-resistant components and tools, new coating materials with enhanced hardness, chemical stability, reduced coefficient of friction, stronger oxidation resistance, and wear resistance have been developed [6]. Surface modification enhancement is a rapidly emerging field since it is less expensive than inventing and manufacturing a completely new material and allows for the preservation of some of the original material's characteristics, such as mechanical capabilities. Surface qualities such as mechanical, biological, and chemical properties, as well as physical properties, can be altered by applying nano- or submicro-coatings to the surface layer [5]. As cutting tool materials, ceramics have great wear resistance, high hot strength, high hardness, and chemical stability, but their fracture toughness is limited by their inherent qualities. With chemical inertness, good high-temperature properties, and oxidation resistance, oxides are the oldest and most widespread

form of ceramic material. Most oxides contain a lot of ionic bonding because oxygen is the most electronegative divalent element. As a result, they have many of the same properties as ionic crystals when they are pure, including optical transparency, high electrical resistivity, poor thermal conductivity, diamagnetism and chemical stability. The largest and fastest-growing category of ceramic tool materials is Al_2O_3-based oxide tool materials [7]. Silicon dioxide (SiO_2), often known as silica, is a typical industrial product with a wide range of applications. It is commonly produced via CVD, and has low thermal expansion and strong thermal shock tolerance at ambient temperature. Silica resists oxidation and is not affected by the majority of chemical reagents [8].

High-speed steel and cemented WC are the most popular substrates. The popularity of coated tools, which make up a large majority of turning and milling inserts, has been steadily increasing. TiC is one of the most common machine tool coatings, and it's usually employed as a bond layer between other layers in a multilayer coating to promote adhesion. Two multilayer coatings are TiC/TiCN/TiN and TiC/Al_2O_3/TiN [6].

In tribology, the properties of multilayer coating systems were investigated. For multilayer coatings, material selection, layer number, individual layer thickness, interlayer type, and layer microstructures. Coating acts as a heat barrier due to its low thermal conductivity as compared to the thermal conductivity of the substrate. Hence, the rate of frictional heat which evaluates in the substrate is minimized and that leads to reduce the temperature of substrate [4]. Thereby, uncoated tools have shorter tool life time compared with the coated cutting tools [9]. The enhancement of the machining process is enabled by trends toward machining of very chemically reactive and hard materials at high speeds, single or multi-layer deposition on cutting tools [10]. The beneficial properties of

the coating layer include: reducing in friction, generated heat, and cutting forces. In this regard, higher feed rate and cutting speed are allowable to be used. Coatings act as a rigorous diffusion barrier, which implies lowering in the diffusion between the surface of the tool and the chip, specifically at higher cutting speed. Also, by reducing tool wear, hard and thin coatings on the cutting tool body cause an increasing of the productivity and tool life duration [11].

It is known that 40% of super-hard tools, 50% of HSS and 85% of carbide tools used in industry are coated [12]. Because coating have a high resistance, hardness, and chemical stability, they improve machining performance and tool life[13].

1.2 Coatings Processes

The choice of a coating technique is a complicated process that is dependent mostly on the component's capacity and cost restrictions. Surface engineering is considered in modern design procedures from the beginning, allowing the technical and economic feasibility of coating technologies, as well as the process's compatibility with the substrate, to be carefully assessed. The most crucial element to be considerd when choosing a coating is its purpose. Coating characteristics, as well as genuine material properties (such as hardness and fracture toughness), may have an impact on its function (such as thickness, surface roughness, residual stress state, and bond strength). The process is subsequently selected based on its technical viability and economic profitability. As a result, a number of process characteristics, as well as process–work piece compatibility, must be studied [6]. As a result, new coating processes including chemical vapor deposition (CVD) and physical vapor deposition (PVD), as well as new preparation procedures like laser cladding, thermal spraying, and sol-gel, have been created [4]. Vacuum

evaporation, sputtering, arc vapor deposition, and ion plating are examples of physical vapor deposition technologies. The three main steps of deposition are evaporation source emission, vapor transit through vacuum space, and vapor deposition on the substrate's surface; however, the technical details of these procedures differ [9].

Sol-Gel is a chemical solution deposition method in which precursor solutions are highly controlled for the deposition of the films .Sol-Gel method involves alkoxides where the macromolecular oxide network is obtained first through the hydrolysis of the alkoxy group after these poly condensation reactions take place[5]. The sol-gel process enables the deposition of solid materials as thin film, at much lower temperature than by traditional methods of thin film deposition. The sol-gel technique is the most effective in the production of O-IH materials due to its specific ability to create a spacious network. Material that has been enhanced, as well as the preparation of porous materials using templates. Industrial production of nano powders large-scale, are easily to be performed and substrates with different shapes and sizes can be coated with low thickness and high optical quality [12]

1.3.Multilayer Coatings

The nano scale multilayer coating provides favorable transformation of thermal mechanical stresses and eliminates superficial defects of the ceramic layer [14].

By comparing between monolayer and multilayers, multilayer coating is less cutting force, stronger adhesion, and a lower friction coefficient. It is possible to reduce the chance of brittle fracture of a tool by using nano-scale multilayer coating. The orientation of the first crack can be considerably modified by the interfaces between layers when a micro crack forms at the top of the coating. When it penetrates deeper into the covering multilayer coatings with various topologies

can be made more resistant to crack propagation. Two or more layers of various materials comprise a multi-layer coating. These layers are composed of the same material and are separated by a sublayer, or they can be built of different materials and separated by an optional sublayer [12,15].

1.4. Factors Affecting Coating Properties

One requirement for a fixed coating design is thickness selection in order to offer the edge a long enough life while preventing coating failure of adhesion due to internal compressive stresses. The style of coating growth and the method of coating growth cause internal tensions in coatings. A mismatch in coating and substrate characteristics, as well as the microstructure of the coating, might create residual stress. The nature and degree of residual stress are frequently influenced by differences in thermal expansion coefficients. The method in which the coating deforms can also be influenced by residual stresses, whether tensile or compressive. Delamination and spalling are more likely in coatings with significant residual compressive stresses, while surface cracking is more likely in coatings with residual tensile stresses. The existence of microscopic defects in the coating can further aid delamination processes. Excessive residual stress will result in the coating being completely removed from the substrate [16].

Coating elements such as deposition process and parameters, composition, thickness, hardness (indentation and scratch) and coating-to-substrate adhesion must be assessed for tribological applications. Prior expertise with the coating (if applicable) and the availability of suitable tribological data are additional important considerations. For effective surface selection, knowledge of the heat and stress distributions induced by the contact for both the coating and the substrate is also essential. Both the coating and the substrate must have Young's modulus, Poisson's ratio, coefficient of thermal expansion, thermal conductivity,

density, and specific gravity. Both materials' temperature and stress limits, as well as any residual stress levels, must be known [12].

1.5. Difficulties of ceramic oxides deposition

Among the differences in physical properties between the metal alloy and ceramics oxides is thermal expansion. Wettability for some metal alloy is poor such as carbon steel [15]. The major limitations of sol-gel processing for coating metals are delamination, crack ability, adhesion, thickness limit, weak bonding, low wear resistance, and high permeability.

Uniform distribution of the coating on the substrate and thermal treatments (drying) are crucial factors that achieve the quality of the coatings. Cracks effect on barrier properties for the coating [16]. Apart from being a great synthesis route, the sol-gel technique also has some serious drawbacks. The foremost ones being the drying of gel and the extreme volume shrinkage at the time of gelation, the elimination of the unwanted residuals (hydroxyls and organics) and the occurrence of large amount of pores. Perhaps, deficient technical and precise knowledge about the sol-gel process is the main disadvantage that creates wide range of complexities in the process [45].

1.6. Application of HSS Tools:

The main use of H.S.S. continues to be in the manufacture of various cutting tools for different machining processes: turning, drilling, milling, reaming, broaching, sawing, etc. One or more of these processes is used to manufacture industrial products of various engineering materials. For example, medium carbon 45 steel (a piece of A519-grade 1045 carbon), which is widely used in the General company for the manufacture of cars and equipment. Shafts, gears, knives and paint scrapers, spindles, and wheels axles include constant velocity axle, half – shaft, solid shaft, Figure (1.1) shows some of the products made of this carbon

steel. Such products are produced by various machining processes using H.S.S. tools. Therefore, it is essential to modify these tools by their coating to increase their performances.

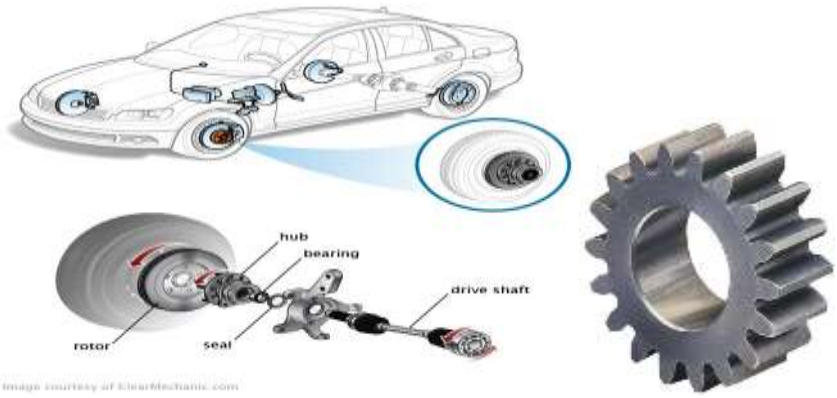

Figure (1.1): Some industrial applications of 1045 carbon steel

1.7. Objectives of the Present Study

This research is aimed at modifying the performance of H.S.S cutting tools by coating them with monolayer or multilayer ceramic oxide coatings, so that it performs better than uncoated tool and a carbide insert in carbon steel (1045) turning. In order to meet these goals, a variety of examinations and tests, such as X-ray Diffraction, Field Emission-Scanning Electron Microscopy, Atomic force, chemical composition, adhesion test, hardness test, wear rate and coefficient of friction test, thermal conductivity, and thermal expansion coefficient, are performed. This research included determining the best coating layers and circumstances for the Sol-Gel technique coating procedure and optimum machining conditions.

.

CHAPTER TWO

Chapter two

Theoretical Part and Literature Review

2.1. Introduction:

This chapter describes the types of hard coatings used on cutting tools in machining processes from a theoretical standpoint. The chapter is divided into three sections, the first discusses the cutting tool's materials of wear resistance, failure modes of cutting tools, tool life and machinability for the work-piece, and wear. The second section discusses cutting tool coating, coating for high speed steel tool, coating process, outlines the challenges of sol–gel deposition of ceramic oxides on high-speed steel and analyzes various ceramic oxides properties. The third section contains a literature review from several approaches for altering cutting tools using ceramic material coatings.

2.2. Cutting Tool Materials

The choice of cutting tool is critical to the success of any cutting procedure. Many factors influence the optimal cutting tool selection, including the material of the work piece, the required surface finish, the type of machining process, and the machine to be utilized. Cutting tool materials are extremely important in the machining process since they determine the chip removal operation's continuously Cutting tool materials also have an impact on the machining operation's quality and quantity outputs, such as surface finish and dimensional accuracy. Toughness, absence of affinity, red hardness, resistance to oxidation, and resistance to thermal

shock are five attributes that must be found in cutting tools in order to have excellent performance, which can be referred to as "perfect cutting tools" [17,18].

Toughness is important in cutting operations that are discontinuous or intermittent. Shock loads and cutting forces are produced during machining; toughness refers to the ability of the cutting tool's edge to endure the shock loads and cutting forces. Lack of kinship Built Up Edge (BUE) formation is caused by any interaction between the work piece and the tool. BUE (a material accumulation against the rake face that seizes to the tool tip, separating it from the chip) causes the work piece's surface finish to deteriorate due to higher forces generated and weaker chip-breaking ability, which are induced by the change in tool geometry caused by BUE formation. To avoid the affinity, any interaction between the tool and the work piece, particularly between the work piece and the cutting edge, must be halted (inert cutting edge).

The temperature rises during metal cutting operation, and the heat generation is undesirable because it damages the tool. The ability of a tool to remain sharp and maintain a consistent cutting edge while machining at a high temperature is referred to as hot hardness. If the tool's hot hardness is insufficient, the tip becomes worthless and rapidly declines. The oxidation is caused by machining at a high temperature, tool wear processes are influenced by temperature. Then to reduce the wear caused by oxidation, the cutting edge should have an oxidation resistance. The condition cycle of cooling and heating causes thermal shock during intermitted cutting in the turning process or during milling operations. If the cutting tool's thermal shock resistance is low, rapid wear rates can be expected.

In the industrial business, a variety of materials are utilized as cutting tool materials, ranging from high carbon steel through carbides and diamonds. There are numerous distinctions between various tools, and it is critical to understand these variances as well as the appropriate use for each tool material. Cutting tools

come in a variety of numbers and names, and each has its own set of applications [19].

Plain carbon steel, (H.S.S) tool, cobalt-base alloys, cemented carbides, ceramics, cermet, polycrystalline cubic boron nitride (PCBN), polycrystalline diamond are the primary eight kinds of cutting tool materials and diamond like carbon [19]. Figure (2.1) shows a comparison of the qualities of these tool materials and their features. Metal cutting processes need tool materials that can endure against the extreme cutting conditions, such as cutting tools face many problems. First material used is the carbon steel; these tools contain 1% manganese and 0.9% carbon, can be employed for aluminum sheet machining and are widely used for wood working. These tools are rarely used for metal machining operations [20].

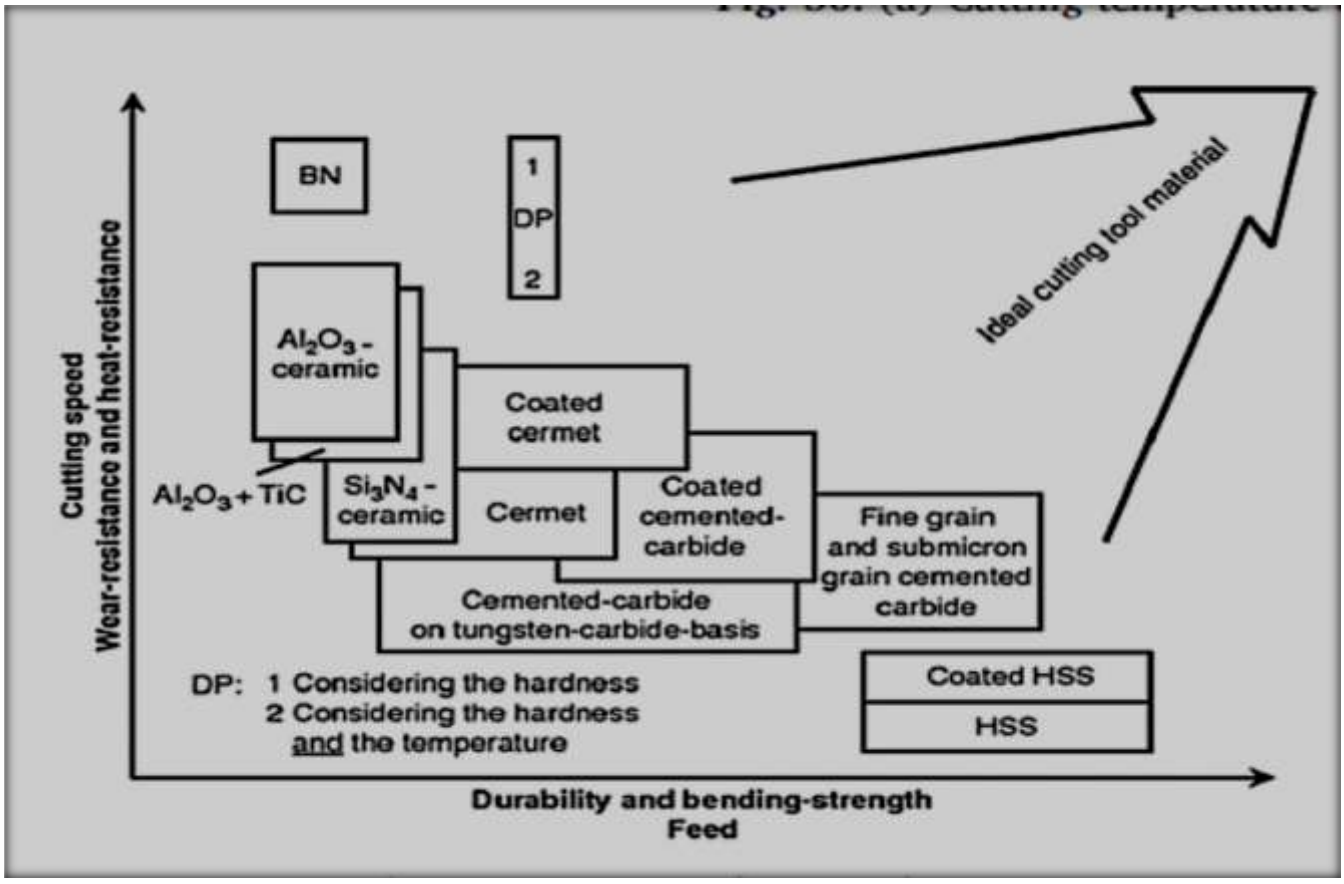

Figure (2.1): Cutting tool materials [20]

In manufacturing processes, (HSS) is the most commonly used in cutting tool material. It's especially crucial for applications with complex tool geometries, such as taps, broaches, drills, and milling cutters. According to AISI, there are two types of HSS tools: tungsten type (T-grades) and molybdenum type (M-grades). Such tools are better suited to shock loading than brittle tools like ceramics and carbides. Stellite tools are manufactured from a cobalt cast alloy containing 40 to 50 % Co, 14 to 19 % W, 27 to 32 % Cr, and 2 %C. Stellite tools are more wear resistant, robust, and heat resistant than standard HSS tools.

After the development of sintered carbides, stellite cutting tools became useless due to their limited grind ability [19]. In the history of cutting tool materials, cemented carbides used in a revolution. Cemented carbides are tungsten carbide (WC)-based hard tool materials using cobalt and nickel as a binder. Cemented carbides cutting tools offer strong compressive strength, high thermal conductivity, good wear resistance, high hardness, good red hardness, and high elastic modulus as general characteristics. Carbides, on the other hand, are less tough than HSS.

Ceramic cutting tools are made of fine-grained Al_2O_3 that has been crushed and sintered at high temperatures and pressured without the use of a binder. Cermets are the most complicated material used in the tool business.

Cermets are made up of titanium nitride (TiN), titanium carbide (TiC), and titanium carbonitride (TiCN) with nickel and/or molybdenum as binders. Using cermet cutting tools results in a better surface polish [22].

Cubic boron nitride is the second hardest substance after diamond (CBN). Steel and nickel-based alloys are the most common materials to be machined with CBN. Tools made of CBN and sintered polycrystalline diamond (SPD) are both costly. SPD tools are made by sintering very fine-grained diamond crystals into suitable shapes at high pressures and temperatures with little or no binder. Diamond tools should not be used to cut steel, due to the carbon atoms react with iron to form iron

carbide at higher temperatures. Nonferrous metal machining, high-speed machining, and machining of nonmetals such as graphite and fiber glass are all common SPD uses [19,21].

2.2.1. H.S.S Cutting Tools

Tool steel is widely used in manufacturing field, for a long service life of a tool made of the tool steel, the tool steel should be sufficient in wear resistance, impact toughness, bending strength and hardness.

Wear resistance of the tool steel depends on the substrate hardness, as well as content, morphology and particle size distribution of the second hard phase in the steel. The second hard phase in the steel comprises M_6C, M_2C, $M_{23}C_6$, M_7C_3 and MX metal carbides, wherein macro-hardness of the MX carbides are higher than other carbides, for providing better substrate protection during operation, thereby reducing wear and improving the service life of molds [23].

Impact toughness and bending strength are key indicators of toughness. In order to improve the toughness of the tool steel, it is important to reduce or refine the carbides. In order to avoid plastic deformation, hardness of the tool steel is usually required to be HRC60 or more [24].

In the conventional H.S.S, carbide segregation occurs and the MC type carbides are large and irregularly shaped. While for both M_6C type and MC type carbides in powder metallurgy high speed steel, a fine and uniform distribution is observed [25].

Because the relatively insoluble primary carbides usually segregate as coarse carbide networks that must be broken down by extensive hot working (after the ingots have been machined) before the steel can be used, the carbides must be present in the materials in cast ingots to produce the best properties in terms of

wear resistance and resistance to impact or fatigue failure. Even after treatment, carbide may remain in the form of stringers, which are localized areas of weakness and thus possible tool failure locations. For this reason attempts have been made recently to fabricate high speed steel by powder metallurgy[25, 17].

Alloy components are designed to prepare a high wear-resistant tool steel, which is sufficient in impact toughness , bending strength and hardness. By adding a large amount of vanadium and carbon alloy elements, the MX carbide is formed, which improves wear resistance. A mount of alloy elements such as chromium, molybdenum and silicon is added for strengthening a matrix and increasing a precipitation amount of the MX carbide [24].

2.2.1.1. The heat treatment of HSS cutting tools

The choice of quenching heating temperature depends on the content of main alloy elements in HSS such as C and W, MO, Cr, V, which determines the temperature range of quenching during final heat treatment of HSS. The final quenching temperature is the most important parameter in the heat treatment process of cutting tool. The proper quenching and heating temperature can ensure that the tool has the necessary high hardness (including secondary hardening), high hardness and good toughness to meet the needs of lathe and machined parts. Generally, HSS with small balance carbon and high carbon saturation should be quenched at a lower heating temperature. Through the study of M2 steel, it is found that each 1% increase in carbon content, the temperature that grain boundary melting drops 11℃. On the other hand, if the carbon saturation is low, the temperature can chose the temperature above the middle limit to heat and quench that the carbide can be dissolved more fully, and obtain high thermal hardness and wear resistance. The morphology and distribution, dissolution and precipitation of abundant alloy carbides in HSS also affect the selection of quenching temperature. Under the

conditions of more large grained carbide, serious carbide segregation, high level of macrostructure and large segregation of components, it should be quenched below the medium limit [23]**.** As shown Figure (2.2):

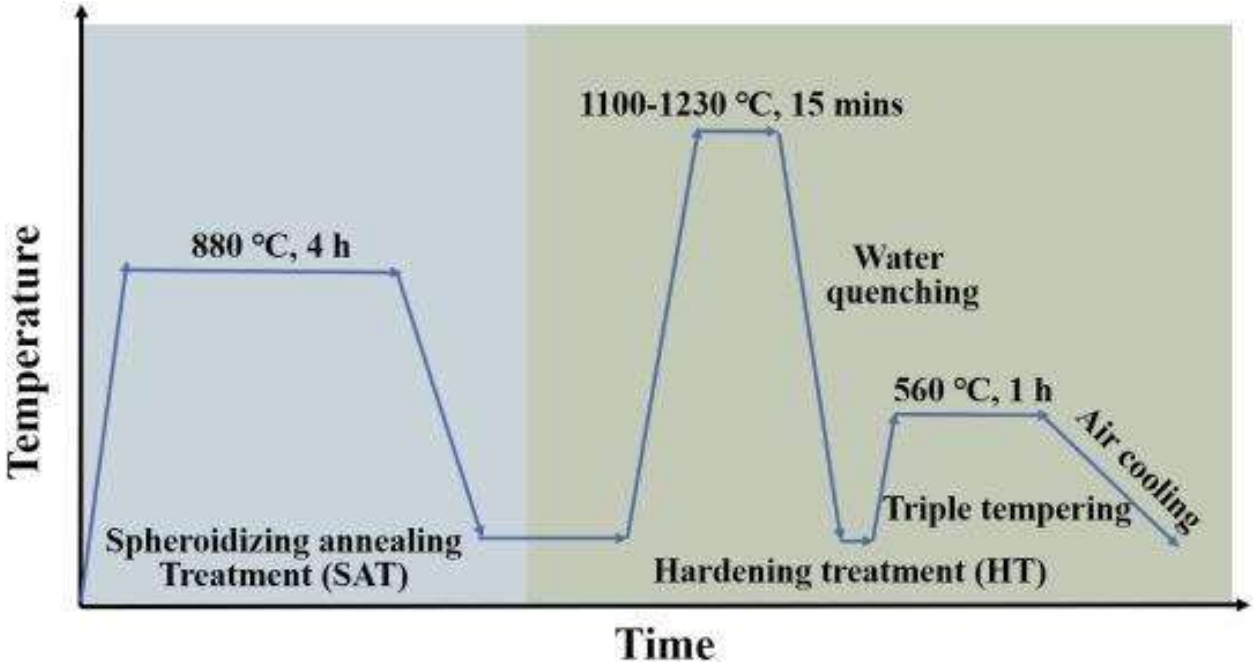

Figure (2.2): Schematic illustration of the heat treatment procedure for the HSS [24]

2.3. Failure Modes of Cutting Tools

In machining, a cutting tool can fail in one of three modes [27]: Fracture failure occurs when the cutting force at the tool point becomes excessive, resulting in brittle fracture failure. When the cutting temperature for the tool material is extremely high, the material at the tool point softens, plastic deformation happens, and the sharp edge is lost, wear and tear over time. This failure is comparable to the temperature failure in that it reduces cutting efficiency, increases and accelerates the tool wear, and causes the tool shape loss. Temperature and fracture failures cause cutting tool loss prematurely, whereas progressive wear allows for prolonged tool use. Gradual wear is unavoidable and cannot be prevented, but it can be slowed to extend the tool's service life [28,29]. The following are some of

the negative effects of tool failure during the process: increased power consumption and high heating on the cutting tool, poor surface finish of the machined material, low dimensions accuracy of the work piece, and the appearance of a burnishing band on the work part surface. There are three types of tool damage: mechanical, thermal, and adhesive. Chipping, abrasion, early fracture, and fatigue are examples of mechanical damage. It is largely unaffected by temperature. The factors that contribute to thermal damage are: heat diffusion, plastic deformation, chemical reaction, and the temperature rise. It's important to remember that heat damage isn't caused by chemical reactions or thermal diffusion. Rather, they provide a weak tool surface so that mechanical shock, abrasion, or adhesion can remove the material more quickly [30].

Wear is defined as a gradual deterioration of the solid surface caused by relative motion with a contacting substance. Wear can be a severe industrial concern because most machinery has moving parts or comes into contact with numerous materials. In practically all machine applications, such as bearings, gears, and cams, wear is undesirable. After a little amount of material has been removed or if the surface has been overly roughened, components may need to be replaced [31].

2.4. Wear in the cutting tool

Wear, in general is the surface damage or removal of materials from one or both side surfaces in sliding, rolling, or impact motion relative to one another. Tool wear is detrimental phenomenon that influences net shape and the unity of machined surfaces. Therefore, increasing the wear resistance of materials used in cutting tools is a major issue in machining. Inhabiting wear in machining is challenging due to the harsh environment of machine operations, especially in machining without using coolant, i.e in dry machining[32].

Cutting tool wear mechanisms are complicated, and they might comprise a variety of interacting effects that are connected together in a complex way. The tool's performance is primarily limited by nose wear, flank wear, crater wear, edge chippings, or a combination of these factors, depending on cutting conditions, work material, and tool material. Wear occurs gradually as a result of abrasive or adhesive wear, plastic deformation, or more discrete material losses as a result of discrete fracture mechanisms, or a combination of these. The enormous mechanical, thermal, and chemical stresses generated could be the cause of these effects. To find the best cutting variables, you'll need to be able to anticipate tool wear. Tool failure, which can damage the workpiece surface and compromise machine tool performance, must also be avoided [33].

Flank wear caused by the adhesive and abrasive actions between work piece and cutting tool [34,34,36]. For a certain cutting tool, the major factors affecting the flank wear are: feed rate, cutting speed, tool nose radius, machining time and depth of cut.

2.5. Machinability

Machinability by definition, is a system property that indicates how easily material can be machined at low cost. It may be described in terms of tool life, ease of metal removal, and work piece quality or surface finish [37].

Only around 8%–10% of the total heat created in machining processes with fixed tool geometries like turning, milling, and drilling goes to the tool, while the rest is split between the work piece and the chip. This heat distribution is difficult to predict and is influenced by the work material, tool material/geometry, and cutting conditions, among other factors. However, because this heat raises the machining

temperature and, in most circumstances, represents a severe concern for productivity and component quality, it must be managed in some way. Reducing the friction coefficient on the chip–tool contact region, which is a practically impenetrable zone, such as by incorporation of free machining elements in the work material, is one technique to reduce heat and temperature. Another method is to use a liquid or gaseous medium to operate as both a lubricant and a coolant at the same time, with one of these features taking precedence over the other. To avoid tool material softening, which leads to deformations and rapid wear, high temperatures at the chip–tool interface must be avoided. Temperature causes large increases in plastic deformation, seizure deformation, and oxidation [32]. Temperature also influences other wear mechanisms/processes such as attrition (adhesion), notch wear, and abrasion. Aside from producing rapid wear, significant heat generation has consequences for surface integrity. Thermal fatigue, phase transition, recrystallization, and microhardness variation are all damaging effects at high temperatures. In general, the machinability can be defined in terms of one or more of the parameters :-required cutting force, quality of the machined surface, tool life, rate of metal removal, required cutting energy, cutting temperature, and types of the resulted chips and others [33].

Forming or material removal operations that modify the geometry of materials with high mechanical characteristics demand more energy. This results in significant plastic deformation and seizure, as well as a lot of heat generation, which leads to higher temperatures. Other factors in the tribological system in machining, such as high friction coefficients between the chip and the rake face of the tool (secondary shear zone) and between the workpiece and the clearance face of the tool (tertiary shear zone), contribute to increasing the seizure stress required to cut the material, as shown in Figure (2.3). High friction coefficients increase

material flow resistance, which is reflected in stresses in the primary shear zone, leading to an increase in shear stress. When the tool presents a reasonable amount of wear, the process is further complicated, because the friction force is proportionally increased. In machining, all of these phenomena acting together cause significant problems, leading to the difficulty in machining cut of some materials, like mould steels, rolling bearing steels [38].

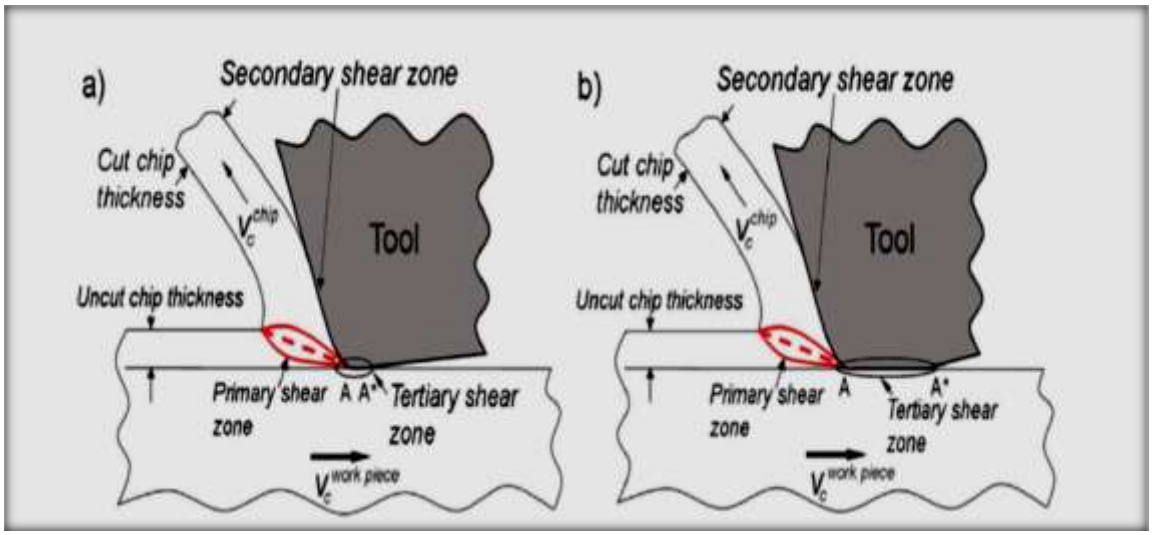

Figure (2.3): Schematic of the cutting tool-workpiece material interaction for (a) new and (b) worn cutting tools. Compare the tertiary shear zone (AA) differences in (a) and (b) (The wear on the tool crater is not depicted in the figures [38]*

. The selection of a 'better' tool material and geometry is not an easy task, and the entire system must be carefully evaluated, among other things, in terms of work material properties, required softening effect, possible chemical affinity with tool material, surface integrity specified in the project, available machine tools, and their rigidity [33].

2.5.1. Surface roughness:

Surface roughness is defined as closely spaced, irregular deviations on a scale smaller than that of waviness. Roughness may be superimposed on waviness . It is expressed in terms of its height, its width, and its distance on the surface along which it is measured [39]. Figure (2.4) shows the surface roughness profile. Surface roughness is an important measure of product quality since it greatly influences the performance of mechanical parts as well as production cost. Surface roughness has an impact on the mechanical properties like fatigue behavior, corrosion resistance, creep life, etc. It also affects other functional attributes of parts like friction, wear, light reflection, heat transmission, lubrication, electrical conductivity; etc. The surface finish produced in a machining operation usually deteriorates as the tool wears. This is particularly true for a tool worn by chipping and generally the case for a tool with flank-land wear [40].

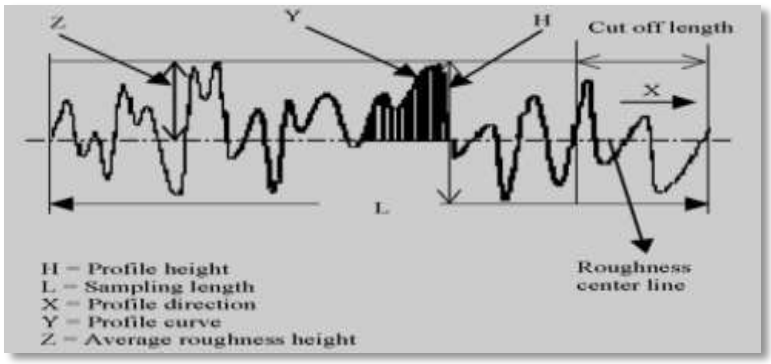

Figure (2.4): The Surface roughness profile [41].

2.6. Tool life

There is no single universally accepted definition of tool life, but in general it can be defined as the length of time that a cutting tool can function properly before it begins to fail, so it needs to be specified with regard to the process aims. It is commonly the quantified by a certain level of the surface roughness

or by putting a limit on the maximum acceptable width for the flank wear, **(V_B *maximum*)**. Mathematically, the tool life can be expressed in the following Taylor's equation [42]:

$$V\,T^{n} = C \qquad (2.1)$$

Where *:* ***V*** (cutting speed in m / min) ; ***T*** (tool life in min) , and ***n*** ,***C*** are constant that may be found for specific workpiece, tool material and feed rate, cutting depth experimentally. Taylor's equation induces the effect of cutting speed only on the tool life, but there are so many modifications for this equation. Besides the effect of the cutting speed, these modifications may introduce the effect on tool life of such parameters as: feed rate, depth of cut, nose radius of the cutting tool, cutting temperature…etc. [43,44].

2.7. Surface Engineering of Cutting Tools

there are many methods to modify the surface properties of a component and this constitutes the field of 'surface engineering'. The processes used in surface engineering can be broadly classified into three groups.

1. Processes which apply a new material, a coating, to the surface, i.e. lead to the formation of a different phase with a distinct boundary between itself and the substrate.
2. Processes that modify the existing surface by inducing a change in composition of the surface engineered layer. This in general leads to a more diffuse boundary between the substrate and the reaction layer, e.g. as in carburizing.
3. Processes that modify the existing surface without a change in composition, e.g. transformation hardening [6].

The coating must be able to resist interaction with other parts or with process media while the substrate material must have sufficient strength to be able to support adequately the highly stressed coating, i.e. the properties of both the coating and substrate must be considered in surface engineering. In addition the coating must be sufficiently strongly bonded to the substrate so that service stresses do not cause it to debond or spall [6].

Surface functionalization is a fast growing field since it is less expensive than inventing and manufacturing a fully new material and allows for the preservation of some of the original material's features, such as mechanical capabilities. Surface properties (such as mechanical, biological, chemical, and physical) can be altered by coating the surface layer with nano- or submicro-coatings. Because changes of surface properties can have both beneficial and negative effects, the breadth of such alterations should always be suited to the eventual requirements [6, 45]. Therefore the deposition of coatings is one of the surface modification techniques which is predominantly adopted for improving the performance of cutting tools [46]. Coating technique is one important aspect in modern cutting tool technology. It reduces manufacturing cost, increases surface finish, decreases setup time, maximizing tool life duration and increases productivity by minimizing tool wear, cutting forces, stresses and temperature of the cutting tool due to their superior wear resistance, great hardness and chemical stability [47].

the domain of producing surface layers has been treated in the form of groups of related techniques, basing on such factors as their modernity, technique of accomplishment, traditional classification and terminology , as shown Figure(2.5) [26].

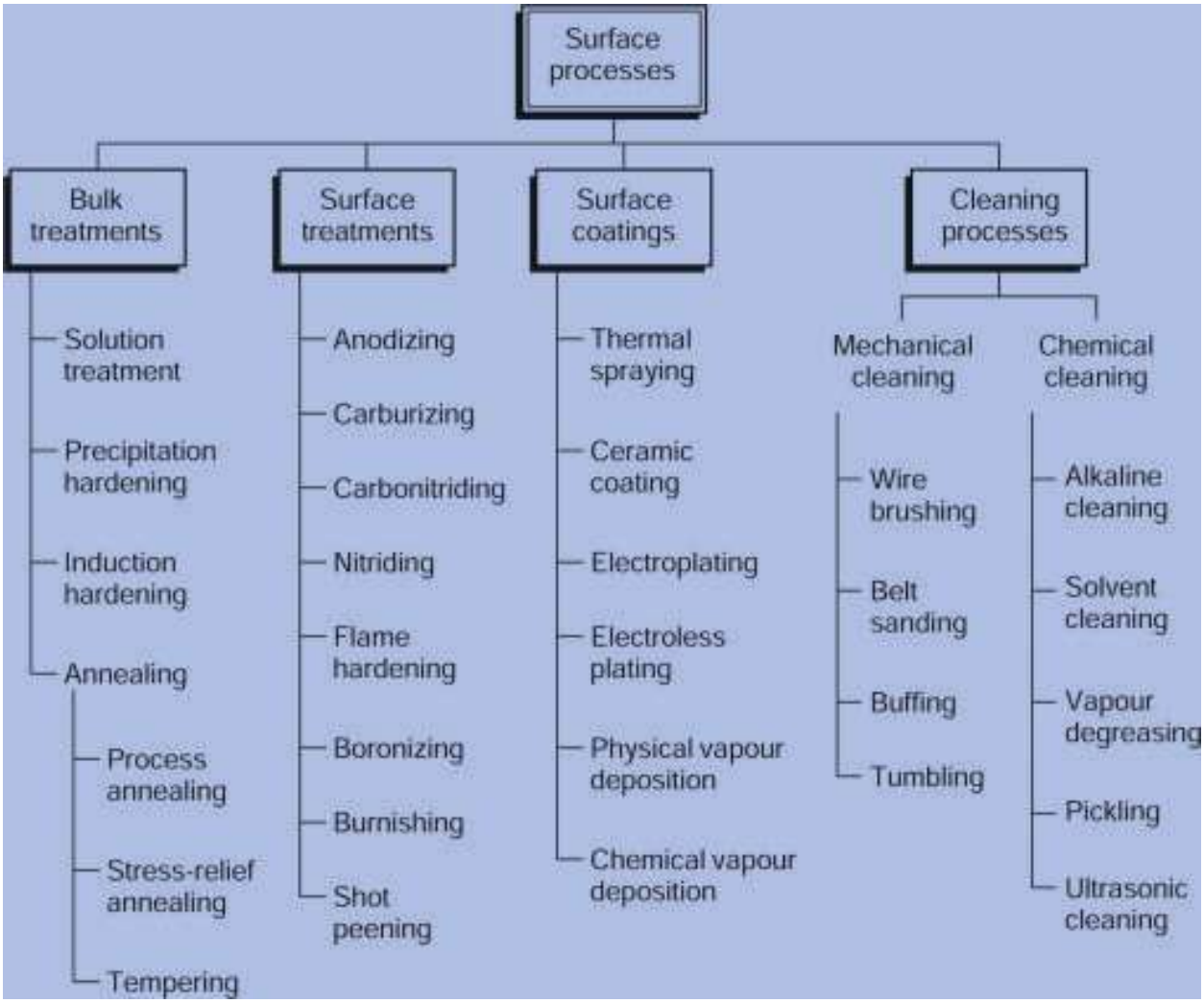

Figure(2.5): Techniques surface engineering [26]

2.7.1. Effect of coating variables on performance of cutting tool

The substrate, the interface, and the coating layers are commonly included in a coating system. Each of these factors has an impact on the system's performance in real-world operations, both collectively and individually. Depending on the coating system's qualities, cutting tool performance can be greatly improved. In order to create a good surface coating layer, each of these constituents needs also have specified qualities [48].

2.7.1.1. Effect of coating thickness

Coating thickness has a considerable impact on cutting tool performance, and there is always an ideal coating thickness for a coating at which the best performance may be obtained. With increasing film thickness, the strain energy and compressive stresses in the coating rise, making coatings more prone to chipping, cracking, spalling, and eventually coating delamination [49]. Coating thickness is a significant element impacting the machining performance of coated cutting tools, but only few studies have been conducted to investigate its impact. In addition, the fluctuation in residual stress with coating thickness is an essential element which is going to be. The cutting tool with 3 μm coating thickness tool exhibited the best machining performance which also demonstrated the best coating/substrate adhesion with minimal tool wear [46].

2.7.1.2. Coating structure

Cutting tool performance is greatly influenced by the coating structure. However, there are just a few studies that compare the performance of coated tools with mono-layer and multi-layer coating structures during machining operations. [50].

The following are the characteristics of monolayer coatings: Microcrack initiation happens at the coating surface and the coating-substrate interface at the same time. In cross-section, propagation fracture owing to coalescence of local micro-crack. The multilayer coatings have the following properties: laminar manner micro-crack develop in vicinity of top surface and in turn the interfaces between layers can substantially change the direction of initial crack when it penetrates deep into the coating. multilayer have multiple structures can enhance

the resistance of coating against crack propagation. lower cutting force, better adhesion, and lower friction coefficient is comparison with monolayer [51].

2.7.1.3.Effect of nano-crystalline coatings

The present section deals with the studies that elaborate the performance of nano composite coatings during turning processes [52,53]. As shown Figure (2.6).

1. ***Decrease grain size***
2. d > 20 nm: hardening – Hall-Petch relation
3. *d* ≈ 10 nm: no dislocations can propagate deformation mainly by grain boundary sliding substantial increase in hardness
4. d < 5 nm: softening (larger fraction of material in grain boundaries)
5. d → 0: amorphous

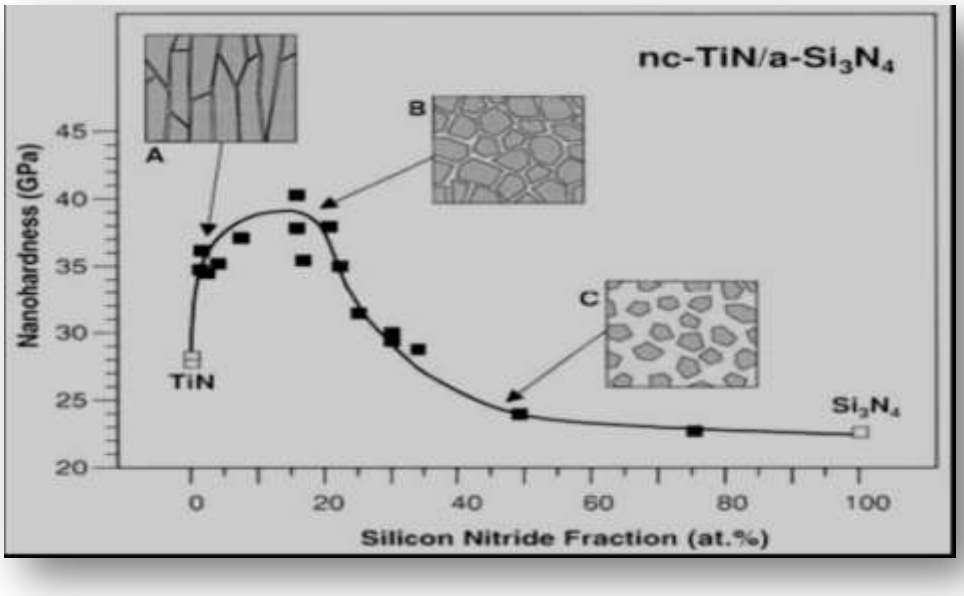

Figure (2.6): When grain size is reduced, no dislocations can propagate, deformation is mostly caused by grain boundary sliding, and hardness is significantly increased [53].

2.7.2. Properties of hard coatings

In general, the properties of thin coatings can be divided into three groups [53]: First group includes: properties of the structural and microstructural systems (thickness, crystal structure, chemical composition, micro structure and texture, surface topography, roughness).The second represents the chemical and the physical characteristics (density, electrical properties, magnetic properties, thermal properties, optical properties, corrosion and oxidation resistance), while the third includes mechanical characteristics (hardness, adhesion, mechanical stresses, fracture strength, wear, friction). From tribological view, properties of hard coatings can be evaluated by thickness, Young's modulus, microstructure, roughness and friction coefficient, corrosion resistance, hardness, adhesion, fracture strength internal stresses, and the thermal properties.

Hardness is defined as a material's resistance to permanent penetration by another harder material. The substrate hardness is critical for tribological applications, and this cannot be overstated. Because it cannot follow substrate deformation, the thin less covering will fracture at relatively low contact stresses if it is not adequately supported.

Coating developers frequently employ hardness measurements to assess coating quality and anticipate coating performance in a variety of tribological applications; nevertheless, the relevance of a high coating hardness should not be overstated. In general, coating materials made of oxides and nitrides have hardness values ranging from 1500 to 3000 HV, whereas carbides and borides have hardness values ranging from 2000 to 3600 HV. When addressing wear characteristics, both hardness and ductility should be considered. Tribological coating development directed towards improved ductility, e.g., by introducing multiple layers or layers

with gradients in hardness and ductility, and towards improved chemical and thermal stability.

It's also crucial to understand that hardness isn't a material constant. Coating thickness, substrate hardness, indenter shape, and a variety of other test parameters will all influence the recorded hardness result. Thin hard coatings' intrinsic hardness values can't be assessed directly using traditional micro-hardness testing because they're frequently heavily influenced by the substrate [49,50].

Adhesion is the interaction between the virtually continuous surfaces of surrounding bodies, such as a film and a substrate. Adhesion is a state in which two surfaces are held together by valence forces, mechanical anchoring, or both. This can be seen in Figure (2.7) [53]. The detailed adhesion understanding to better predict the behavior of the adhesion is to view its effect film quality, durability, and environmental stability [49].

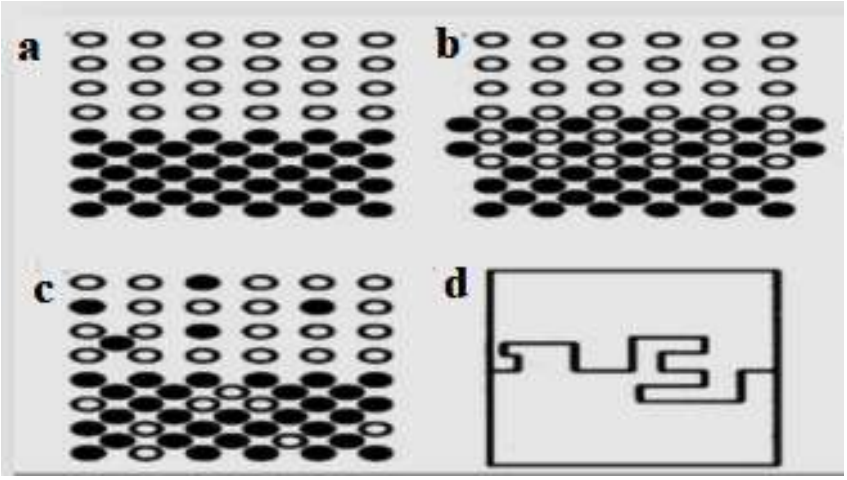

Figure (2.7): Four types of adhesion; (a)smooth transition, (b)compound layer, (c)diffusion bond, (d)mechanical locking [53]

Adhesion of tribological coatings is routinely tested using the scratch test.From a thermodynamic standpoint the work *WA* required to separate a unit area of two phases forming an interface is expressed by equation (2.2) [53]

$WA = \gamma f + \gamma s + \gamma fs$. (2.2)

The quantities γf and γs are the specific surface energies of film and substrate, and γfs is the interfacial energy. A positive *WA* denotes attraction (adhesion) and a negative *WA* implies repulsion (de-adhesion). The work *WA* is largest when materials of high surface energy come into contact such as metals with high melting points. Conversely, *WA* is smallest when low-surface-energy materials

Young's modulus is difficult to determine due to the low thickness of the coatings. On the other hand, its value has a strong influence on the contact stress field, coating delamination and detachment, coating fracture, residual stress state within the coating, etc. Usually, thin hard coatings have a Young's modulus higher than the substrate, and also often a lower coefficient of thermal expansion.

Coating wear often involve crack initiation and propagation processes. Hard coatings, particularly those produced by PVD techniques, are usually brittle, i.e., their tensile strength is low compared with their yield stress in compression. This is a result of their structure, with columnar grains often extending through the whole coating thickness. Fracture strength is a critical parameter in situations where the coating has to deform to accommodate substrate deformation. Therefore, in the tribological contacts operating at high contact pressure, mechanical impact or rapid heating, the fracture strength can be more important than the coating hardness. The possible mechanisms of coating failure are illustrated in Figure (2.8).

In the case of a monolayer coating micro crack initiation occurs simultaneously at the coating surface and the coating-substrate interface. Thus, coating fracture develops through the entire cross-section as a result of the propagation and coalescence of local microcracks. On the other hand, for multilayer coatings, microcracks develop mainly in the vicinity of the top surface and, in turn, the interfaces between layers can substantially change the direction of the initial crack when it penetrates deep into the coating. This means that multilayer coatings fail in

a laminar manner. In consequence, multilayer as well as multiple structures can enhance the resistance of coatings against crack propagation [53].

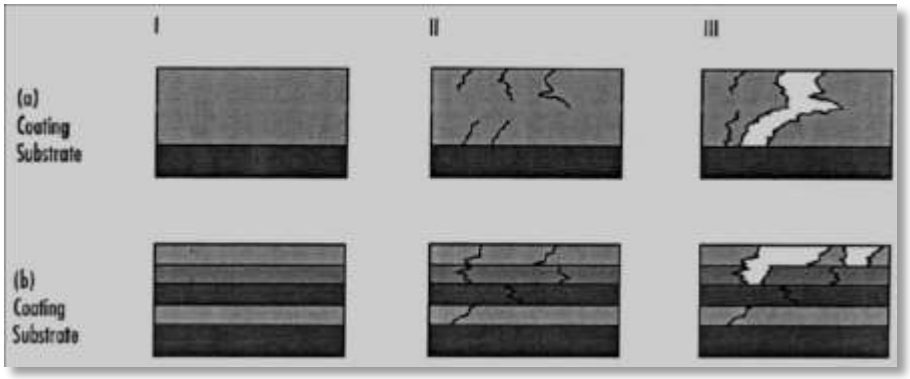

Figure (2.8): Schematic representation of mechanical destruction of single layer (a) and multilayer coatings (b). I—schematic coating structure; II, III—successive stages of failure [53].

2.8. Coating Processes & Coating Materials:

The choice of a coating technique is a complicated process that is dependent mostly on the component's capacity and cost restrictions. Modern design procedures take surface engineering into account from the start, allowing the technical and economic feasibility of coating technologies, as well as the process' compatibility with the substrate, to be properly weighed. Coating a component, on the other hand, is still frequently used to improve its qualities when it has already been discovered to fail at an unacceptable rate [6].

2.8.1.Chemical vapor deposition (CVD):

The substrate is heated to the appropriate temperature in the reactor, which is frequently at or below atmospheric pressure (760 torr). Either a hot-wall or a cold-wall reactor can be used. The chamber walls of a hot-wall reactor are normally heated by resistive heating or radiation from heating devices comprised of high-temperature materials like graphite. The substrates in a cold-wall reactor are typically heated using inductive coupling, electrical resistance, or infrared heating.

Precursor gases are injected into the reactor during deposition, sometimes with a carrier gas such as hydrogen or argon, where they are transferred to the substrate and then breakdown and/or react to produce a coating on the substrate's surface. The decomposition is usually thermally induced, although this can also be accomplished by other energy sources such as microwave plasma. See Figure (2.9)[6].

For wear resistant hard coatings refractory borides, carbides, nitrides, and oxides. CVD coatings can be used on parts that require wear resistance, oxidation resistance, corrosion resistance, and electrical, optical and tribological properties, Hard coatings for wear resistance such as refractory borides, carbides, nitrides, and oxides. [54]

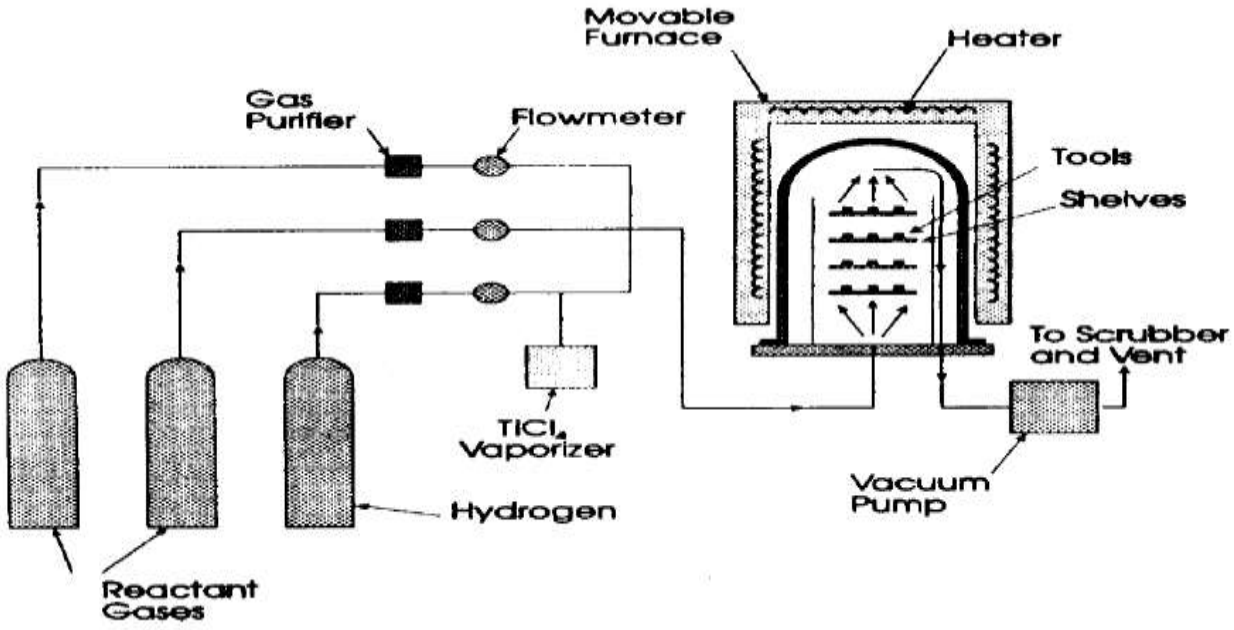

Figure (2.9): Schematic diagram of the CVD process [7].

2.8.2.Physical vapor deposition (PVD):

PVD is a vaporization-based technology for depositing solid material on a pure material or alloy in a controlled environment [6]. The PVD coating technique

involves atom-by-atom deposition of the coating from the vapour phase. There are four stages to this: physical creation of the vapor flux (evaporation or sputtering), gas-phase transport of coating atoms from target to components, deposition of coating elements on component surfaces, and incorporation of coating atoms into the layer [6]. A schematic design is shown in Figure (2.10)[54]. Application of PVD in Nano-coating prepared an adaptive Nano-multilayer coating a significantly lower coefficient of friction at elevated temperatures. Physical vapor deposition was first applied to tools and molds. By depositing TiC coating, the life of the mold can be extended; depositing coatings on high-speed steel tools can improve the wear resistance, chip resistance and cutting speed of the tools. At the same time, the coated tools also have high hardness, high chemical stability, high toughness and low friction coefficient [54].

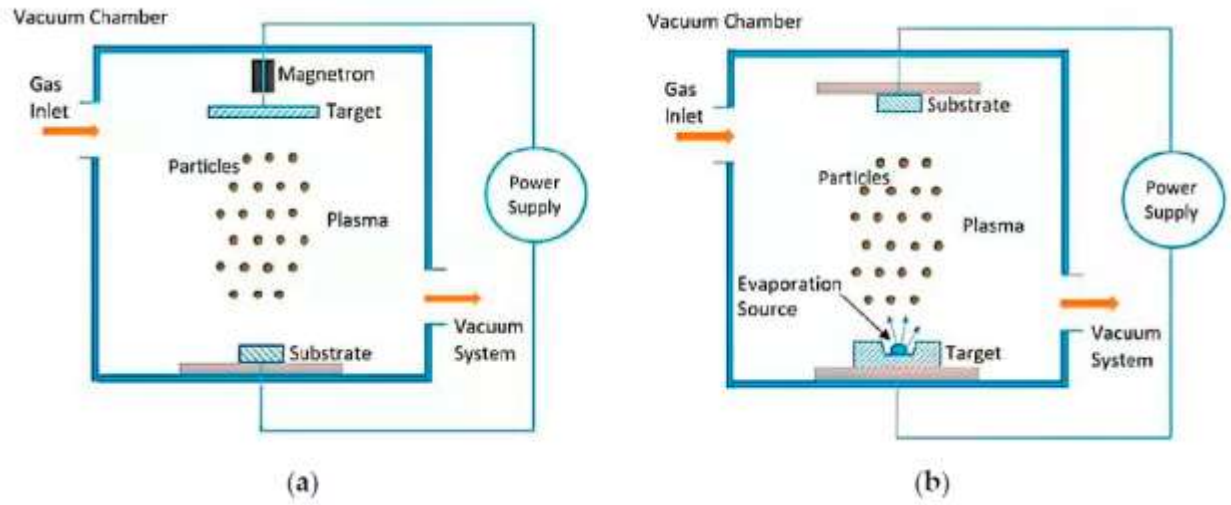

Figure(2.10):Schematic diagram of physical vapor deposition (PVD) sputtering coating methods [4].

2.8.3.Laser coating:

Laser cladding is a process in which the cladding material is melted on the surface of a component using a high power laser beam. The molten material solidifies forming a metallurgical bond with the component, cladding can be described as covering one material with another, within surface engineering, cladding involves the creation of a new surface layer having a different microstructure and /or composition than that of the base material. Laser cladding can be used to improve the hardness, wear resistance, corrosion resistance or it should be considered as a coating process [55]. As shown Figure (2.11) [56].

Laser coatings are used to produce surfaces which are resistant against abrasive , erosive, and adhesive wear, wet corrosion, high temperature oxidation and corrosion [55, 56].

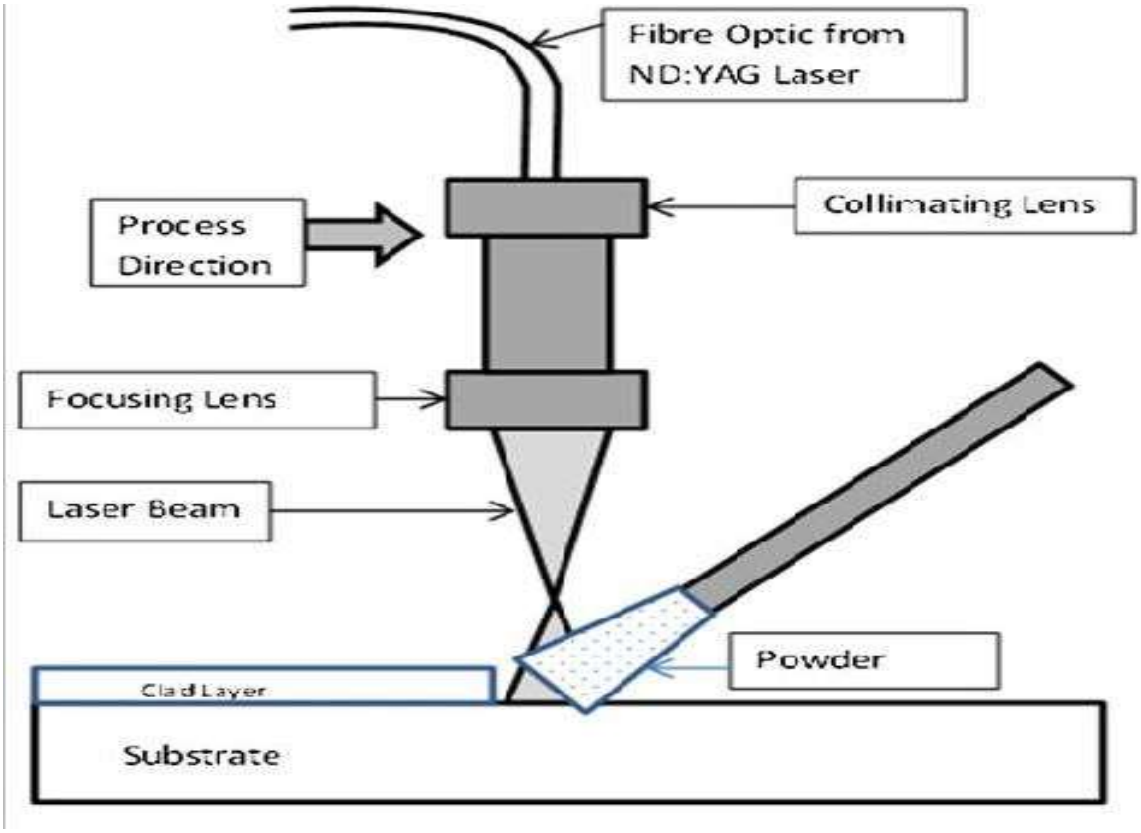

Figure (2.11): Schematic diagram of the laser cladding process [56].

2.8.4. Thermal spray:

Thermal spray is a generic term used to describe a group of processes including flame spraying, plasma spraying, arc metallization, detonation gun, high velocity oxyfuel, and cold spray, that can be used to apply a variety of different coating materials, Figure (2.12) shows High Velocity Oxyfual process .

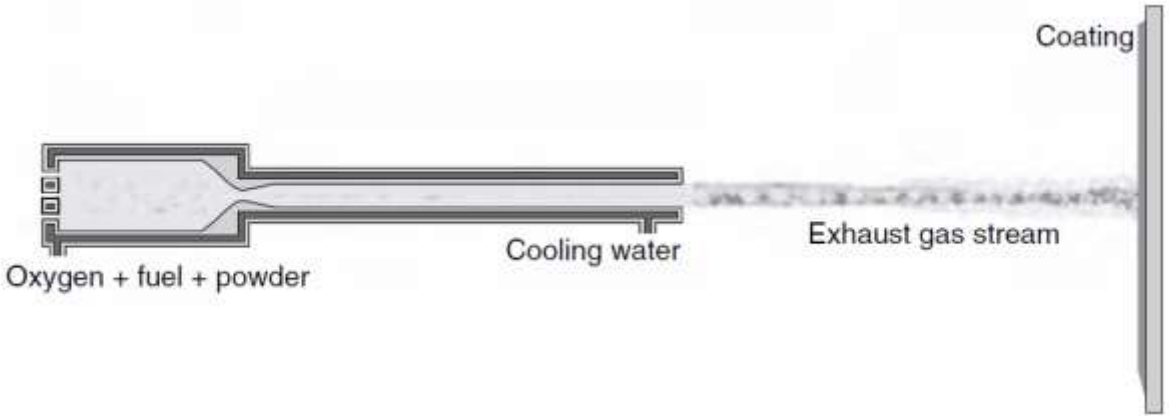

Figure (2.12): High Velocity Oxyfual HVOF [58]

Although these processes encompass a wide range of equipment needs, costs, materials selection and application, they can all be treated belonging to the same family since the processing variables that are being altered are temperature and particle velocity, nature of the material that is used to form the coating [58]. The main disadvantage of thermal spraying is that their inherent high temperature inevitably leads to changes in the microstructure of the coating, resulting in oxide inclusions, which can affect the hardness and wear resistance of the coating [54]. nanostructures have a qualitative leap in wear resistance, corrosion resistance and thermal barrier performance compared with micron level coatings, and their service life can be extended by 3–5 times [57].

2.8.5. Sol- Gel:

The sol-gel process is a wet-chemical technique for the fabrication of materials, employing low temperature, starting either from a chemical solution or colloidal particles (sol for solution or nano-scale particle) to produce an integrated network (gel). In general, sol-gel process can be regarded as the preparation of the sol, gelation of the sol and removal of the solvent. The overall sol-gel process can be represented by the sequence of transformations, which includes [59]: Precursor → Sol→ Gel → Product.

Precursors are starting materials, in which the essential basic entities for further network formation are stoichiometry. Typical precursors are metal alkoxides, metal chlorides, metal nitrate etc. Sol is a colloidal suspension of particles in a liquid, the particles typically ranging from 1-100 nm in diameter. The solid particles in the colloidal phase are stable due to short-range forces such as Van der Waals attraction and surface charges.

Conditions for sol-gel synthesis:- PH of the hydrolysis, rate of addition of water, temperature of gelation, aging of gels, drying control chemical agents (DCCAs), calcination temperature [59].

Sol-gel method includes the formation of a colloidal suspension –sol – followed by polymerization leading to the formation of three-dimensional structure dispersed in a solvent–gel. The gel can be modified with a large number of dopants leading to products with single properties. When drying takes place, under conditions of pressure and temperature. The resulting dry gel is generally referred as xerogel and can be reduced in volume between five to ten times when compared with the initial wet gel.

Sol-Gel process has more advantages than other methods for film deposition those discussed above. These advantages are:

- Low temperature is required in sol-gel method.
- Sol-Gel technique is an economical method.
- Coating of large surface using sol gel method is very easy.
- Capable of making small thickness films, it provides high optical and quality films.
- Sol gel method can produce thick coating to provide the corrosion protection performance.
- Sol-Gel can easily shape material into the complex geometries in the gel state.
- Sol-Gel method has the ability to precisely control the microstructure of the deposited film like surface area, volume & size of the pores.
- Materials prepared by sol-gel synthesis is high homogeneity, high purity.

The sol-gel method consists of three steps that are as follows: a) The desired colloidal particles once dispersed in a liquid to form a sol. b) The deposition of sol solution produces the coatings on the substrates by spraying or dipping or spinning. The particles in the sol are polymerized through the removal of establishing components and produce a gel in a state of a continuous network. c) The final heat treatments pyrolysis the remaining organic or in organic components and form an amorphous which can be change into crystalline by the use of annealing method [45], as shown in Figure (2.13).

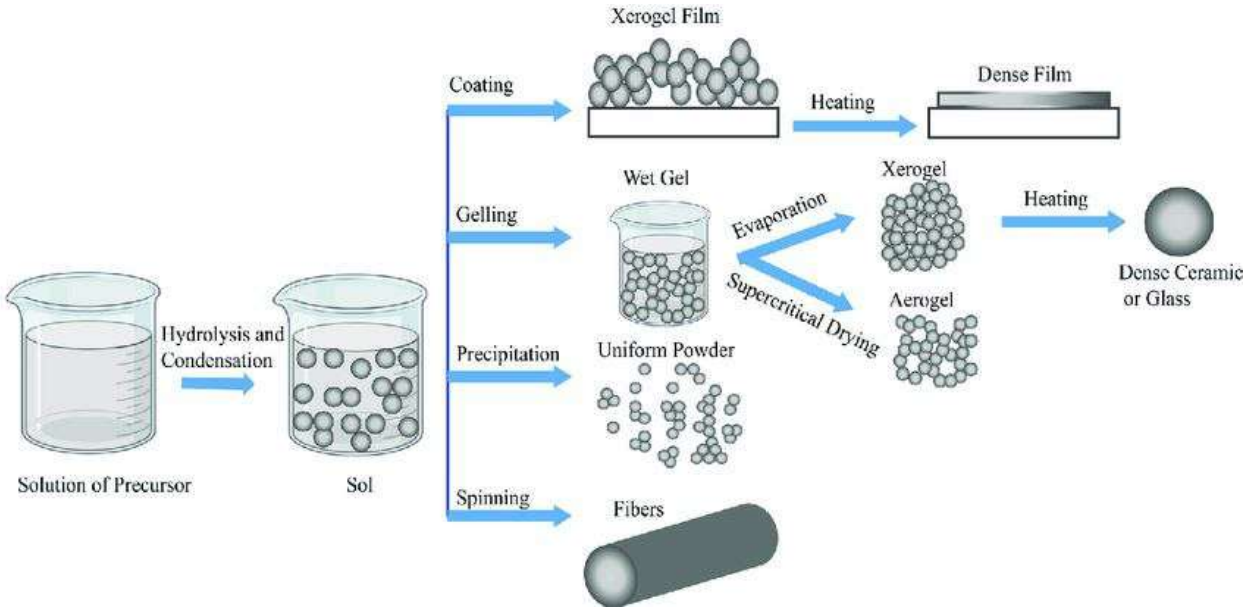

Figure (2.13): Steps involved in controlling the absolute morphology of the desired material [45].

2.8 5.1. Thin Film

The sol gel method of synthesis of thin films offers potential advantages over traditional techniques. First, it is a low-temperature process that avoids decomposition both the coating and substrate material and also allows the introduction of thermally sensitive molecules if needed. It is important that the process is relatively cost-effective, easy to perform, and substrates with different shapes and sizes can be coated. It is cost effective because of the small amount of material required for the coating procedure. Coatings with low thickness and high optical quality can be obtained by carefully controlled conditions during the film deposition process. Sol gel is a chemical method in which reagents are mixed at an atomic scale resulting in a homogeneous material[5].

Thin films are types of layers ranging in thickness from fraction of nanometers to fraction of micrometers. This process is used to modify the reflectance, absorption or transmitting quality of an optical object. The use of sol-gel protective

coating could be performed on either metals or glasses. Composite sol-gel compounds are getting attention in cases that reinforced structure or matrix is needed. Another application of sol-gel process could be preparing powders, grains and spheres that might be expensive or difficult to prepare while using some other hi-tech processes. Ceramic powders are used in catalysts, pigments, abrasive applications and fillers in electric or magnetic devices and mechanism [45]. parameters' influence on properties for nano-coating layer by sol- gel: type precursor, PH, temperature, molar ratio of reactants, solvents composition, sequence of added precursors**,** catalyst (acid or alkaline) [5, 16].

Thin films are prepared by depositing precursor solutions onto various substrates. The amorphous gel films are pyrolysis at relatively low temperatures (300℃ to 700℃) to form amorphous or crystalline oxides followed by annealing at relatively high temperature to allow crystallization. A sol gel coating can be applied to a substrate through various techniques, such as dip coating, spin coating, spray coating, flow coating, capillary coating, and roll coating [12].

2.8.5.2 Dip Coating:

It is the most straightforward process for producing thin films from chemical solutions at a high rate and with the greatest degree of control. This approach can be utilized to deposit coatings on big surfaces in specialized high-tech instances. The basic premise is to extract the substrate at a steady speed after it has been dipped in a solution. The joint impact of capillary rise and viscous pull causes the solution to stretch evenly and naturally on the plane of the material (substrate) at this stage of the dipping process. The final coat is then solidified by evaporation, either naturally or artificially.

A fine adjustment of the evaporation conditions (relative vapour pressure and temperature) and withdrawal speed is necessary to perfectly control the

characteristics of the film which includes the thickness of the film and the inner structure. Amid all accessible methods used for this function, dip coating provides the exceptional prospect to precisely direct the vital parameters, see Figure (2.14) [14,1].

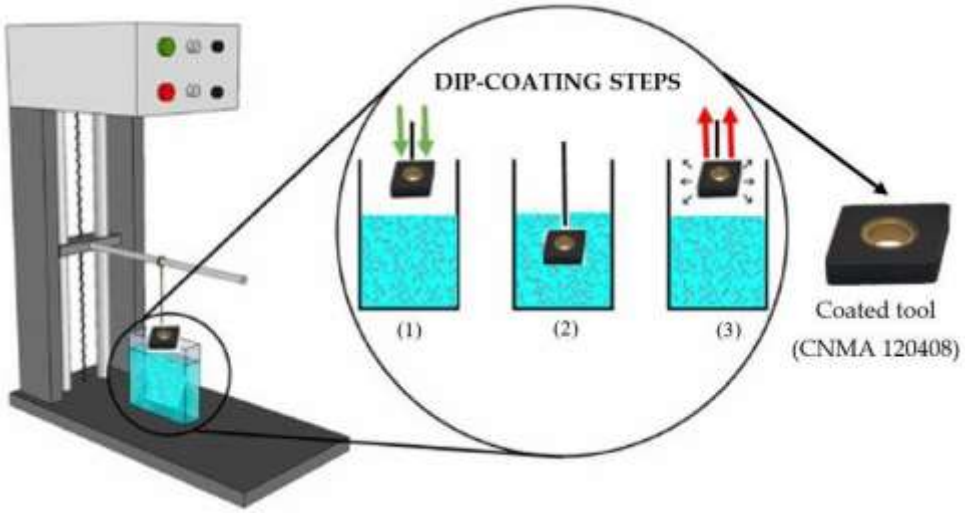

Figure (2.14): Dip coating steps [1]

Advantages: Fast production, cost effective, no need for skilled operator ,and high operating speed [14].

2.8.5.3. The material coating by sol gel

Oxides are the oldest and most common type of ceramic material, with chemical inertness, good high-temperature characteristics, and oxidation resistance. Because oxygen is the most electronegative divalent element, most oxides have a lot of ionic bonding. This material's properties include transparency, high electrical resistivity, poor thermal conductivity, diamagnetism, and chemical stability. The largest and fastest-growing group of ceramic tool materials is Al_2O_3-based oxide tool materials [60].

2.8.5.3.1. Alumina (Properties& structure)

The main reasons to use alumina as a coating tool its presents a high relatively high hardness at elevated temperatures, and good mechanical anti- corrosive properties [1]. Chemical and thermal stability, relatively good strength, thermal and electrical insulation characteristics combined with availability in abundance have made aluminum oxide Al_2O_3, or alumina, attractive for engineering applications. Alumina has several allotropic forms. Alumina has a melting temperature of about 2040 ℃. It has Elastic modulus about 300GPa. Engineering grade polycrystalline alumina products are usually made by sintering alumina powder at high temperature 1300℃. Alumina is graded into two main groups, the first of high-alumina grades with at least 99% Al_2O_3 and the second of alumina grades between 80%and 99% Al_2O_3. The difference between the grades is mainly in the amount of impurities and some deliberate alloying agents such as sintering [60].

The only thermodynamically stable crystallographic modification of alumina is α-Al_2O_3. The ions O_2 are arranged in close hexagonal arrangement, with the cations Al^{3+} occupying two-thirds of the octahedral interstitial positions. Except for the thermodynamically stable a modification, there exist also numerous metastable modifications, denoted γ,δ, θ. These modifications are often used as supports for catalysts. All metastable modifications have a partially deformed closely packed hexagonal oxygen sub lattice with various configurations of interstitial aluminum atoms. On approaching the equilibrium, the crystal lattice becomes more ordered until the stable a modification is formed. The type of metastable polymorph influences the morphology of the formed α-Al_2O_3 particles, as shown Figure (2.15) [63,64].

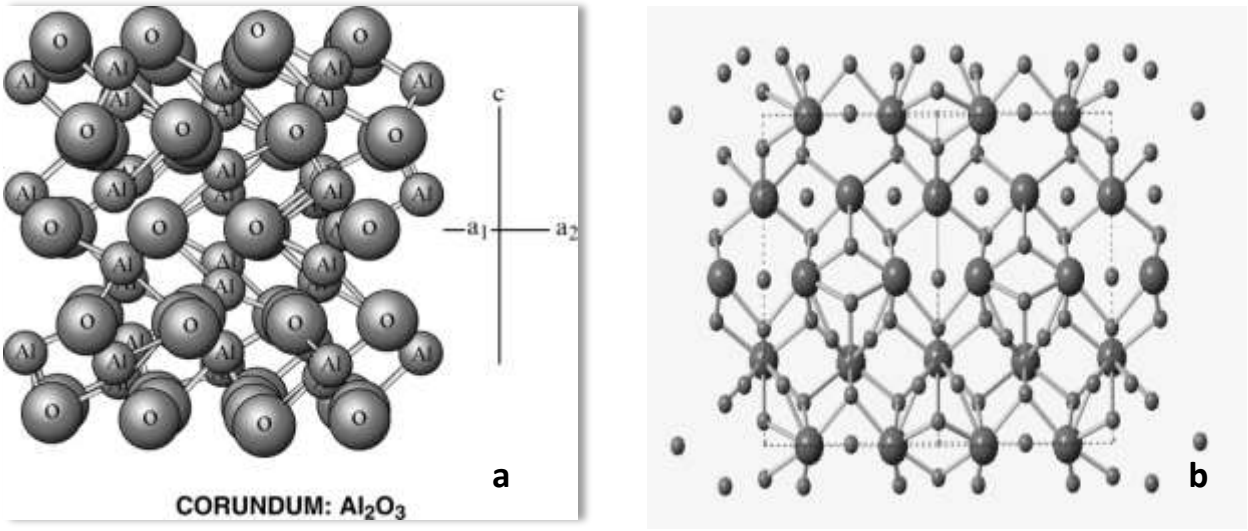

Figure (2.15)Crystal structure of, (a): α-Al_2O_3, (b) γ-Al_2O [64].

2.8.5.3.2. Titania (Properties and structure)

The existing and promising applications of TiO_2 nanomaterials include paint, toothpaste, UV protection, photocatalysis, photovoltaics, sensing, and electrochromics as well as photochromics. TiO_2 nanomaterials normally have electronic band gaps larger than 3.0 eV and high absorption in the UV region. TiO_2 nanomaterials are very stable, nontoxic, and cheap. The continuing breakthroughs in the synthesis and modifications of TiO_2 nanomaterials have brought new properties and new applications with improved performance. Accompanied by the progress in the synthesis of TiO_2 nanoparticles are new findings in the synthesis of TiO_2 nanorods, nanotubes, nanowires, as well as mesoporous and photonic structures. It has an extremely high melting point of 1843℃ and boiling temperature of 2972℃. TiO_2 is insoluble in water, and it is also insulater. Thermal expansion coefficient for TiO_2 is 9.943 $*10^{-6}$ K^{-1} [61].

Titanium oxide forms three polymorphs: rutile, brookite, and anatase : Rutile is a tetragonal mineral usually of prismatic habit, often twinned. Each titanium atom

is surrounded by an approximate octahedron of oxygen atoms, and each oxygen atom is surrounded by an approximate equilateral triangle of titanium atoms.

Anatase is a tetragonal mineral of octahedral habit.

Anatase and brookite are metastable phases, and their exothermic and irreversible conversion to rutile at high temperatures has been widely investigated. Both, ultrafine anatase and brookite transform upon coarsening to rutile when they reach a certain particle size. Once rutile has been formed, it grows much faster than anatase. The thermodynamic analysis of this phase stability indicates that anatase becomes more stable than rutile for particle sizes <14 nm, as shown Figure (2.16) [63, 64].

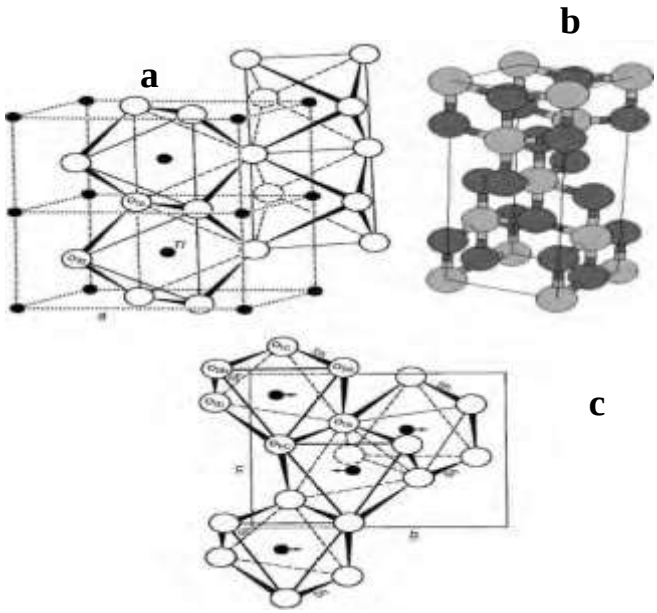

Figure (2.16): Crystal structures of, (a): rutile,(b): anatase, (c):and brookite [64]

2.8.5.3.3. Zirconia (properties &structure)

Zirconium oxide (ZrO_2) has a very high melting point (2680℃) chemical durability and is hard and strong; because of these properties, it has long been used for refractory containers and as an abrasive medium. At temperatures above 1200℃ it becomes electrically conductive and is used for heating elements in furnaces operating with oxidizing atmospheres. Zirconia-based materials have

similar thermal expansion characteristics to metallic alloys and can be usefully integrated with metallic components in heat engines. In addition to these established applications, it has been found practicable the structural transitions of zirconia, thereby reducing notch-sensitivity and raising fracture toughness values thus providing a new class of toughened ceramics. This approach is an alternative to increasing the toughness of a ceramic by either adding filaments or introducing micro cracks that will blunt the tip of a propagating crack.

Zirconia is known to exist as three, well-defined polymorphs, namely monoclinic, tetragonal, and cubic, although the existence of a high-pressure orthorhombic form has also been reported . Monoclinic zirconia consists of a sevenfold coordinated Zr^{4+} cation, such that the oxygen ions with O^{11} coordination are almost tetrahedral, but with one angle in the structure differing significantly from the tetrahedral value. zirconia contains the eightfold-coordinated Zr^{4+} cation with four oxygen ions placed at a distance of 2.065 Å in the form of a flattened tetrahedron, and four at 2.455 Å in an elongated tetrahedron rotated through 90 The high temperature cubic polymorph has a face-centered CaF_2 structure with an eight fold coordinated Zr^{4+} atom with oxygen ions arranged in two equal tetrahedral [63, 64]. As shown Figure (2.17).

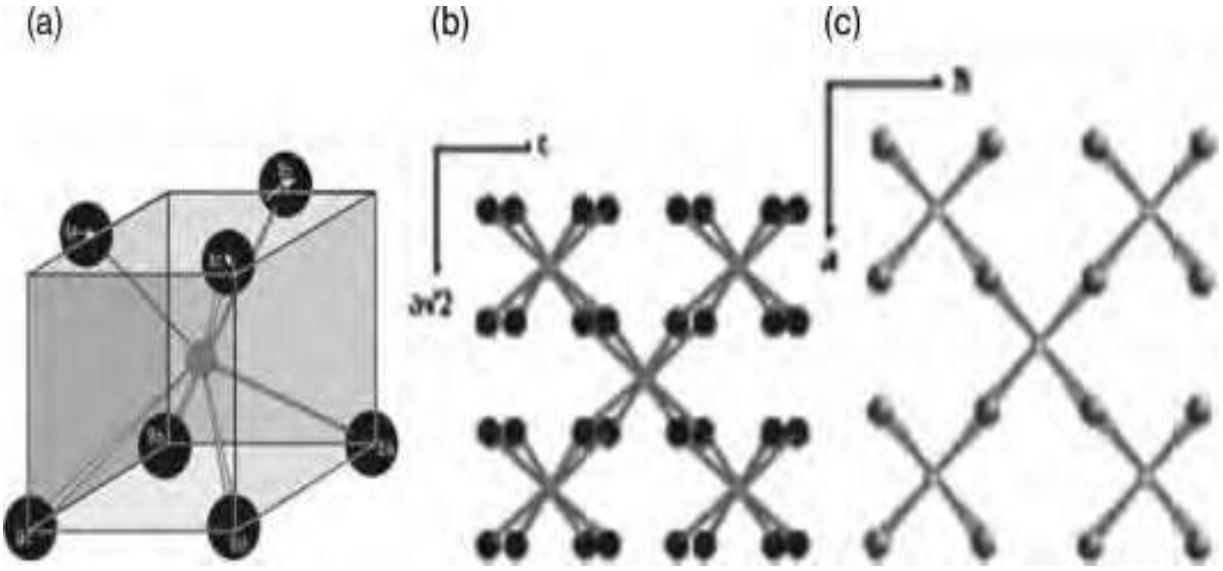

Figure (2.17): Crystal structures of (a) monoclinic, (b) tetragonal, and (c) high-temperature cubic ZrO_2 polymorphs [64].

Ceramic oxides (such as, alumina and zirconia thin coatings) have been deposited on metal alloys via sol gel- due to their excellent mechanical and chemical resilience, high hardness, and corrosion resistance. These coatings are widely used as protective layers in the optical, electrical, and car industries, as well as aerospace applications, and good performance demonstrating high wear resistance. These deposition processes were discovered to be multi-difficult [63].

2.9. Design of Experiments

It specifies the techniques for designing, assessing, and organizing experiments so that objective and valid results can be drawn effectively and sufficiently. It is necessary to integrate sophisticated and simple statistical methodologies to the experimental design approach in order to obtain statistical findings from an experiment. Planning, precise design selection, and statistical data analysis are all necessary for the successful implementation of any industrially planned experiment. The Taguchi approach is a useful tool for optimizing the design of high-quality systems [60, 61]

2.9.1.Taguchi Method

Dr. Genchi Taguchi (a Japanese scientist) created a powerful technique for creating and improving product quality by parameterizing performance attributes. This method was developed using typical design of experiment, DOE. The Taguchi technique will separate the factors that affect the products into two categories: control factors and noise factors. The noise factors are used to identify all factors that produce deviations, whereas the control factors are used to determine the best production or design stability conditions. DOE is used in conjunction with other

methods to investigate the effects of many variables. Taguchi's approach is a type of DOE with a unique set of applications. Taguchi found that the manufacturing process stage and the product design stage are the optimal time periods for minimizing variation. As a result, the Taguchi rule for production has three stages [65,66]: system layout (conceptual level); parameter design (also known as " robustification"); design for tolerance. Taguchi's technique [67] relies on the orthogonal array, signal-to-noise ratio, and analysis of variances (ANOVA). By achieving performance consistency, quality can be improved by eliminating deviations around the target. Experiment design is a method for influencing both of these performance qualities. [68].

2.9.2.Optimization by Grey relational Analysis

The Taguchi system can be combined with Deng Julong's suggested Grey Relational Analysis (GRA). GRA converts a multi-response problem into a single-response problem, and then evaluates the best solutions. Using Grey relational grades, this approach is a trial and error method for estimating the degree of approximation among the sequences (GRG). The GRG is utilized to optimize method factors, and the Taguchi technique can be used to evaluate the optimum method factors setting using GRG as a performance index [69]. The following phases are included in the Grey Relational method based on Taguchi technique:

1st step: The signal to noise (S/N) ratio is used to measure the quality and identify the variables. A greater S/N ratio indicates that the factor is performing better. Eqs. (2.3) and (2.4) can be used to calculate the S/N ratio. When a response maximum is desired, equation (2.3) represents the higher-better S/N ratio type, whereas equation (2.4) represents the lower-better type [70].

$$\text{S/N ratio } (X_{ij}) = -10 \text{ Log}_{10}\left[\left(\frac{1}{n}\right)\left(\sum_{ij=1}^{n} \frac{1}{X2}\right) \right] \qquad (2.3)$$

$$S/N \text{ ratio } (X_{ij}) = -10\text{Log}_{10}\left[\left(\frac{1}{n}\right)\left(\sum_{ij=1}^{n} X^2\right)\right] \quad (2.4)$$

Where, n = number of repetitions; X_{ij} = the response, i = 1, 2. . . n; n is the number of the test in the orthogonal array; j = 1, 2,. . ., m. m is the number of the process response.

Step 2: The second step of GRA is to normalize S/N ratio, in the range between 0 and 1, using formulations (2.5) and (2.6) to maximize and minimize the quality properties respectively [71].

$$X_{ij} = \frac{(Xij) - \text{Min}(Xij)}{\text{Max}\,(Xij) - \text{Min}\,(Xij)} \quad (2.5)$$

$$X_{ij} = \frac{\text{Max}(Xij) - (Xij)}{\text{Max}\,(Xij) - \text{Min}\,(Xij} \quad (2.6)$$

Step 3: Calculation of deviation utilizing the formula, $\Delta = 1 - xij$, where xij = Normalized S/N ratio.

Step 4: After treating the results, Grey Relation Coefficient (GRC) for the jth response in the ith experiment can be stated as follows:

$$GRC = \frac{\Delta\text{min.} + \gamma\Delta\text{max}}{\Delta + \gamma\Delta\text{max.}} \quad (2.7)$$

Where Δ is the deviation of the response; Δ min is the minimum value of Δ; Δmax is the maximum value of Δ; γ is the distinguishing factor (0.5 is widely accepted) [71].

Step 5: After computing GRC, Grey Relational Grade (GRG) can be calculated via the next formulation:

$$GRG = \frac{1}{m}\sum_{i=1}^{m} GRC \quad (2.8)$$

The number of responses is represented by m. For each experiment, the GRC and GRG have been determined. The maximum value of GRG for optimal technique factors is close to the product quality. The maximum GRG value is given an order of 1, and the rankings are done in decreasing order [71].

Step 6: ANOVA is used to classify the significant variables. The analysis of variance's major goal is to find out why things are the way they are. The application of a statistical method to determine the influence of individual components is known as ANOVA. The effect of each element on the method results can be determined very clearly using ANOVA results. The total number of squared deviations, the sum of the squared deviations due to each technique element and the sum of the squared error are the two sources of total sum of squared. The percentage contribution of each method factor to the total sum of squared deviations SST can be used to assess the impact of method-factor changes on performance attributes. When the F value is high, changing the method factor usually has a significant impact on the performance characteristic [72].

2.10. Literature Review

A preview of the recent studies about using coating to modify the cutting tool will be discussed in this item.

In (2004) Pakula et al. [73] investigated good properties of the multi layer CVD on substrate from Si_3N_4 nitride ceramics. The Si_3N_4 inserts were multi layer coated in the high –temperature CVD process with a combination of the TiC, Ti(C,N), Al_2O_3, and TiN layers. The adhesion test found double layer coatings of the Ti(C,N)+TiN and TiC+TiN types are very good adhesion to substrate, the highest value of the critical load Lc=83N, at which beginning of spalling was observed the double layer TiN+Al_2O_3coating.The highest hardness of 32.57GPaof all coating put down demonstrates the double –layer TiN+Al_2O_3one. The highest value of the roughness parameters was Ra=0.6µm for the substrate with the TiN+Al_2O_3+TiN+Al_2O_3+TiN coating and lowest value of the roughness was Ra=0.06µm for the tool uncoated.

In (2005) Dobrzanski and J.Mikula [74] studied the structure and properties of the coatings deposited with the PVD and CVD techniques on cutting inserts made from the Al_2O_3+TiC oxide tool ceramic to grey cast iron machining. The Al_2O_3 + TiC ceramics microhardness is 1970MPa and grows significantly after deposition of the PVD and CVD coatings, except the TiCN + TiN coating. The maximum microhardness of HV0.07 = 40.3 GPa was observed in case of the TiN+ multi TiAlSiN + TiN coating deposited onto the Al_2O_3 + TiC ceramics substrate . The roughness parameter values for the Al_2O_3 + TiC ceramics substrate is *R*a = 0.07 and depositing the TiAlN and TiCN + TiN coatings on to the examined substrate does not cause increase of the roughness parameter. Depositing other PVD and CVD coatings on to the examined substrate causes increase of the roughness parameter from *R*a = 0.21µm for the TiN coating to 0.37µmfor the TiN+ TiAlSiN + TiN coating. Comparison of the approximated values of the VB wear of the Al_2O_3 + TiC based ceramics: uncoated and coated with the PVD and CVD coatings, depending on machining time. From all the investigated materials, the minimum roughness of *R*a = 2.23µm at the final machining stage was revealed in case of the TiN+ multiTiAlSiN + TiN coating deposited onto the Al_2O_3 + TiC ceramics substrate.

In (2011) Hakim et al. [75] study the performance of four cutting tools in the machining of medium hardened HSS : polycrystallinec-BN (c-BN+TiN), TiN coated polycrystalline c-BN(c-BN+TiN), ceramic mixed alumina (Al_2O_3+TiC), and coated tungsten carbide (TiN coated over a multilayer coating (TiC/TiCN/Al_2O_3). For each of the four cutting tools tested. Increasing the cutting speed from 100 to 200 m/min reduced the tool life about 60%. Cutting test soft the HSS were carried out with four different cutting tools. Mixed alumina ceramic and coated carbide tool materials can see longer tool life than cBN tools when

machining the selected workpiece material. Both c BN tools showed poor behavior with this HSS at higher cutting speeds.

In (2012) Grigoriev et al. [76] provided the raised toughness, oxidation resistance, high hardness, and strength of tool material by made of layered composite ceramics LCC coating with nano-scale. These results also testify to higher cutting properties of LCC inserts with NMC, especially at cutting of hard to- machining Ni-alloy. The LCC-NMC tool life exceeds that of standard coated carbide tools and standard coated ceramic tools about 2.5-8.0 times. The developed coated LCC tools allows for increase of cutting productivity in 1.2-1.5 times not only in comparison with the coated carbide tools, but also in comparison with the coated ceramic tools.

In (2013) Cadena et al.[77] studied a thin nanocomposite film (AlCrN) coating to enhance tribological properties of tungsten carbide tool for Ti6Al4V machining. Monolayer coating of AlCrN-T was deposited on a tungsten carbide by cathodic arc (PVD)and used nitrogen atmosphere. It can be observed that the coating very homogeneously with a thickness a round 3.8 µm. The energy dispersive spectroscopy EDX analysis indicates that the chemical composition resulted in at%: Al 32.31, Cr27.85, N39.84. XRD shows two structures of the coating CrN and AlN. By contrast, the flank wear decreases dramatically when Vc of 100 m/min and feed per tooth fz of 0.04 mm are used. It is also important to note the productivity reached by the operation with the lower levels of cutting speed Vc and fz. The machinability study with the coated carbide tool and a workpiece of titanium alloy presented improved results.

In (2015) AL-Dulaimi et.al.[78] investigated the coated inserts are a coating layer of TiC on a tungsten cemented carbide using PVD, substrate lower surface roughness comparing the uncoated carbide insert by (41-53)% through turning AISI1020 steel. An optimum machining conditions for minimum surface

roughness are spindle speed =315 rpm, feed =0.2mm/rev and depth of cut =0.7mm for coated insert, while spindle speed =500 rpm, feed =0.4 mm/rev, and depth of cut=0.6mmfor uncoated insert.

In (2017) Thamir et al. [79] studied the Ti-B-C-N coatings doped with Al which have been deposited on the H.S.S tools by using a mixed gas phase deposition process technique (PVD and CVD) as a new route for the hard film deposition. Multicomponent hard coatings (Ti-B-C-N) were deposited on a molybdenum high-speed tool steels (AISI M52). The investigations indicate an increase in the film thickness from 1.9 to 3 μm for samples deposited at 550 °C, to ~5 μm for samples deposited at 650 °C, 9 μm for samples deposited at 750 °C, 12-13 μm for samples deposited at 850 °C, and 20 μm for samples deposited at 950 °C. A better thermal stability during the process of the wear test than the uncoated H.S.S samples, with a great enhancement in the wear resistance values for this coating film.

In (2017) Puneeth and Smitha [80] studied characteristics of HSS drill bit with Titanium Nitride (TiN) and Titanium Aluminium Nitride (TiAlN) coated by PVD on HSS for machining of EN8 material under dry machining condition and compare between them. Tool life was calculated theoretically using Taylor's tool life equation and compared with the experimental work. It was found experimentally that TiAlN coated HSS twist drill had greater tool life of 110 holes compared to TiN coated HSS of 80 holes and uncoated HSS of 20 holes twist drill. The results showed that the maximum thrust force of 126 kgf was developed in TiAlN coated HSS compared to TiN coated and uncoated HSS of 47 kgf and of 90 kgf, whereas the torque produced in all the twist drills were at an average of 0.5 Kgm.

In (2017) Hu et al. [81] investigated effects and working mechanisms of fluorinated surfactants-based coatings on HSS-Co-E for titanium cutting (Ti-6Al-

4V). Coating process was performed by sol-gel dipping. Finish milling tests were carried out on CNC machining center with maximum speed 120rpm. The average roughness of coated pin is 4.75nm, while the one of uncoated pin is 0.87nm. At room temperature, coefficient of friction of coated pin is about 0.4 while COF of uncoated pin is about 0.55. After entering the normal wear stage, flank wear of coated tool is slightly lower than that of uncoated tool. However, un- coated tool enters into rapid wear stage at 70min,while coated tool is still in normal wear stage. Eventually, uncoated fails at 91min,while coated one is still in normal wear stage. Tool life of coated tool is almost 50% longer than uncoated one.

In (2017) Rabio et al. [82] studies the drilling of a sandwich composite material consisting of aluminium and polyethylene core (PEALL). The drilling tests were carried out using a TiO_2-coated high-speed steel drills (HSS drills) deposited by sol–gel process. The results underline that the TiO_2-coated tool exhibits the best performance and improves the hole quality. Thus, the sol–gel method is a promising technique to coat the complex geometries of the HSS tools.

In (2018) Zheng et al. [83] discussed the effect of cutting parameters on tool wear behavior and surface roughness in high-speed turning of 300M high-strength steel is conducted with coated carbide tool. 300M (40CrNi2SiMoVA) is used as work piece material which is low alloy medium carbon martensitic steel. In general, the resultant cutting force is not very large in the initial cutting stage, which is about 130 N-240 N. The smaller resultant cutting force of the coating tool for high-speed turning of 300M can be obtained at a low level of cutting speed and feed rate. The tool flank wear is accelerated as the cutting parameters increase. ν_c has the greatest effect on the tool surface wear, followed by ∫. A longer tool life can be obtained at ν_c=300–500 m/min, ∫=0.10–0.25 mm/rev and d =0.10–0.25 mm. The major failure type of the coating tool is wear, and the flank wear is uniform. As the average flank wear increases, Ra has a tendency to rise. In

particular, Ra increases rapidly after the average flank wear over 0.25 mm exhibited on the rake face at v_c=600 m/min, such as peeling off, micro-chipping.

In (2019) Rezende et al. [1] investigated of the effect multilayer coatings TiO_2/Al_2O_3on tribological conditions, by sol-gel . The carbide tungsten tools were K10 class for cast iron machining. The test of scratch with a Rockwell indenter, the failures start close to 25 N for the Al_2O_3 coating, and for the multilayer coating between 30 and 40 N. Therefore the adhesion of the multilayer coating is higher than the one of the Al_2O_3 coating. The coated tools presented lower friction coefficients up to 100 m. The ANOVA showed that the main parameter that influenced the resulting cutting force was the feed. The tool and cutting speed have minor influences.

In (2019) Pereira [84] investigated the new coating consists in a silicon dioxide (SiO_2) deposited on HSS by sol-gel process, and its performance was studied by means of drilling tests in nodular cast iron. Four outputs were investigated: thrust force, hole average surface roughness, hole average diameter (DA), and tool wear (VB_{Bmax}). The results indicated that the SiO_2 coating achieved performances significantly superior to the uncoated tools. The "number of holes/maximum flank wear ($VB_{Bmax)}$" ratios were calculated, indicating a performance 315% better for the SiO_2-coated tool when compared to the uncoated one.

In (2019) Al-Ethari et al.[85] evaluated tool life for individual cutting circumstances for an uncoated P10 carbide tool and one coated with titanium carbide by PVD to machine low carbon steel. The results show that the wear width on the lateral surface (VB) for an uncoated tool is two to three times higher than for coated tools. Coated tools have a four-fold longer life than non-coated tools, but as spindle speed, feed rate, and cutting depth increase, their life decreases. When using uncoated tools, surface roughness Ra is higher than when using coated

tools. The surface temperature of a TiC-coated P10 insert is higher than that of an untreated P10.

In(2020) Liborio et al. [86] described the improvement in surface hardness of high speed steel through titanium nitride coating using cathodic cage plasma and solid lubrication (molybdenum disulfide) coating to reduce friction coefficient using magnetron sputtering. Hardness test shows highest hardness with TiN (1371HV)coating while the sample with TiN and MoS_2 layers decrease in hardness and friction coefficient. AFM shows decrease the number of the particles on surface and increase their size with multiple layer. Surface roughness increasing with number of layer increased. As well as for the substrate steel without coating, friction coefficient was raised and changed rapidly that refers to wear and reduce in hardness. Monolayer for each coating MoS_2, TiN decrease in coefficient of friction due to lubricating MoS_2 coating. The results obtained in this study clearly reveal that the cathodic cage plasma deposition can be used effectively for hardness improvement and magnetron sputtering for the combination of solid lubrication/ hard coating. Therefore, using this combination of treatment, the friction coefficients and thus failure to coatings can be minimized.

In (2020) Manivannan et al. [87] investigated the improvement in the surface properties of H.S.S rod by PVD multilayer coating. The PVD coating process was carried out by sputtering and thermal evaporation technique to coat thin films of Al_2O_3, SiC, and B_4C. The maximum coating thickness attained by this process is 1.9 µm. The wear test was performed on three coated samples of coating thickness 1.1, 1.7, and 1.9µm. The wear test results show that uncoated material has a wear rate of 441µm and as the coating thickness increases from 1.1 to 1.9 µm, the wear rate reduces from 24 to 20 µm. The maximum frictional force reduces 19.8 to 12.2 N for uncoated to the coating layer thickness increase from 1.1 to 1.9 µm. the frictional force in 1.9 µm coated was 50% lesser as compared to uncoated

specimen. Minimum coefficient of friction of 0.371 was attained for 1.9 μm coated specimen and maximum coefficient of friction of 0.452 for uncoated specimen. The hardness value was obtained from the Vickers indentation, the highest hardness of 37.2 GPa for 1.9μm coated material. Thermal stress for the coated specimen is 25 times better than uncoated specimen. As compared to uncoated specimen the cutting tool life of HSS coated with Al_2O_3. SiC. and B_4C using PVD coating process could be increased about 7 times.

2.10.1. Summary for the Literature Review

Study	Machining process, Cutting tool,	Coating type	Thickness of layer	Coating process	Improve The machining performance for the cutting tool
Rezende et.al.[1] (2019)	Carbide tungsten K10 for cast iron machining through turning process	TiO_2, Al_2O_3	5μm	Sol-gel	Lower friction , good adhesion, and higher hardness with multilayer coating
D.Pakula et.al.[73] (2004)	Si3N4	TiC, Ti(C,N), Al_2O_3, TiN	1.7-9.5μm	CVD	Highest adhesion with double layer (Ti(C,N)+TiN and TiC+TiN While highest hardness with double layer TiN+Al_2O_3
R.Manirannan et.al. [87], 2020	HSS, AISIM2	Al_2O_3+SiC+B_4C	1.9μm	PVD	Wear rate was reduced by 20-24% , frictional force in 1.9μm coated 50% lesser compared uncoated, highest hardness with 1.9μm,tool life for HSS increase 7 times Coefficient of friction was 0.371
L.A.Dobrzanski and J. Mikula [74] 2005	Al_2O_3+TiC oxide tool ceramic for machining grey cast iron	TiN+TiAlSiN+TiN TiCN+TiN TiAlN	1.1-5.8μm	PVD+CVD	Microhardness max with TiN+TiAlSiN coating layer
L.Cadenaet al.[77], 2013	WC to machine Ti6Al4V through milling process	AlCrN	1.97—13.7μm	Cathodic arc PVD	Improve machinability condition

Natalia Fernanda Santos Pereira [84], 2019	HSS to machine cast iron through drilling process	SiO_2	For SiO_2 nano thickness layer	Sol-gel	With coated reduce each of thurst force, coefficient of friction, width wear
Juan Carlos Campos Rabio et.al. [82], 2017	HSS to drill sandwich composite Al/PE	TiO2	Nano thickness layer	Sol-gel	Reduce coefficient friction, improve hole quality
Meng Hu et al. [81], 2017	HSS-Co-E for titanium cutting (Ti-6Al-4V	fluorinated surfactants	---	Sol-gel	The tool life of a coated tool is over 50% longer than that of an untreated tool.

According to the literature review, the sol–gel coating approach has been successfully used to improve machining responses: tool life, surface roughness, and temperature, mechanical properties such as: hardness, wear rate, and coefficient of friction, as well as various physical properties: thermal conductivity for cutting tool. Few studies employed the sol gel technique to coat HSS cutting inserts with ceramic oxides monolayer. Several studies have also looked into the effect of multilayer coating on machining results for HSS tools, carbide inserts, and ceramic inserts utilizing a different coating technique (PVD, CVD). There has been no research into the effect of a multilayer coating by sol-gel on HSS tool through traditional machining.

2.11. Research Originality

This research investigated the ideal conditions for coating HSS inserts with ceramic oxides (TiO_2/Al_2O_3/ ZrO_2) utilizing the sol-gel process, as well as the majority of its characteristics. These conditions involved viscosity, aging time, and PH, for each coating precursor. Addition, deposition conditions such as immersion time, number of coating cycles, dry temperature and calcination temperature to obtain nano structure of coating layers.

Then, Deposited multilayer of ceramic oxides on HSS insert with thickness layer don't exceed 5-6 µm at low temperature.

CHAPTER THREE

Chapter Three

Experimental part

3.1 Introduction

The current study's program is described in this chapter.Techniques, experimental setup, equipment, and preparation method of coating precursor for coating processes. It also contains several tests such as: physical and mechanical tests, and the machining experiment schedule. The preparation for uncoated insert and mechanical tests for coated and uncoated inserts such as, wear test, coefficient of friction, micro hardness were carried out at the laboratories of the Metallurgical Engineering Department/College of Materials Engineering at the University of Babylon. All samples were sorted and drilled and then machining tests were carried out at the Training and Workshop Center/ University of Technology. Metallography was carried out by Field Emission Scanning Electron Microscope (FESEM) at the Nclher Land, at Nano Lab, in Al-khora Company.

3.2. Program of the present study

Figure (3.1) shows the experimental program of the present work.

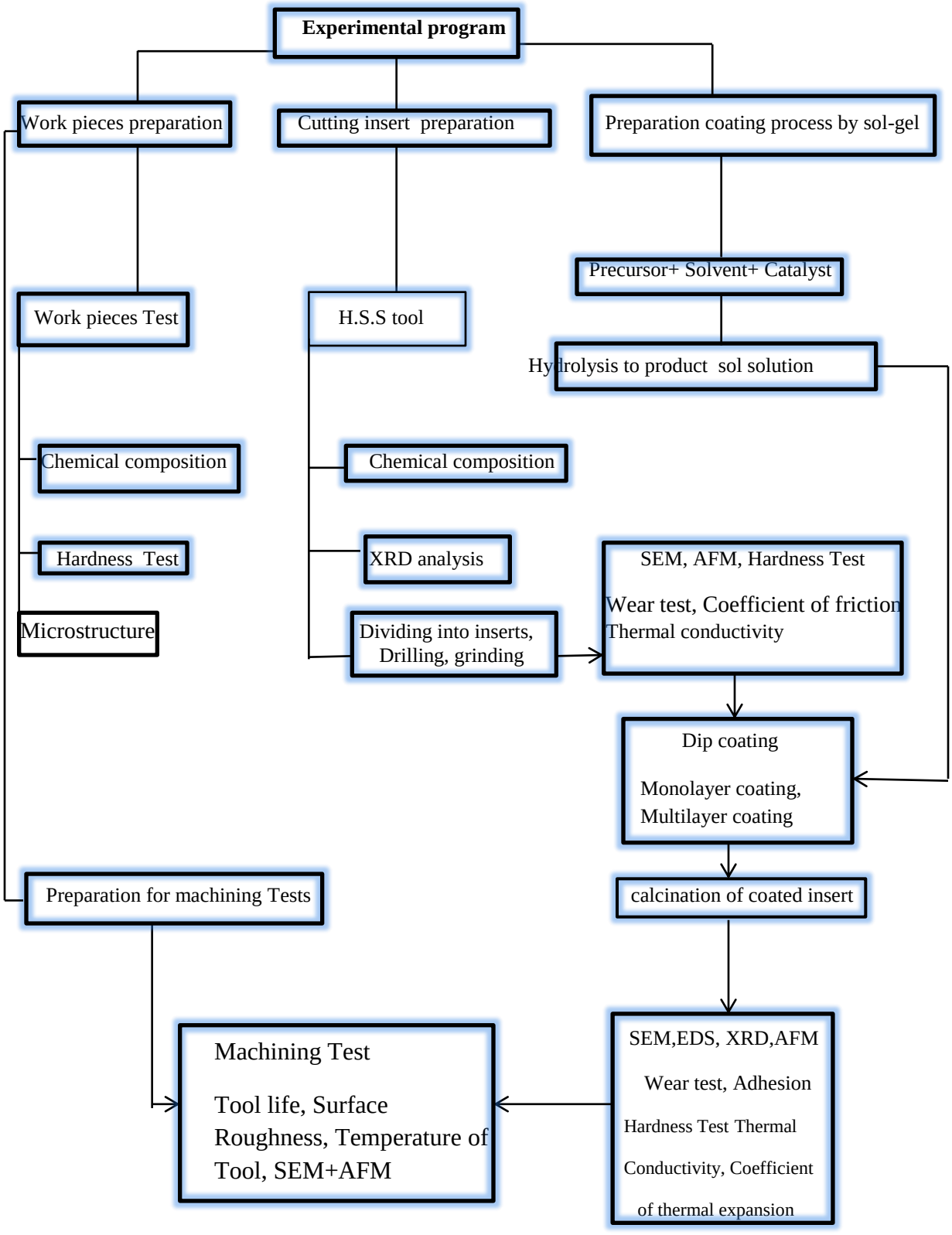

Figure (3.1):Experimental program of the present study

3.3. Materials and their tests:

3.3.1 Cutting tool preparation:

A single point AISI M3 high speed steel tool having a length of 200mm and a square cross section with side of 12.75 mm was used to prepare the cutting inserts for turning purpose. Wire cut machining was used to divide this tool into 5mm thick parts, then a spark machine was used to drill a 5mm diameter central hole in each part. obtained cutting insert was a rake angle (α) equal to zero and a flank angle (γ) equal to zero also. Figure (3.2) shows the prepared cutting insert.

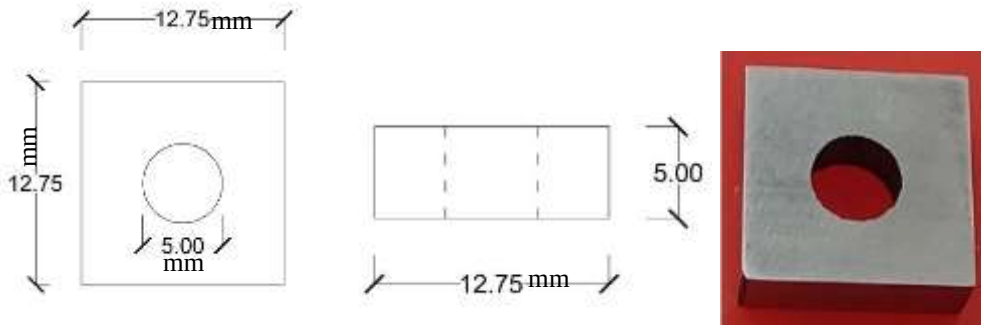

Figure (3.2): AISI M3 HSS cutting insert

The grinding was carried out at the laboratories of the Metallurgical Engineering Department/College Materials Engineering at the University of Babylon. Conventional grinding was used to prepare the surfaces of the cutting insert specimen began at grade 220 and progressed to 600 in phases. The grinding was performed for all specimen to a achieve a uniform roughness for all of its surfaces. To eliminate adherent contaminations, the specimens were first washed in an ultrasonic acetone bath for 15 minutes and then trichloroethane for 10 minutes before being dried in air. Grinding and polishing were achieved via the device type (Metallographic lapping/ polishing machine, MTI Corporation, model UNI POL-820).

3.3.1.1. SEM and EDS analysis

Following the fabrication of the cutting inserts, several emery paper grades (300, 400, 600, 800, 1000, 1500, and 2000) were used to grind the surface of the specimen to an adequate fineness, and it was then rinsed with water. The HSS insert was polished using a diamond paste with a grain size of (0.1-0.3)µm. MAX3, was carried out at ALKHORA with the use of a Field Emission Scanning Electron Microscope (inspect F50) with an Electron Dispersive Spectroscopy EDS detector. The SEM morphology of the uncoated HSS implant is depicted in Figure (3.3).

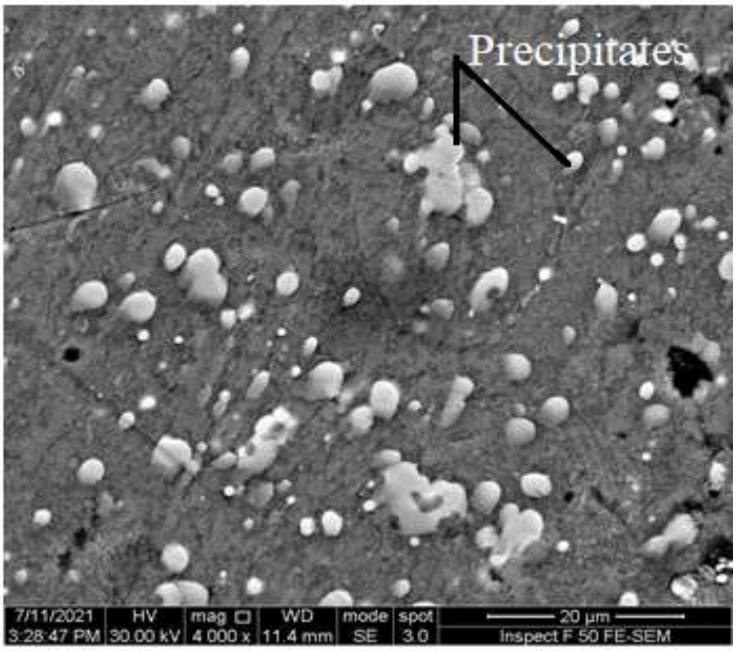

Figure (3.3): Microstructure image for HSS cutting insert

3.3.1.2. Chemical composition

The chemical composition analysis for the HSS tool was carried out at the General Company for Inspection and Engineering Rehabilitation-Baghdad. The analyse shows that the HSS is of AISI M3 class1 high speed steel-UNST11223[88]. Table

(3.1) demonstrates the standard composition and the result of the performed analyze see appendix A1.

Table (3.1): Chemical composition of the H.S.S tool [88]

Element wt%	C%	Cr%	Mo%	Mn%	V%	P%	W%	S%	Si%	Ni%	Cu%	Fe%
Standard [88] ASTM A600M3Class1	1.06-1.10	3.75-4.5	4.8 - 6.500	0.1500-0.400	2.25-2.275	0-0.03	5-6.8	0-0.03	0.2-0.45	0-0.3	0-0.25	Bal
A 600M3Class1	1.03	4.03	5.3	0.308	1.99	0.0292	6.8	0.0129	0.271	0.136	0.0927	Bal

3.3.1.3.Hardness Test:

The specimen of uncoated insert had been appropriately ground and polished prior to the hardness test. The test was performed on a United Manufacturer Rockwell hardness gadget type at the General Company for Inspection and Engineering Rehabilitation in Baghdad (TRU-BLUE11).The hardness test was achieved for uncoated insert using a Rockwell hardness device type (TRU-BLUE11) with a load (150kg) HRC and a tip (120)degree for 10 seconds. The resultant hardness of the HSS tool is shown in Table (3.2), with the standard value for this parameter, see appendix A2-A3.

Table (3.2): Mechanical properties for HSS[88].

Material	Tensile strength MPa	Hardness HRC
Standard[88] A600M3Class1	2180	66
A600M3Class1	------	65.7

3.3.2. Work piece Preparation:

The machining experiments were conducted on a work piece of medium carbon steel , having a length of 225 mm and a diameter of 50mm. ASTM A519- grade

1045 is unalloyed medium carbon steel. It may be machined in any condition and has a wide acceptance in engineering applications. The work piece was divided into regions as shown in Figure (3.4).

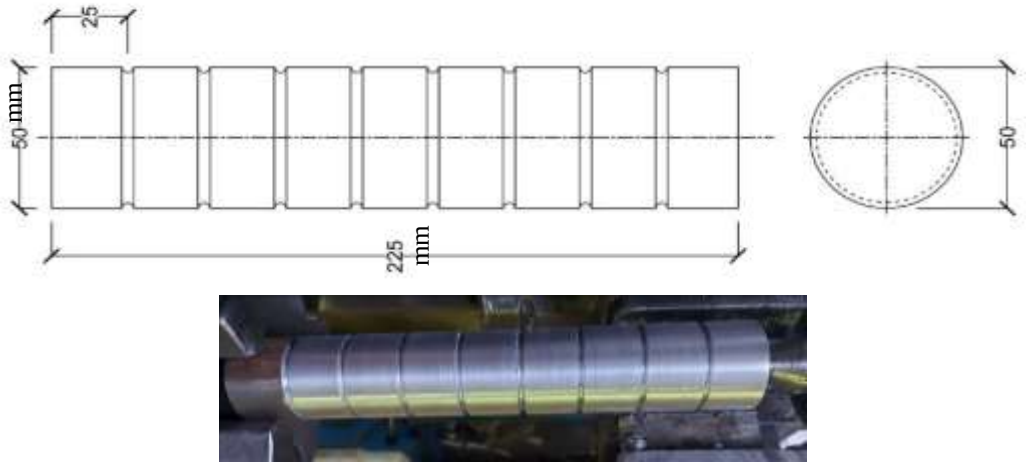

Figure (3.4): Work piece regions

3.3.2.1.Optical microscope

The specimen was prepared for microstructure examination which involves the following steps. Sample was cut to the cross-section area for easier handling and wet grinding process was carried out by exposing the sample surface to rotary disk with using emery papers of (SiC) with different grades in sequence (180, 400, 800, 1000, 1200, 1500, 2000)). Then the sample washed by water and dried by hot air. Polishing process was carried out, this process continues until the sample surface becomes as mirror, and then it is washed by the water and alcohol and dried by hot air. Etching process was doing by immersion the sample for 30 s with Nital (2ml Nitric acide+98 ml Ethanol) [89]. Figure (3.5) illustrates the optical microscope examination of the work piece.

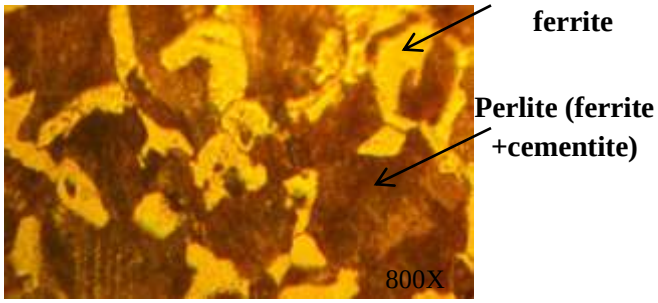

Figure (3.5): Microstructure image 800X for work piece

3.3.2.2.Chemical composition

The work piece was examined using a spectral analysis device at the General Company for Inspection and Engineering Rehabilitation-Baghdad. Table (3.3) shows the resulted chemical analysis of the work piece and its standard composition [88]. See appendix A4

Table (3.3): Chemical composition of the work piece [88]

Element wt%	(C)	(Si)	(S)	(Mn)	(P)	(Mo)	(Ni)	(Cr)	(Fe)
Standard [88] A519 -1045	0.43-0.50%	0.17-0.37	0.05%	0.50-0.80%	0.04%	0.0153%	0.4%	0.4%	Bal.
A519-1045	0.505%	0.304%	0.0432%	0.610%	0.030%	0.0097%	0.135%	0.128%	Bal.

3.3.2.3.Hardness &Tensile strength Tests:

Before the test, the specimen was properly ground and polished. The test was performed on the work piece according to ASTM E384 standard. The test was carried out at the General Company for Inspection and Engineering Rehabilitation-Baghdad, on a United Manufacturer Rockwell hardness device type (TRU-BLUE11), using load of (100kg) HRB with (0.0625mm) diameter. While in Brinell hardness device, using load 62.5Kpa with 2.5mm diameter at 10 sec. Table (3.4) shows the resulted hardness and the tensile strength of the work piece with the

standard values of these properties [88]. The tensile test was performed on the workpiece according to (ASTM A519) [88]. The test was carried out at the General Company for Inspection and Engineering Rehabilitation-Baghdad, via a tensile test device typeWDW- 200 E. Figure (3.6) shows a sketch with the dimensions for the used specimen and the specimen before and after the test, see appendix A5-A6.

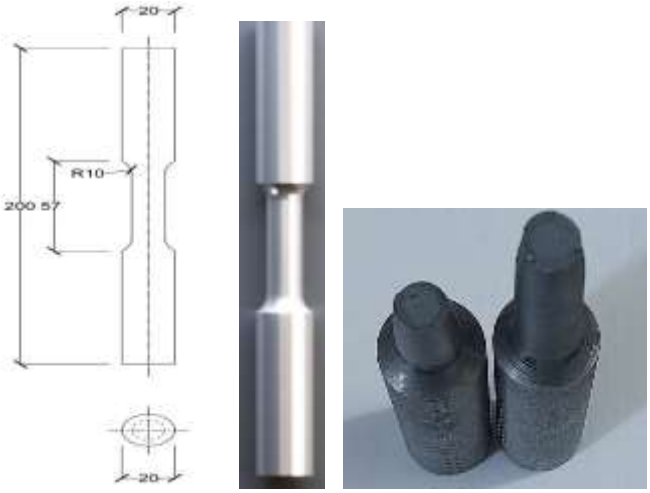

a b c

Figure(3.6): The work piece (a): sketch with the dimensions, (b): before the test, and (c): after the test

Table (3.4): Mechanical Properties of 45-steel carbon steel [88]

Material	Tensile strength MPa	Hardness HRB	Hardness HB
Standard ASTM A519-Grade 1045 [88]	620	94	201
ASTM A519-Grade 1045	611	93	195

3.3.4. Carbide tool

Tungsten cemented carbide tips were used to compare with coated HSS cutting inserts. All the inserts have identical geometry designated by the American National Standard Institute (AISI) as [TNMG 160408], as shown Figure (3.7).

Chemical analysis for the carbide insert was carried out in Faculty of sciences X-Ray Lab, Tarbiat Modarres Univesity/Iran. Instrument (XRFPW2404) Calibrate with Philips Analytical X-Ray B.V.standards. Table (3.5) shows the chemical compositions of the used carbide inserts.

Figure(3.7): Carbide inserts used in the present work

Table (3.5): Chemical composition for carbide tool

Tool carbide	Material	Co	W	C	Ti
	%	9	65	12	14

For carbide cutting tool, use a load (150 kg) HRC with a tip (120)degree at 10sec. The average of three measurements was used to calculate the hardness value. The value of hardness is equivalent to (60 HRC), see appendix A7 .

3.4. Sol-Gel Coatings Preparation

Table (3.6) shows all chemical materials which need for precursor preparation

Table (3.6): Chemical materials for each precursor preparation

Type precursor	Source	catalyst	Solvent	Dispersion materials
Titania	titanium tetra-isopropoxide	0.7NHCl	isopropanol	Triethanolamine
Alumina	aluminum isopropoxide IPA	HNO_3	H_2O	Triethanolamine
Zirconia	Zirconium 70 percent n-propoxide	Glacial acetic acid	Deionized water	Ethylene glycol+glycerol

3.4.1. TiO_2 coatings

The coating was prepared using the methods outlined in Figure (3.8). The $Ti(OH)_4$ precursor was prepared utilizing titanium tetra-isopropoxide (TTIP),as the titanium source precursor from SIGMA-ALORICH CHEMIE GmbH, product of USA Group, 0.7N-hydrochloric acid (HCl) as a catalyst, and isopropanol IP as a solvent. It had a molar ratio of TTIP: IP: 0.7NHCl= 1:26.5; 1.5 in its usual composition. After 30 minutes of stirring in a closed system, the solution TTIP+IP was added to triethanolamine TEOA at a molar ratio of TTIP:TEOA= 1:2 and stirred for one hour.

In a closed system, solution of IP+o.7NHCl was mixed with a magnetic stirrer for one hour at room temperature. 0.7NHCl +IP was added to the TTIP +IP solutions, and the mixture was stirred continuously for another hour at room temperature with a withdrawal speed of 10cm/min.

The PH and viscosity of the produced $Ti(OH)_4$ precursor were measured and recorded as 6.46 and 8.74cPs, respectively. The $Ti(OH)_4$ coating was achieved after 5 seconds of immersion time for each cutting insert specimen, at a continuous withdrawal speed of 10 cm/min then dried at 335℃ for one hour, and calcinated at 500 ℃ for 2 hours.

After the dip coating step, this technique produces a thin film that has strong adherence to the substrate and reduces residual stress, reaction (3.1) was represented about titania precursor preparation.

$$C_{12}H_{28}O_4Ti+4C_3H_7OH+4HCl\rightarrow Ti(OH)_4+4C_3H_7Cl+C_{12}H_{24}+4H_2O\ldots\ldots\ldots\ldots(3.1)$$

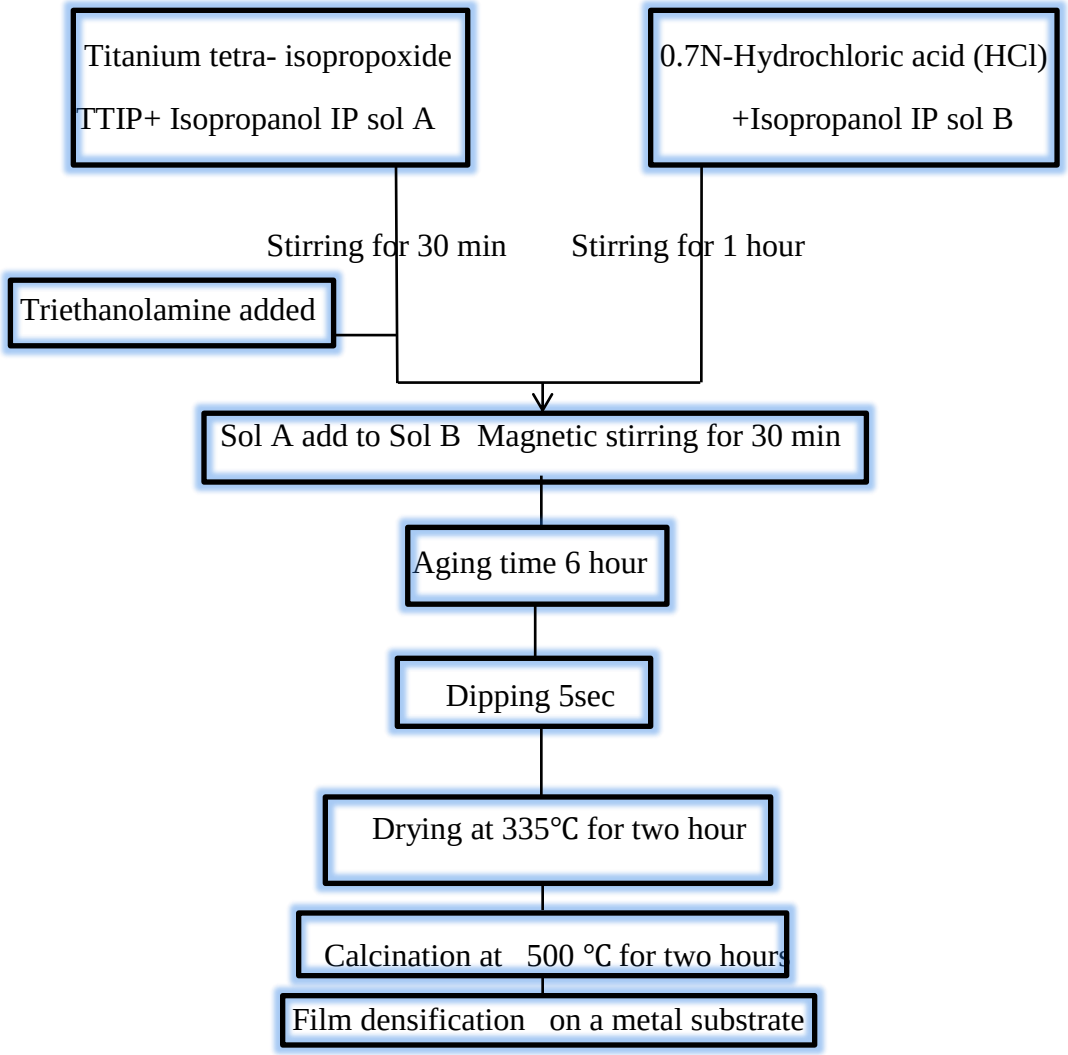

Figure (3.8): Experimental procedure for coating with TiO_2 layer

3.4.2. Al_2O_3 coating

The Al_2O_3 coating films were created by dipping cutting inserts in alumina hydroxide ($AL_2(OH)$) sol, which was prepared by combining aluminum isopropoxide IPA with using deionized water H_2O, and nitric acid (HNO_3). In XRD results of IPA, peaks of 31.8958º, 29.4008º, and 22.5604º, are matching well with the JCPDS No. 12-0472 for $Al(NO_3).9H_2O$, as shown Figure (3.9) and appendix A8.

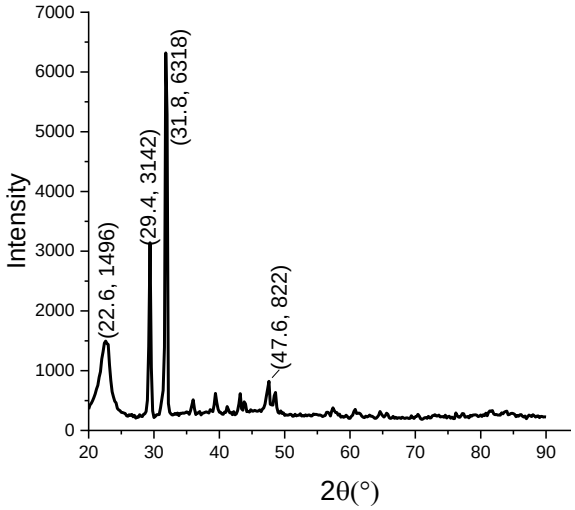

Figure (3.9): XRD for aluminum isopropoxide

The IPA:H_2O:HNO_3 molar ratio was 1:60:0.1. The temperature was raised to 85℃ and, 0.63 g of HNO_3 was added after one hour stirring of IPA+H_2O solution. The solution mixture was stirred continuously for two hours at 85°C with a withdrawal speed of 5cm/min. The produced aluminum hydroxide precursor had a PH of 5 and a viscosity of 8.11 cPs. In order for the hydrolysis to proceed, the sol-gel precursor has to be aged for at least 12 hours. The Al_2O_3 layer was applied to the insert in multiple layers by dip coating, at a constant withdrawal speed of 6 cm/min. Time immersion was used as (10, 30, 60,90)sec. After the immersion the coating were dried at 355°C for one hour to reach the required film thickness, with a 6°C/min temperature increase. The insert were then calcinated in a furnace for two hours at 500 ℃ to achieve densification of the sol-gel layers. Figure (3.10) explains the procedure for prepare coating and reaction (2) revealed into precursor alumina preparation.

$$Al(NO_3).9H_2O+2HNO_3+H_2O \rightarrow Al_2O_3+H_2+O_2+N_2 \ldots\ldots\ldots (3.2)$$

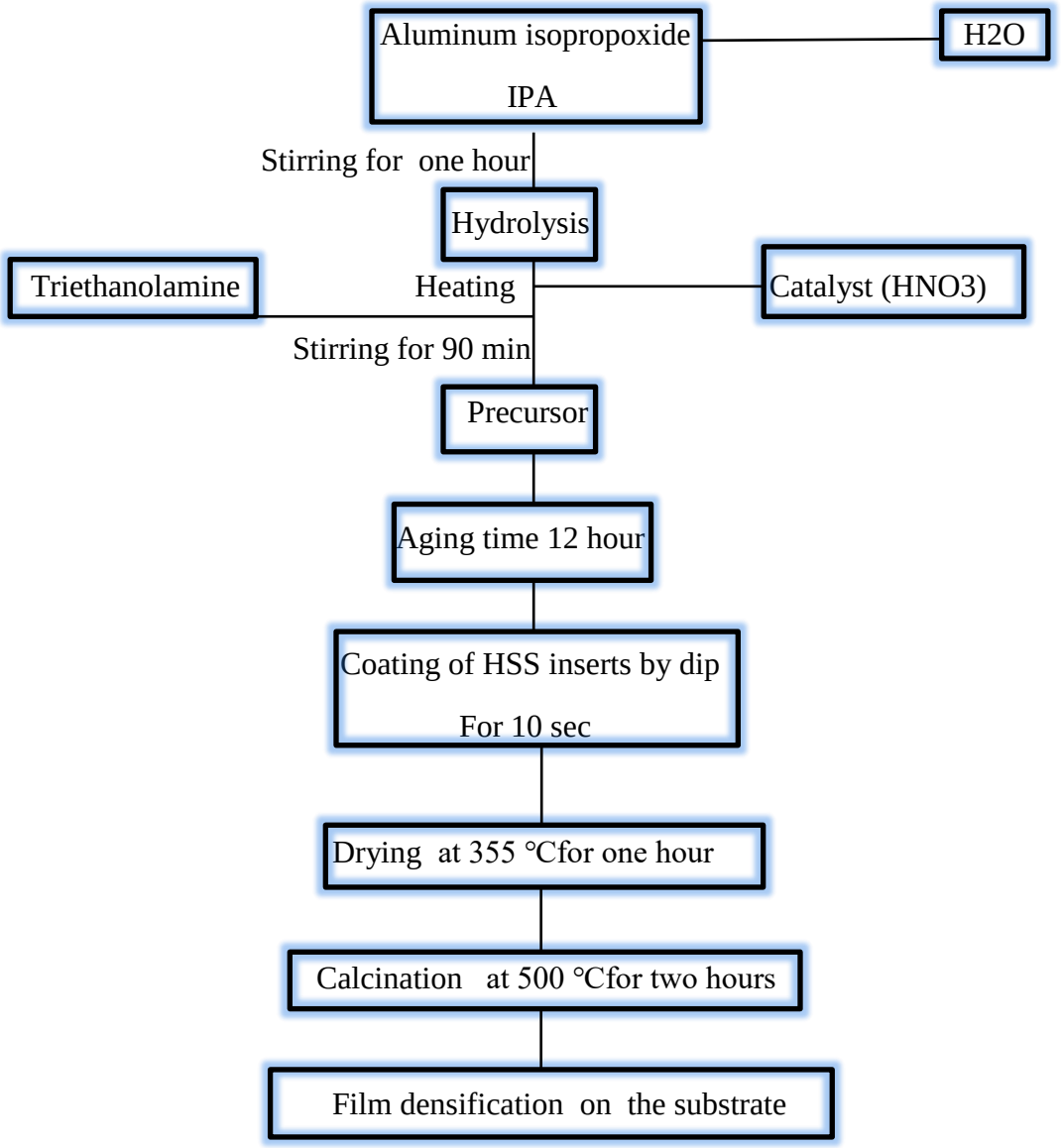

Figure (3.10): Experimental procedure for Al_2O_3 layer preparation and deposition.

A furnace of a maximum temperature of 1800℃, and a quartz tube with a 37mm internal diameter was employed in calcination process to give protection under the argon gas. Figure (3.11) shows the dip coating device, while Figure (3.12) shows the furnace used in this process.

Figure (3.11) : Dip coating device

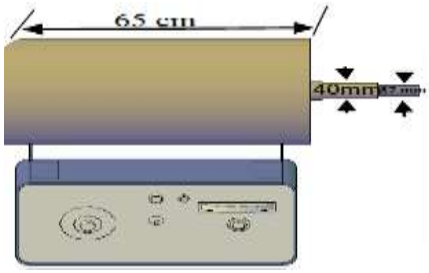

Figure (3.12): The furnace used in the calcination process

3.4.3. ZrO_2 coating

Zirconium 70 percent n-propoxide (Zr(OC3H7)4) as the zr source precursor from, glacial acetic acid, ethylene glycol, and glycerol were used to prepare the mixture. n-propanol was utilized to dissolve a 2.23 solution of zirconium(IV) npropoxide as a Zr precursor. At a 1:1.7 v/v ratio, glacial acetic acid was added to the precursor solution and agitated. In an ice bath, the solution was ultrasonically sonicated for 25 minutes. Deionized water was added to the solution after 20 minutes of sonication. According to mechanical and high temperature testing, the new ultrasonic aided sol-gel technique is an efficient way to create thin, well-adhered ZrO_2 layers on the substrate. The resulting sol was chilled and matured for

one day before rapidly spinning in the ethylene glycol and glycerol. The volume ratio of H_2O/CH_3COOH was 1:2.5, while the volume ratio of $H_2O/(CH_2OH)_2/C_3H_5(OH)_3$ was 25.

To slow down hydrolysis and solvent evaporation, ethylene glycol and glycerol were utilized. Impurities were removed from the support samples using an alkaline solution of n-propanol, acetone, and distilled water. To promote adhesion between the tool HSS surface and the deposited material, the samples were treated with alumina, a thin alumina coating .

At a continuous withdrawal speed of 3 cm/min, the samples were dip-coated in the sonocatalyzed zirconium sol solution. The coated HSS supports were then dried in 80°C vented oven. The method of dip-coating in zirconium sol was repeated three times .

Then, using rate of heating of 6 °C/min, calcination for 2 hour at 500 °C. Figure (3.13) demonstrates the steps at experimental procedure for coating with ZrO_2 layer. Reaction (3) gives Zr precursor preparation.

$$C_{12}H_{28}O_4Zr+4CH_3COOH+H_2O\rightarrow Zr(OH)_4+C_{12}H_{28}+4CH_3COOH+OH^-+4CH_3COO^- +4H_2O\ldots\ldots..(3.3)$$

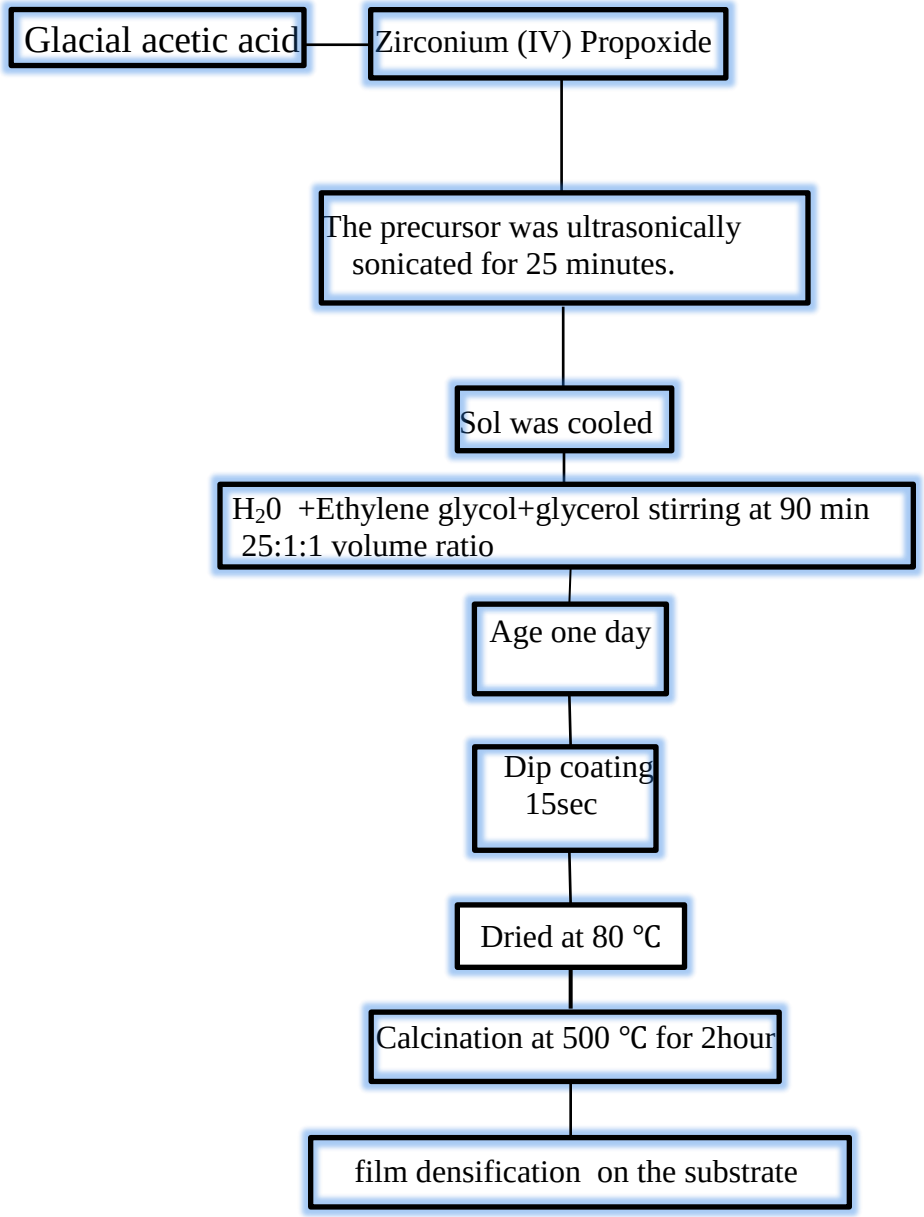

Figure (3.13): Experimental procedure for ZrO_2 layer preparation and deposition

Properties of the coating (TiO_2, Al_2O_3, ZrO_2), are demonstrated in Table (3.7)

Table (3.7) **:**Physical properties of the substrate and coatings materials ASTM-[91].

Properties	**HSS**	**Al_2O_3**	**TiO_2**	**ZrO_2**
Melting point (℃)	1620	2072	1843	2680
Thermal Conductivity (W/m.k)	26	29	11.8	5
Thermal expansion $10^{\wedge -6}$/K	11-14	4.5	8.4	9.7

3.4.4. Viscosity and contact angle measurements

The viscosity of precursor was measured at room temperature with a viscometer(LVmodel) having a rotating drum. Cone-plate viscometer BROOK FIEID. Contact angle for each precursor was measured.

These are the function of the precursor viscosity [62]. After (10, 30, 60, and 90) sec of immersion in low viscosity of each sol, the wettability of the HSS tool in each (aluminum and zirconium) hydroxide sol solution was measured, while the time immersion in titanium hydroxide was measured (5sec or 10sec).Vino for Contact Angle Meter-CHINA Manufacturer was used. These tests were carried out at the University of Babylon's/ College of Materials Engineering.

3.4.5. Conditions of coating

The coating condition studied on the quality and thickness of the coating layer is shown in Table (3.8).

Table (3.8): Coating conditions

Number of layer	**Coating layer type**	**Immersion time (sec)**
Monolayer	Al_2O_3	10
Monolayer	Al_2O_3	30

Monolayer	Al_2O_3	60
Monolayer	Al_2O_3	90
Double layers	Al_2O_3+TiO_2	10
Double layers	Al_2O_3+TiO_2	30
Double layers	Al_2O_3+TiO_2	60
Double layers	Al_2O_3+TiO_2	90
Triple layers	ZrO_2+Al_2O_3+TiO_2	30
Triple layers	ZrO_2+Al_2O_3+TiO_2	60
Monolayer	ZrO_2	30

3.5.Tests and measurements of coatings :

3.5.1. X-Ray Diffraction

X-ray diffraction XRD was used to identify the for the uncoated HSS substrate ,HSS coated with Al_2O_3, TiO_2, ZrO_2 layer at a speed of 5 degrees per minute HSS and 3 degrees per minute for each thin layer. When compared to the diffraction data card (060696), XRD of the substrate HSS with the help of EDX analysis reveals the elemental distribution to estimate the phases. X-Ray instrument type (XRD), Shemadzu manufacturer, XRD dfractometer-XRD-7000, volt 40 kV, current 30mAmp, tube Cu, at Iraq Geological Survey was used. The detector was moved during an angles of 2θ = 10 to 90º degrees.

3.5.2. SEM-EDS Analysis

The microstructure analysis and the thickness measurement of coatings were performed. Using FESEM, inspect F50, made in Nclher Land, at Nano Lab. In Al-khora Company. The FESEM was equipped with an Electron Dispersive Spectroscopy EDS detector to indicate Al, Ti, O, and Zr elements and other elements.

3.5.3 Atomic Force Microscopy Test

The goal of using this technique is to determine the integrity of HSS inserts both uncoated and coated. The surface morphology of uncoated and coated HSS inserts was studied and assessed before machining. Because of the tip's vertical mobility, it creates a topographical image of the surface with an accuracy of a few µm or less. AFM was performed using Advanced angstrom (AA3000) Model made in USA at the department of Chemical Science / College of Science /University of Baghdad.

3.5.4. Hardness Test:

The hardness of the coatings was examined according to ASTM E384 standard by using Vickers hardness with a load of (50g) for 10sec. A micro Vickers hardness gadget with a diamond pyramid and square base, type Digital MicroVickers hardness tester TH717, was used to conduct the hardness test. The test was performed at the University of Babylon/ College of Materials Engineering. For each specimen, the hardness value was recorded as the average of three measurements.

3.5.5. Wear test and coefficient of friction

Pin-on-disc technique was used to conduct this test according to ASTMG9 . Type MT4003 version 10.0 control and data collecting software for friction and wear testing. The experiment was carried out at room temperature (32°C), for an intervals of 15min and a load of 15N. The sliding velocity was(65m/min) and the distance of sliding was (95m). The pin was a ball that is pressed against the revolving disc. Martensitic steel ball with a hardness of (990 HV.) was used for wear testing the cutting insert. The coated and uncoated inserts were subjected to the wear tests. Weighing the specimens by a sensitive scale with an accuracy of

before and after the test to calculate the weight loss was done. The wear rate of the specimen is calculated according to the following equation [90]:

$R.W = \Delta w / 2\pi$ rnt…….(3.1)

Where:-

R.W:- wear rate (gm/mm)

ΔW:- weight lost (gm) which is the difference in weight of the samples before and after the test.

t:- Sliding time (min.).

r:- The radius of the sample to the center of the disc (4mm).

n:- Disk rotational speed (250 rev/min).

3.5.6. Adhesion and scratch test for the coated inserts

The basic pull-off test to measure bond strength in accordance with ASTM C633-79 [91] is the simplest test procedure in concept. In this tests a stud is adhered to the coating using adhesive and ripped off using a force-recording mechanical testing device in this test. The problem with this test is that the maximum adhesive strength that can be measured. Surface tension of high-performance adhesives is typically less than 100 MPa. In order to achieve this amount of stress in a practical test, careful approaches must be used to increase coating adherence and keep the force direction perpendicular to the sample. The test was performed at the University of Babylon /college of materials engineering via the adhesion test device Posi Test AT-M adhesion device, manufactured by Defelsko Corporation (Figure 3.14) [6].Adhesion tests were performed for all types of the prepared the coated inserts.

Figure (3.14): Adhesion device ASTM D4541 pull-off test

A scratch test apparatus type, having a silicon carbide indenter, was used to evaluate the moving indenter along the inspected specimen's surface. The test was carried out with a continuously rising force to investigate coating adhesion to the insert. The test was performed at the University of Babylon /college of materials engineering. The test was performed according to ASTM D4541, the following parameters were used in the tests: The penetrator travels at a speed of 1mm/s and a distance of 4mm, with a load range of 5-30N [92]. Equation (3.2) was used to get the scratch hardness. [16].

$$Hs=\frac{4qw}{\pi d\wedge 2}\ldots\ldots\ldots\ldots\ldots\ldots\ldots\ldots\ldots\ldots\ldots\ldots\ldots\ldots\ldots\ldots(3.2)$$

Where q is a quality factor for ceramics and metals, and 2 is a dimensionless variable. w: Newton's normal force, d: scratch width in millimeter.

3.5.7.Coefficient of thermal conductivity

The Hot Disk Thermal Constants Analyzer is a transient plane source (TPS) thermal characterization tool. The Hot Disk sensor used is a heat source and a dynamic temperature sensor in one. The measurement was carried out by passing an electrical current through the sensor to raise its temperature by several degrees, and then recording the increase as a function of time. The experiment was conducted with the Hot-Disk TPS 500 model, Sweden. The device's specifications are shown in Table (3.9). The following equation depicts heat transfer by conduction [93].

: $Q_{cond} = -KA\frac{dT}{dX}$ ……..(3.3)

$K = m\,c\frac{hp}{\pi\,(R_B)^2(v1-v2)}(\,2\,hp + \,Rp)/(2\,Rp + 2hp)\left(\frac{\Delta v}{\Delta t}\right)$ (3.4)

K: thermal conductivity coefficient (w/m.k).

m: mass of copper plate (0.824 kg).

C: specific heat capacity of copper plate.

hp, Rp: thickness and radius of copper plate.

R_B: cross section of specimen is 12.75mm.

v1,v2: voltage of thermocouple 1,2 at heating.

Δv: difference in voltage at cooling.

Δt : difference in time at cooling.

Table (3.9): Specifications of the Hot Disk TPS500

Hot-Disk TPS500	
Thermal Conductivity	0.03 to 100 W/m/K using standard isotropic method. 5 to 200 W/m/K using slab or one-dimensional methods
Measurement time	2.5 2560 seconds
Accuracy	Better than 5% (thermal conductivity)
Temperature range	-100 ˚C to 300 ˚C

The samples were prepared in a (12.75 * 12.75) mm^2 squire shape. The sensor 5501 TPS having a radius of 6.4 mm was used during the measurements. Hot-Disk TPS 500 analyzer was used to measure the thermal conductivity for the sample. The test was performed at room temperature (21 ˚C). Figure (3.15) shows the Hot-Disk TPS and the sample. This test was performed at University of Anbar/ College of Science / Department of Chemical Science .

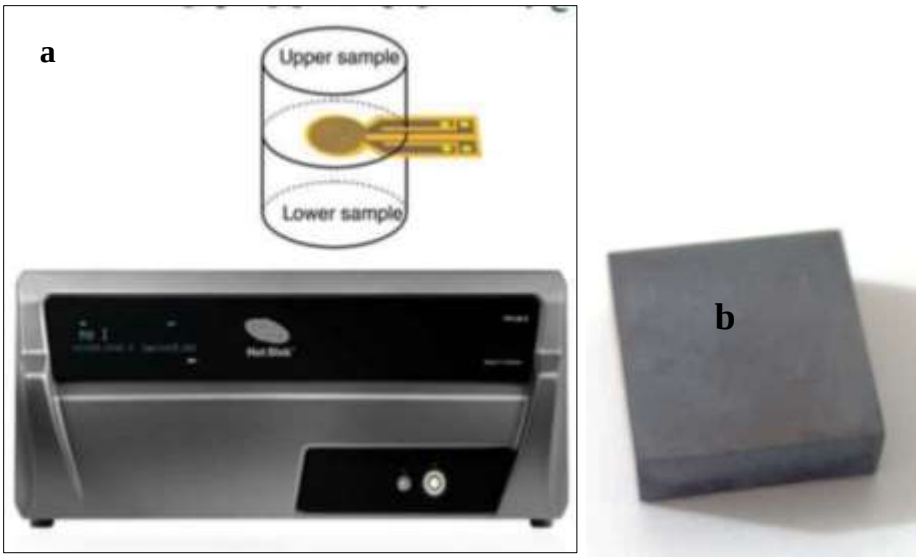

Figure (3.15): (a):Hot-Disk TPS 500, (b): sample coated HSS steel were used in this test .

3.5.8. Coefficient of thermal expansion measurement (α)

Dilatometery is a technique for measuring a substance's dimensional change as a function of temperature while it is subjected to a controlled temperature program. This approach and the exact procedure are described in ASTM D 3386. Dilatometer 101 is a bench top system that includes a furnace (for a wide range of temperatures, including sub-ambient); a sample holder system (fused silica or high alumina); a control / sample thermocouple; a sample displacement measuring system (probe rod and LVDT sensor); and a furnace controller data acquisition system (stores temperature and displacement data). Dil 101 is an excellent tool for calculating thermal expansion coefficients (CTE). The test was performed at the Unit 01, No. 8, 9th Andishe St, Andishe St, Motahari Ave / Iran. Figure (3.16) shows the device and the HSS specimen. The dimension of sample 50mm in length and the area of the cross section in 2.5 *2.5 mm^2, as shown (3.16)-b.

Figure (3.16): (a): the device of thermal expansition measurement, (b) the HSS sample of test

3.6 Machining Test

The topic of this study requires initial requirements which contain three aspects :

- Measurement of the cutting tool wear due to the cutting operation.
- Measurement of the surface roughness of the machined work piece.
- Measurement of the temperature during machining

3.6.1 Machining Program

In this work, external longitudinal turning operation was used. The machining experiments were performed via a turning machine type (MDAENb 1A616), spindle speed 45-1800rpm, feed 0.065-0.91 mm/rev, total power 2.2KW at the Training and workshop center/ University of Technology. The dry cutting condition was used in all of the machining trials. For each of the three feed rates (0.065, 0.165, and 0.265 mm/rev), three spindle speeds (355, 560, and 710 rpm) were used. With the above spindle speeds and feed, three values for the depth of cut (0.2,0.5,0.7 mm) were employed. The machining program was carried out using coated and uncoated high speed steel inserts. The inserts used were rigidly mounted on a tool holder type (**TAK Holder**) as shown in Figure (3.17). During

the machining operations, measurements related to the width of the flank wear, surface roughness, and machining temperature were recorded.

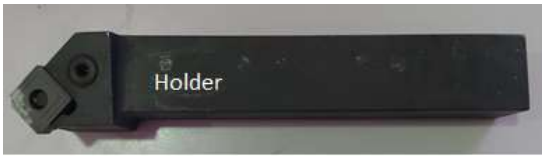

Figure (3.17): Tool holder type tak holder

3.6.2 Flank Wear Measurement

Cutting tool wear mechanisms are complex, involving a variety of interacting variables that are connected together in a convoluted manner. Because flank wear is the most common type of wear, the width of the flank wear V_B was the primary parameter examined in this study. According to ISO 3685 for carbide tools, a maximum width of 0.3mm was utilized as a flank wear criterion for it's tool life [94]. Moreover, according to ISO 3685:1993 for HSS insert, the maximum width of 0.3-1 mm was utilized as a flank wear criterion [95]. The tool life was determined using a one-minute time test. In this method the cutting conditions will be continued for one minute, then the operation will be stopped to measure the width of the flank wear. The process will be repeated under the same cutting conditions and using the same cutting edge until the width of the flank wear reaches its criterion limit. FESEM type (inspect F50) was used to determine the flank wear.

3.6.3 Surface Roughness Measurement

For each cutting operation under the required cutting conditions, the surface roughness of the coated, uncoated, and the carbide inserts were measured. Using surface roughness tester type (TR200 hand-held roughness tester, modelTA620Stan and Co, by time group Inc.). All measurements were carried out after the first minute of machining. In each case the sample was mounted on a flat

base then the distance to be tested was appointed and the probe of the measuring instruments was attached by special lever to the surface of the sample, after that the instrument was switched on with continuous movement of the probe into front and behind. The instrument registration board gives the roughness value (Ra) directly and the maximum reading was recorded.

3.6.4 Machining Temperature Measurement

The machining temperature is a key factor that limits the productivity and cutting speed and accelerates the cutting tool wear. The effect of machining conditions on machining temperature was investigated. An infrared thermal imaging camera model Ti32 has been used during the machining operation to measure the tip temperature of the tool to make better understanding of the machining zone and coating effect. Temperature is measured at one spot, namely tool-work piece contact area. Figure(3.19) shows the setup of the temperature measuring process.

Figure (3.19): Set up of Temperature measurement

3.6.5 Design of Experiments:

Design of Experiments (DOE) is an essential tool for engineers and scientists. The wide range of (DOE) has improved the performance of processes and the development of the new process. Taguchi orthogonal array of Program (Minitab 17) was used to investigate statistically the combined effect of machining variables (cutting speed, feed, depth of cut) on the flank wear, surface roughness of the workpiece, and the machining temperature. The designed experiments were performed for each type of the prepared cutting inserts.

CHAPTER FOUR

Chapter Four

Results and Discussions

4.1 Introduction

This chapter presents and discusses all the results obtained from several tests (physical, mechanical and machining tests of the coated and uncoated cutting inserts) that were conducted throughout this work. This chapter can be divided into three parts, The first part contains the best conditions for coating HSS with ceramic oxides using the sol-gel process and to determine the majority of its qualities. The second part reveals the characterization, mechanical, and physical examinations of coating layers under ideal coating conditions. Finally, the third part points to dry turning tests for coated HSS cutting inserts, after which Grey Relational Analysis (GRA), based on the Taguchi Method, is used to determine the best machining conditions.

4.2. Coating Conditions

This section, reveals the best conditions for coating HSS with ceramic oxides using the sol-gel process and determines the majority of its qualities. These conditions involved :viscosity, PH, and the aging period of the precursor, the number of coating cycles, dispersions materials, immersion time, calcination temperature, and dry temperature which have an effect on the layer thickness, adhesion, surface roughness, and homogeneity for coating layer.

4.2.1. Dispersion type Effect

The FE-SEM surface morphology of the TiO_2 coating is shown in Figure (4.1). The topographical features of the top coating surface at 500℃ calcination temperature, with a reasonable amount of ethanolamine added via hydrolysis process, are shown in Figure(4.1)-a. The agglomeration nanocrystalline formations

with cavities that developed from the segregation duplex in this image characterize the surface during the condensation reactions. Figure (4.1)-b illustrates a more uniform coating with no apparent cavities or agglomeration as a result of adding the appropriate amount of triethanolamine TEOA during the hydrolysis process and condensation condition (slow reaction). TEOA must have contributed to the stability of the metal hydroxide gel in some way.

As a result, under typical conditions, uniform ceramic oxide particles were generated. TEOA appeared to boost the pH influence on nucleation rate, resulting in a wide range of size control. TEOA functions as a stabilizer of M ion against hydrolysis to M in the alkaline range (OH). TEOA, on the other hand, is a term that refers to the process of converting one thing into another. The conversion of M(OH) to MO is inhibited. Third, TEOA controls the form of metal oxide. TEOA has a lower PH than ethanolamine, which has a PH of 11.6 and a PH of 14.6. TEOA also has a particle size that is larger than ethanolamine's particle size [96].

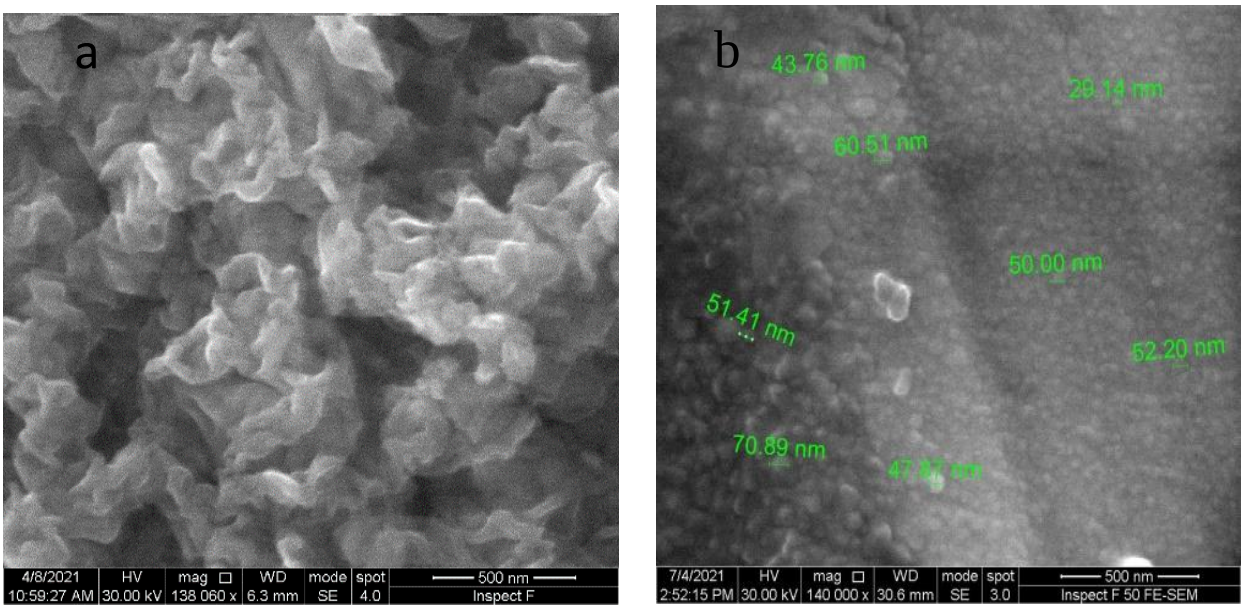

Figure (4.1): SEM image (a) TiO_2 coating with agglomeration,(b)TiO_2 coating uniformity

4.2.2. Viscosity Effect

Each coating precursor's effective dynamic viscosity (Titania, Alumina, and Zirconia) was determined using a conventional method (ASTM D7945-21). All of the measurements in this investigation were done at room temperature, 31°C**.**The coating was also non-uniform on the substrate steel, as shown in Figure (4.2). Non-uniformity of the coating layer is due to a rise in precursor viscosity to 12 cPs. The contact angle increases with increasing viscosity, although it plateaus at roughly 75 degrees above 10cPs. When the contact angle is less than 90 degrees, good wetting occurs [97].

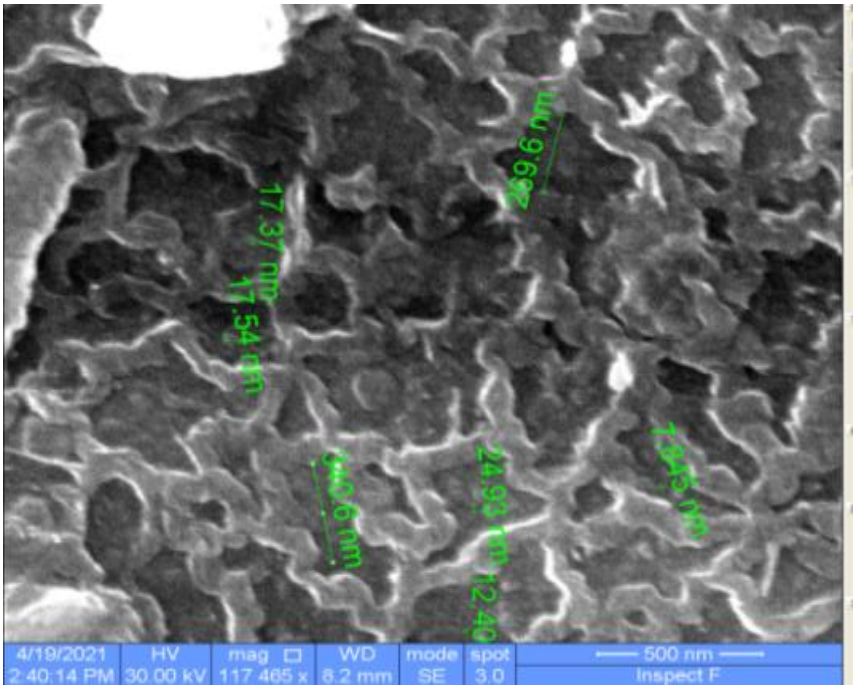

Figure (4.2): FE-SEM image of the non-uniformity of Al_2O_3 coating insert with a viscosity of coating precursor 12cPs

The enhanced wettability behavior of the coating precursor can be explained by the production of OH groups in precursor, which lead to bonding with the substrate surface during hydrolysis [98]. The wettability of aluminum hydroxide precursor on the substrate HSS was good in this study, with the viscosity of aluminum hydroxide coating measured at 8.11 cPs after, as shown in Figure (4.3).

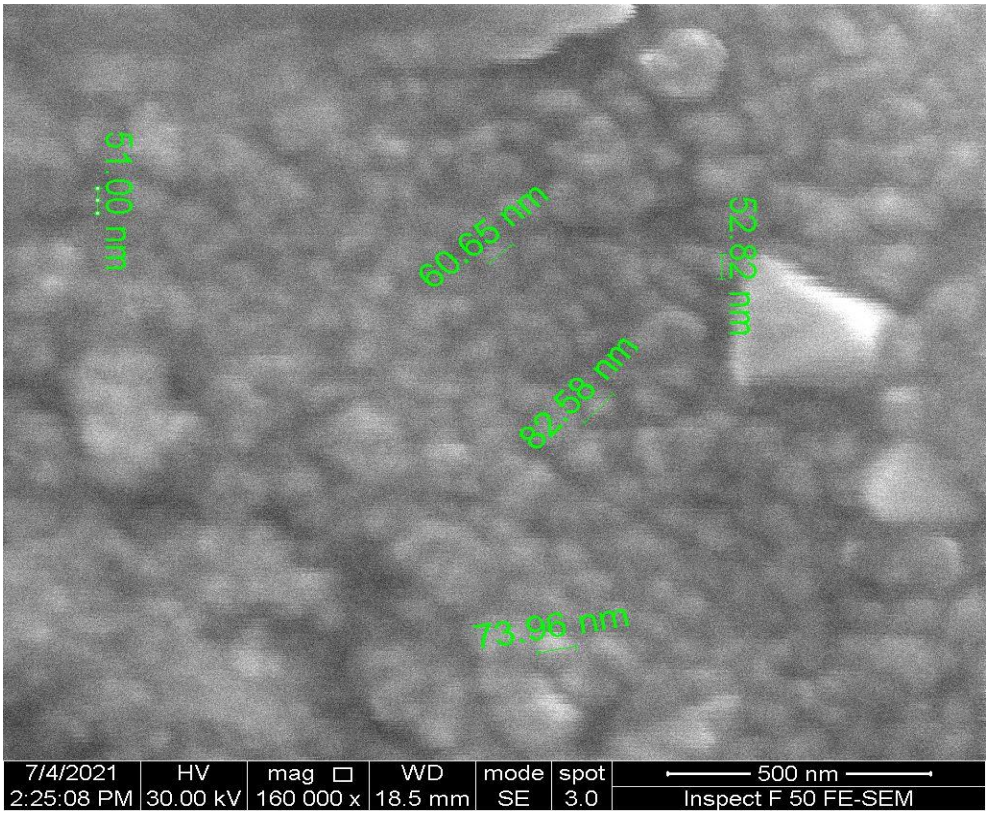

Figure (4.3): FE-SEM image of HSS coated with good homogeneity coating insert with viscosity 8.11 cPs of Al_2O_3 and 8.74cPs of TiO_2 precursors.

The magnitude of viscosity is selected for each precursor in the test when the shear rate is more than (10) 1/sec and the speed is employed in the dip coating procedure. As shown Figure (4.4). At speed 10cm/min in dip coating process, for titania precursor, viscosity 8.74cPs, 72.66 1/sec shear rate. At speed 6cm/min in dip coating for alumina precursor, 40.00 1/sec shear rate , equal 8.11 cP. Finally, at speed 3 cm/min in dip coating zirconia precursor, 20 1/sec shear rate , 7.94cPs, see appendix B1.

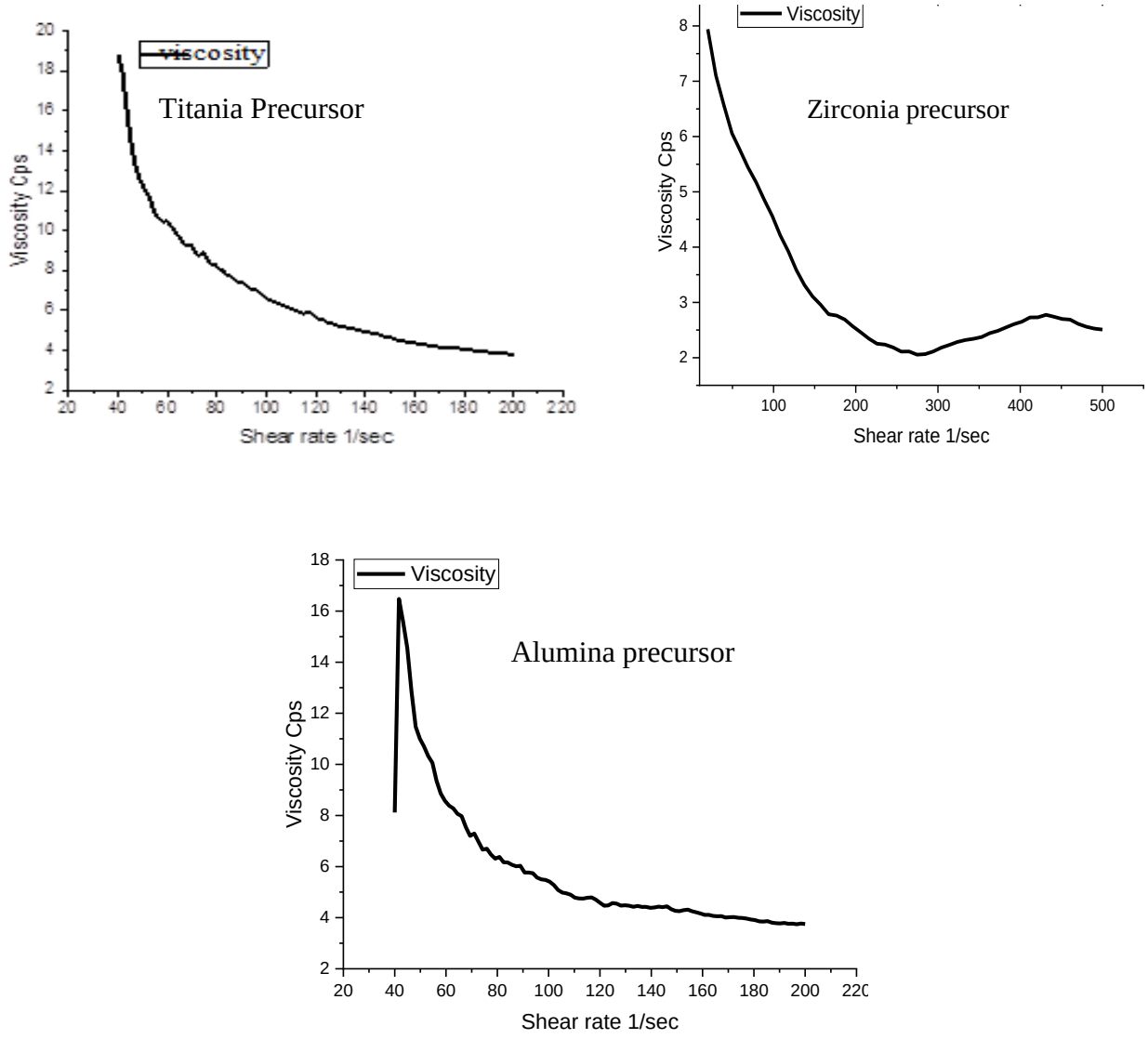

Figure (4.4):Relation between shear rate and viscosity for each precursor

Figure (4.5) revealed PH for each precursor dependent on value of viscosity for each one. From obvious values of viscosity and PH for each precursor, coating good distribution on HSS, can be obtained s shown in Figure (4.6).

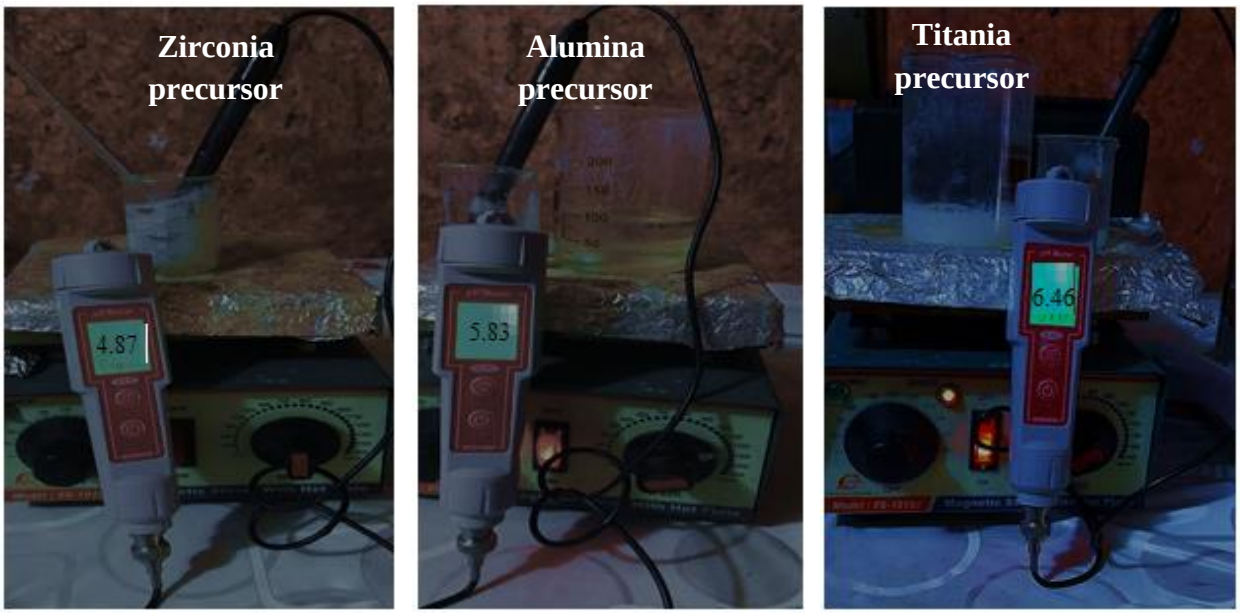

Figure(4.5): PH of coatings precursors

Figure(4.6): Triplex layers $TiO_2/Al_2O_3/ZrO_2$ coated HSS cutting inserts

4.2.3. Number of Coating Cycles Effect

The thickness of the layer grows with less homogeneity when four number of coating cycles are run, resulting in the formation of cracks in the coating film on the substrate, as shown in Figure (4.7).

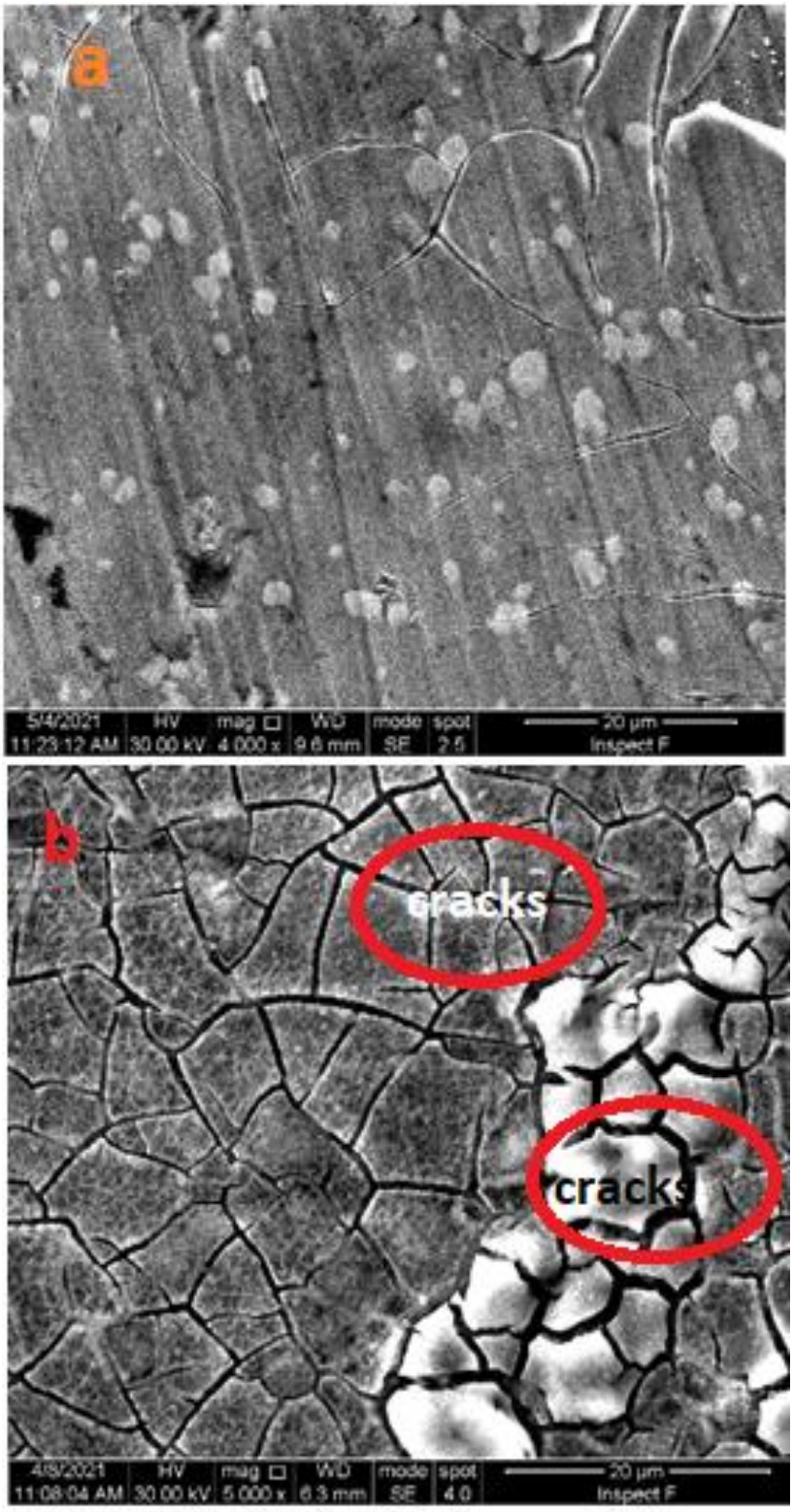

Figure (4.7): (a) FESEM image of TiO_2/Al_2O_3coating on HSS insert with three numbers of coating cycles, (b) FESEM Image of a multilayer coating on HSS insert with four numbers of coating cycles

On the nano scale, atomic force microscopy allowed the preservation of surface morphology. The AFM images of sol-gel coated cutting insert with multiple coatings, Figure (4.8-a) has two coating cycles at 5 sec immersion time, while Figure (4.8-b) has three coating cycles at the same time. According to Cadena et al. [99], as the number of coating cycles grows, the number of particles on the substrate's surface reduces while their size increases.

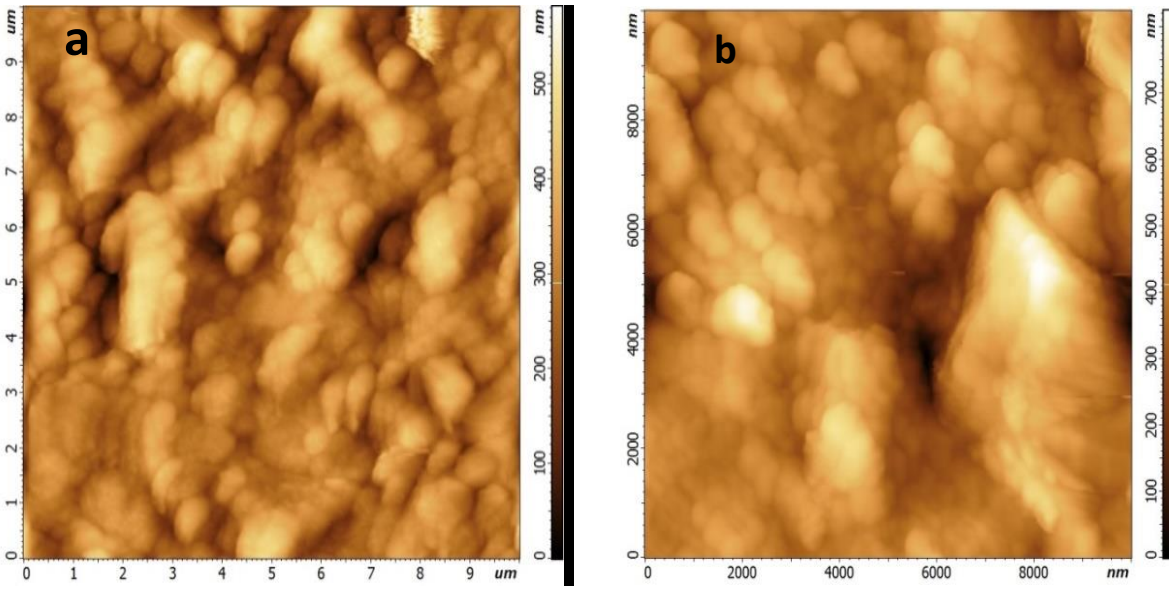

Figure (4.8): AFM for multilayer coating (a) AFM topography of two number of coating cycle, (b) AFM topography of three number of coating cycles

Figure (4.9)-a-b-c-d shows a distinct rise in surface roughness from 1.2 to 1.8 µm as the number of coating cycles grows, the distribution's homogeneity declines.

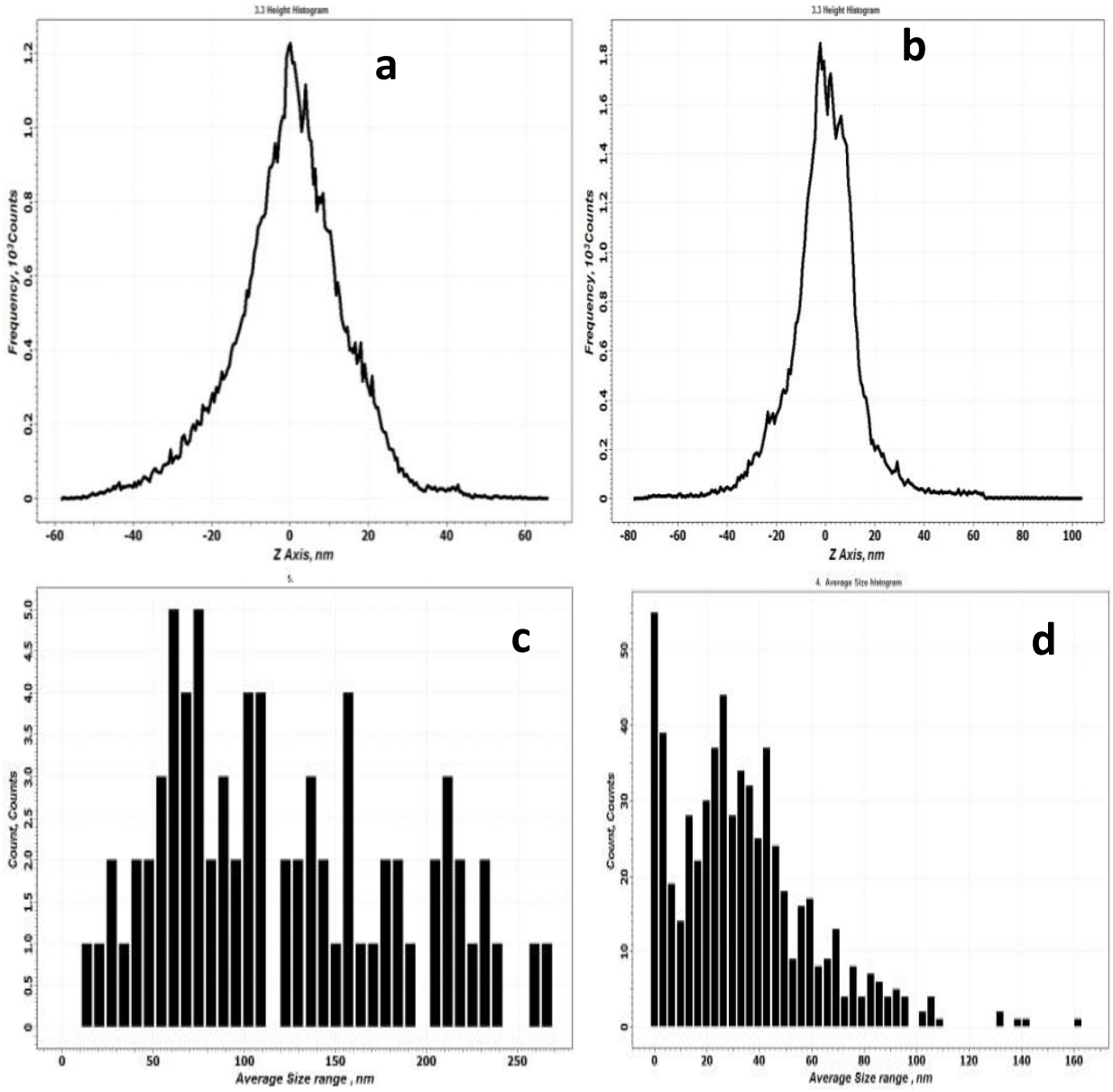

Figure (4.9): (a) Average of surface roughness of coating with two numbers of coating cycles, (b) Surface roughness of coating with three of coating cycles, (c) degree of uniformity in distribution for two numbers of cycles, (d) degree of uniformity in distribution of three numbers of cycles.

Figures (4.10) show FESEM micrographs of cross sections of TiO_2/ Al_2O_3 films deposited on the HSS substrate. As shown in Figure (4.10)-b, coatings with the four numbers of coating cycles having more cracks, non-homogeneous, and higher thickness than those of three numbers of coating cycles. The number of

coating cycles has greater impact on the thickness of the film than viscosity; this agrees with previous study[97].

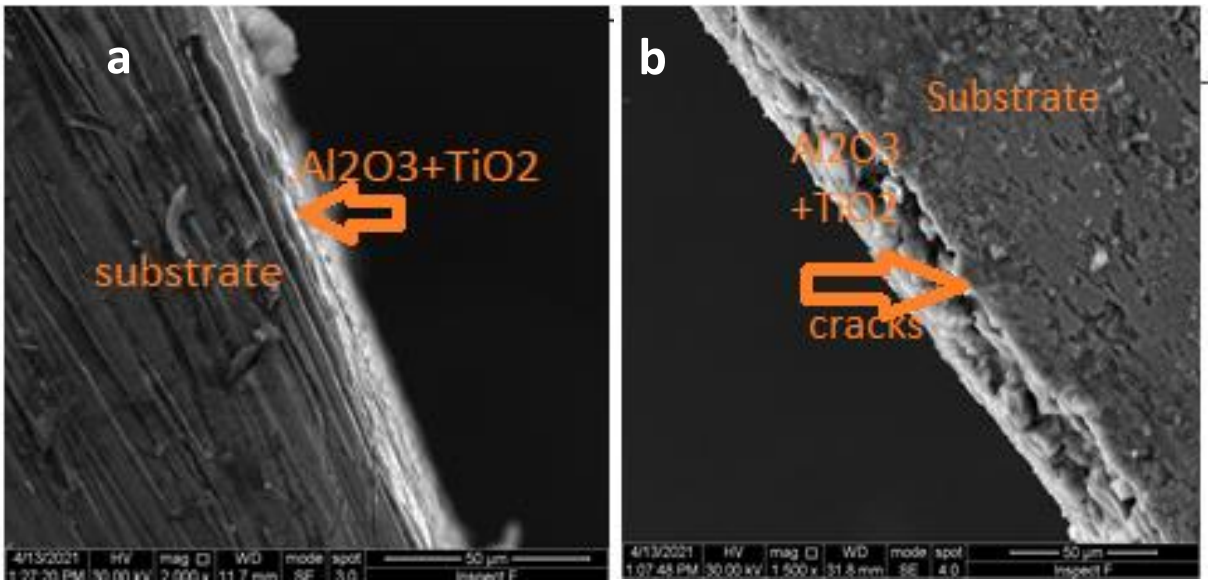

Figure (4.10): (a) Effect of two number of coating cycles on coating layer, (b) Effect of four number of coating cycles on coating layer

4.2.4. Aging Time Effect

As indicated in Figure (4.11), after 15 hours of aging for each coating precursor, the thickness of the coating layer has increased, making it unsuitable for machining operations, which reveals the effect of aging time for precursor.

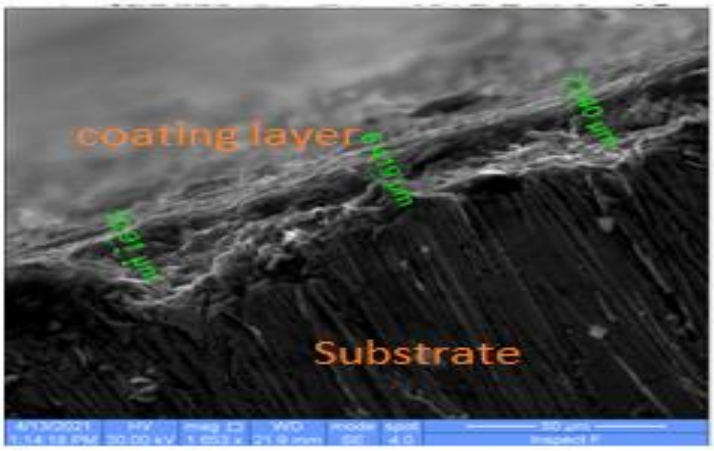

Figure (4.11): Thickness of multilayer coating TiO_2/Al_2O_3 after 15 days aging time of the coating precursor.

While the TiO_2/Al_2O_3 layers were obtained with varied thicknesses (3.6, 5.2, 8.6) µm at varied aging times for coating precursor (12 hours, 3 days, 7 days) using two immersions each lasting 30 seconds, as shown in Figures (4.12), 3days with a layer thickness of 5.2 µm were deemed better acceptable for HSS machining processes.

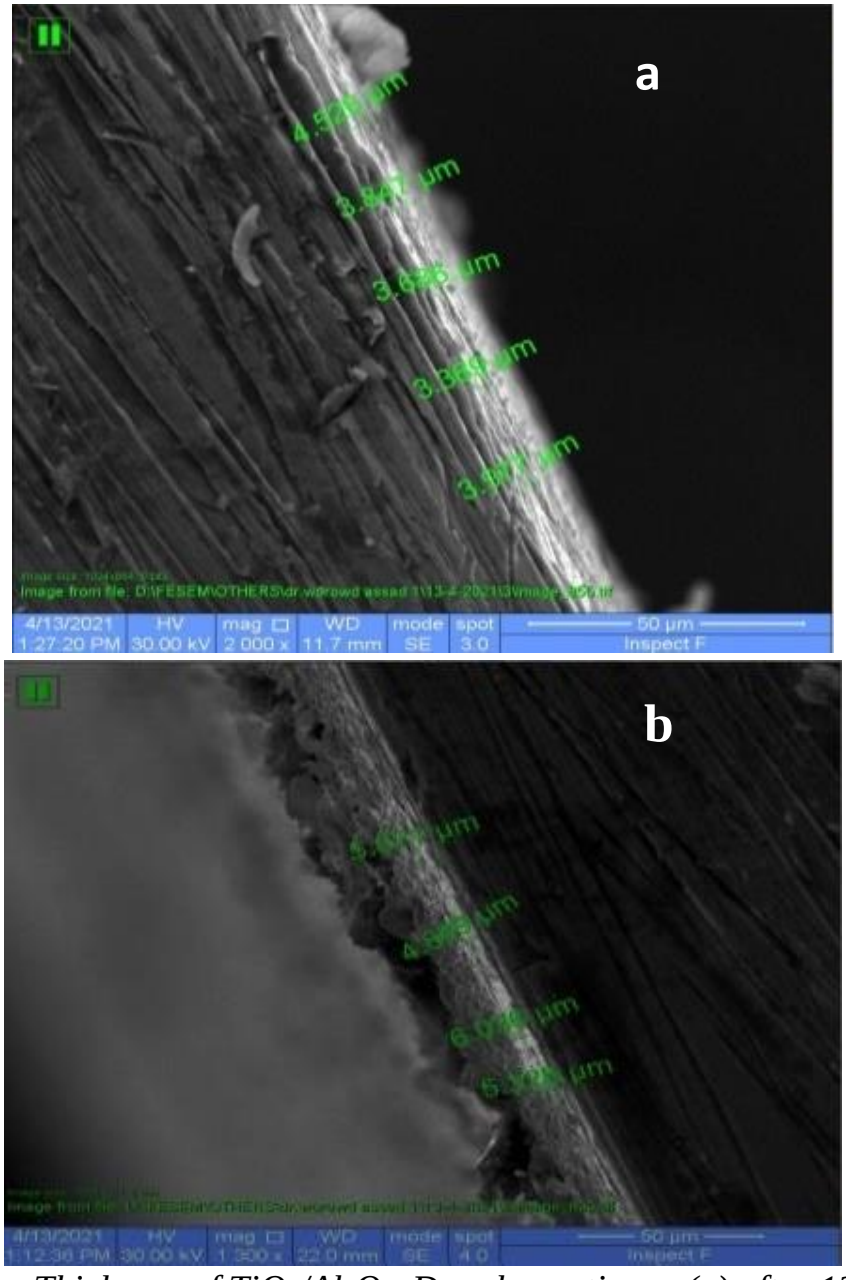

Figure (4.12): Thickness of TiO_2/Al_2O_3 Douple coatings (a) after 12 hours aging time, (b) 3 days aging time, (c) 7 days aging time

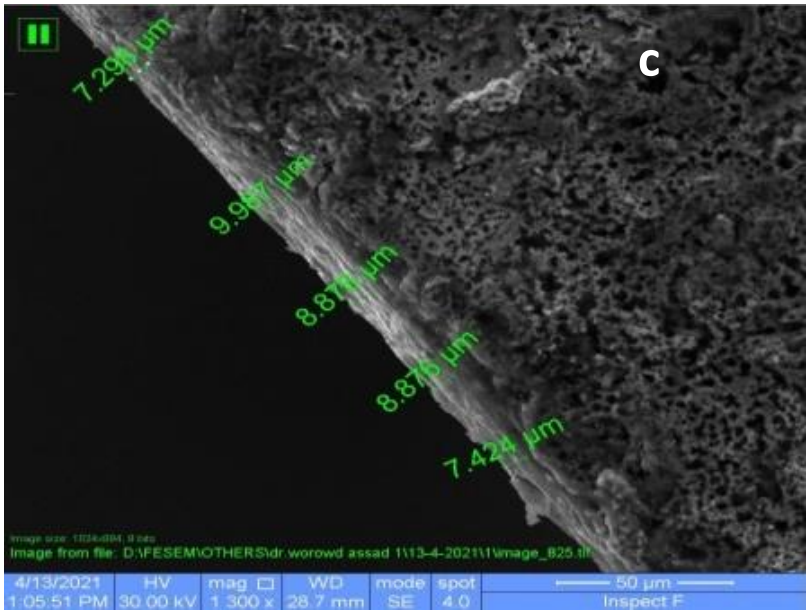

Continue Figure(4.12)

4.2.5. Wettability Effect

After 5-60 seconds, contact angle tests are undertaken to determine precursors wetting compatibility. Because of the differences in interfacial energy between H.S.S substrate and precursor, evaluating their interactions is important. When the contact angles of various drops for each precursor coating on HSS substrate and another ceramic coating layer on HSS were measured, the titania precursor has strong wetting ability on HSS with a contact angle of 27.266 after 5 sec.

After five sec, alumina precursor, exhibits poor wetting ability on HSS at a contact angle of 90.0400. The wettability of the alumina precursor improved on the titania layer coating that was deposited on HSS, and the contact angle reached 38.7750.

Also, wettability of zirconia precursor on alumina layer higher comparing wettability of it on HSS. When contact angle between zirconia precursor and HSS 59.395and contact angle between zirconia precursor and coated HSS with alumina 35.038 at five sec immersion time , see Figure (4.13).

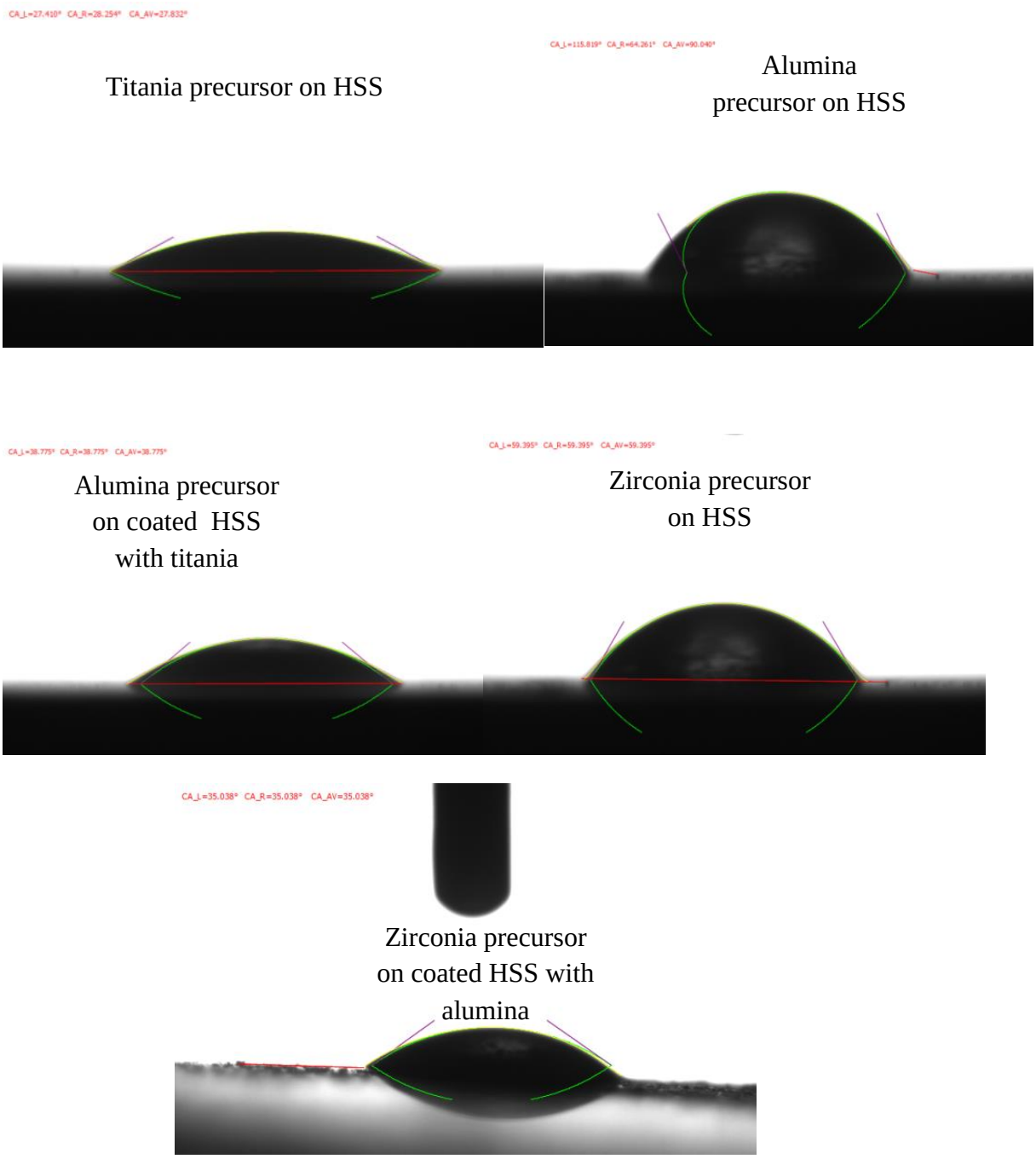

Figure (4.13): Contact angles between substrates and coating precursors

At the same immersion time (5sec), it can be noticed that the difference in wettability among five types of specimen, that related to particle size, homogeneity for each coating precursor added compatibility degree to the material of substrate and coating precursor, as shown in Figure (4.14).

The good wettability behavior of the coating solution can be explained by the production of OH groups in solutions leading to bonding with the surface of the substrate during the hydrolysis . The occurrence of cracks and separation in the coating film may be attributed to reduction of OH group which required for bonding with the substrate in accordance with the hydrolysis reactions[97].

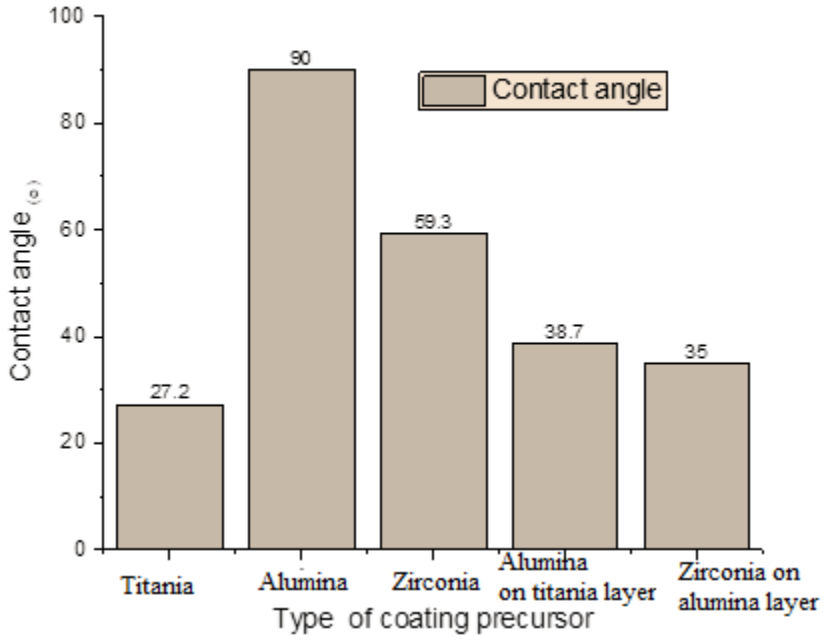

Figure (4.14): Contact angle^{o} with different coating precursors

It is possible to investigate that the contact angle increases for each drop precursor on HSS as immersion time in sec increases. This means that as the immersion period increases, the wetting ability between the precursor and the substrate decreases. Figure (4.15) and Table (4.1) show this behavior.

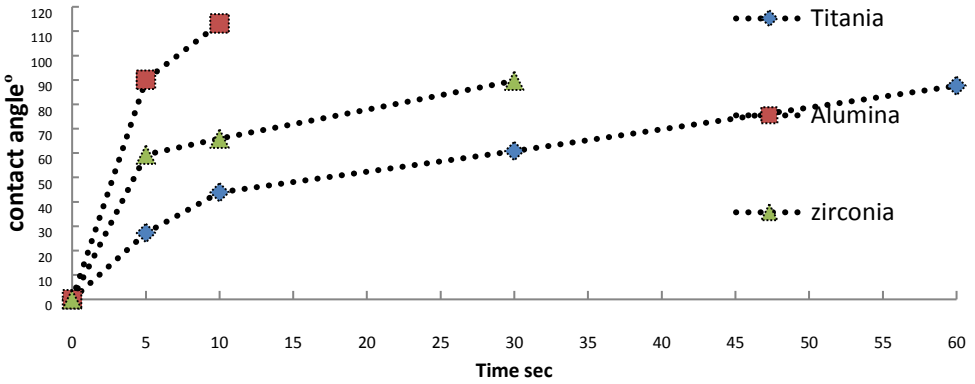

Figure (4.15):The relation between contact angle and immersion time for different precursors on the HSS substrates

Table (4.1): Immersion time and contact angle for each precursor on HSS

Time sec	Titania	Alumina	Zirconia
0	0	0	0
5	27.26604	90.04	59.395
10	43.93106	113.1379	65.889
30	60.86903		89.668
60	87.60409		

4.2.6. Titania layer Effect

The scratch test shows that the monolayer Al_2O_3 coating fail at around 15 N with a line of scratch width of 102 µm, whereas the multilayer coating fails at 25 N with a line of scratch width of 63.5 µm, in agreement with Rezende et al. [1]. As a result, the (douple layers TiO_2/Al_2O_3) multilayer coating appears to have better adhesion than the monolayer Al_2O_3layer,which is consistent with D.Pakula et al.[73]. Figure (4.16) show the scratch width for monolayer and multilayer coating. To obtain a comparable coating adhesion value, multiply the normal force at the time of coating detachment by the scratch hardness values to obtain the critical load that near [100]. Table (4.2) shows that multilayer coatings have a higher scratch hardness than monolayer layer.

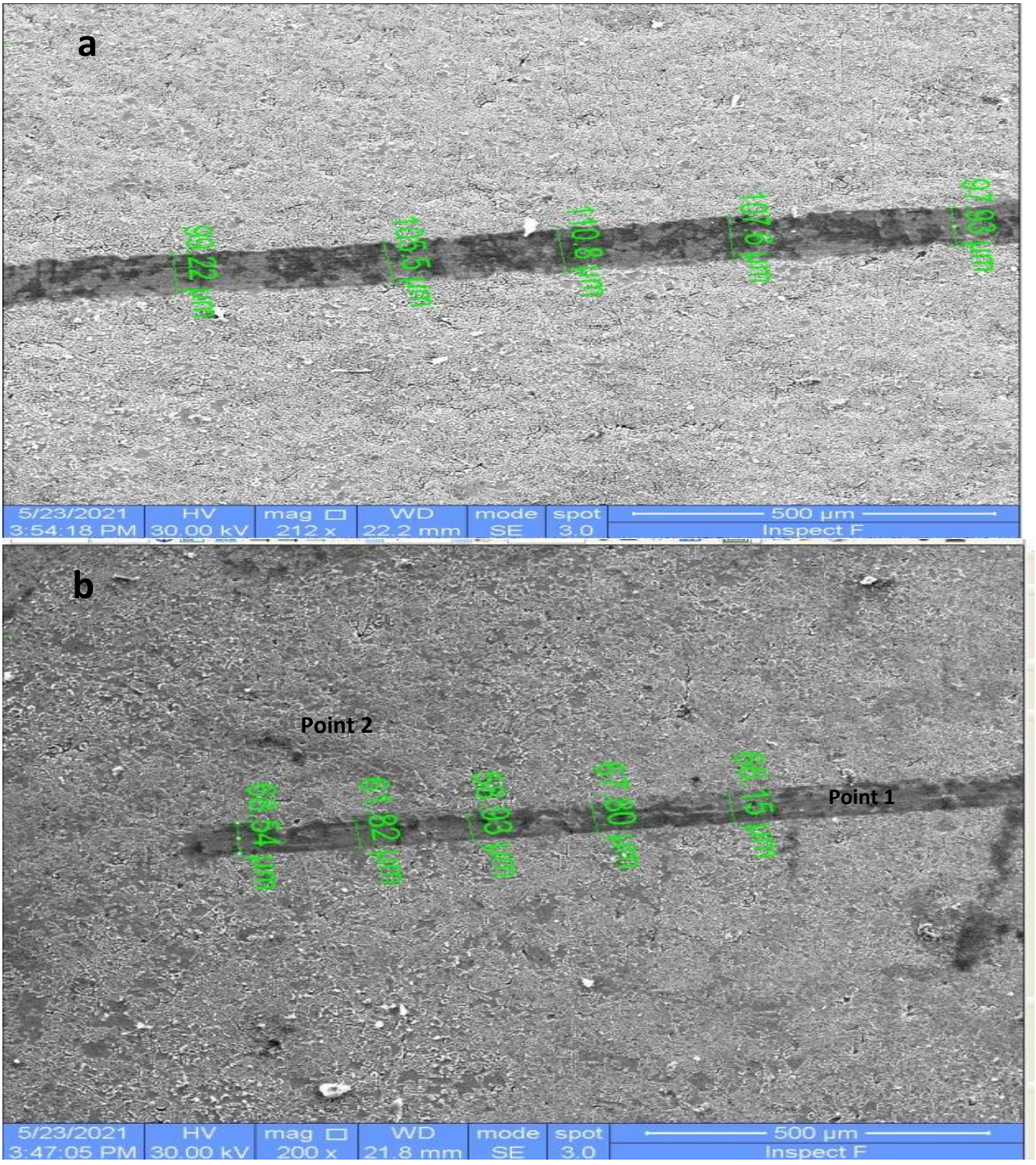

Figure (4.16): (a)FE SEM image of the scratched Al_2O_3monolayer (b) FESEM image of the scratched TiO_2/Al_2O_3 multilayers , (c) EDS spectrum from the point one in (b), and (d) EDS spectrum from the point two in (b)

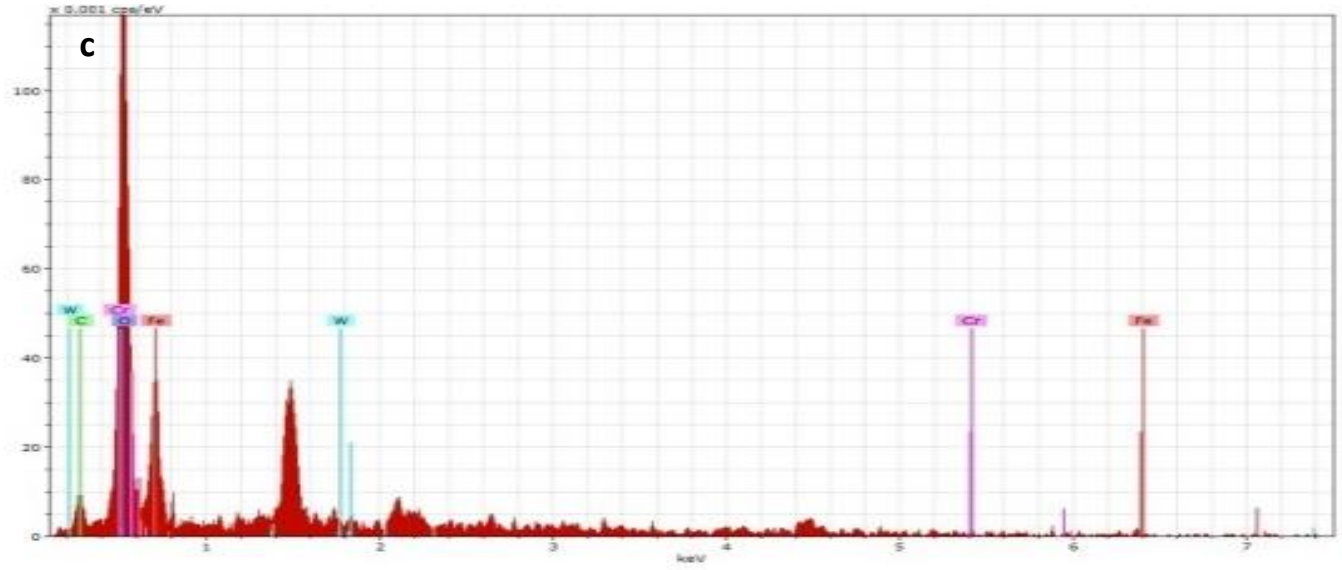

Spectrum: Acquisition 4129

El	AN	Series	unn. C [wt.%]	norm. C [wt.%]	Atom. C [at.%]	Error (1 Sigma) [wt.%]
O	8	K-series	82.63	82.63	86.22	18.66
Fe	26	K-series	8.12	8.12	2.43	2.90
C	6	K-series	8.05	8.05	11.19	5.33
W	74	M-series	0.98	0.98	0.09	0.27
Cr	24	K-series	0.23	0.23	0.07	0.24

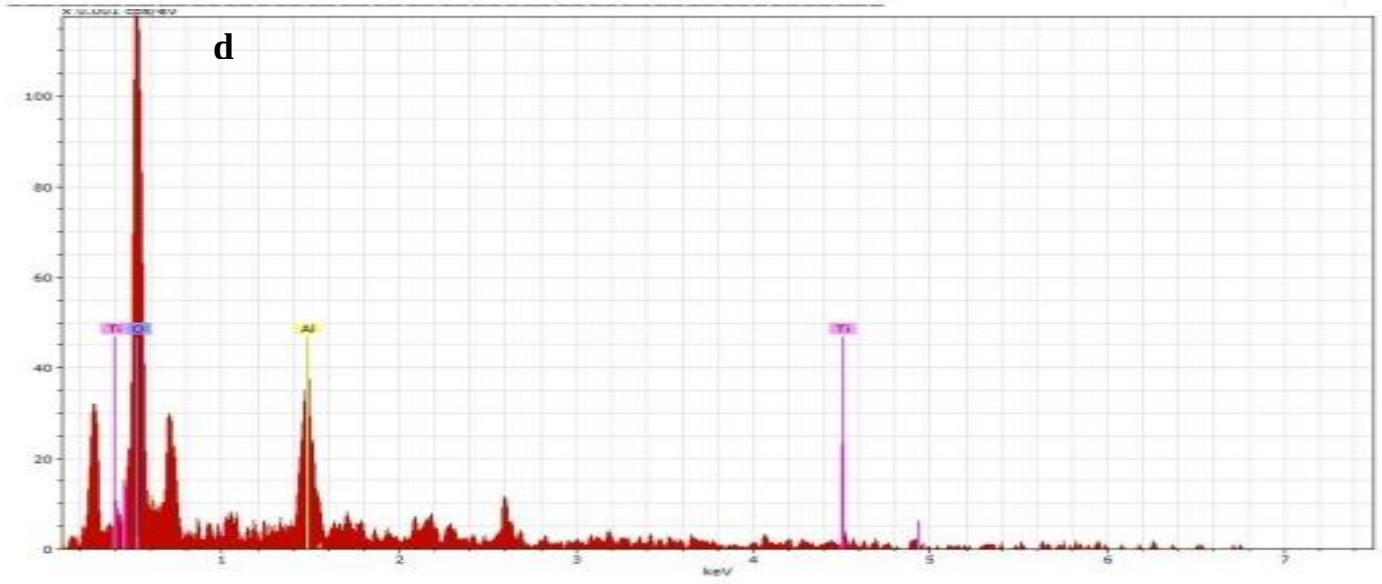

Spectrum: Acquisition 4131

El	AN	Series	unn. C [wt.%]	norm. C [wt.%]	Atom. C [at.%]	Error (1 Sigma) [wt.%]
O	8	K-series	17.12	80.63	88.77	4.40
Al	13	K-series	3.06	14.42	9.41	0.31
Ti	22	K-series	1.05	4.96	1.82	0.29

Continue Figure (4.16)

Table (4.2): Mechanical and functional properties of uncoated and coated monolayers, multilayers.

Coating layer	Microhardness HV	Critical load Lc (N)	Scratch hardness GPa
Monolayer	1046.1	15	0.374
Multilayer With suitable hardness	1393.3	25	1.010

4.2.7. Adhesion test

The adhesive strength of the polymer utilized in the pull off test was at 94.78 MPa. Table (4.3) shows the results of the adhesion test and the coating thicknesses, Figure (4.18) shows FESEM for coating at different time immersion with the thicknesses. Figure (4.17) provides surface tension values for coating and failure position.

Table (4.3): Coating conditions

Layer number	**Coating layer type**	**Immersion time (sec) for each coating precursor**			**Adhesive Strength MPa**	**Thickness layer µm**
		Titania precursor	Alumina precursor	Zirconia precursor		
MA5	Al_2O_3		5		10.65	2.707
MA30	Al_2O_3		30		1.14	6.165
MA60	Al_2O_3		60		0.94	11.6
DAT10	Al_2O_3+TiO_2	5	5		21.31	3.666
DAT 30	Al_2O_3+TiO_2	5	25		86.59	5.027
DAT 60	Al_2O_3+TiO_2	5	55		23.55	17.006
DAT90	Al_2O_3+TiO_2	5	85		18.71	22.985
TZAT30	ZrO_2+Al_2O_3+TiO_2	5	10	15	93.60	6.350
TZAT60	ZrO_2+Al_2O_3+TiO_2	5	25	30	24.29	11.613
TZAT90	ZrO_2+Al_2O_3+TiO_2	5	40	45	19.47	19.433
MZ10	ZrO_2			10	11.12	4.577

Maximium adhesive strength was recorded for multilayer deposition, as marked in Table (4.3), appropriate for achieving good adhesion with thickness layers of 6.350 µm. Increasing immersion duration resulted in decreasing of adhesion and increasing of layer thickness. This is attributed to wettability, which decreased as immersion time increased indicated by the rise in contact angle [101]. With out layer, the monolayer alumina layer has the lowest adhesive strength. When compared to another specimen with similar wettability on HSS, Al_2O_3 has the lowest adhesive strength (0.94), at 60 sec immersion time.

Figure (4.17): Adhesion test

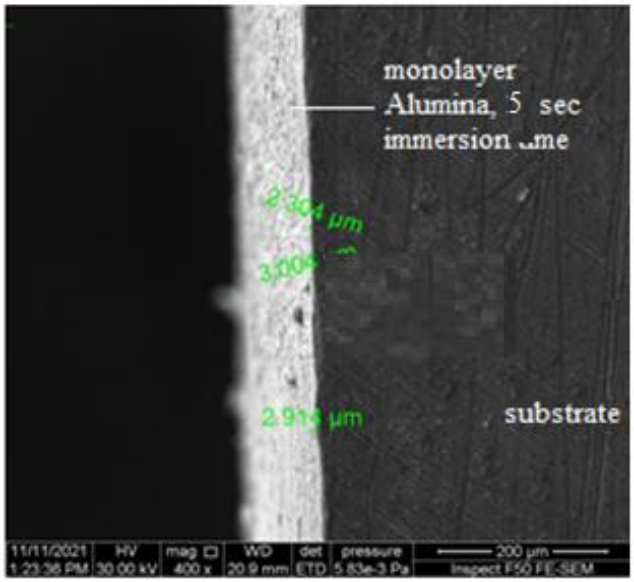
monolayer
Alumina, 5 sec
immersion time
2.913 µm
substrate

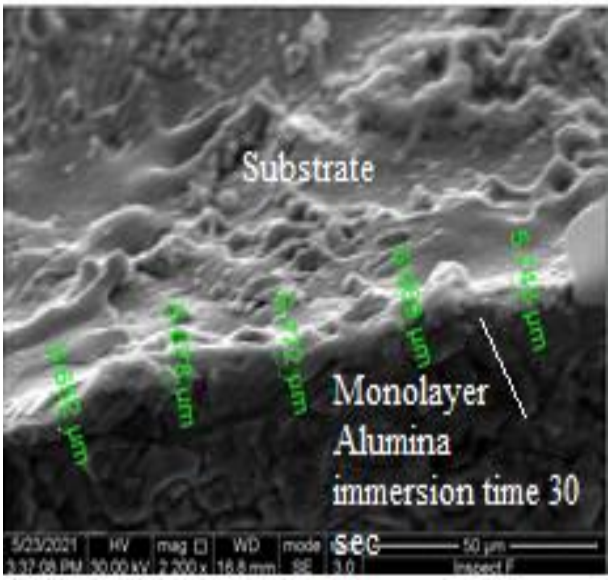
Substrate
Monolayer
Alumina
immersion time 30
sec

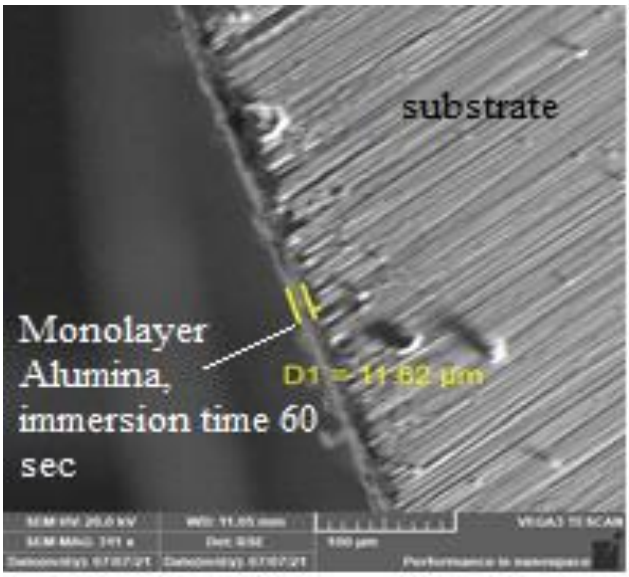
substrate
Monolayer
Alumina,
immersion time 60
sec
D1 = 11.62 µm

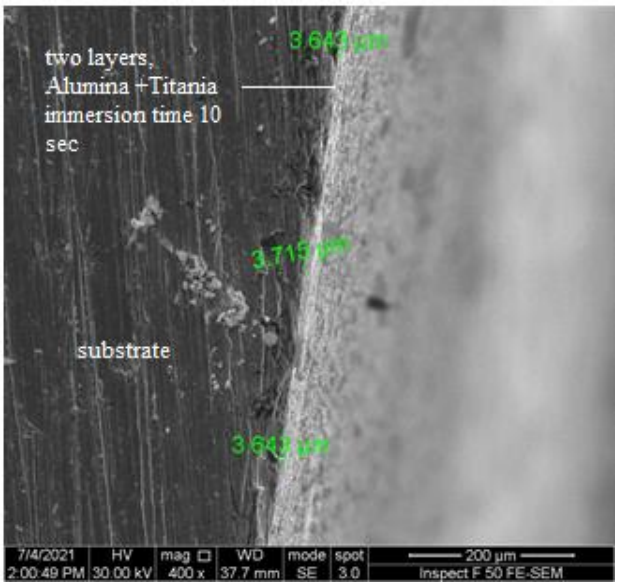
two layers,
Alumina +Titania
immersion time 10
sec
3.643 µm
substrate
3.643 µm

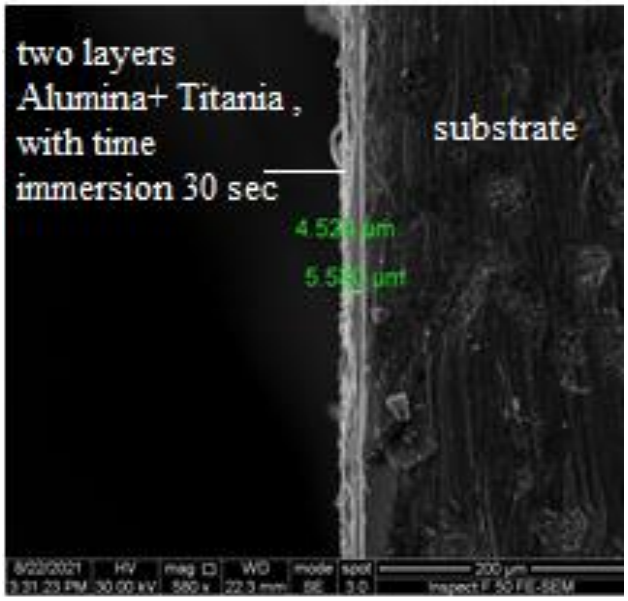
two layers
Alumina+ Titania ,
with time
immersion 30 sec
substrate

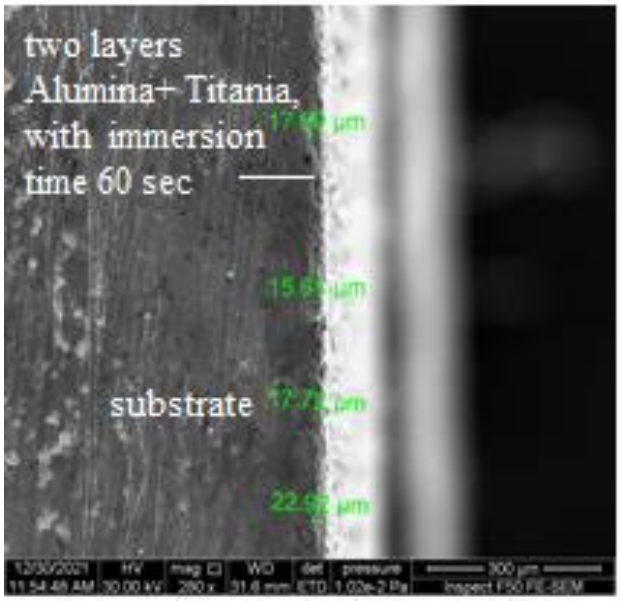
two layers
Alumina+ Titania,
with immersion
time 60 sec
substrate

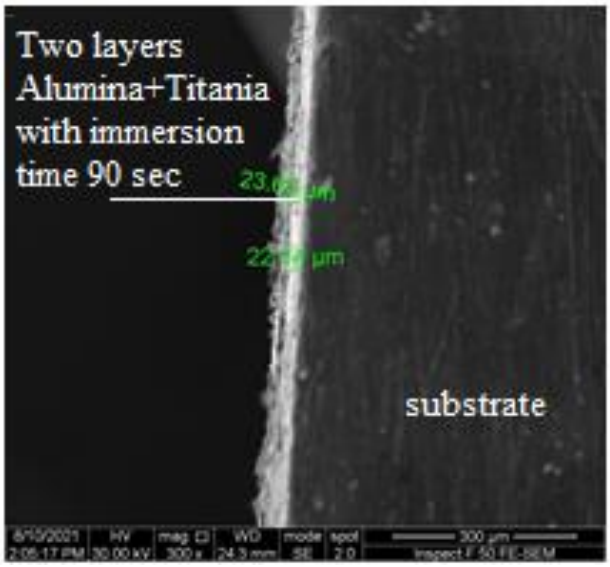
Two layers
Alumina+Titania
with immersion
time 90 sec
substrate

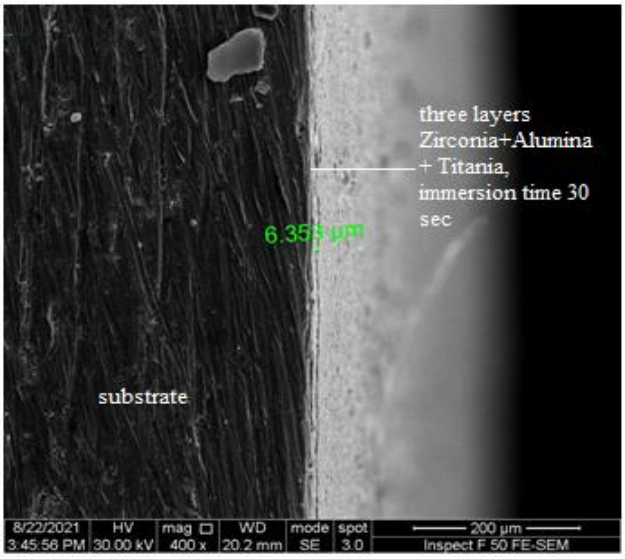
three layers
Zirconia+Alumina
+ Titania,
immersion time 30
sec
substrate
8/22/2021 HV mag WD mode spot 200 µm
3:45:56 PM 30.00 kV 400 x 20.2 mm SE 3.0 Inspect F 50 FE-SEM

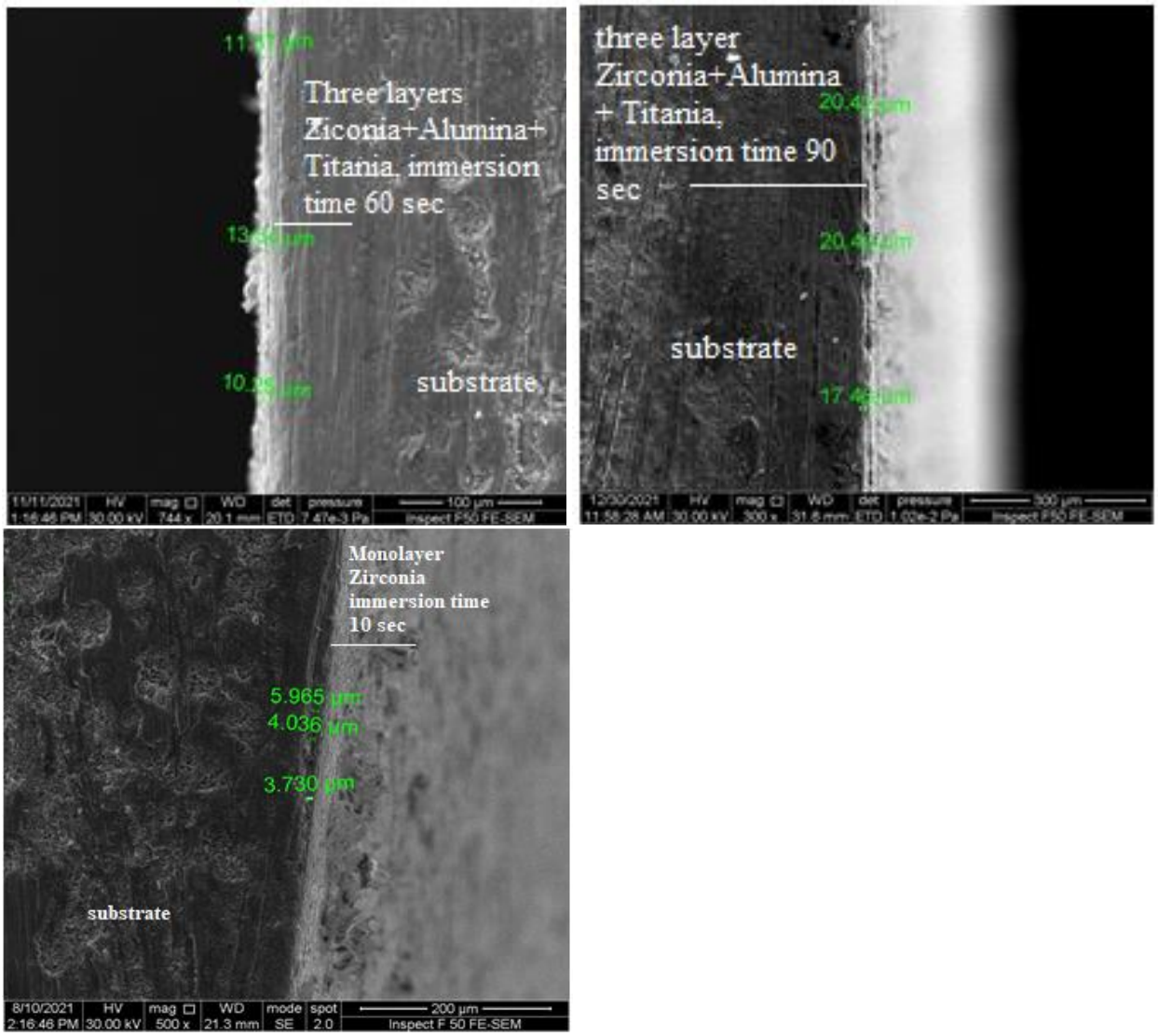

Figure (4.18):FE SEM images of different coatings

The wettability of the Al_2O_3precursor was improved on the TiO_2layer coating that was deposited on HSS, and that effected by an immersion time. At 30 sec total immersion time, the wettability of the alumina precursor improved on the titania layer coating that was deposited on HSS , when the contact angle reached 38.77º, shows Figure (4.19). While at the immersion time 90 sec, the TiO_2layer had poor distribution on HSS, as shown in Figure (4.20).

Figure (4.19): Coated HSS at specify of use conditions of coating

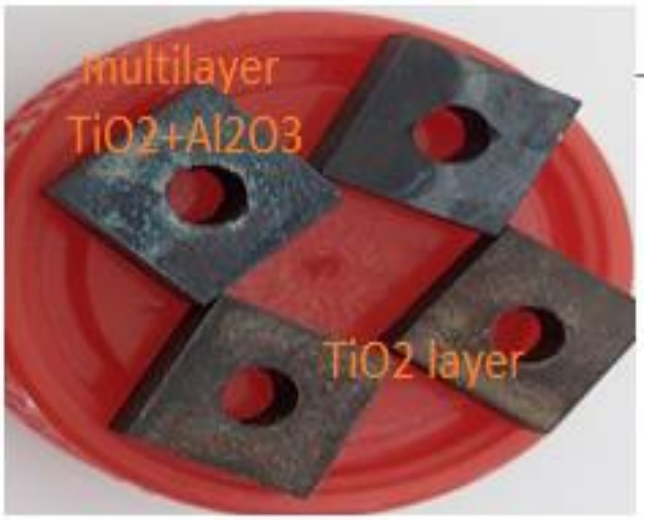

Figure (4.20) Immersion time effect on adhesive and homogeneity coating layer

From the aforemtioned results, can be found that the best conditions for coating of HSS with ceramic oxides using the sol-gel process, to obtain thickness of multilayer good adhesion without exceeding 5-6 μm that acceptable in machining, the inserts were calcinated for two hours at 500 ℃ with a 6°C/min temperature increase of the furnace, are shown in Table (4.4).

Table (4.4): Ideal coating conditions for coating of HSS cutting insert with ceramic oxides by sol-gel process

Type of coating precursor	Viscosity cPs	Aging time Hour	PH	Number of coating cycles	Immersion time (sec)	Dry temperature	Dispersion type
Titania precursor	8.74	6	6.46	1-2	5	100-355 ℃	TEOA triethanoamine
Alumina precursor	8.11	12	5.83	2	10	100-355℃	TEOA triethanoamine
Zirconia precursor	7.9	24-48	4.87	2-3	15	195—290 ℃	ethylene glycol and glycerol

4.3. Characterization of the Coatings:

In this section, metallurgical examination, physical and mechanical tests were performed on the best multilayer coating (two and three layers) which have good adhesive strength (89.56, 93.60) MPa with acceptable thickness in machining (5-6)µm. Furthermore, it was investigated the attributes of each monolayer coating: Al_2O_3 layer, ZrO_2 layer with highest adhesive strength (10.65,11.15) MPa. All of this is based on mentioned conditions of coating in Table (4.4).

4.3.1.Metallurgical Examination

4.3.1. 1. HSS

Figure (4.21) depicts the morphology of the substrate, which contains many precipitates in the matrix to provide high strength for this type of the H.S.S tool. Figure (4.22) reveals peaks associated with Fe, W, Mo, C and O that are mostly visible in the substrate region.

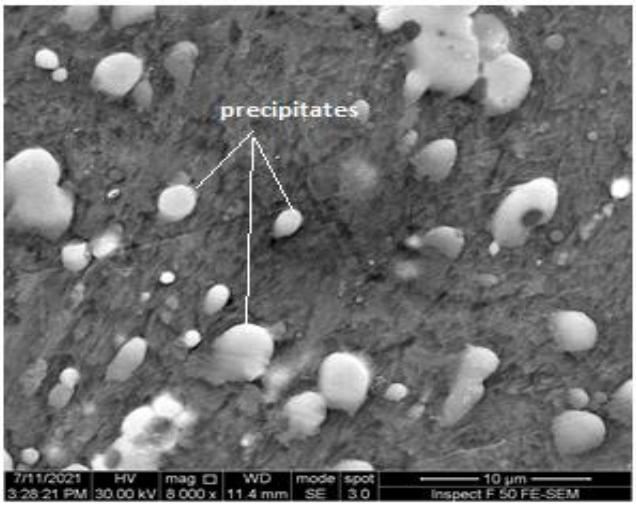

Figure (4.21): FE-SEM image for the surface of uncoated insert

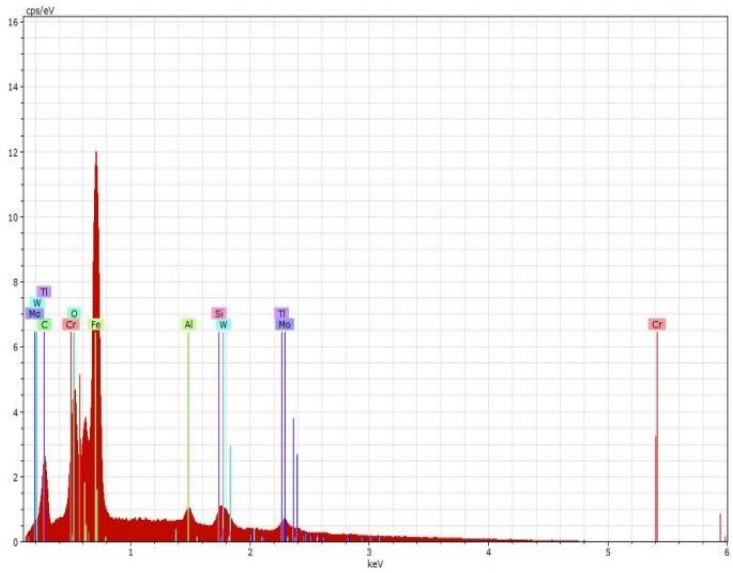

Spectrum: Acquisition 4998

El	AN	Series	unn. C [wt.%]	norm. C [wt.%]	Atom. C [at.%]	Error (1 Sigma) [wt.%]
Fe	26	L-series	45.86	66.66	51.25	5.27
O	8	K-series	5.47	7.95	21.34	0.74
Cr	24	L-series	4.06	5.91	4.88	0.67
W	74	M-series	3.57	5.19	1.21	0.21
Mo	42	L-series	3.43	4.99	2.23	0.22
C	6	K-series	2.68	3.90	13.93	0.41
Tl	81	M-series	1.67	2.42	0.51	0.13
Si	14	K-series	1.11	1.61	2.47	0.09
Al	13	K-series	0.94	1.37	2.18	0.08
		Total:	68.80	100.00	100.00	

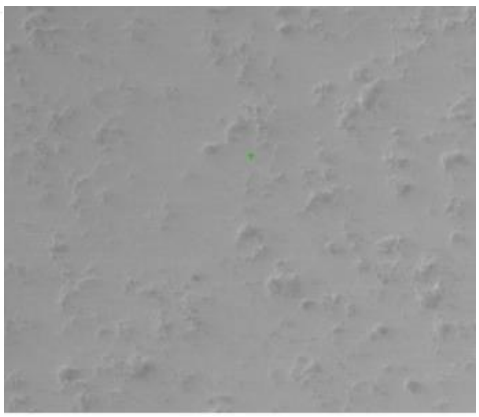

Figure (4.22): EDS spectrum from the substrate region of the insert

4.3.1.2.TiO_2

Figure (4-23)-a shows the nano-layer of titania with high adherence on the substrate, titania achieves good adhesion on the substrate and ignore mismatch between the substrate and the alumina + zirconia layer that agree with the study of Rezende et.al, [1]. Cross section of the TiO_2 thin coatings deposited on substrate, is shown in Figure (4.23) -b.

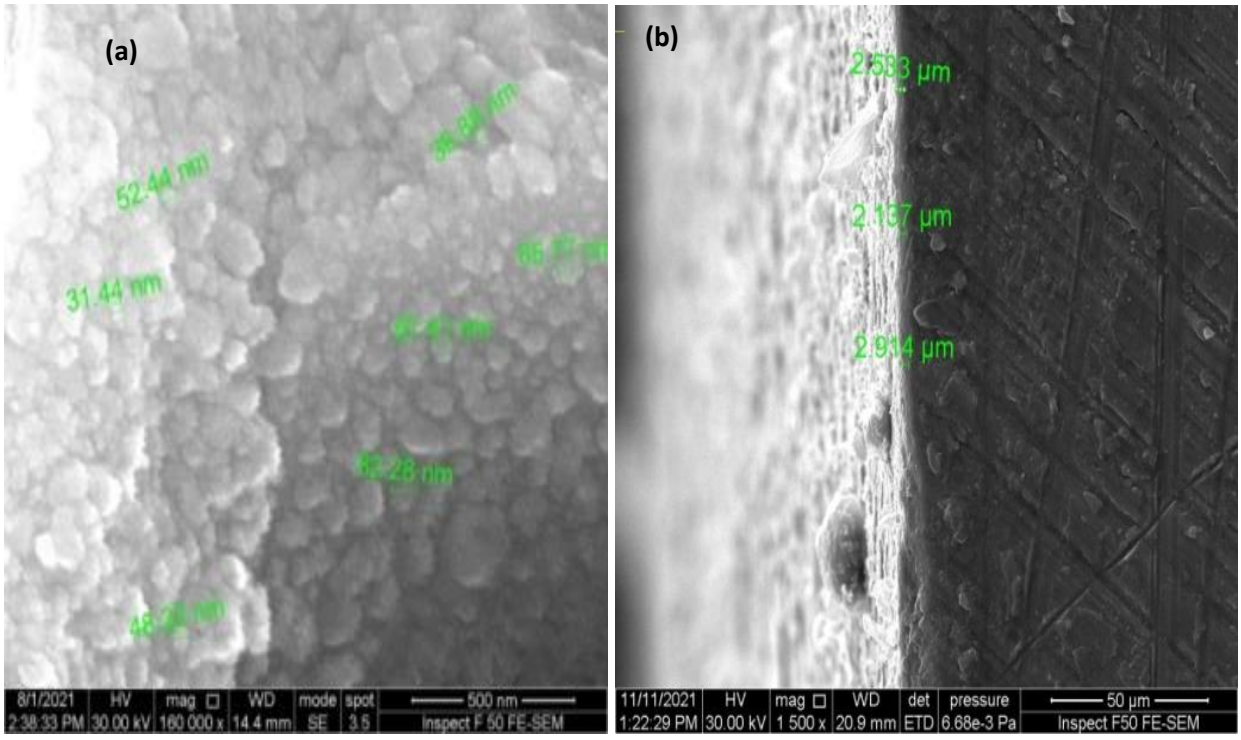

Figure (4.23):FE SEM image of TiO_2 coating after calcination for two hour at 500 ℃, (a): for surface , (b): for cross –section

Figure(4.24)-a shows a FESEM image of a TiO_2 layer which formed after two immersions for 5 sec. Peaks of Ti and O may be seen in the coating zone, indicating that the TiO_2 coating has been applied in Figure (4.2 4) -b-c.

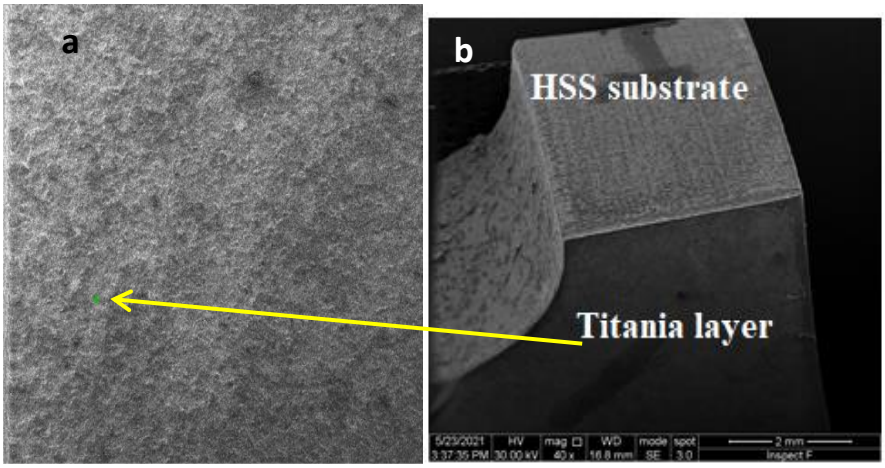

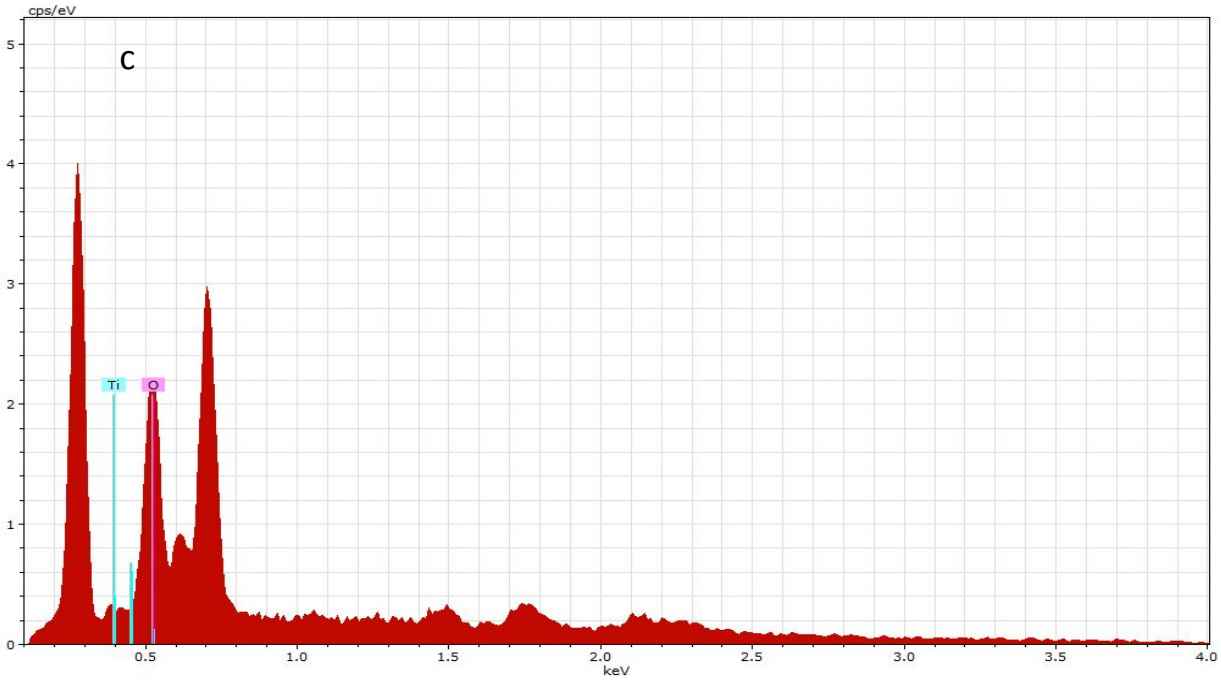

Spectrum: Acquisition 4486

El	AN	Series	unn. C [wt.%]	norm. C [wt.%]	Atom. C [at.%]	Error (1 Sigma) [wt.%]
O	8	K-series	69.55	69.55	87.24	13.47
Ti	22	L-series	30.45	30.45	12.76	10.41
		Total:	100.00	100.00	100.00	

*Figure (4.24): (**a**)FE SEM image of the TiO_2 layer (**b**)cross section of coated insert (**c**) EDS spectrum from the TiO_2 coated region of the insert.*

4.3.1.3.Al_2O_3

After 500°C calcination for two hours, the Al_2O_3layer is shown in Figure (4.25)-. Figure (4.25)-b shows that the alumina layer is deposited unevenly with cracks. a layer of alumina just with many cracks due to the layer's lack of adhesion and mismatch in physical attributes with the substrate.

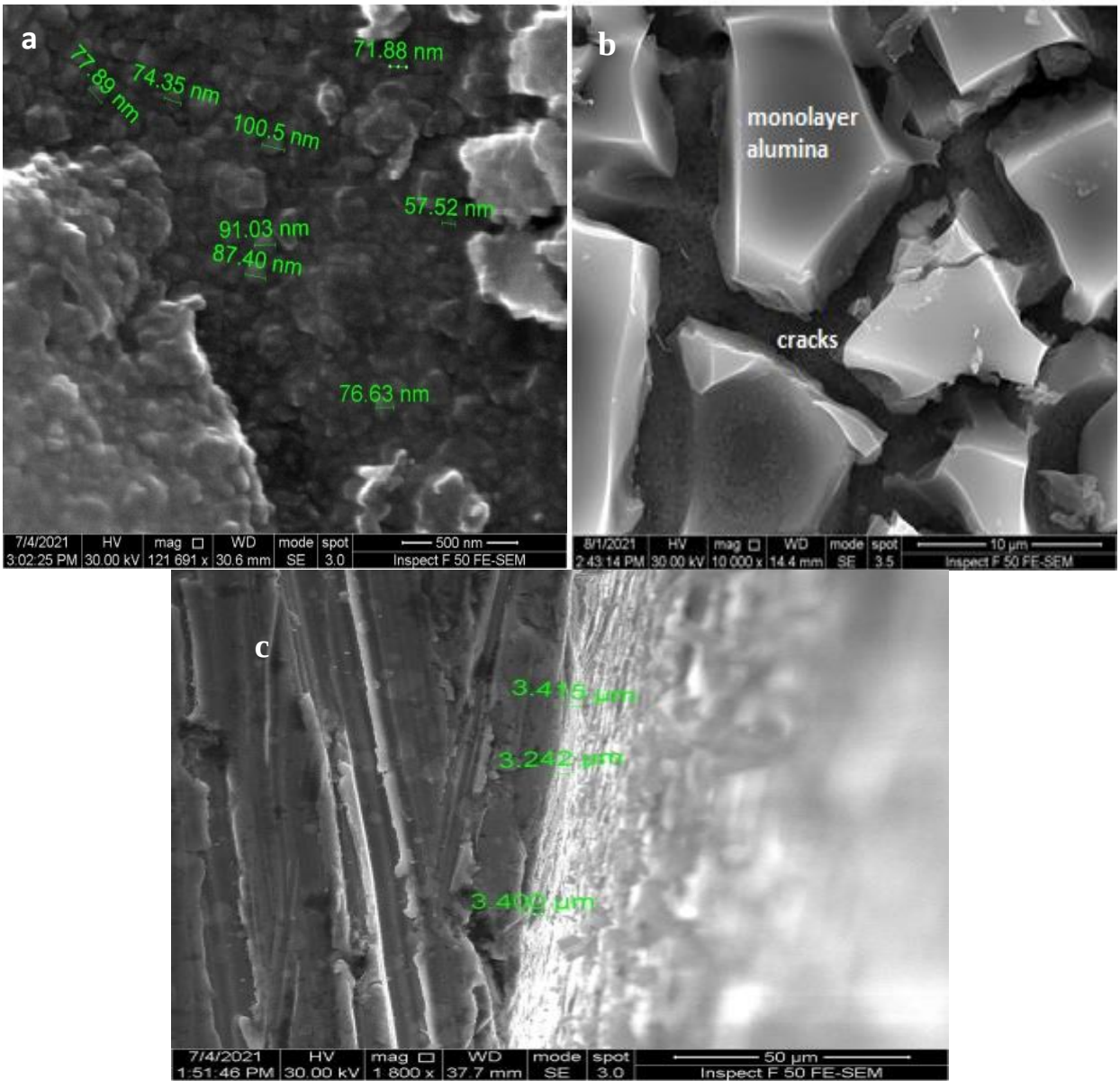

Figure (4.25):FESEM of Al_2O_3 after calcination for two hour at 500 ℃(a-b): for surface, (c): for cross –sectional

FESEM image of the Al_2O_3 layer which formed after three immersions for 15sec is shown in Figure (4.26)-a . Peaks associated with Al and O are mostly visible in the coated region, showing that the substrate tool is coated with alumina. See Figure (4.26)-b-c.

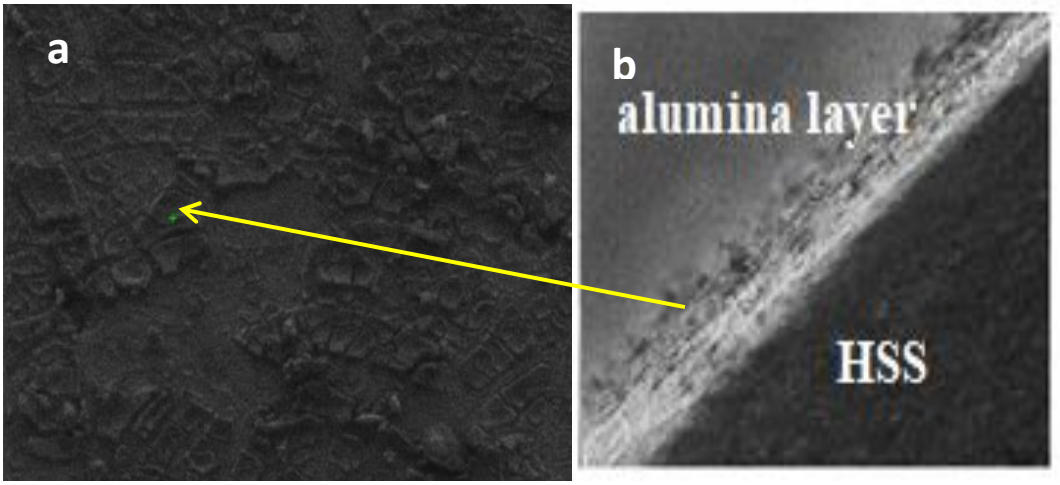

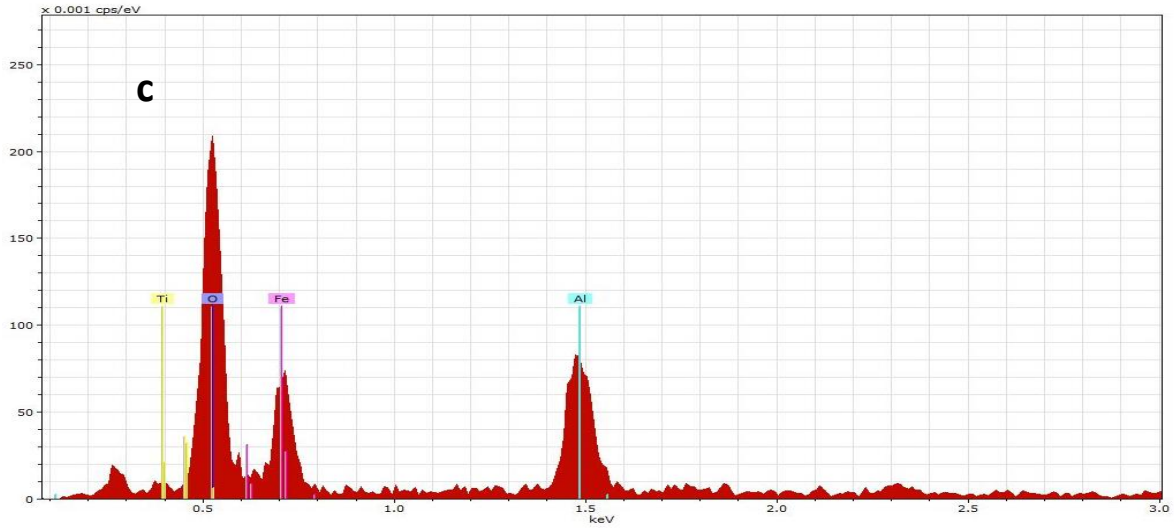

Spectrum: Acquisition 4007

El	AN	Series	unn. C [wt.%]	norm. C [wt.%]	Atom. C [at.%]	Error (1 Sigma) [wt.%]
O	8	K-series	20.44	72.75	83.39	4.64
Al	13	K-series	6.12	21.79	14.81	0.47
Fe	26	K-series	1.48	5.26	1.73	0.71
Ti	22	K-series	0.06	0.20	0.08	0.09
		Total:	28.09	100.00	100.00	

*Figure (4.26): (**a**) SEM image of the Al_2O_3 coating (**b**)cross section of coated insert, and (**c**) EDS spectrum from the Al_2O_3 coated region of the insert*

4.3.1.4.ZrO_2

Figure (4.27) shows the morphology for the surfaces of the coated insert monolayer ZrO_2 at 500 ℃ for two hours shows growth of agglomeration circular particles. Comparing between the present study and S.K.Tiwari image of ZrO_2 layer heated at 500 ℃ for two hours from povious study [102] is also presented in Figure (4.27)-d .

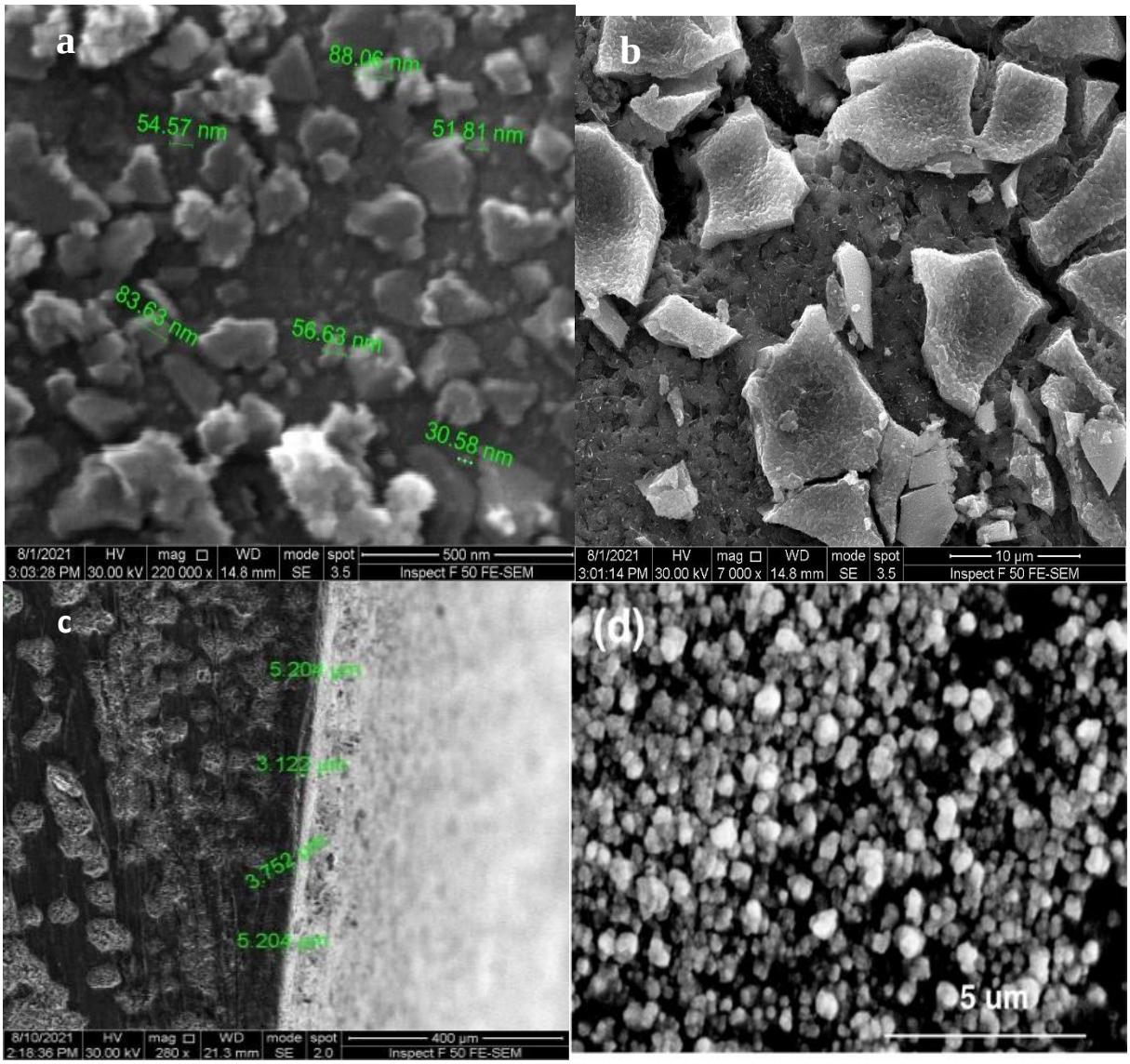

Figure (4.27): FESEM micrograph of ZrO_2based coatings for two hours at 500 ℃ (a-b):for surfaces, (c) : for cross-section, (d): ZrO_2 layer in previous study [102].

FESEM image of the ZrO_2 layer. After two immersions for 10 sec, the ZrO_2layer was formed as shown in Figure (4.28). Peaks associated with Zr and O are mostly visible in the coated region.

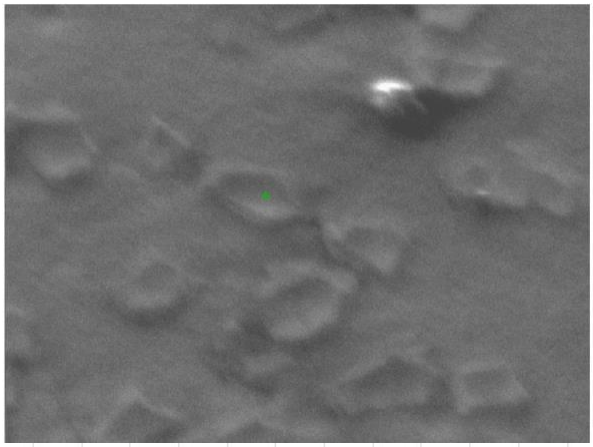

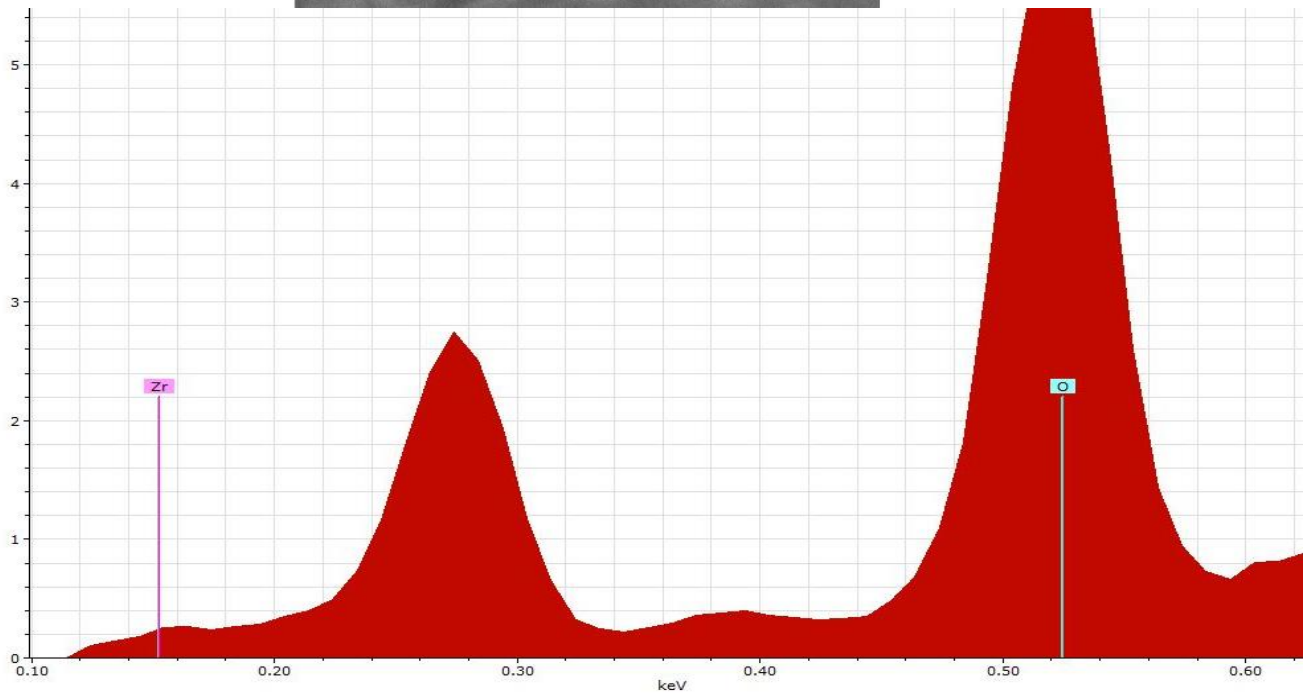

Spectrum: Acquisition 4440

El	AN	Series	unn. C [wt.%]	norm. C [wt.%]	Atom. C [at.%]	Error (1 Sigma) [wt.%]
O	8	K-series	91.47	91.47	98.39	13.12
Zr	40	L-series	8.53	8.53	1.61	0.89
		Total:	100.00	100.00	100.00	

*Figure (4.28**):** EDS spectrum from the ZrO_2coated region of the insert surface*

4.3.1.5. Multi- layer coating

4.3.1.5.1. Douple layers

The FE-SEM image of the multilayer (TiO_2/Al_2O_3) coatings on the HSS insert is shown in Figure (4.29). The coating thickness was also measured of 4.5-5.5 µm using a FESEM, this thickness is acceptable for machining with high-speed steel according the research [103]

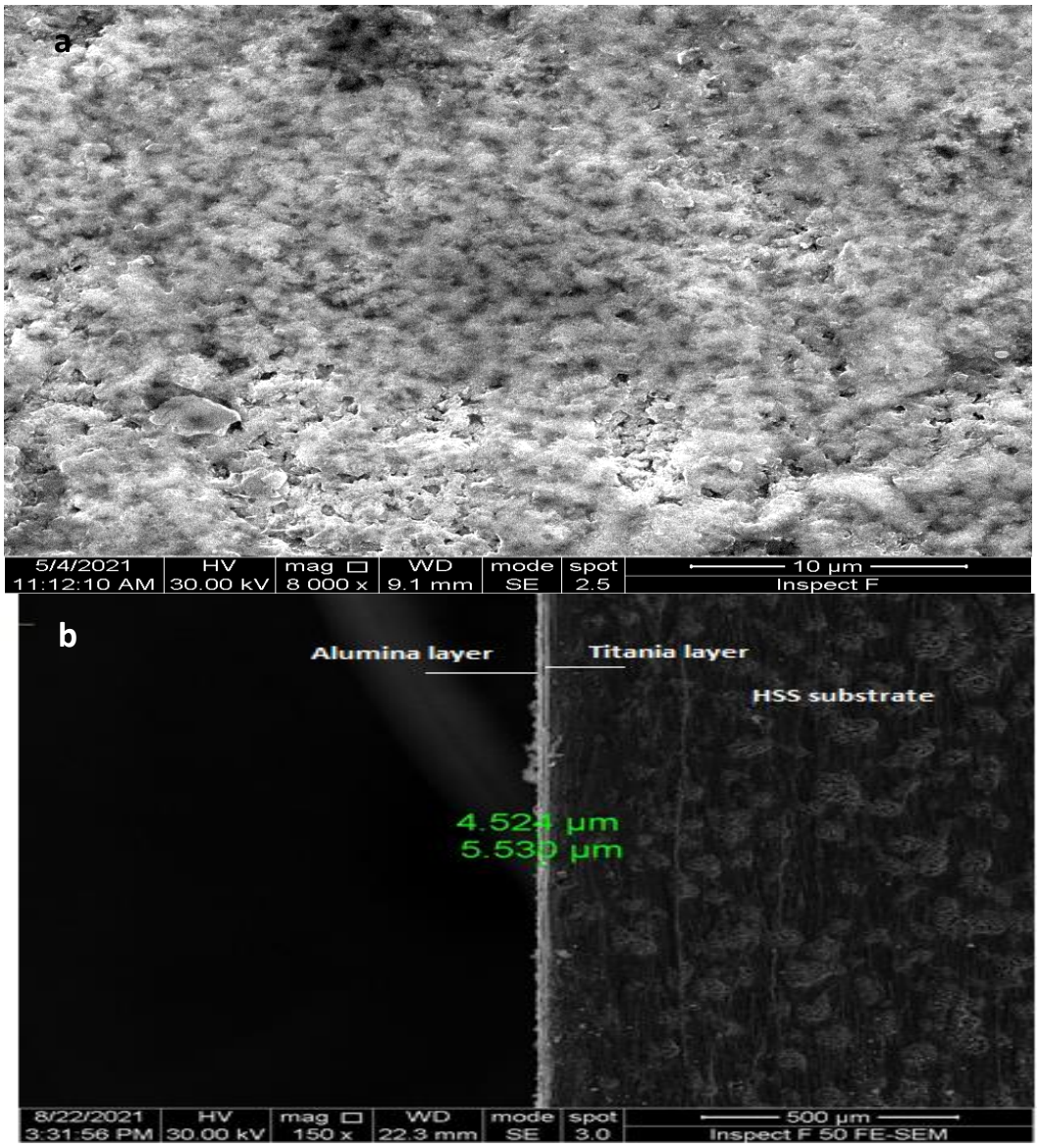

Figure (4.29): FE-SEM images of the douple layers coating, (a): for surface, (b): for cross –section

The EDS spectra of the substrate and coated portions of the tool are exhibited in detail from the coating region. The peaks of Ti and O confirm the deposition of TiO_2 directly on the substrate in the titania layer region, the peaks of Al and O demonstrate the deposition of Al_2O_3 Figure (4.30)-a-b. In Figure (4.30)-c, the maxima of Al, O, and Ti at the interface between two layers, indicating that Al_2O_3 and TiO_2 layers were deposited and the diffusion occurred between them, respectively. Figure (4.30)-d shows the elements of W, Cr, and Fe in HSS in the substrate region.

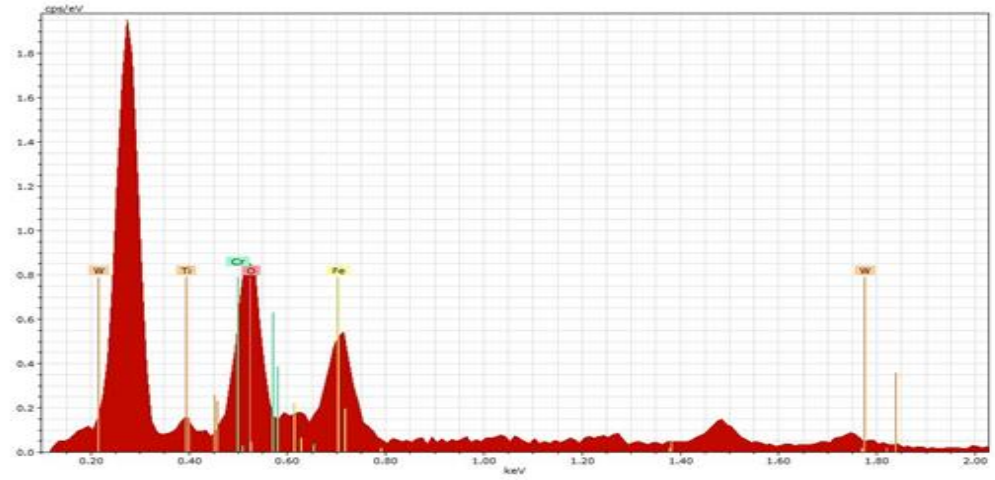

Spectrum: Acquisition 4451

El	AN	Series	unn. C [wt.%]	norm. C [wt.%]	Atom. C [at.%]	Error (1 Sigma) [wt.%]
Fe	26	L-series	41.42	41.42	24.12	11.62
O	8	K-series	27.70	27.70	56.31	6.96
Ti	22	L-series	18.18	18.18	12.35	8.54
Cr	24	L-series	11.06	11.06	6.92	5.72
W	74	M-series	1.63	1.63	0.29	0.46
Total:			100.00	100.00	100.00	

a

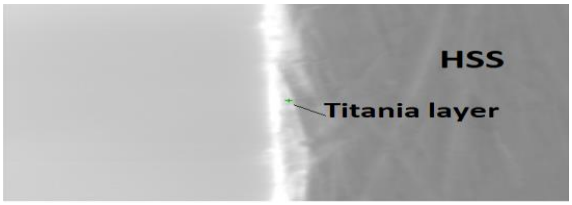

Figure(4.30): EDS spectra from the coated regions in the cross section of the insert, (a) region of TiO_2layer, (b) region of Al_2O_3layer, (c) region of the interface between two layers, (d) region of substrate HSS

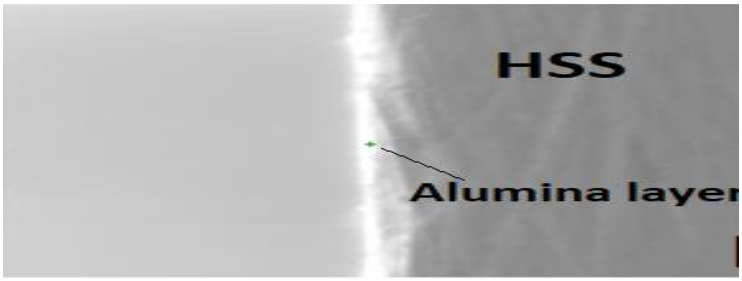

b

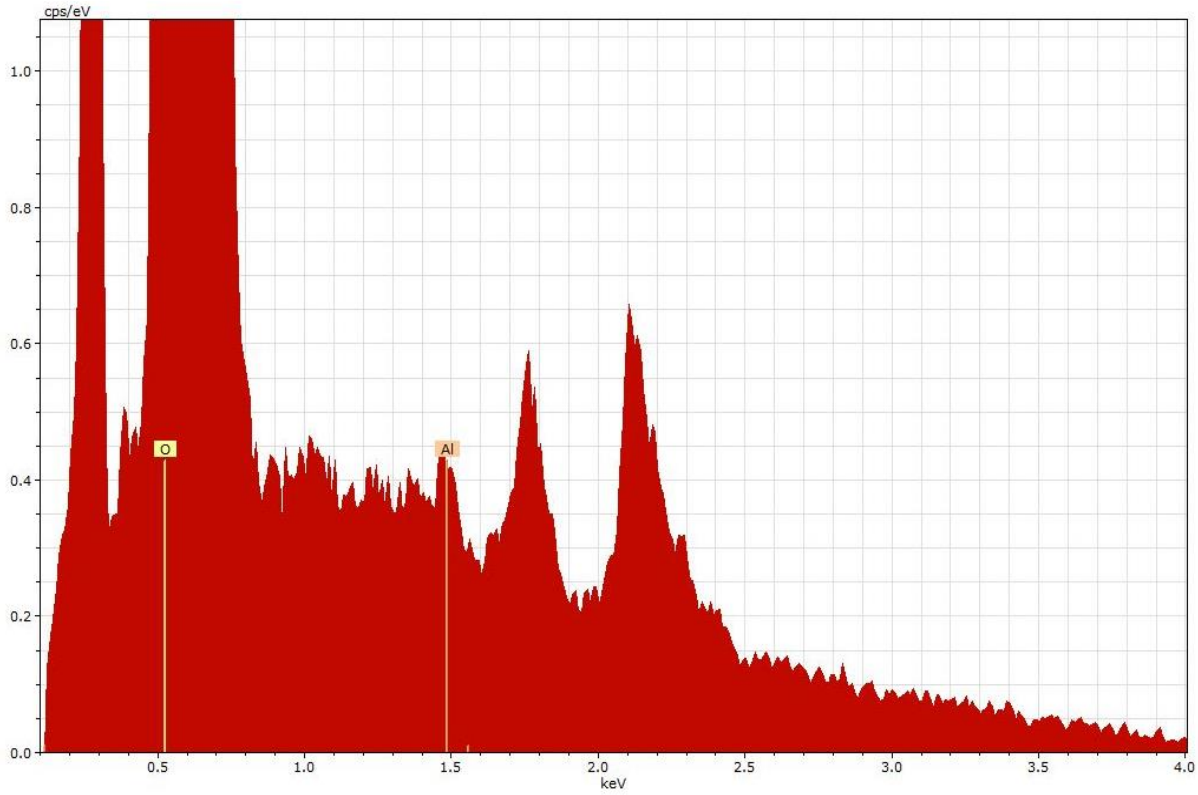

Spectrum: Acquisition 4496

El	AN	Series	unn. C [wt.%]	norm. C [wt.%]	Atom. C [at.%]	Error (1 Sigma) [wt.%]
O	8	K-series	95.81	95.81	97.47	19.37
Al	13	K-series	4.19	4.19	2.53	0.71
		Total:	100.00	100.00	100.00	

Continue Figure (4.30)

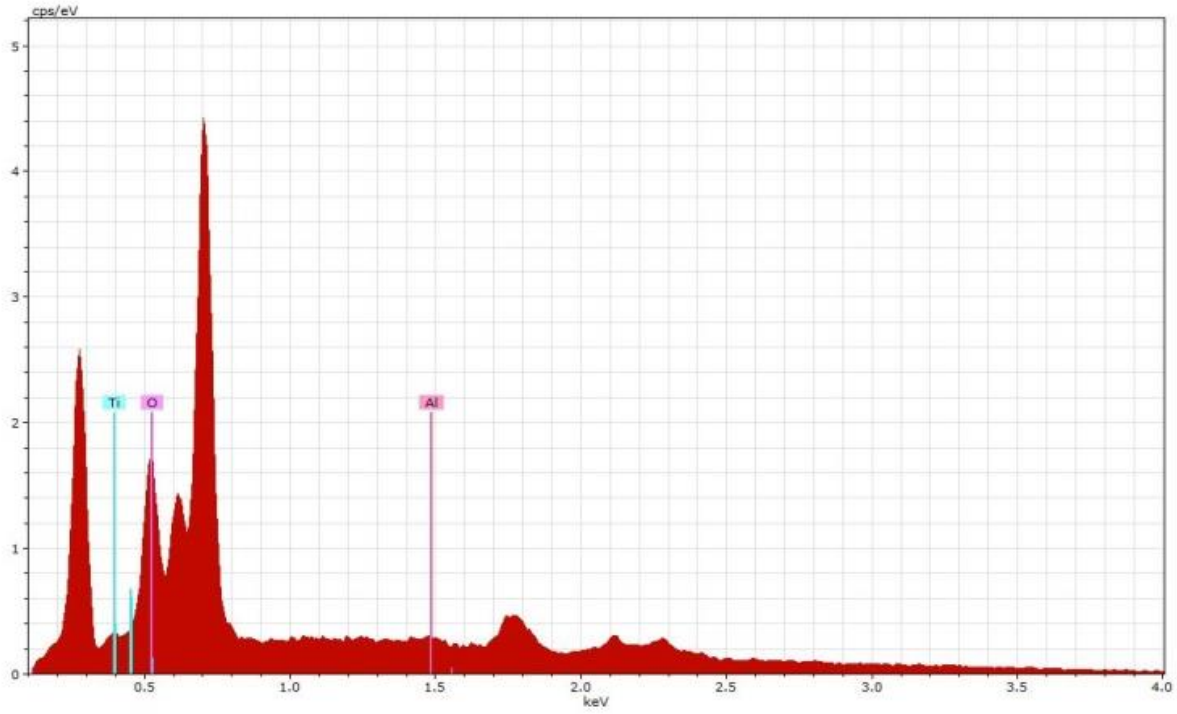

El	AN	Series	unn. C [wt.%]	norm. C [wt.%]	Atom. C [at.%]	Error (1 Sigma) [wt.%]
O	8	K-series	66.50	66.50	84.97	16.87
Ti	22	L-series	31.29	31.29	13.36	16.82
Al	13	K-series	2.20	2.20	1.67	0.56
		Total:	100.00	100.00	100.00	

c

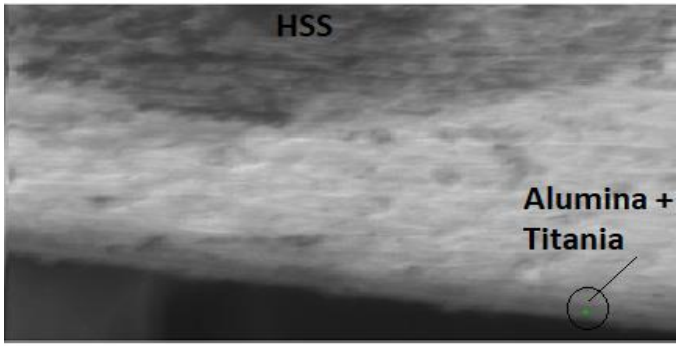

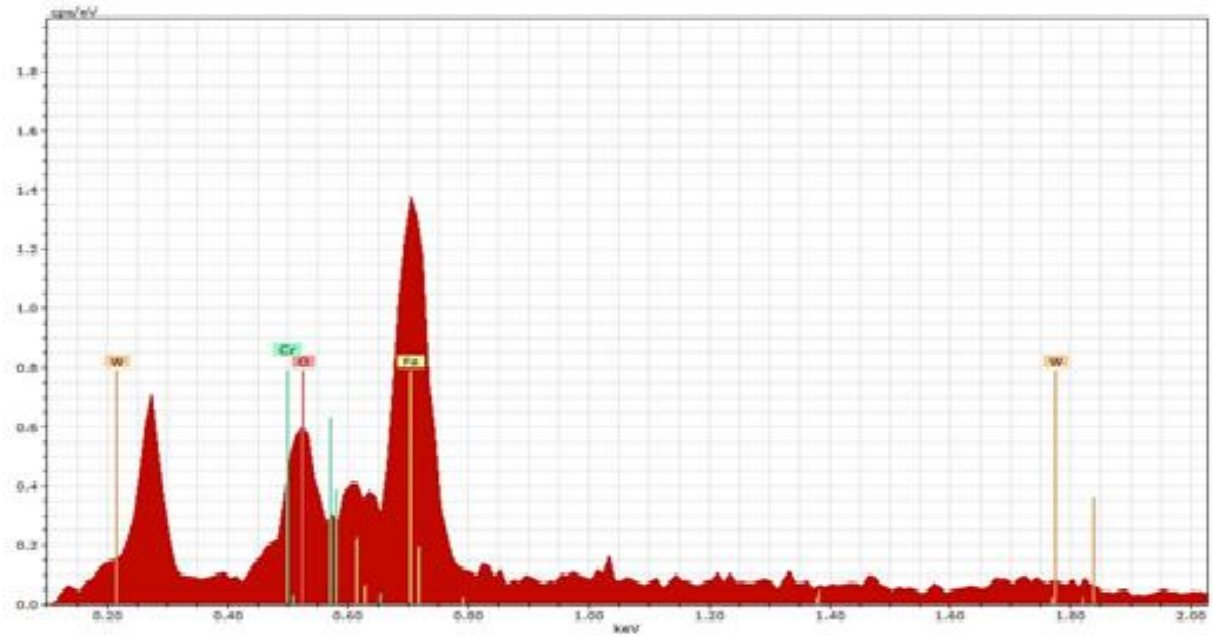

Spectrum: Acquisition 4453

El	AN	Series	unn. C [wt.%]	norm. C [wt.%]	Atom. C [at.%]	Error (1 Sigma) [wt.%]
Fe	26	L-series	81.67	81.67	67.28	17.80
O	8	K-series	9.34	9.34	26.85	3.27
Cr	24	L-series	5.71	5.71	5.05	3.61
W	74	M-series	3.29	3.29	0.82	0.70
		Total:	100.00	100.00	100.00	

d

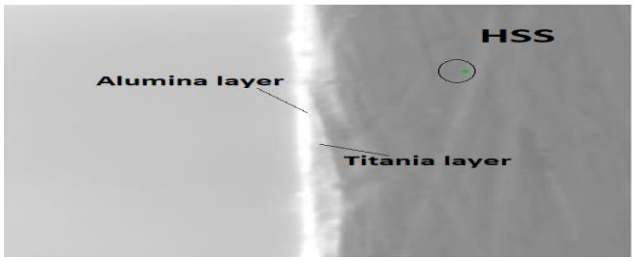

Continue Figure(4.30)

Relevant peaks of the chemical elements C, Cr, and CO, as well as additional peaks characteristic of the Ti, Al, and O elements, related to the multilayer coating chemistries, can be seen in the EDS collected from the multilayer coated portion

of the insert, as shown in Figure (4.31)-a-b. Peaks of Ti, Al, and O are found in the coating region, confirming the presence of TiO_2 and Al_2O_3 layers on the tool's surface.

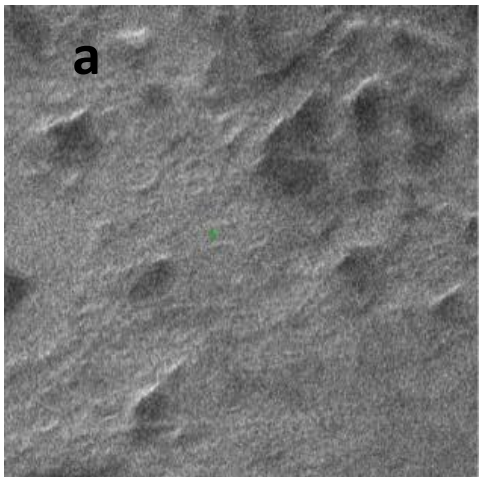

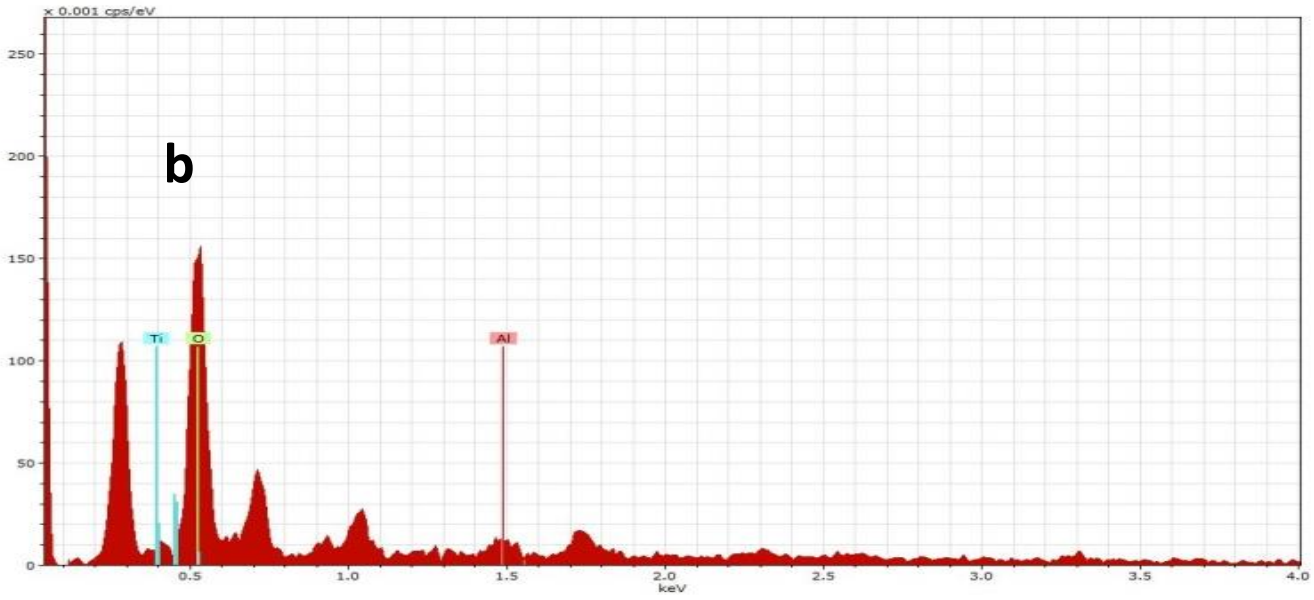

Spectrum: Acquisition 4083

El	AN	Series	unn. C [wt.%]	norm. C [wt.%]	Atom. C [at.%]	Error (1 Sigma) [wt.%]
O	8	K-series	94.87	94.87	97.00	17.25
Al	13	K-series	4.70	4.70	2.85	0.53
Ti	22	K-series	0.43	0.43	0.15	0.29
		Total:	100.00	100.00	100.00	

Figure (4.31): (a) SEM image of douple layers coating top surface; (b) EDS spectrum of douple layers-coated tool region

Figures (4.32) a-b show FESEM image of a multilayer coating applied on an HSS substrate, as well as EDS spectra taken in the cross section of coated insert areas. The coating had good adherence to the HSS substrate. Diffusion and chemical bonding are most likely the bonding mechanisms between the $Al_2O_3$and the substrate according obvious research [97].

The EDS spectra of the substrate and coated portions of the tool are shown in detail, from the coating region, peaks of Al ,O and Ti, O are present, confirming the deposition of Al_2O_3 layer and TiO_2 layer respectively.

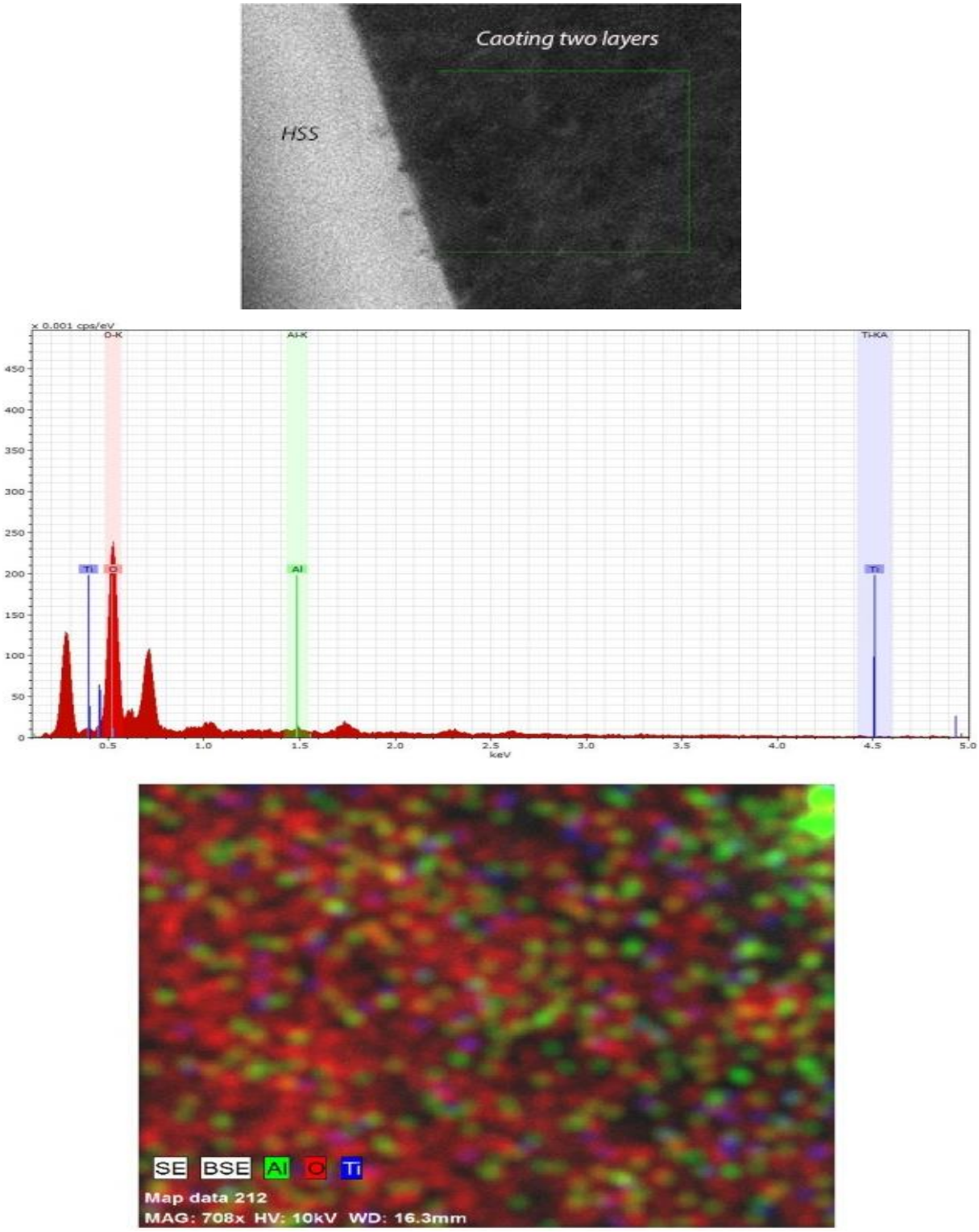

Figure(4.32): (a) EDS spectra from the douple layers coated regions of the cross section of the insert,(b) SEM picture of the douple layers coating

4.3.1.5.2. Triplex layers

Figure (4.33) shows the image of TiO_2, Al_2O_3, and ZrO_2 triplex coating respectively, that confirmed good adhesion of the layers and a low porosity

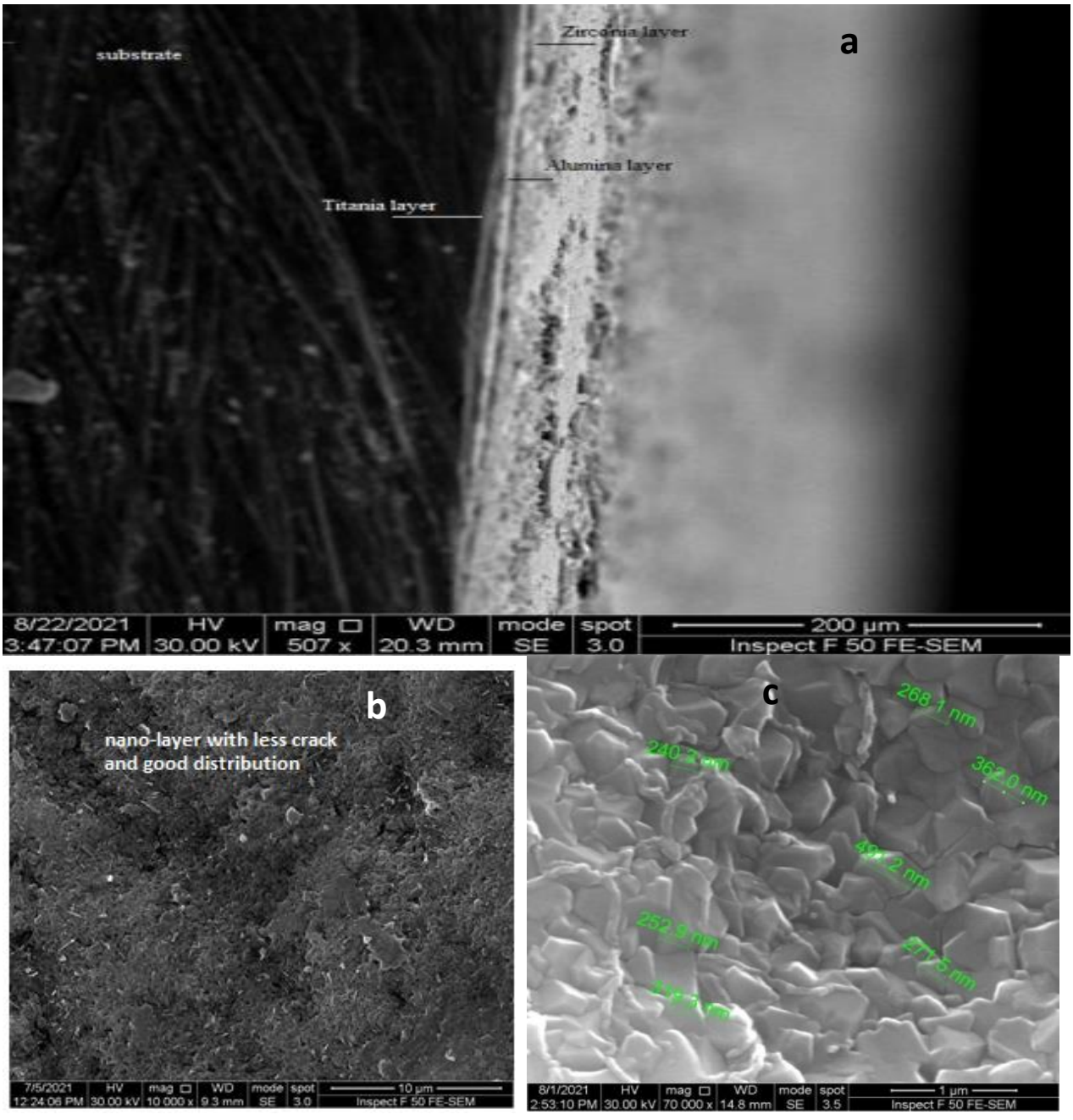

Figure (4.33): FE-SEM images of the triplex coating, (a): SEM cross –sectional image (b): Image of surface for $TiO_2/Al_2O_3/ZrO_2$, (c): Surface SEM image for Zirconia microstructure

The EDS spectra of the substrate and coated portions of the tool are exhibited in detail from the coating region. The peaks of Ti and O confirm the deposition of TiO_2 directly on the substrate in the titania layer region, the peaks of Al and O demonstrate the deposition of Al_2O_3, as shown in Figure (4.34)-a. In Figure (4.34)b shows the maxima of Al, O, Zr and Ti at the interface between two layers Al_2O_3–TiO_2, Al_2O_3-ZrO_2 indicating that ZrO_2, Al_2O_3 and TiO_2 layers were deposited and the diffusion occurred between them, respectively. Figure (4.34)-c shows the peaks of Zr and O confirm the deposition of ZrO_2 directly on the alumina layer in the zirconia layer region.

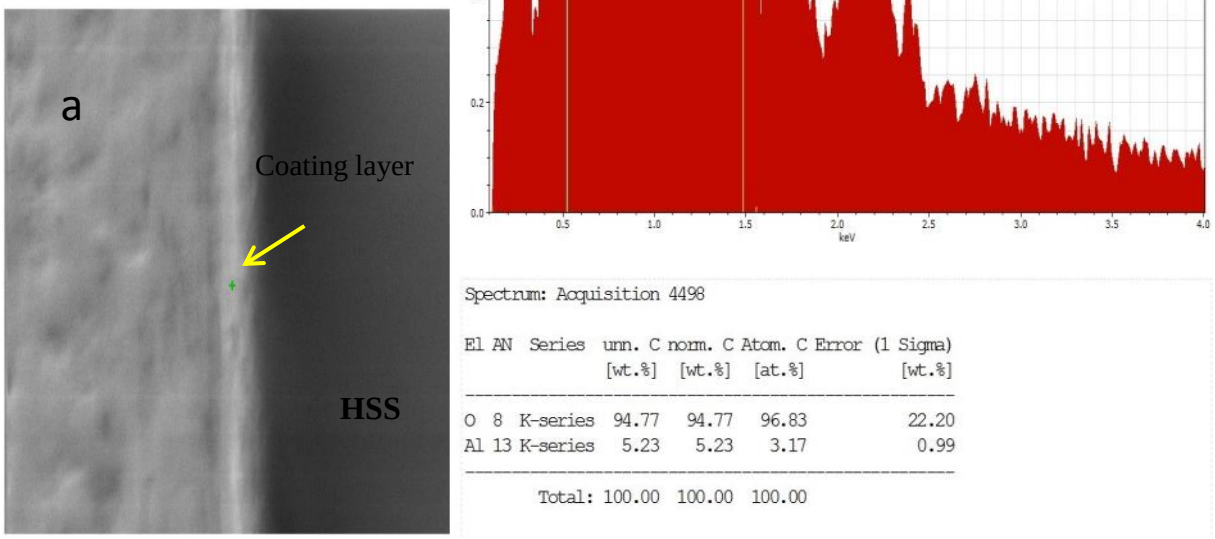

Figure(4.34): EDS spectra from the coated region of the cross section of the insert, (a) region of Al_2O_3layer, (b) region of the interface between TiO_2-Al_2O_3 layers and region of the interface between Al_2O_3–ZrO_2layers, (c) region of ZrO_2layer

b

Spectrum: Acquisition 4505

El	AN	Series	unn. C [wt.%]	norm. C [wt.%]	Atom. C [at.%]	Error (1 Sigma) [wt.%]
Zr	40	L-series	22.78	60.59	27.57	1.33
O	8	K-series	8.12	21.60	56.05	1.82
Ti	22	L-series	6.17	16.40	14.22	2.49
Al	13	K-series	0.53	1.41	2.17	0.09
		Total:	37.60	100.00	100.00	

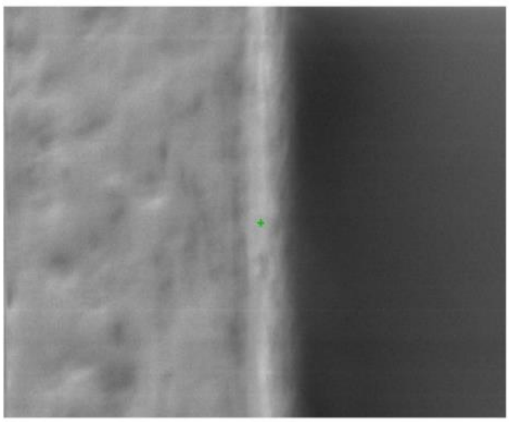

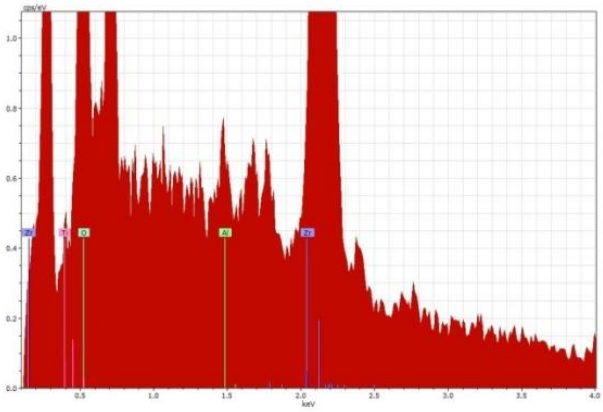

c

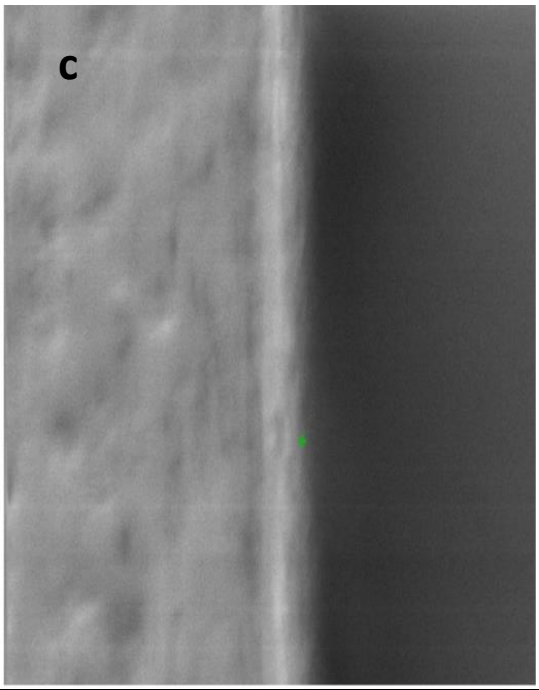

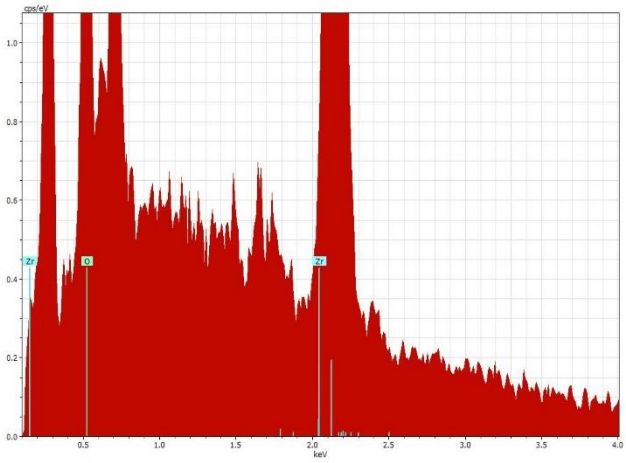

Spectrum: Acquisition 4497

El	AN	Series	unn. C [wt.%]	norm. C [wt.%]	Atom. C [at.%]	Error (1 Sigma) [wt.%]
Zr	40	L-series	18.32	64.26	23.97	1.22
O	8	K-series	10.19	35.74	76.03	2.57
		Total:	28.52	100.00	100.00	

Continue Figure (4.34).

To determine the elemental distribution of cross sectional image for the three layers, EDS mapping were performed. The results were summarized in Figure (4.35), which shows the spatial distribution of Zr, O in ZrO_2 layer, Ti, Al, and O diffusion between the three layers.

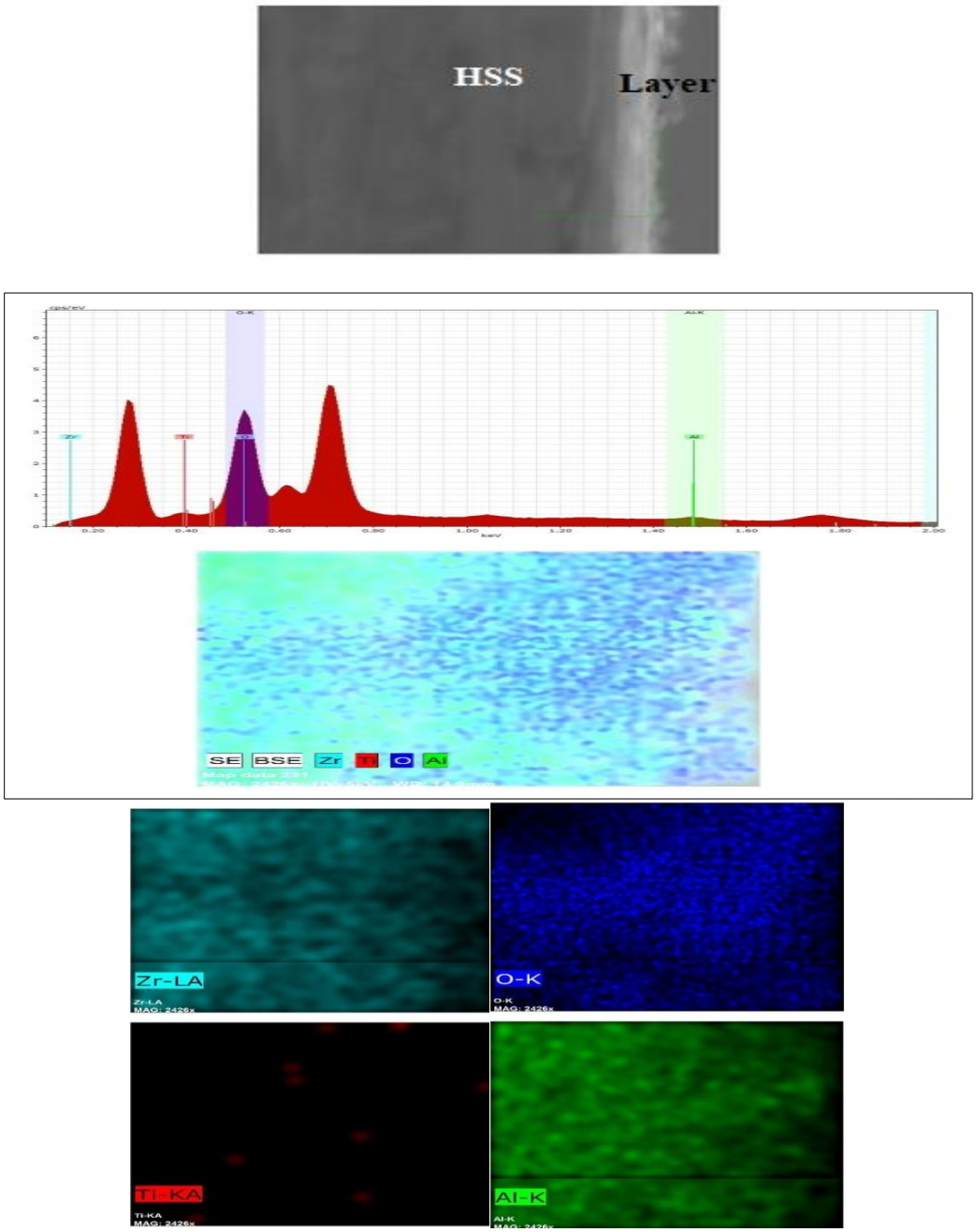

Figure(4.35): EDS mapping of prepared cross sectional sample triplex layers coated insert

4.4.X-Ray Diffraction

X-ray diffraction (XRD) analysis was used to identify the phases for the substrate, at speed 5 degree per minute. XRD pattern of the substrate with the help of EDX analysis reveals the elemental distribution of the phases. Figure (4.36) shows the XRD pattern of standard tool steel substrate (Fe base, 4%Cr, 6.8%W, 5.3%Mo, 1.03% C). The mean strong peaks at 22.3˚, 44.8˚ and 64.9˚ are matching with the standard JCPDS No. 00-041-1224 of chromium iron (Cr-Fe). While the other diffraction peaks are excellent matches with the standard JCPDS No. 01-078-1990 of Iron Tungsten Carbide (Fe_3W_3C). These results are in close agreement with the results of the other work[104, 105]. See appendix B2

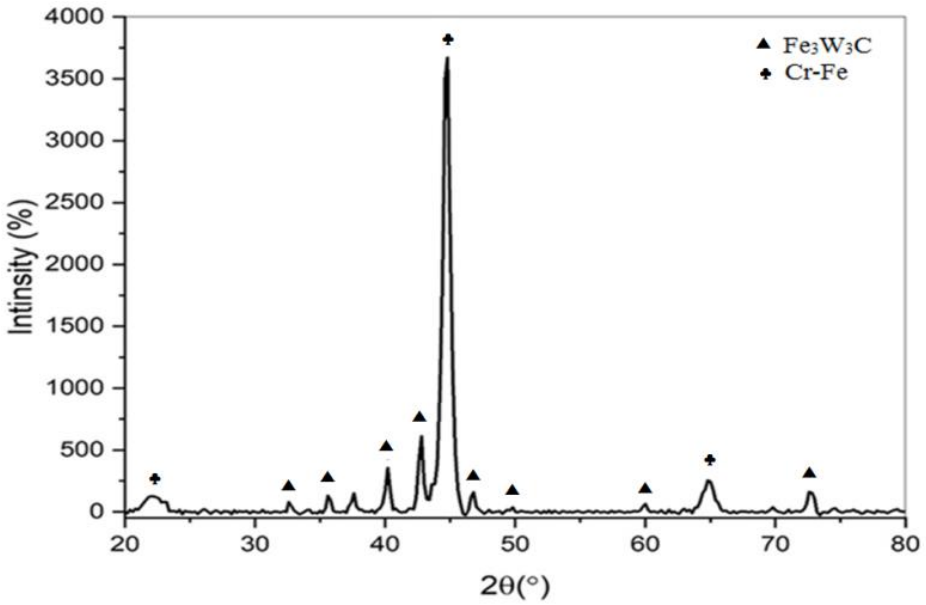

Figure(4.36). XRD pattern of tool steel HSS.

Figure(4.37)-a-b shows the XRD pattern of TiO_2 coating layer on a tool steel substrate, at speed 3 degree per minute. From the figure, it can be seen that most of the diffraction peaks of the tool steel substrate sample appeared. With addition diffraction peaks at diffraction angles of 27.69˚, 36.43˚, 42.67˚, 54.45˚, 62.8˚ and

70.03˚. Those results are excellent matches with the standard JCPDS No. 01-078-1510 of the rutile TiO_2 phase[106]. Figure (4.37)-a shows a two-hour calcination at 650°C, while Figure (4.35)-b shows a two-hour calcination at 500°C. As shown appendix B3

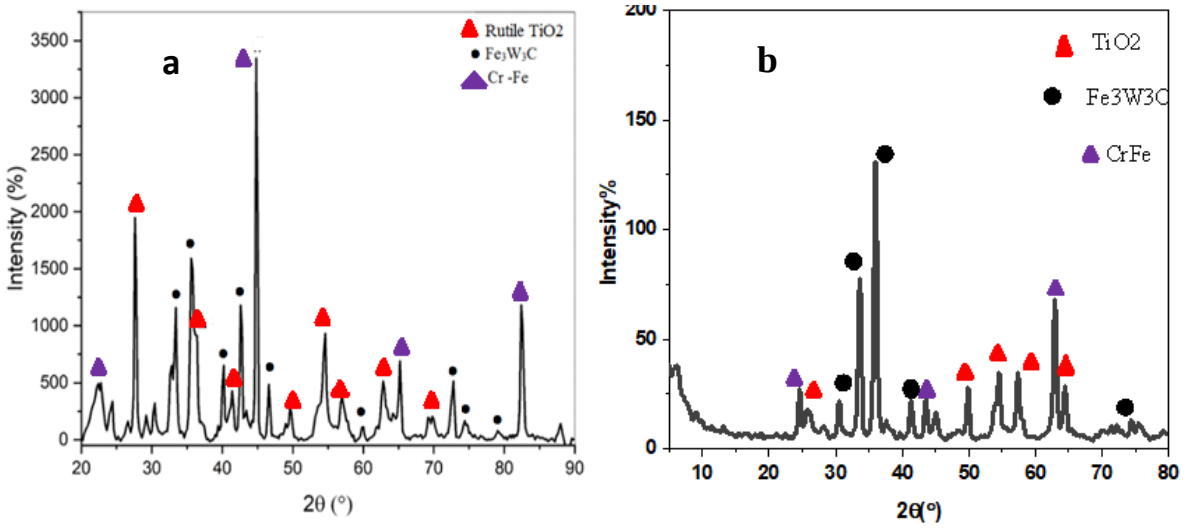

Figure (4.37): XRD of TiO_2 coating , (a): calcinated at 650℃for one hour,(b): calcinated at 500℃for two hours

Figure(4.38) shows coated specimens the XRD analysis of Al_2O_3. The intensity peaks were observed in the pattern matched with Fe_3W_3C and Fe-Cr composite and agree with the JCPDS No. reference pattern file of them. The X-ray diffraction peaks of 24.3˚, 33.3˚, and 49.6˚, are matching well with the JCPDS No. 00-034-0412 for Iron Chromium Oxide. The results showed the presence of one peak of γ-Al_2O_3 at a diffraction angle of 37.6º, 44.8˚, and 66.7º and this result corresponds to JCPDS No. 00-29-0063[107]. See appendix B4

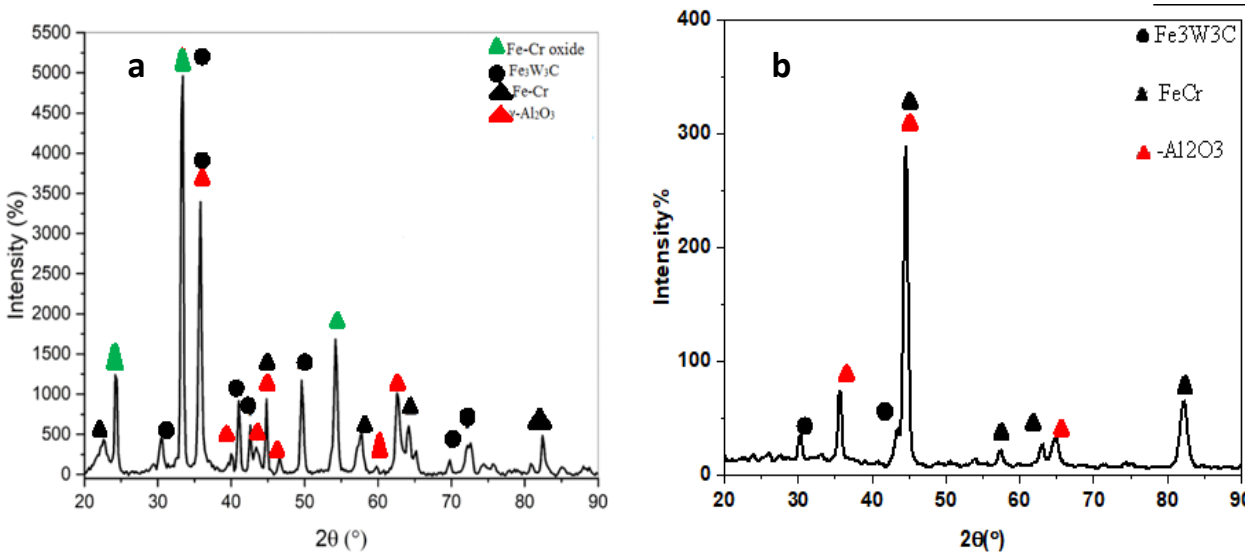

Figure(4.38):XRD of Al_2O_3 coating,(a): calcinated at 650℃ for one hour,(b): calcinated at 500℃for two hour

Figure (4.39) shows the XRD pattern of ZrO_2 coated specimen . The results show that most of the diffraction peaks are due to Fe-Cr oxide with high diffraction intensity at angles. This behavior is repeated in most Al_2O_3 coating due to the presence of an abundance of iron in the alloy, each layer that was deposited on the substrate was extremely thin (2 µm).

The results indicate that multi diffraction peaks appear at angles 27.5º, 35.1º, and 42.8º matches with the standard JCPDS No. 00-041-0017 of cubic ZrO_2 [108]. At 650℃ calcination temperature, the iron Chromium Oxide appeared with peaks of 24.3˚, 33.3˚, and 49.6˚, these are matching well with the JCPDS No. 00-034-0412. See appendix B5.

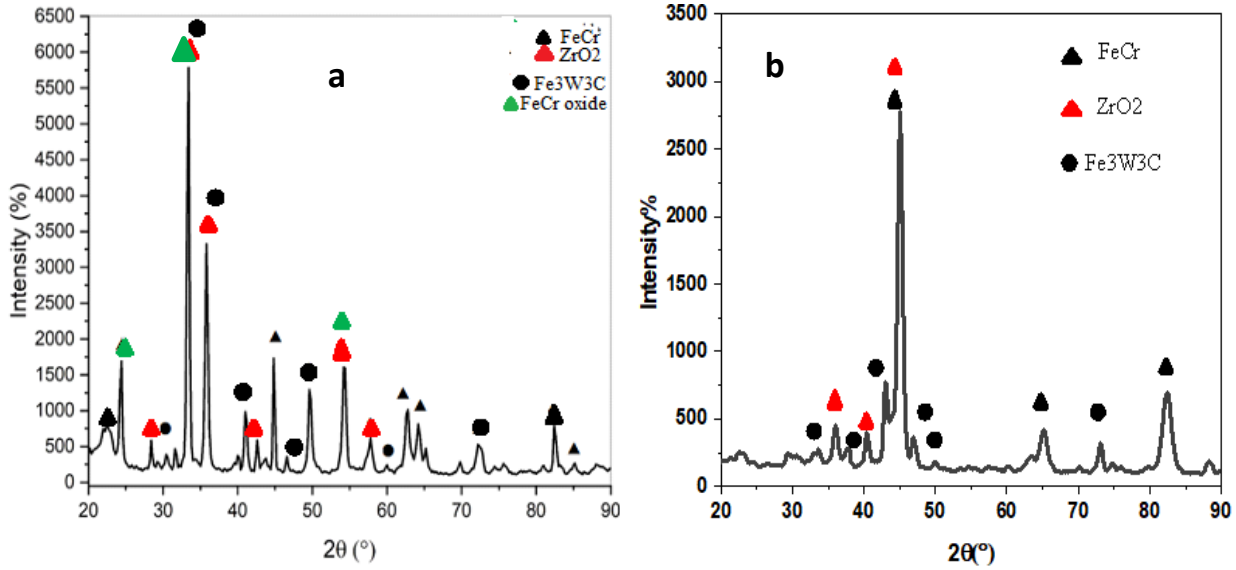

Figure(4.39): XRD of ZrO_2 coatings, (a): calcinated at 650℃ for two hour,(b): calcinated at 500℃for two hour

4.5. Surface Roughness

Figure (4.40) shows the AFM maps of the structured surfaces. Table (4-5) shows the surface roughness and the average of the particle size for each coating layer, see appendix B6-B8. In Al_2O_3 coated monolayer insert, the resulting layer is nanoparticles and some uncovered areas can be noticed in Figure 4.40 -a. The image (4.40)-c shows how the deposition of a double layer reduces the existence of unprotected areas. For coated inserts with triplex $TiO_2/Al_2O_3/ ZrO_2$ the image displays high homogeneity and good distribution, as well as minimal surface roughness compared with another inserts. The surface roughness for the coated two layers insert has less value 15.5nm, see Figure 4.40 -d.

Table (4.5): Surface roughness and average of the size for monolayer, multilayer coated, and uncoated cutting insert.

Type of tool	Surface roughness Ra (nm)	Average particle size (nm)
Monolayer coated/ Al_2O_3	48.4	89.38
Monolayer coated TiO_2	23.3	69.73
Monolayer coated ZrO_2	18.5	84.36
Douple layers coated/ TiO_2/Al_2O_3	15.5	72.31
Triplex layers coated/ $TiO_2/Al_2O_3/ZrO_2$	14	71.36
Uncoated insert	37.6	90.86

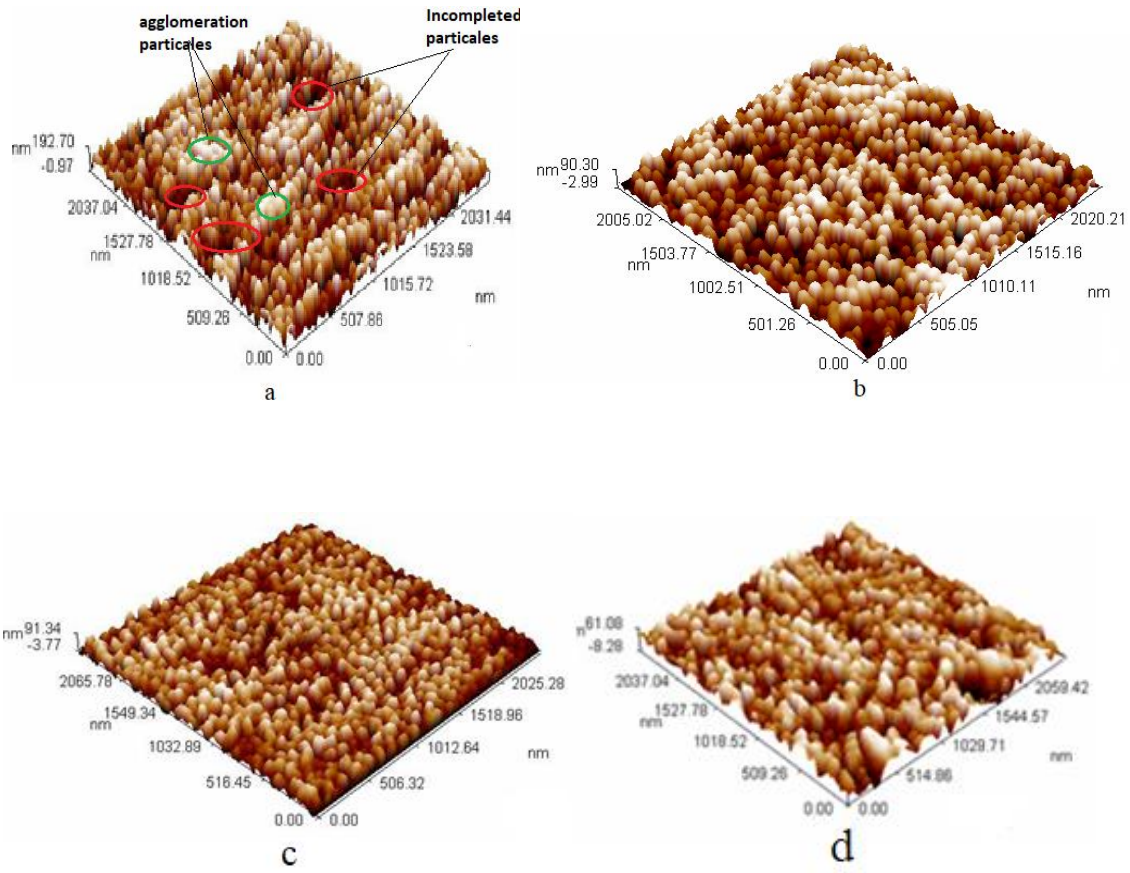

Figure (4.40): AFM (a): for (Al_2O_3), (b): (TiO_2) (c): for (Al_2O_3/TiO_2), (d): for $TiO_2/Al_2O_3/ ZrO_2$, (f): for (ZrO_2) (e): for HSS

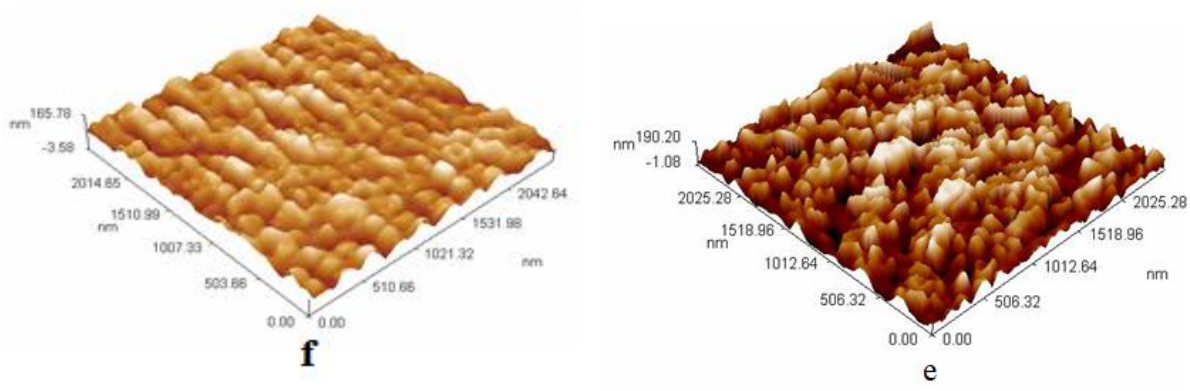

Continue Figure (4.40)

In Figure (4.41)-e describs the distribution for the deposition particles on the substrate HSS insert. When compared to another layer put on the substrate, $TiO_2/Al_2O_3/ZrO_2$ was deposited on the cutting insert with a high distribution.

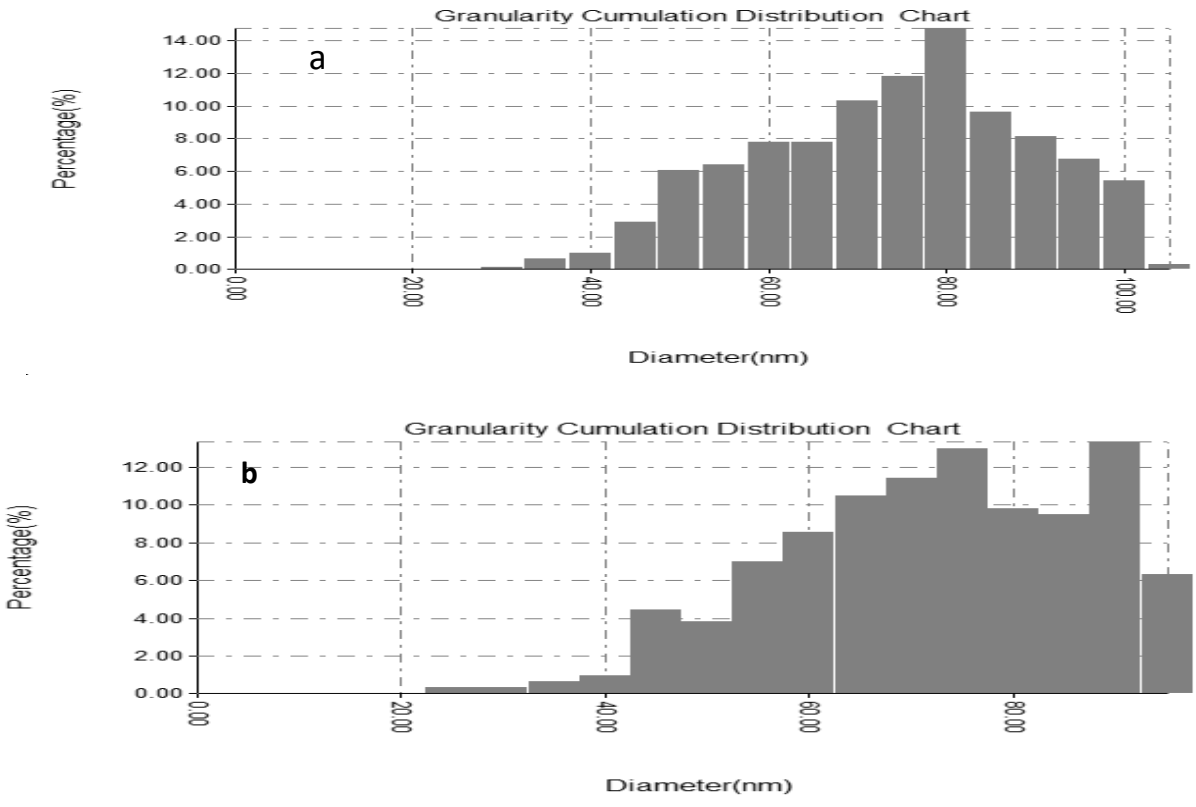

Figure (4.41): Degree of uniformity in distribution, (a): for TiO_2/Al_2O_3 ZrO_2(b) for TiO_2, (c) for Al_2O_3

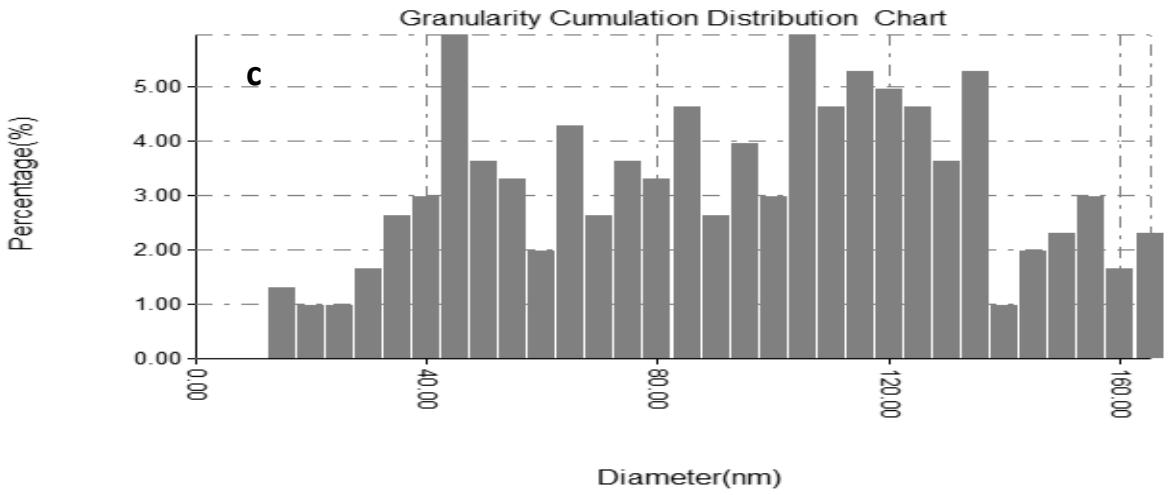

Continue Figure (4.41)

4.6. Physical tests

4.6.1. Coefficient of thermal conductivity

Thermal conductivity of the ceramic coatings was measured using the transient plane source (TPS). Generally, thermal conductivity of the ceramic coating are significantly lower than that of the bulk HSS. Triplex layer ($TiO_2/Al_2O_3/ZrO_2$) coating has the lowest thermal conductivity and thermal diffusivity (measured at 21℃ at room temperature (10.53W/m.k, 2.799 mm^2/sec respectively).

Thermal conductivity and thermal diffusivity of Al_2O_3 and TiO_2 coating layer at room temperature was measured to be (13.99W/m.k, 5.376mm^2/sec for alumina and 11.47 W/m.k, 4.932mm^2/sec for titania respectively) which was higher than that of monolayer ZrO_2 (9.640W/m.k, and 0.1866mm^2/sec).

Although pores could be counted as defects and have deteriorating effect on hardness, a certain quantity of pores are required to enhance the thermal resistivity and mechanical compatibility of coatings[109]. Andi M.Limarge et.al. referred into Al_2O_3 exhibits lower level interconnected porosity compared to ZrO_2. Therefore

thermal conductivity for mono layer ZrO_2 coated insert less than multilayer coated insert, see Figure (4.42). This result near the Andi M.Limarge et.al. [108]

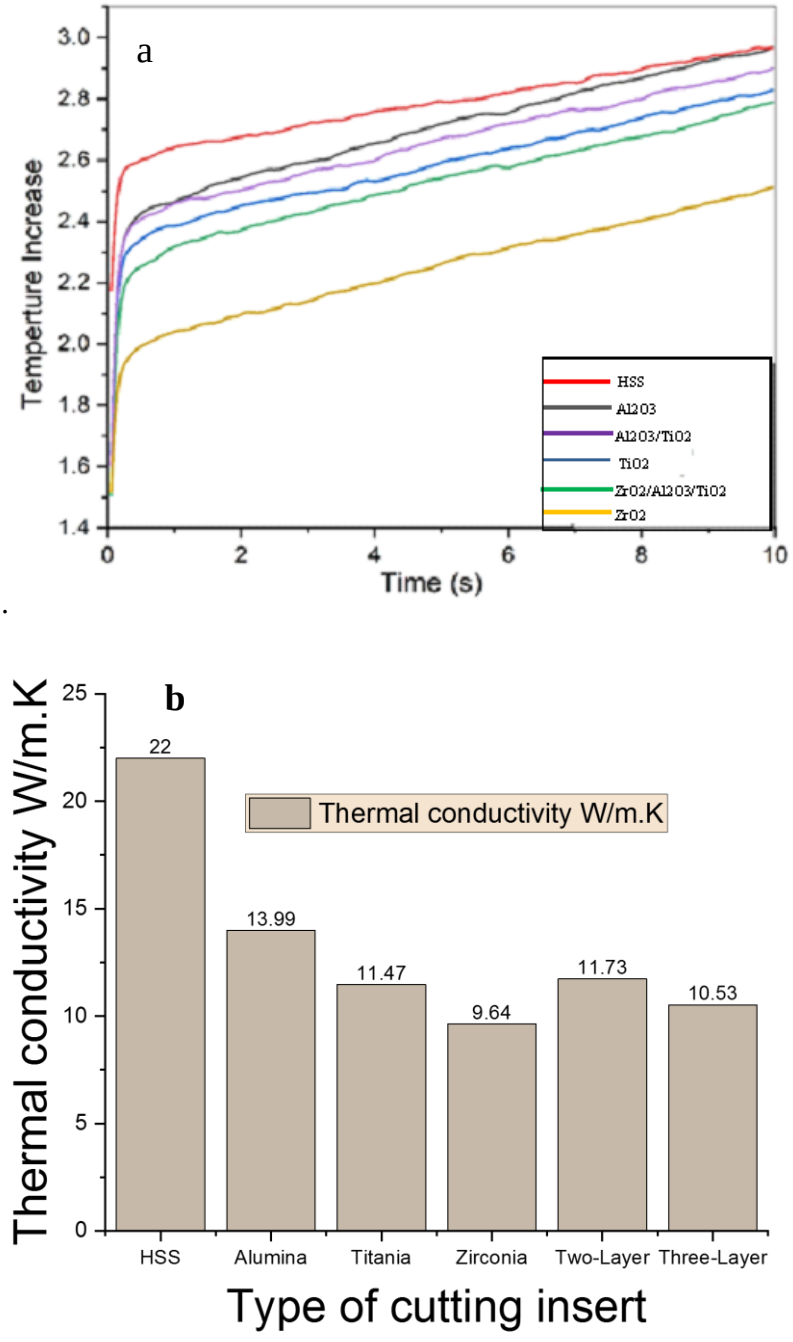

Figure (4.42): (a)Transient graph of thermal conductivity; (b) Thermal conductivity of specimens.

4.6.2. Coefficient of thermal expansion

Figure (4.43)-a-b demonstrated that the average thermal expansion coefficient of the titania ceramic coating is generally quite close to the thermal expansion coefficient of the bulk HSS ($11*10^{-6}$, $13*10^{-6}$ 1/K) approximately. While alumina ceramic coating and zirconia ceramic coating have ($3.652*10^{-6}$, $3.752*10^{-6}$ 1/K). That confirming titania coating in significantly eliminate the mismatch in physical properties between the metal alloy HSS and another ceramic coating which deposited on it.

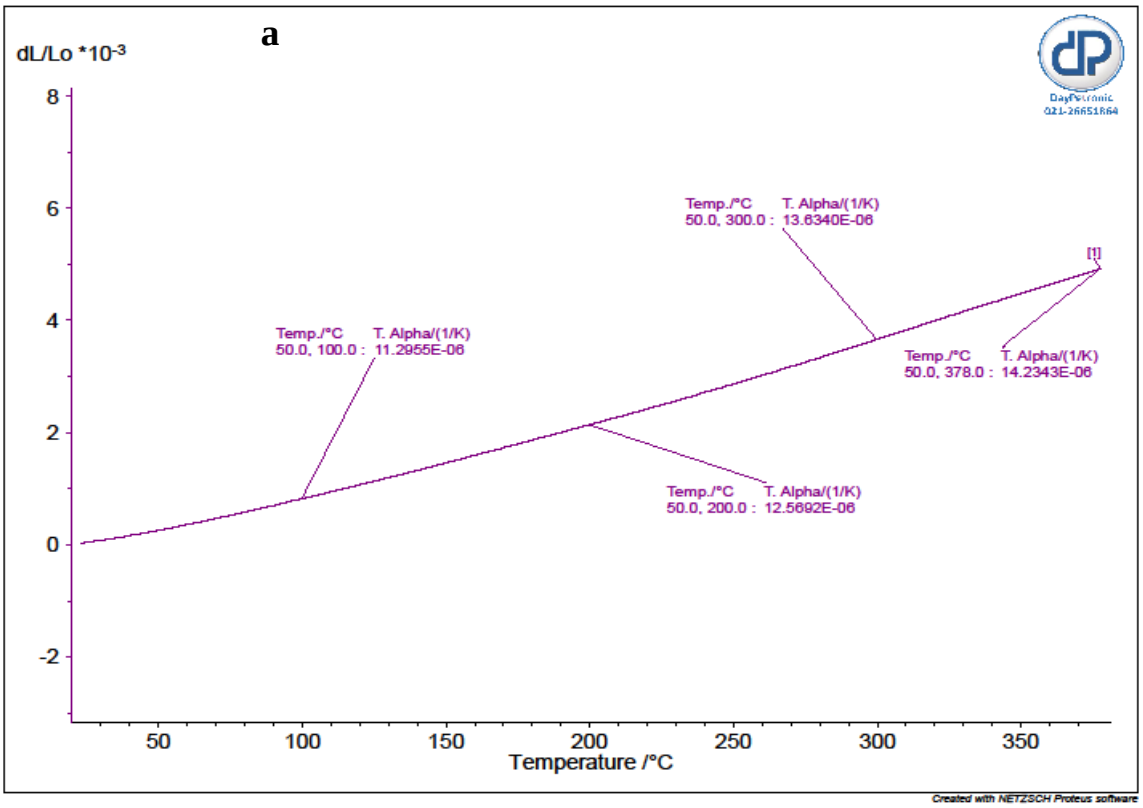

Figure (4.43): Coefficient of thermal expansion,(a): for HSS, (b): forTiO_2, (c): forAl_2O_3, (d): for ZrO_2

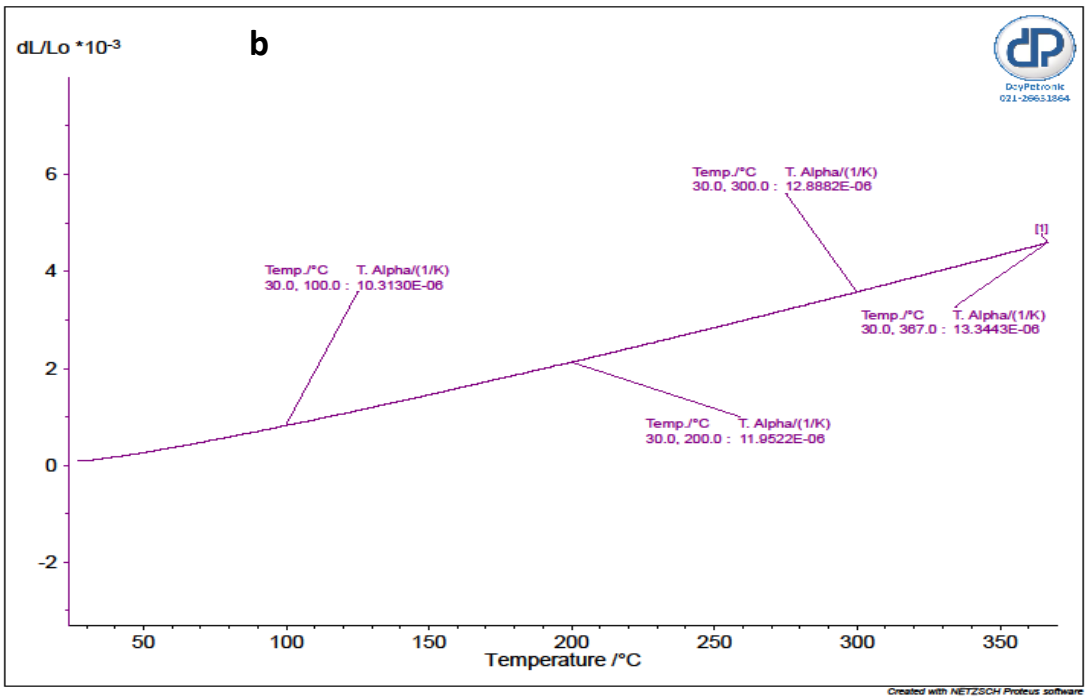
b
dL/Lo *10-3
Temp./°C T. Alpha/(1/K)
30.0, 300.0 : 12.8882E-06
[1]
Temp./°C T. Alpha/(1/K)
30.0, 100.0 : 10.3130E-06
Temp./°C T. Alpha/(1/K)
30.0, 367.0 : 13.3443E-06
Temp./°C T. Alpha/(1/K)
30.0, 200.0 : 11.9522E-06
6
4
2
0
-2
50
100
150
200
250
300
350
Temperature /°C
Created with NETZSCH Proteus software

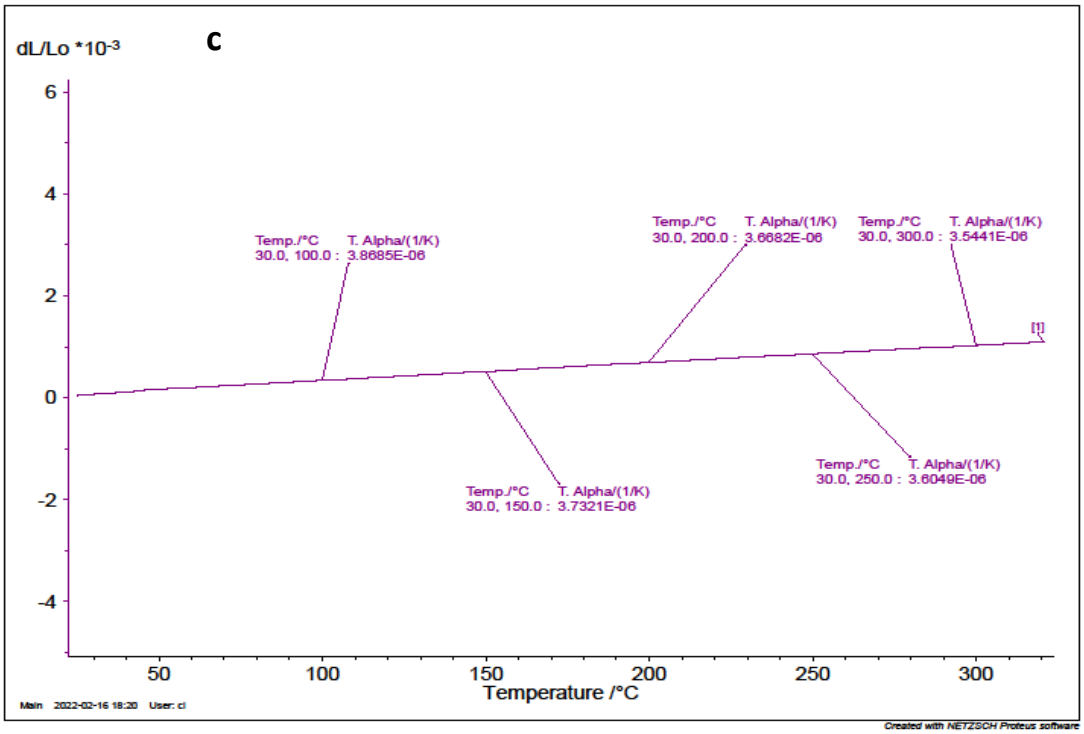
c
dL/Lo *10-3
Temp./°C T. Alpha/(1/K)
30.0, 100.0 : 3.8685E-06
Temp./°C T. Alpha/(1/K)
30.0, 200.0 : 3.6682E-06
Temp./°C T. Alpha/(1/K)
30.0, 300.0 : 3.5441E-06
[1]
Temp./°C T. Alpha/(1/K)
30.0, 150.0 : 3.7321E-06
Temp./°C T. Alpha/(1/K)
30.0, 250.0 : 3.6049E-06
6
4
2
0
-2
-4
50
100
150
200
250
300
Temperature /°C
Main 2022-02-16 18:20 User: ci
Created with NETZSCH Proteus software

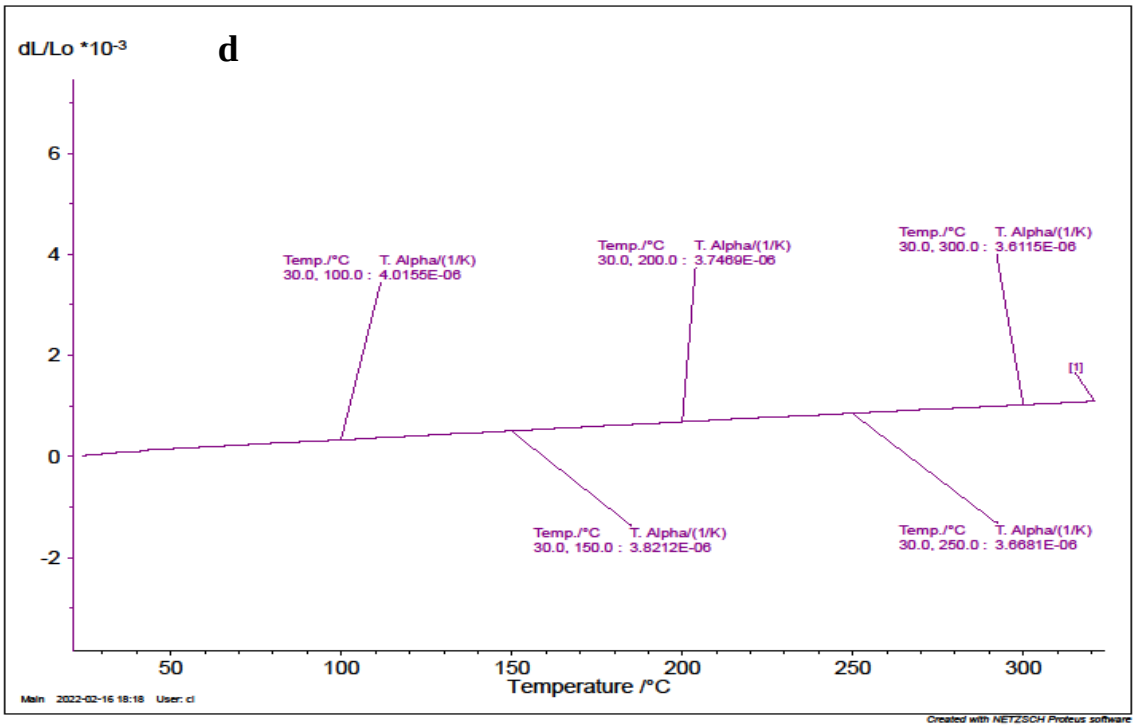

Continue Figure (4.43)

4.7. Mechanical test

4.7.1.Micro-hardness

The results from surface micro hardness of the substrate and coated inserts are shown in Figure (4.44) at 40X. Three layers coated inserts have the ability to improve a surface's micro hardness. These results can be attributed to the good adherence and uniform distribution of ceramic oxides deposited on the cutting insert. The hardness of the (monolayer Al_2O_3) cutting insert is lower than those of douple or triplex coating.

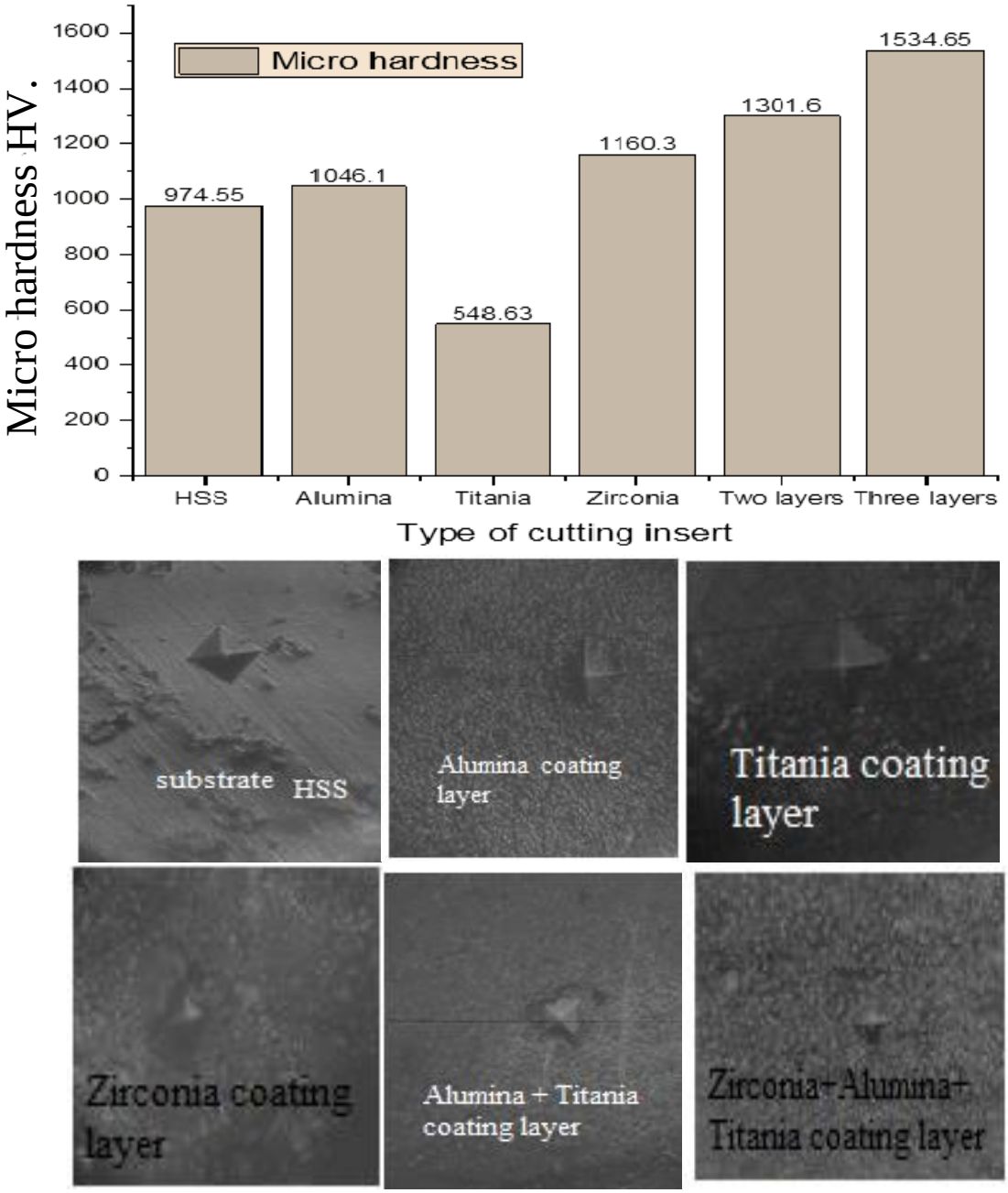

Figure (4.44): Hardness test and results 40X

4.7.2. Wear rate and coefficient of friction

The effect of the multilayer on the wear rate was studied at load (15N)for a period of 15 minutes. Due to high hardness of zirconia and alumina coatings (1160, 1046 HV respectively), and their good adhesion on HSS substrate, and highest hardness (1534 HV) of titania coating, coated inserts with three layers

essentially have the lowest rate of wear compared to uncoated, monolayer, and two layers coated inserts. Figure (4.45) shows that wear rate of uncoated insert is maximum but as douple and triplex layers coated insert wear rate is drastically reduced and it further drops down.

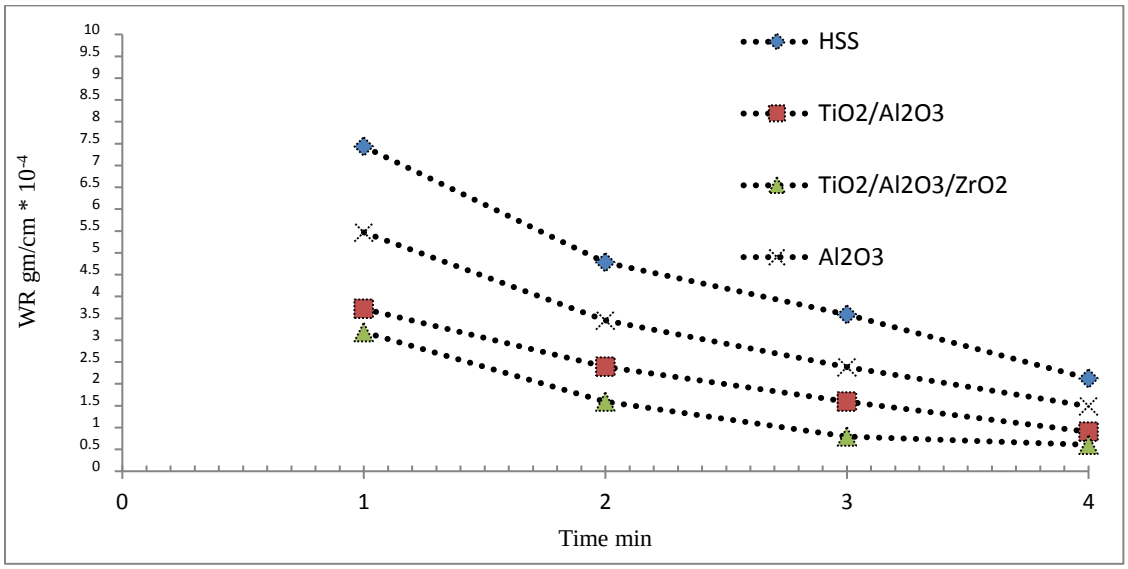

Figure (4.45): Wear rate test for uncoated insert and coated insert

Figure (4.46) shows a deep and wide wear track; the lamellar debris of uncoated insert that delamination happens through wear tests. In contrast coated insert could have less wear rate due to prevent the generation of excessive heat through the wear test; thus, a smooth surface along without plastic deformation and with fine grooves can be observed in the SEM image.

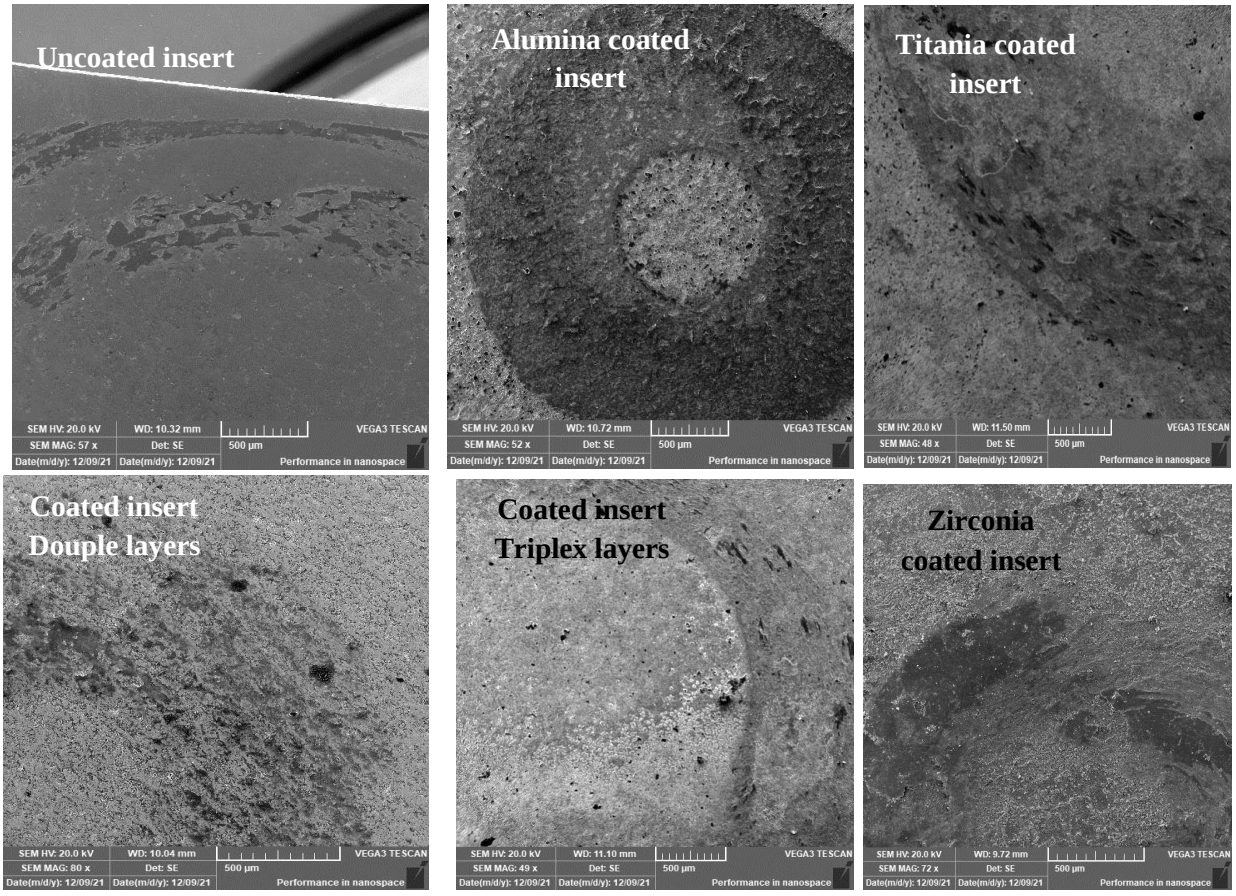

Figure (4.46): SEM micrographs of wear track of coated and uncoated inserts

The behavior of the coefficient of friction (μ) for uncoated and coated inserts versus sliding distance is shown in Figure (4.47).

The multilayer coated HSS has slightly lower initial friction coefficients than those of uncoated HSS. The friction coefficient for an uncoated insert was 0.59, while they were 0.12 and 0.25 for coated inserts with three layers and two layers, respectively. This mutation has been linked to a high level of chemical inertness [1]. In addition, the ceramic coatings have a decreased thermal conductivity, a good adhesion test for triplex and douple layers (93.6 and 89.56 Mpa, respectively), and a minimum surface roughness of 14,15.5 nm from obvious examination.

Monolayer Al_2O_3 layer, on the other hand, has the highest friction value when compared to an uncoated insert, which is associated with weak adhesion of 10.65 MPa and non-homogeneous surface roughness of 48 nm.

Despite having a minimum adhesive strength of 11.15MPa, ZrO_2 has a friction coefficient of 0.46, which is lower than monolayer Al_2O_3 and uncoated inserts due to their low surface roughness of 18 nm. The behavior of the coefficient of friction (μ) for uncoated, Al_2O_3, TiO_2 and multilayer coating cutting insert (TiO_2 /Al_2O_3), (TiO_2/Al_2O_3/ZrO_2) versus sliding distance is shown in Appendix B9.

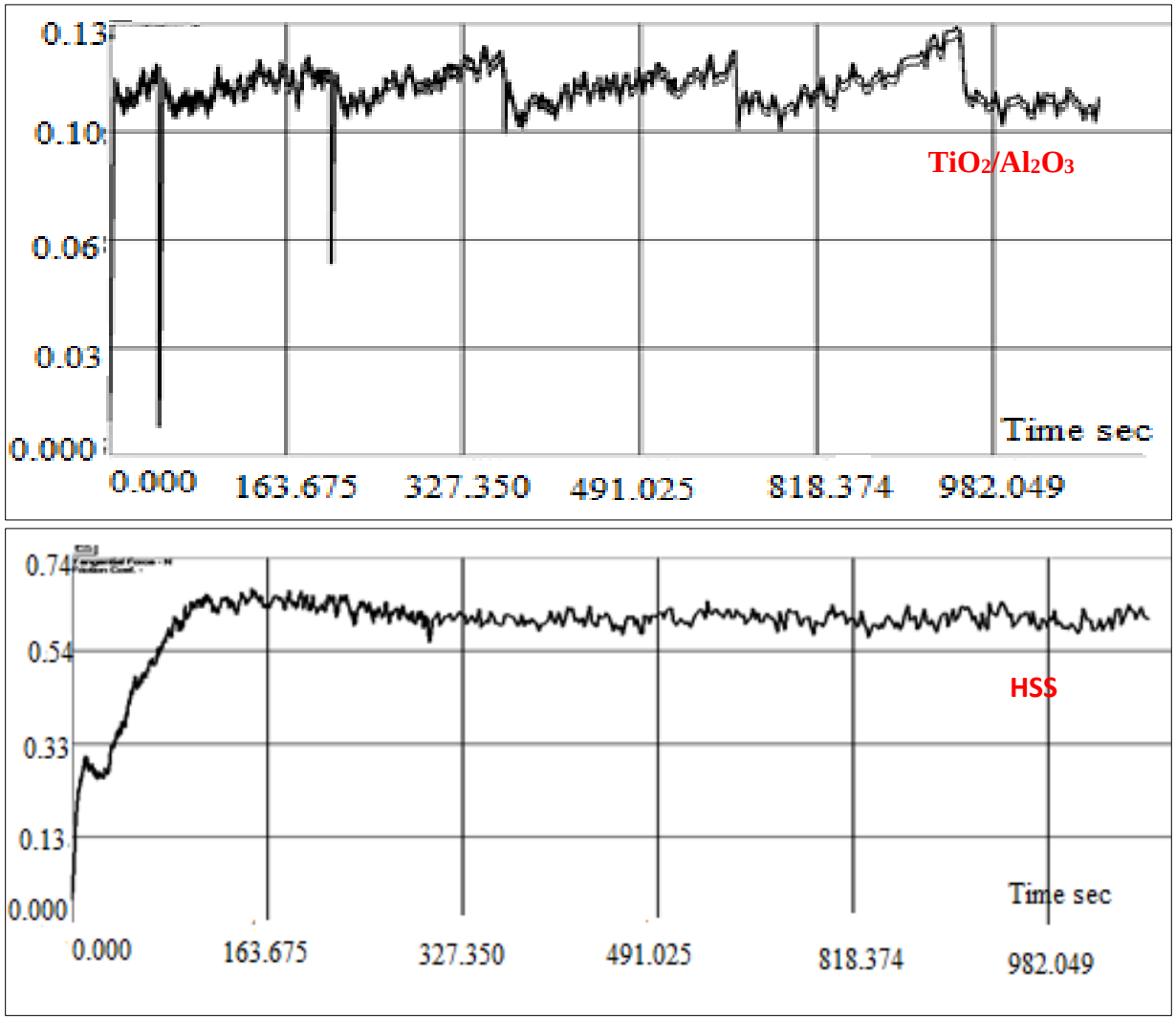

Figure (4.47): Coefficient of friction versus sliding distance.

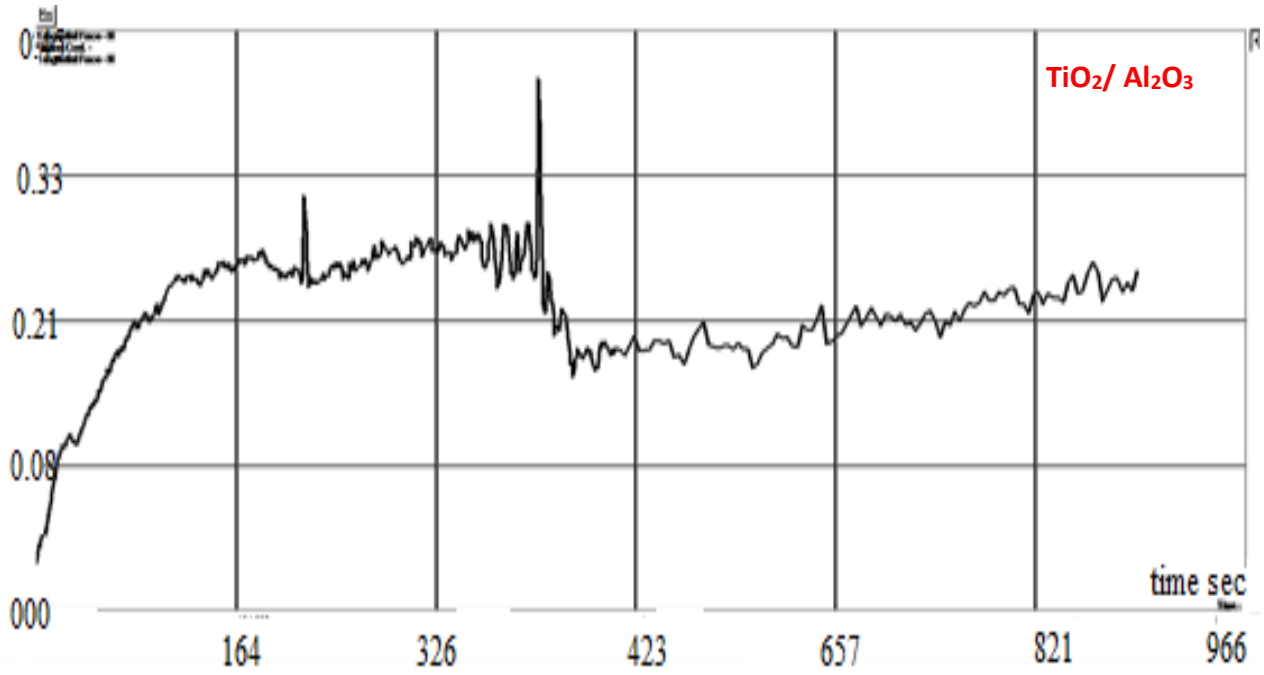

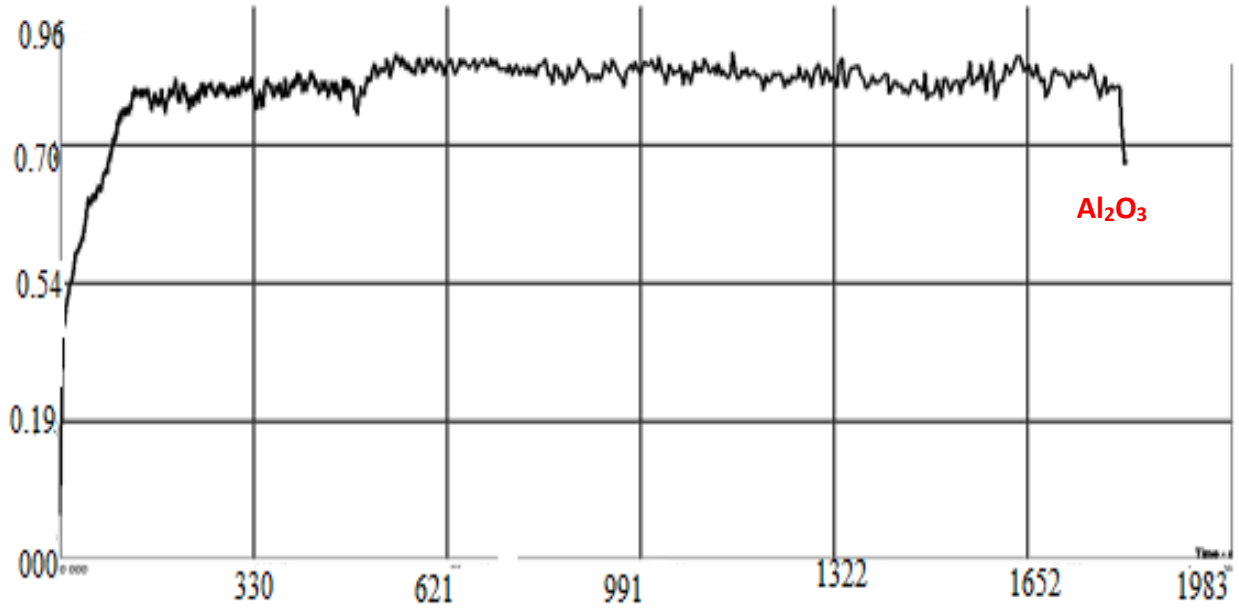

Continue Figure(4.47)

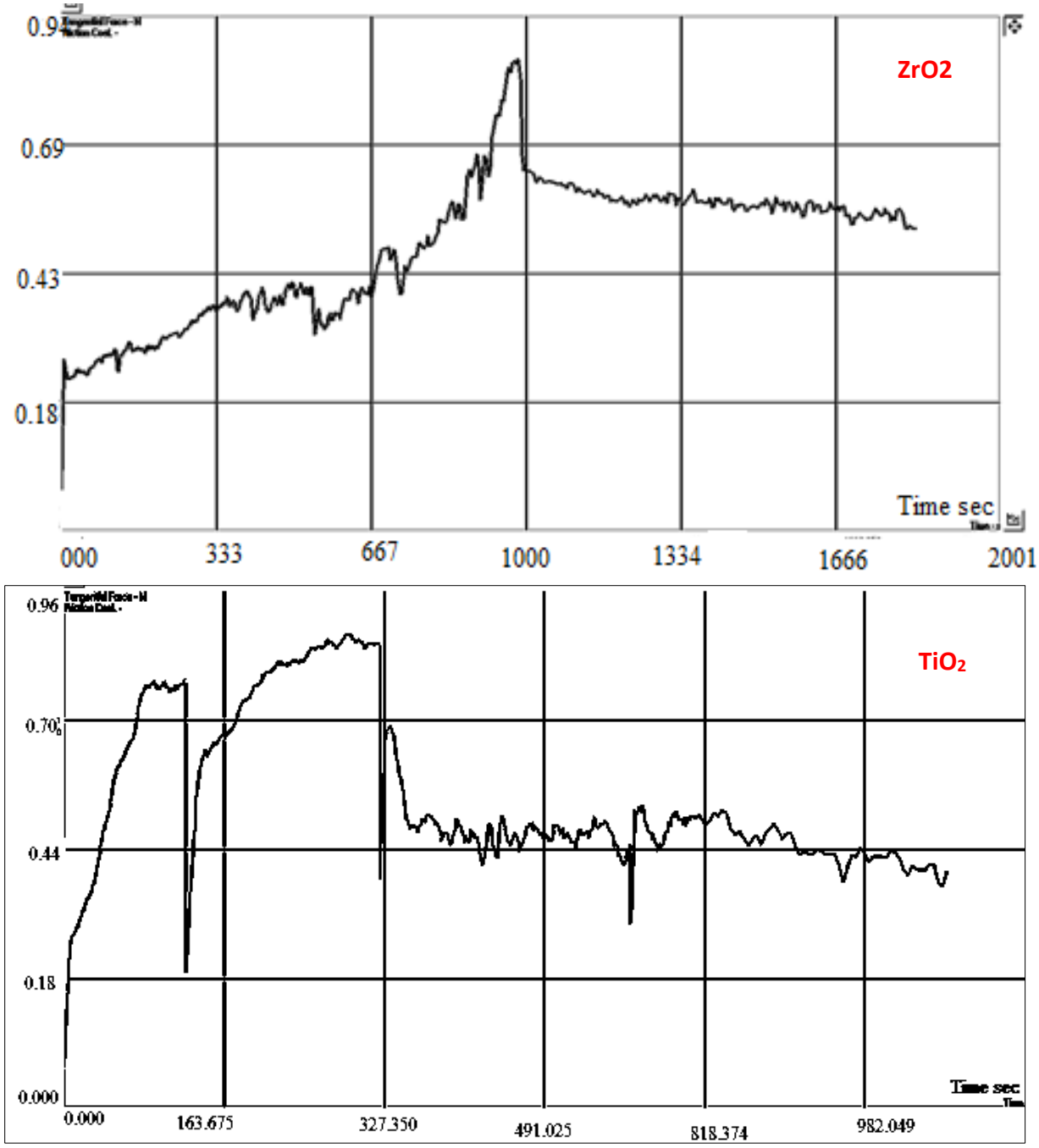

Continue Figure (4.47)

Figure (4.48) shows the coefficients of friction at 15 min for uncoated and coated inserts that agree with the study of Rezende [1].

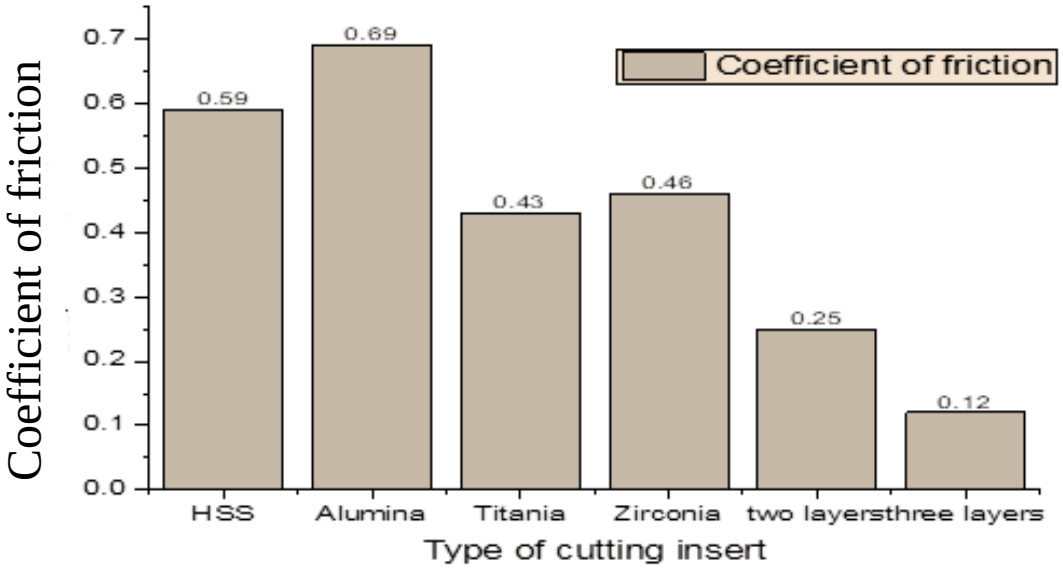

Figure (4.48): Coefficients of friction for cutting inserts

4.8. Machining Test

Three cutting velocities (56, 88, and 112 m/min) for each of which three feeds 0.065, 0.165 and 0.265 mm/rev were used with the three depths of cut (0.2, 0.5, and 0.7mm) as shown in Table (4.6).

Table (4.6): The cutting parameters and their levels for coated and uncoated cutting inserts

Parameters		Coded/Actual levels		
		1	2	3
Cutting velocity (m/min)	v	56	88	112
Feed (mm/rev)	ʃ	0.065	0.165	0.265
Depth of cut (mm)	t	0.2	0.5	0.7

The experiment was planned by considering three levels for each of the three input process parameters. The selected responses were the tool life, the surface roughness, and the cutting temperature.

The machining experiments were designed for each cutting insert(uncoated, coated monolayer Al_2O_3 with 10.65 Mpa adhesive strength at 5 sec immersion time, TiO_2/Al_2O_3 coated insert at 30 sec immersion time with 89 MPa in adhesive strength, and TiO_2 /Al_2O_3 /ZrO_2 coated insert at immersion time 30 sec with 93 MPa adhesive strength), based on Taguchi L9 orthogonal array via Mintab 17 software.

Then, to determine the degree of improvement achieved for coated HSS inserts, it compared to carbide inserts under the same machining conditions. The maximum wear width of carbide cutting insert was (0.3 mm) utilized as a flank wear criterion ISO 3685.

4.8.1.Tool life

Field emission scanning electron microscope type (inspect F50)was used to measure the width of the flank wear. The tool life was measured according to the flank wear criterion. A maximum flank wear width of 0.4mm was considered as the criterion of the tool life [95].

Figure (4.49) is evident which depicts FE-SEM of the machining zone that excess in width of wear with uncoated HSS insert and monolayer coated insert compared with multilayer coated HSS insert at the final minute which exceed 0.4mm flank wear.

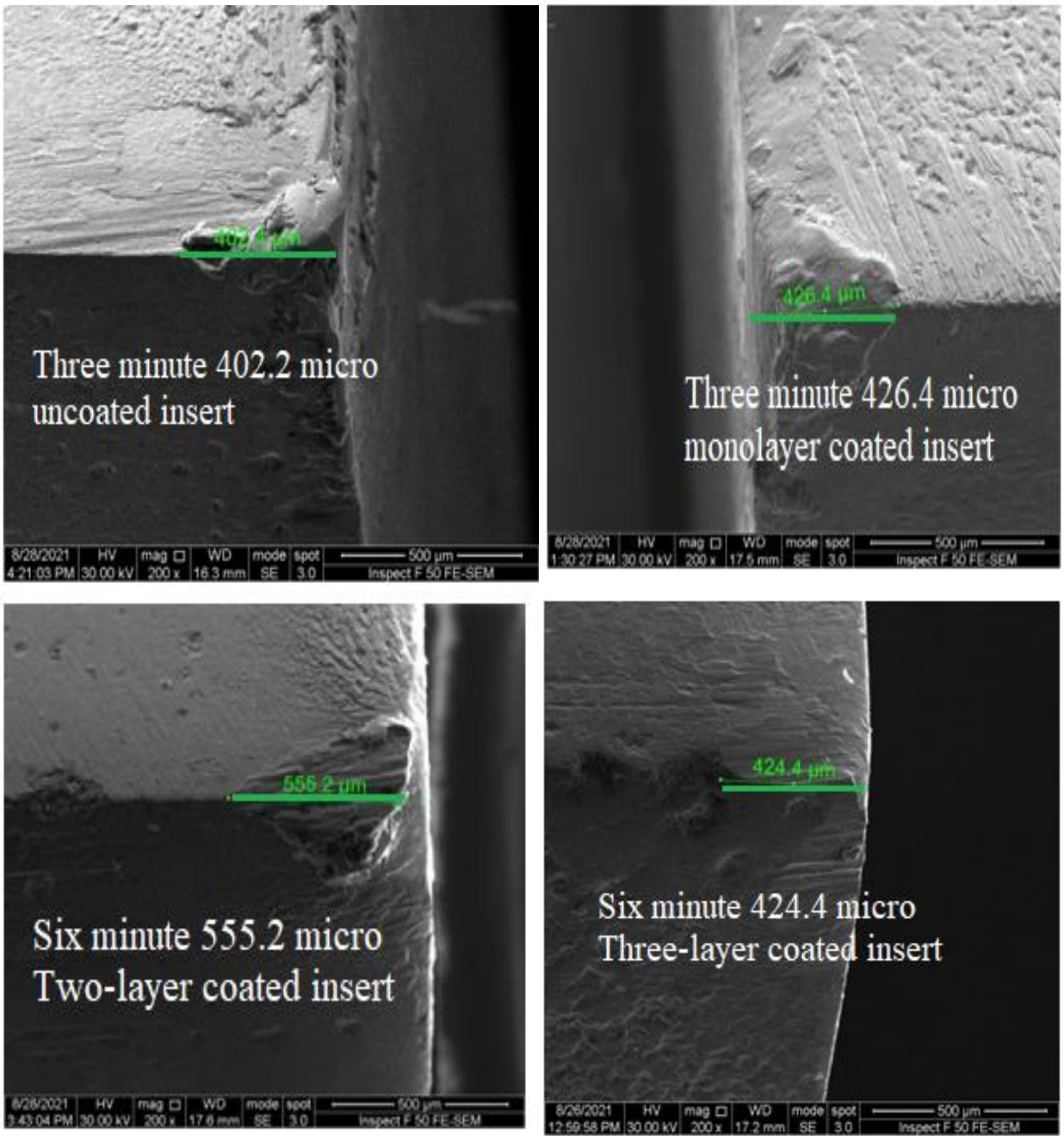

(a) 56m/min, 0.065 mm/rev, 0.2mm

Figure (4.49): The evaluation of maximum flank wear at failure minute during machining

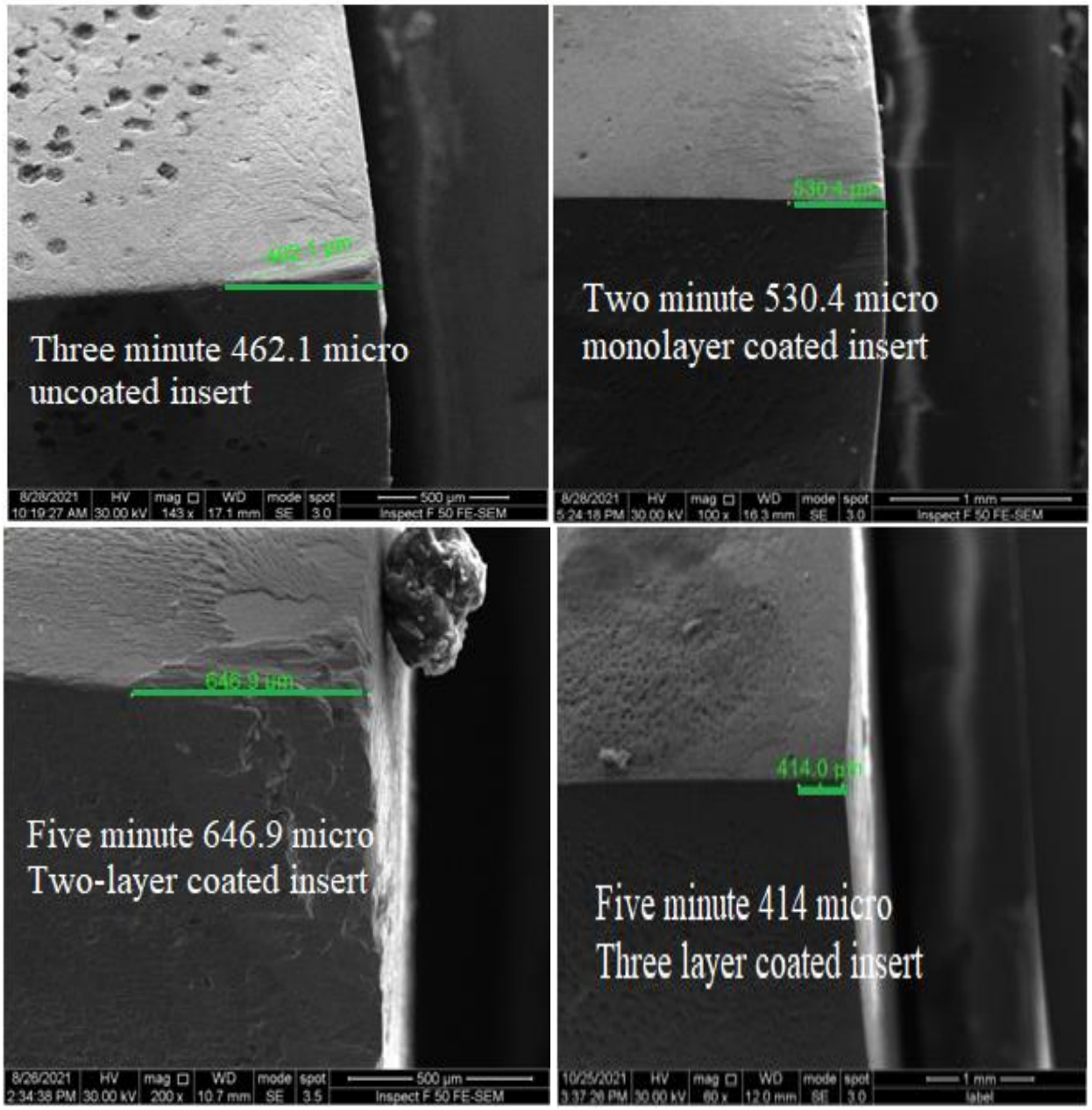

(b) 56m/min,0.165mm/rev, 0.5mm

Continue *Figure (4.49)*

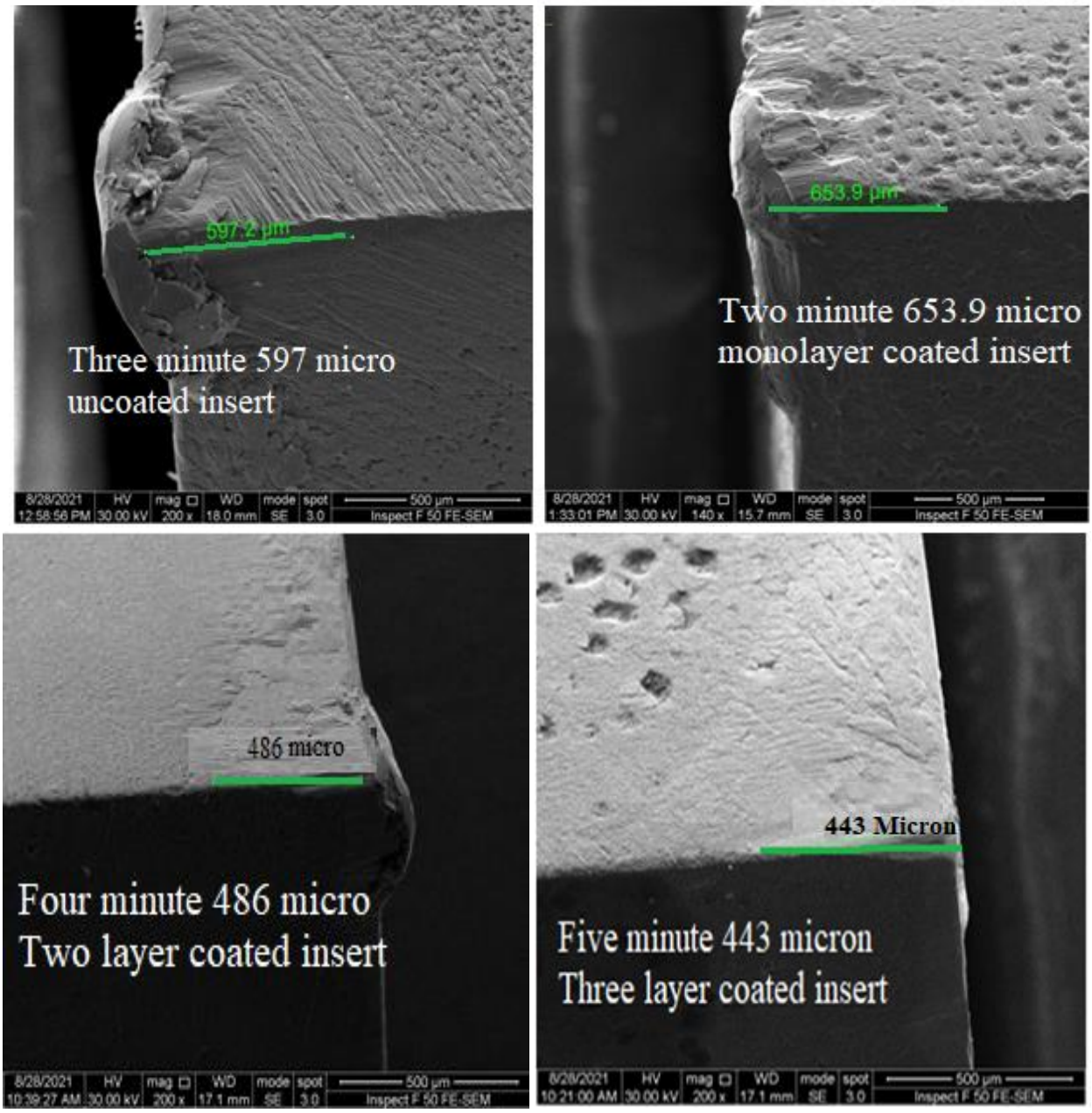

(c)56m/min, 0.265 mm/rev, 0.7mm

Continue *Figure (4.49)*

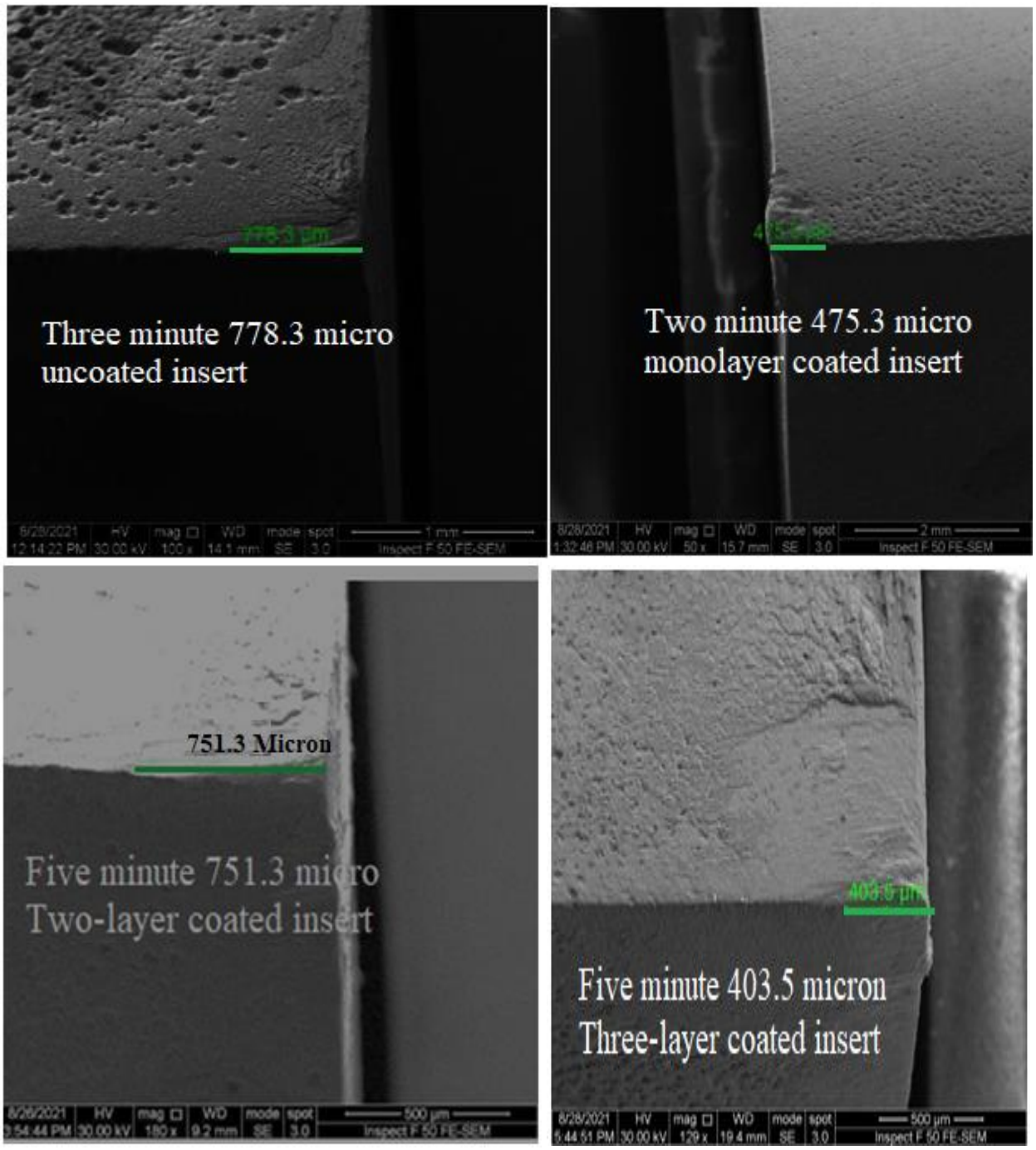

(d)88m/min, 0.065mm/rev, 0.5mm

Continue *Figure (4.49)*

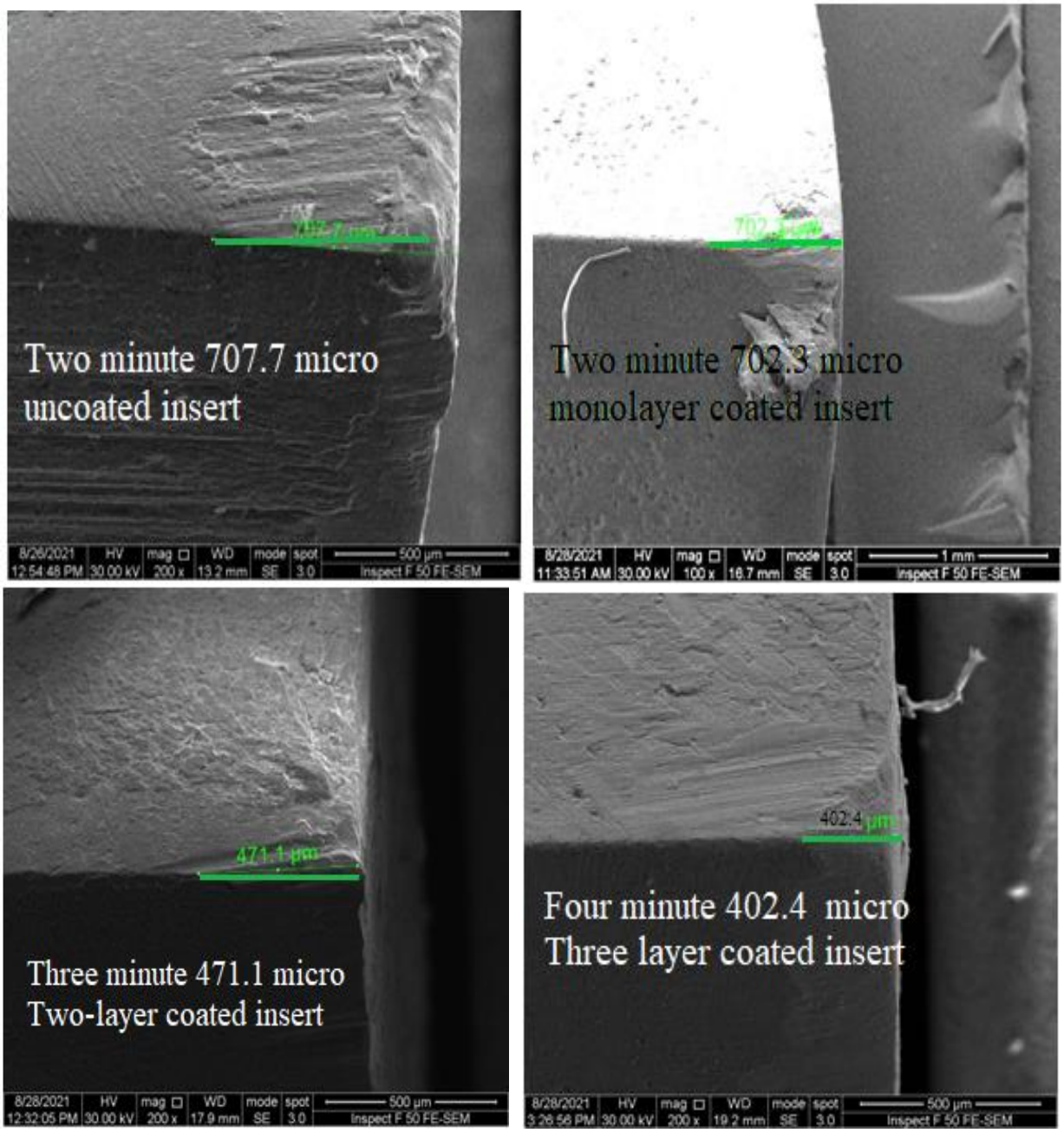

(e)88m/min, 0.165mm/rev, 0.7mm

Continue *Figure (4.49)*

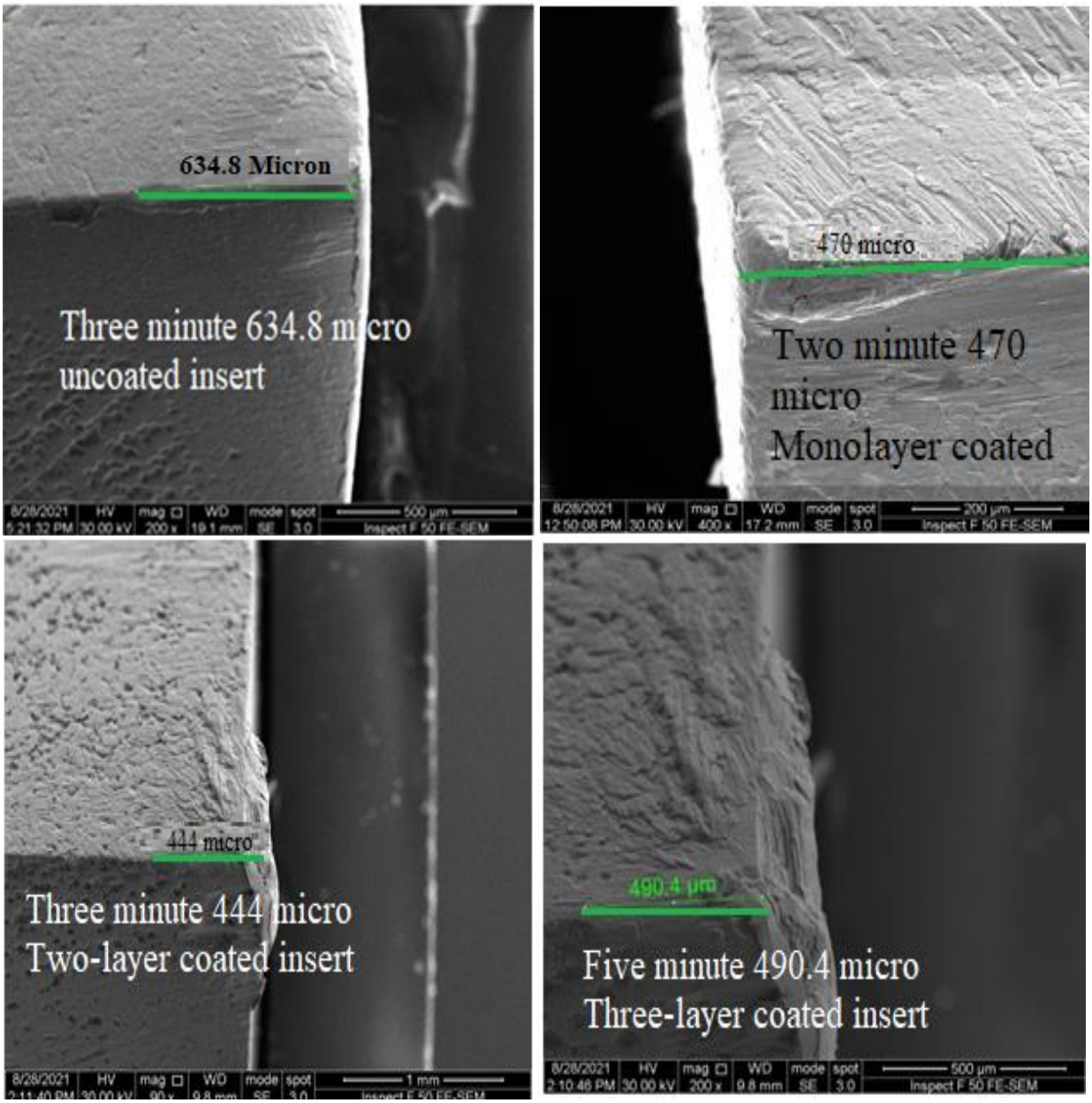

(f)88m/min, 0.265mm/rev, 0.2mm

Continue *Figure (4.49)*

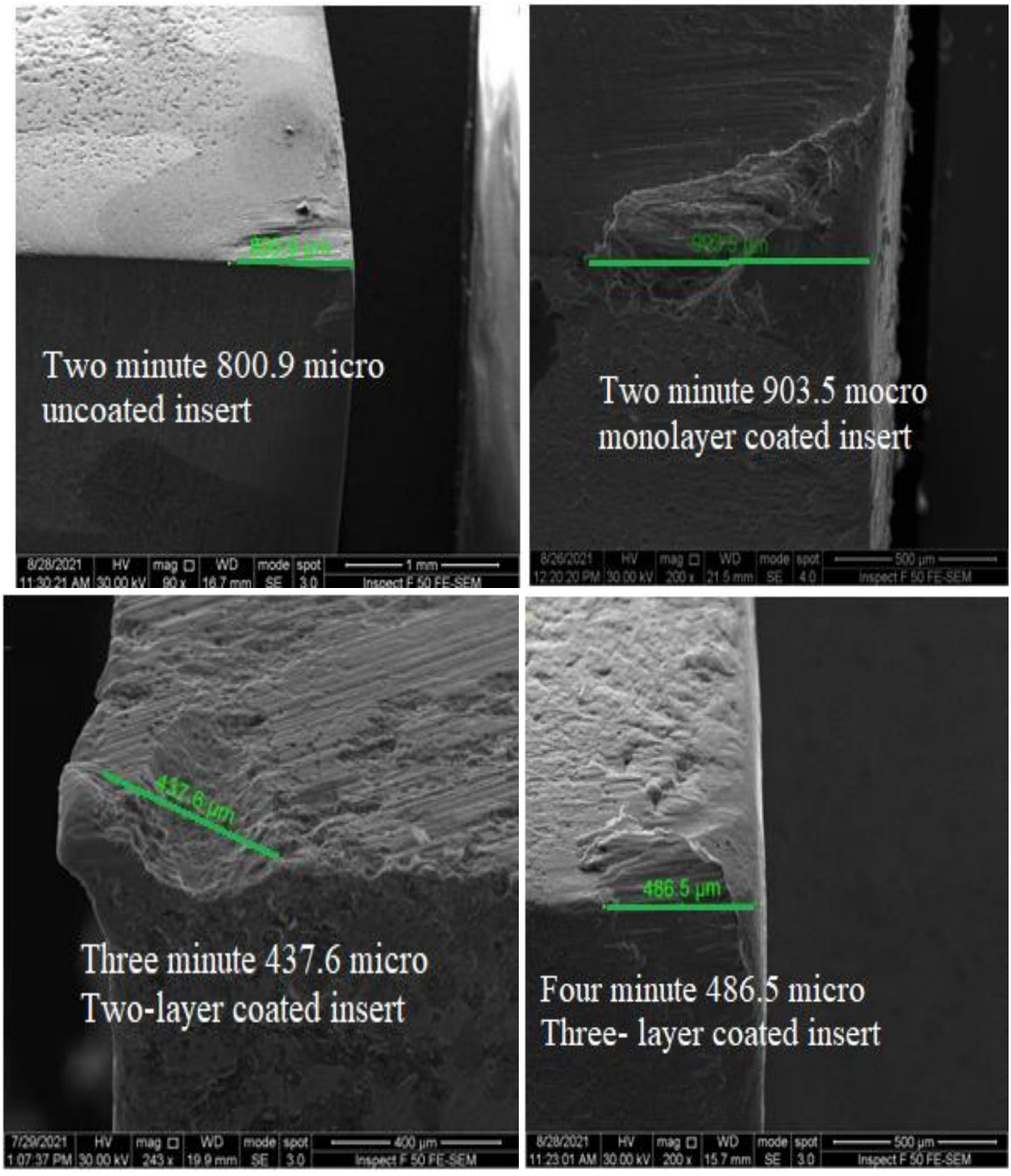

(g) 112m/min, 0.065mm/rev, 0.7mm

Continue *Figure (4.49)*

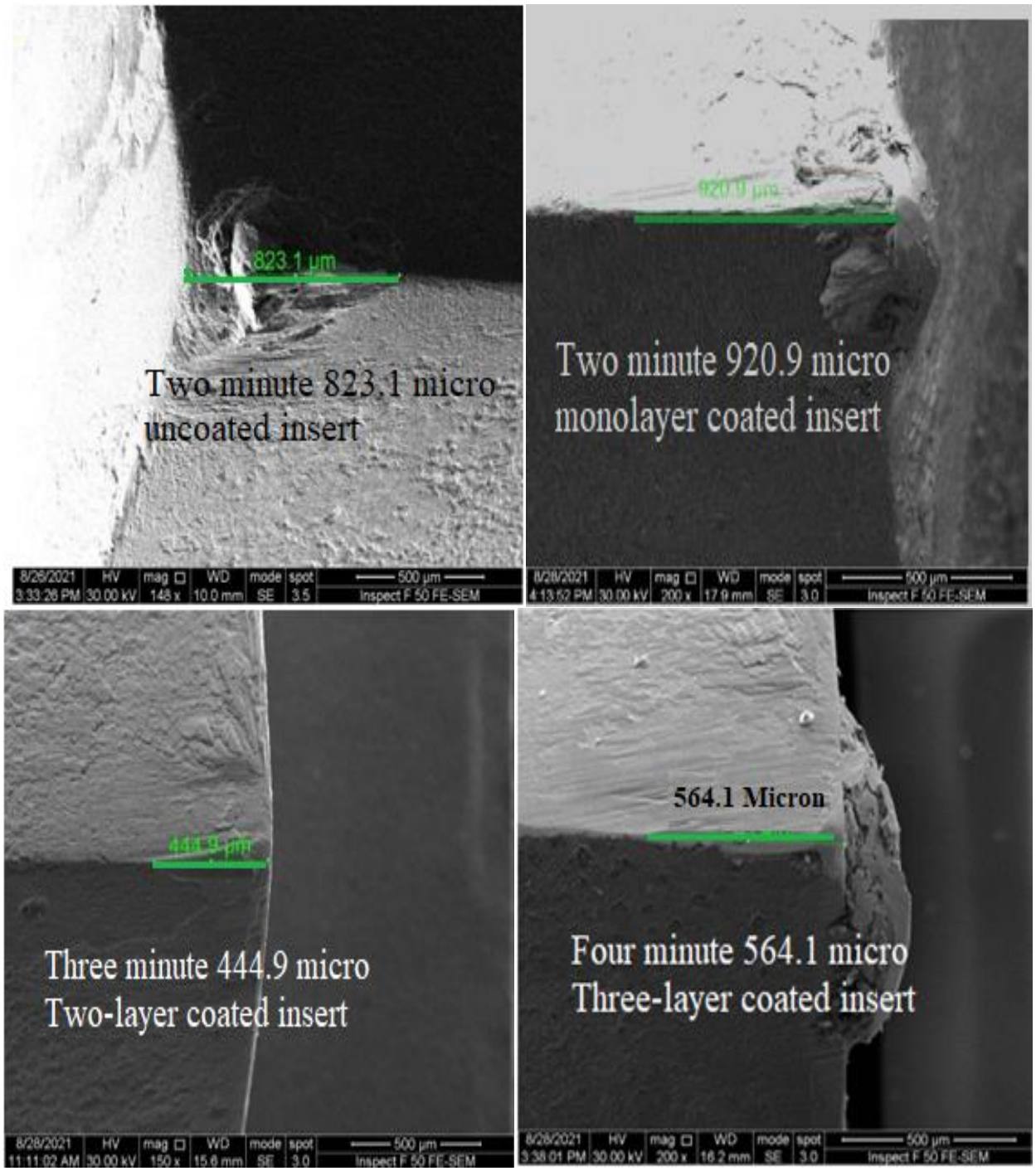

(h) 112m/min, 0.165mm/rev, 0.2mm

Continue *Figure (4.49)*

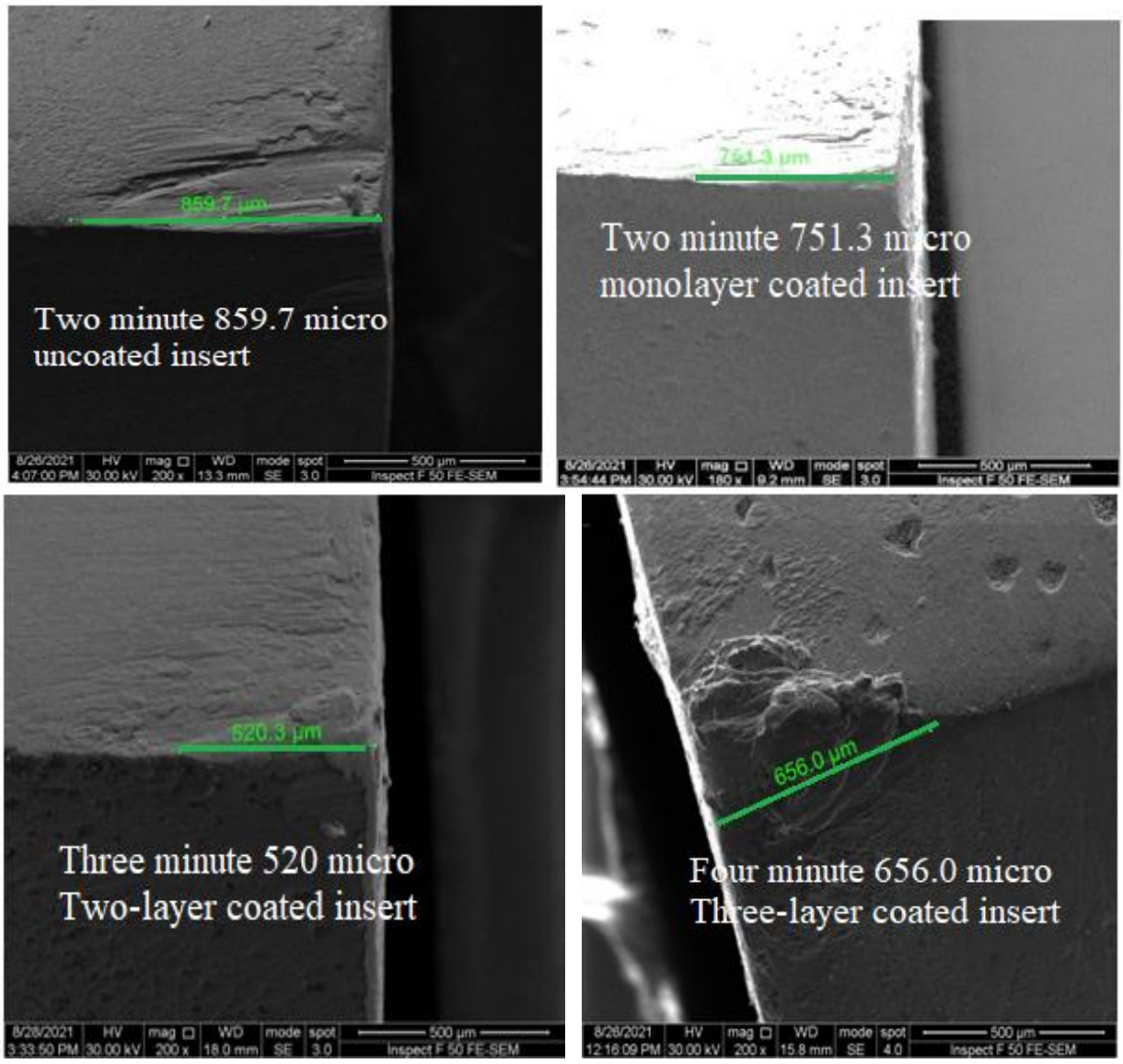

(k)112m/min, 0.265mm/rev, 0.5mm

Continue Figure (4.49)

Figure (4.50)represents examples for the method used for estimating the tool life according to used machining conditions. The results showed that the maximum tool life was recorded for the multilayer (triplex) coated HSS insert. This is attributed to the good chemical inertness, low friction coefficient (0.12) and good adhesive strength 93.60 MPa, good wear resistance, high hardness (1534.6) HVand lower thermal conductivity of the ceramic coating (10.53 W/m.K) [109].

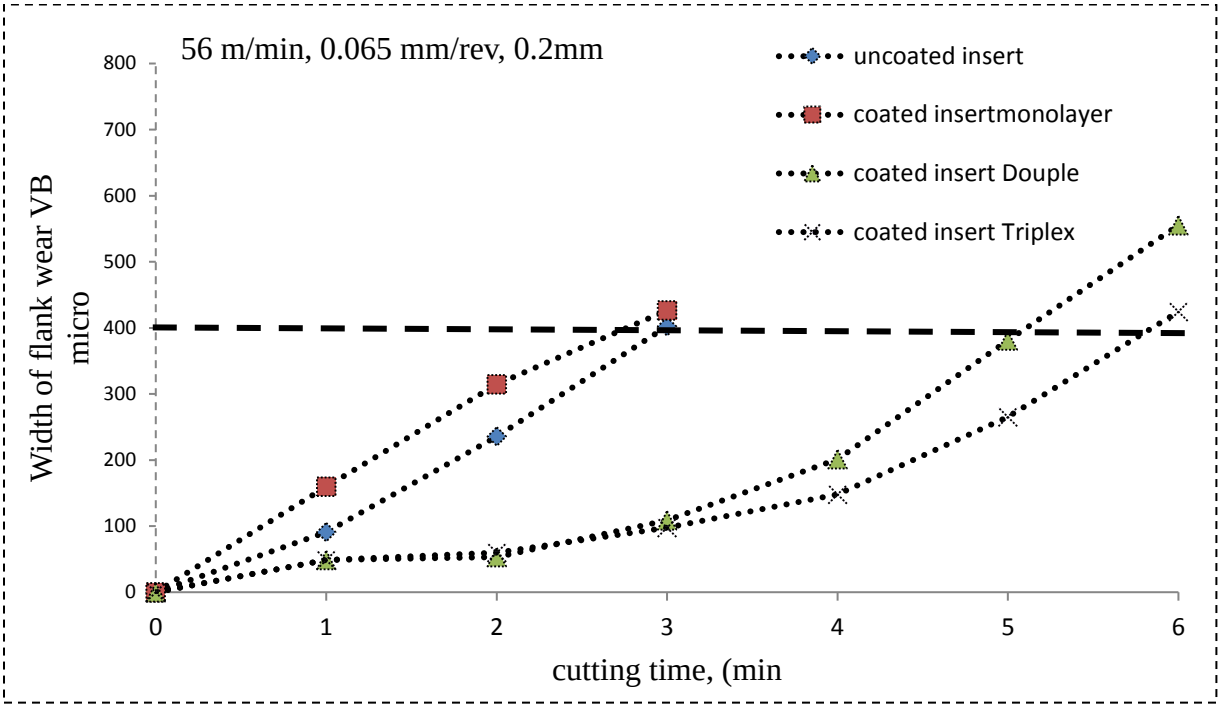

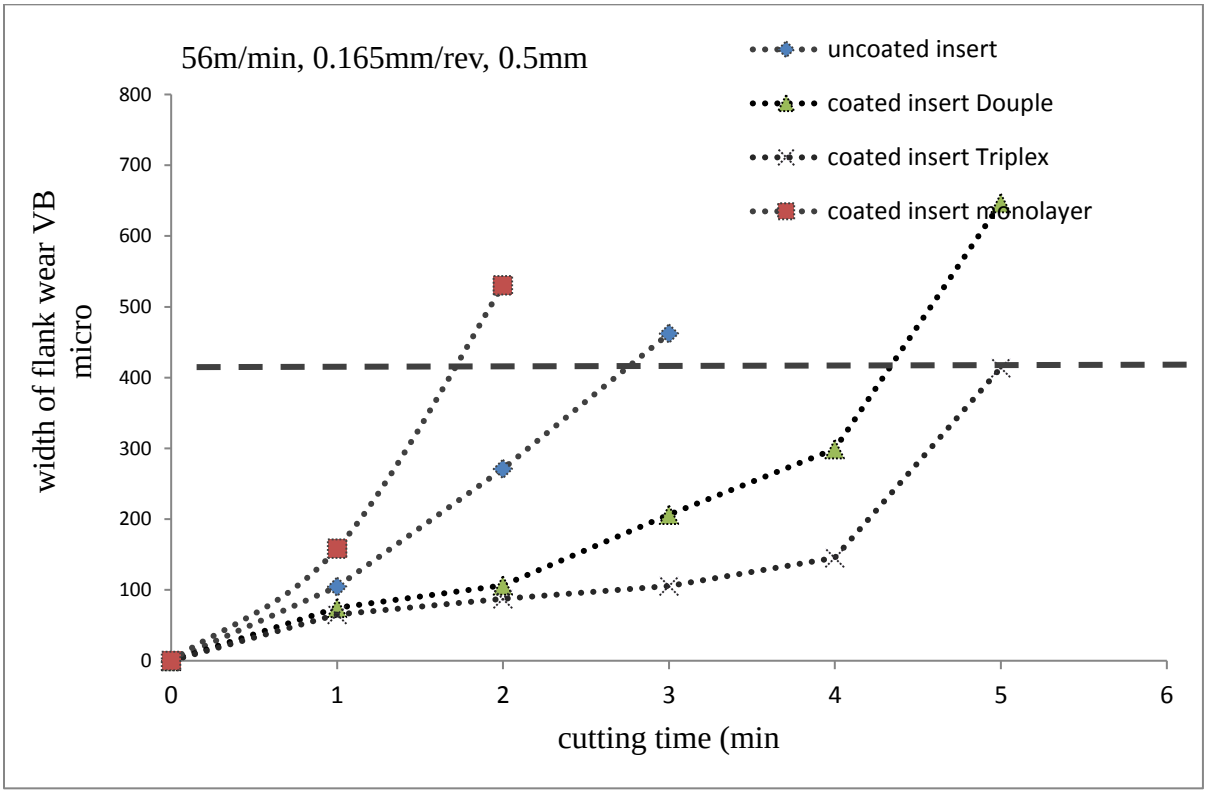

Figure (4.50): Estimation results of the tool life for the coated and uncoated HSS cutting inserts

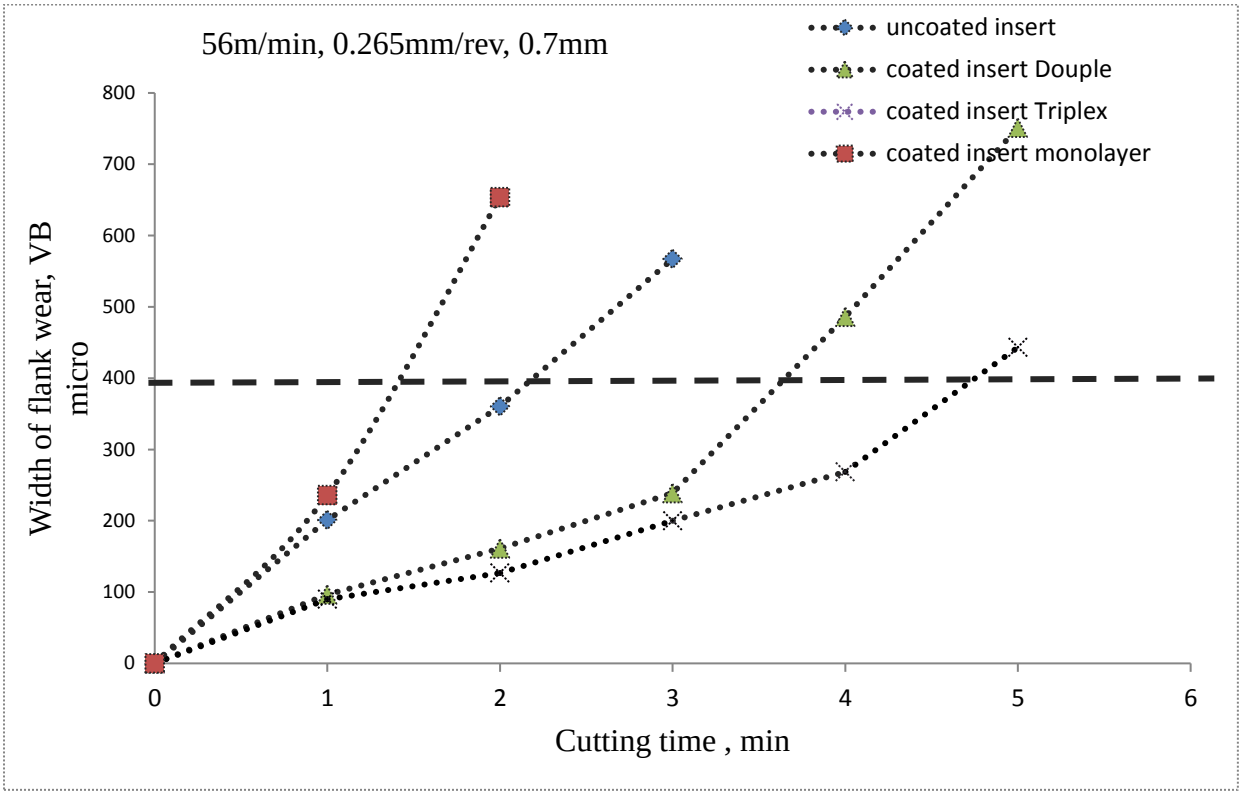

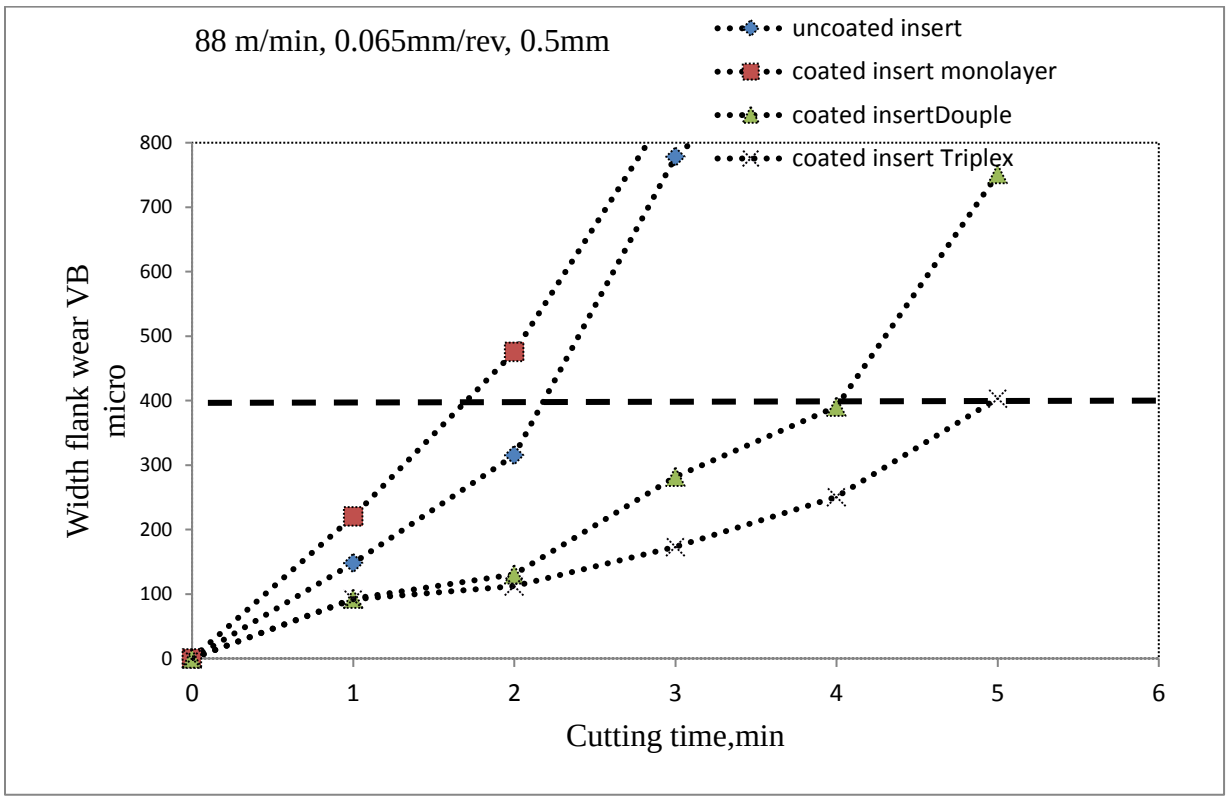

Continue Figure (4.50)

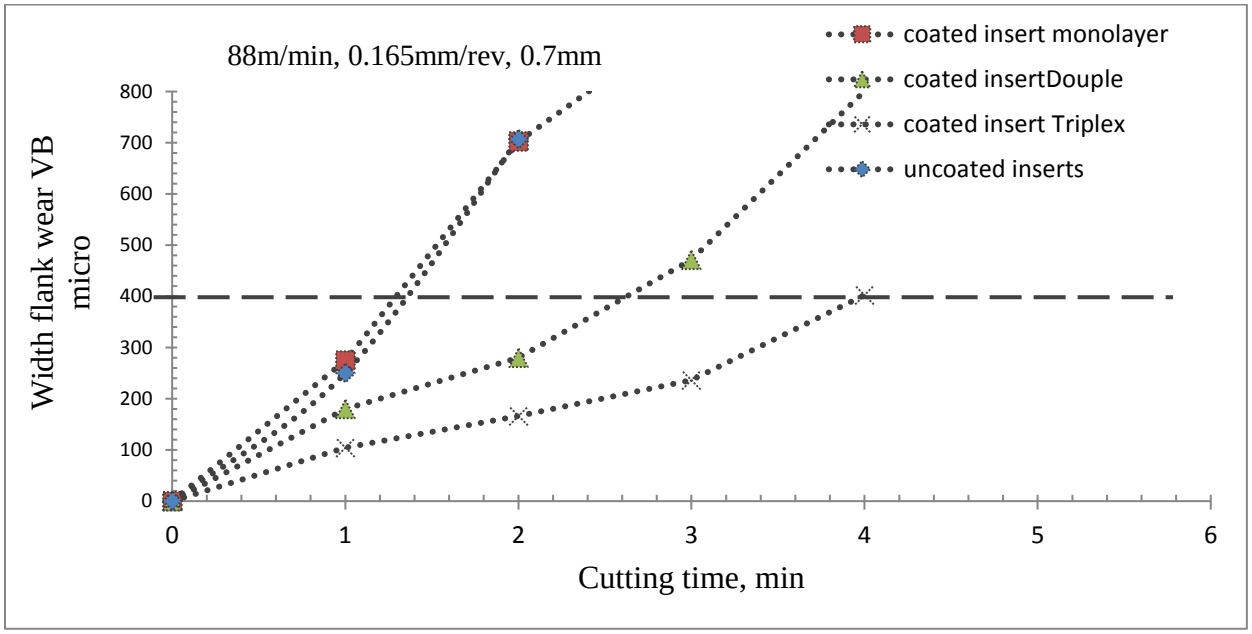

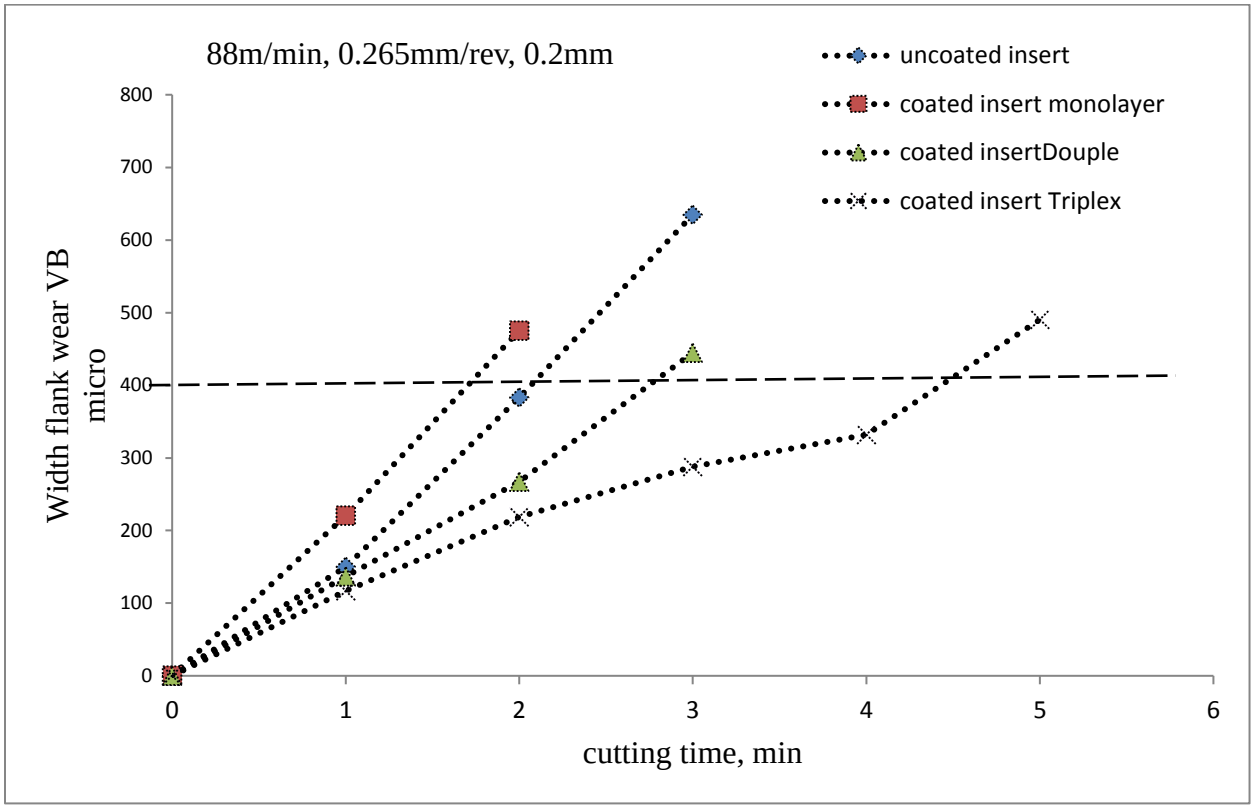

Continue Figure (4.50)

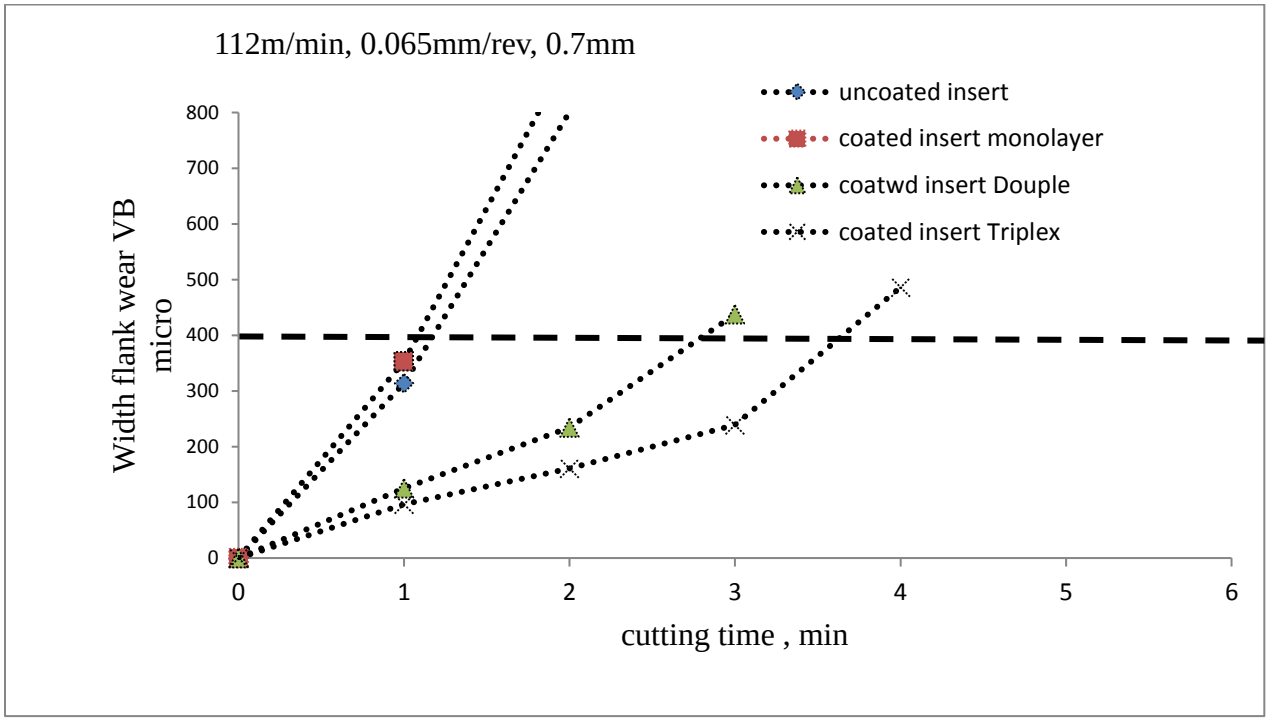

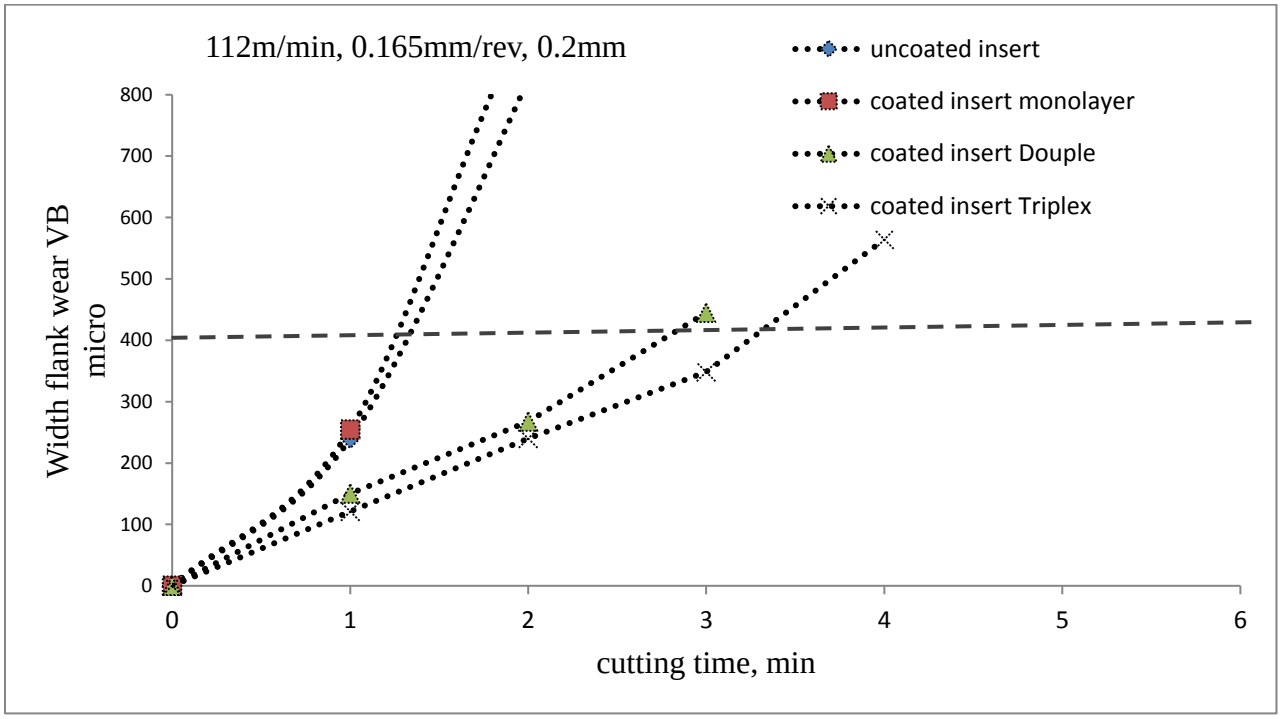

Continue *Figure (4.50)*

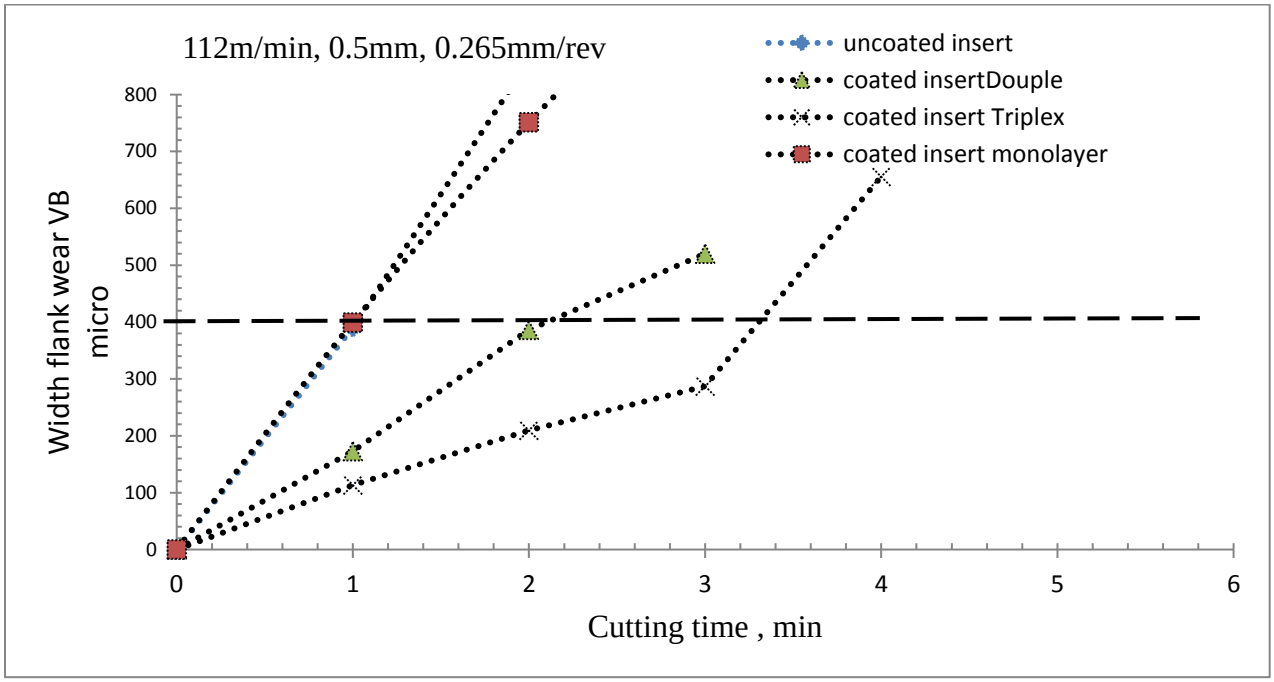

Continue Figure (4.50)

Table (4.7) demonstrates the width of the flank wear through the machining time up to the criterion width. Also, the estimated tool life of each tested tools were recorded. It is clear that the minimum wear can be noticed for the triplex layer coated insert while the highest at the monolayer coated insert considered for all of the machining conditions. The increase in cutting velocity and feed leads to an increase in wear width along the lateral surface.

For machining with monolayer coated inserts the time to reach *VB* = 0.4 mm was 2.6 min or less depending on the cutting speed. For uncoated insert, the time to reach VB=0.4mm was about 2.9 min or less depending on machining parameters. But for the two and three layer coated insert, the machining time increases to approximately 5.1 and 5.8 min respectively.

Monolayer coated HSS inserts have the minimum tool life compared with the other inserts at the same condition. This is due to it is high coefficient of friction

(0.69), less homogenous in coating particles and in distribution, lack adhered for monolayer on substrate.

Flank wear was caused by friction between the flank face of the cutting insert and the machined surfaces. When the surface of the HSS cutting inserts was coated with ceramic oxides which had a low friction coefficient and anti-adhering property, low thermal conductivity, high hardness, low wear rate, lead the adhesion of workpiece on the cutting edge can be suppressed therefore decreasing cutting resistance.

Reduced formation of built-up edge led to maintain the sharpness of the edge, and thus improve the machinability and the quality of the work materials. Coated HSS insert perform better than uncoated HSS insert due to the reduction in friction, in generation heat, and in cutting forces, also reduction in the diffusion between the chip and the surface of the tool, especially at higher speeds (the coating acts as a diffusion barrier).

Table (4.7) Wear width and tool life of cutting inserts

Exp. No.	Wear width µm uncoated insert			Wear width µm monolayer			Wear width µm Douple layers						Wear width µm Triple layers						Tool life (F) min			
	1 (min)	2	3	1 (min)	2	3	1 (min)	2	3	4	5	6	1 (min	2	3	4	5	6	uncoated insert	monolayer	Douple	Triple
1	91.03	235.7	402.2	159.6	314.8	426.4	48.83	53.03	108.8	201.1	381	555.2	48.96	59.9	97.63	148.1	265.2	424	2.9	2.6	5.1	5.8
2	104.9	2714.	462.1	158.5	530.4	--	74.75	106.5	206.2	299.2	646.9	-	65.57	87.43	105.6	145.3	414		2.7	1.7	4.4	5
3	201.1	360.4	567	236.2	653.9	--	96.31	161	239	486	----	-	89.92	126.7	200	268.5	443.3		2	1.4	3.8	4.7
4	148.1	315.1	778.3	220.5	475.3	--	92.37	130.8	281.9	390.4	751.3	-	91.84	112.2	173.2	250.8	403		2.2	1.7	4	5
5	250.2	707	-	274.7	702.3	--	179.8	280.1	471	--	-	-	104.3	166.1	236.2	402.4	-	-	1.3	1.2	2.4	4
6	150	382.9	634.8	218	470	-	136.6	297.3	444	-	-	-	117.1	218.6	288	331.9	490.4		2	1.7	2.8	4.5
7	313.9	800.9	-	353	903.5	-	125.3	234.5	437.6	-	-	-	96.31	161	239	486			1.1	1.1	2.7	3.2
8	239.4	823.1	-	254.5	920.9	-	150	267.3	444.9	-	-	-	121	240	348.5	564.1	-		1.2	1.2	2.8	3.4
9	390.4	859.7	-	399.2	751.3	---	173.2	386.1	520.3				113.2	209.6	287.1	656	-		1	0.9	2	3.1

For each cutting insert, the wear width increased at machining time increased as shown Appendix(C1-C27). Figure (4.51) shows the effect of the machining conditions on the tool life of the tested inserts. All types of the cutting inserts are impacted by parameter (ν), (ʃ), and (t) in the same way. The results indicate that a higher cutting speed and feed causes a higher value of VB, due to the accompanying increase in cutting temperature, which causes the increase in width of wear on tool cutting edge, also it may soften a very thin surface layer of the tool cutting edge. In addition to that a higher cutting speed means a higher repeated contact between the machined surface and the flank surface which increases the scratching action of machined material. The significant decrease in tool life for coated HSS insert at higher depth of cut can be attributed to increasing temperature [44,103].

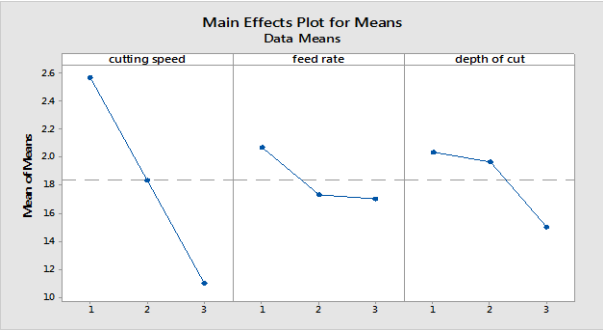

Tool life of uncoated insert

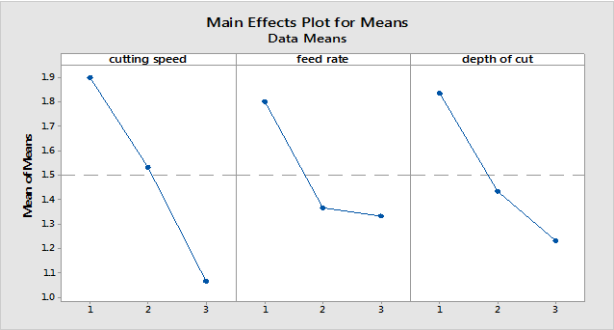

Tool life monolayer

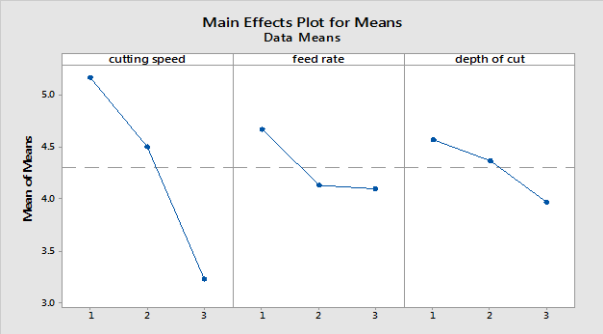

Tool life of triplex layers

Tool life douple layers

Figure (4. 51): Main effect plot of tool life for cutting inserts

4.8.2. Surface roughness

The values of surface roughness for cutting inserts after first minute machining can be noticed in Table (4.8).

Table (4.8): Surface roughness after first minute machining for cutting inserts

Exp.No.	Machining conditions			Surface Roughness (µm)			
	cutting velocity (m/min)	feed (mm/rev)	Depth of cut (mm)	Uncoated insert	Triplex layers	Monolayer	Douple layers
1	56	**0.065**	**0.2**	**1.49**	**0.933**	**1.737**	**0.99**
2	56	**0.165**	**0.5**	**2.49**	**1.769**	**2.929**	**1.882**
3	56	**0.265**	**0.7**	**3.827**	**2.652**	**3.91**	**2.98**
4	88	**0.065**	**0.5**	**0.986**	**0.45**	**1.15**	**0.579**
5	88	**0.165**	**0.7**	**2.882**	**1.104**	**3.41**	**1.254**
6	88	**0.265**	**0.2**	**0.706**	**0.124**	**0.925**	**0.462**
7	112	**0.065**	**0.7**	**0.991**	**0.544**	**1.605**	**0.579**
8	112	**0.165**	**0.2**	**0.462**	**0.018**	**0.882**	**0.11**
9	112	**0.265**	**0.5**	**1.077**	**0.7**	**1.482**	**1.04**

It is obvious that douple and triplex multilayer coated HSS insert exhibited a better surface finish compared with the uncoated and monolayer coated HSS insert.

The triplex layer coated HSS inserts with the limit thermal conductivity and lower the friction coefficient (0.12), roughness(14)nm, and strong adhesive strength (93)MPa showed the minimum surface roughness. Monolayer coated inserts exhibited the highest surface roughness because they have the highest coefficient of friction (0.69), roughness (48)nm, minimum adhesive strength (10.65)MPa and poor homogeneity.

Figure (4.52) plots the relationship between the roughness parameter Ra and cutting parameters. Analysis of the results showed that the lowest surface roughness is achieved at the lowest feed, depth of cut, and maximum cutting speed.

This effect can be explained as follows. Due to the higher cutting speed, the material removal rate is very high. The tool is in contact with the work piece for a very short period of time, and this contributes to a low roughness value. In addition, the higher cutting speed reduces edge chipping and thus improves the surface quality.

The low feed results in a shorter peak-to-rough distance, which helps to achieve a lower surface roughness. Another important issue is machine vibrations. A lower cutting speed also contributes to vibration in the machine, which in turn adds height to uneven peaks and troughs and deteriorates the quality of the machined surface. The above results are similar to those presented in[109].

When depth of cut (t) increases, the roughness of the work piece also increases, due to high plastic deformation appeared on the work piece surface.

The maximum surface roughness at the largest value for coated inserts with douple and triplex layers is (ʃ).

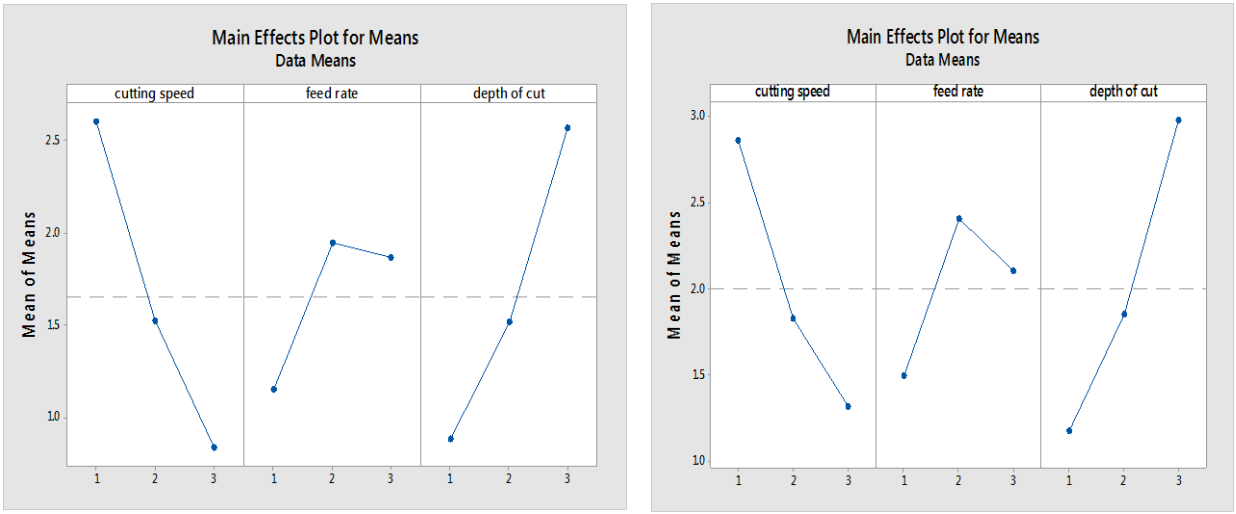

Figure (4.50): Estimation results of the tool life for the coated and uncoated HSS cutting inserts

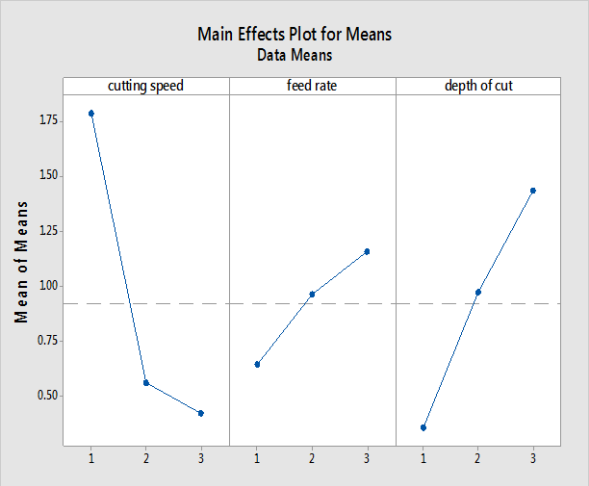

Surface roughness of triplex layers

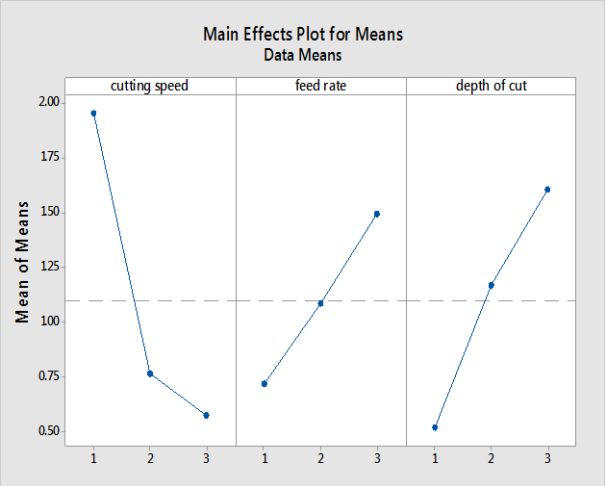

Surface roughness of douple layers

Continue Figure (4.52):

4.8.3.Temperature

The two main heat sources during machining are plastic deformation of the workpiece and friction of the workpiece–tool contact zone [111,2]. The thermal conductivities for the HSS insert and three layer coating are 22 W/m.k and 10.53(W/m K), respectively, which are different. This means that the coating is a thermal barrier and the heat flux is not transferred to the bulk of the insert.

Also it depends on the fact that coating insert leads to decrease of the tool–work piece contact area, decrease of the thickness of the secondary shear zone and of the temperature at this interface, which leads to a decrease of the heat flux transmitted to the cutting insert , since the flux transmitted depends on the contact area and the heat created at this interface (heat flux density) [85]. The lower amount of the generated heat was recorded during machining with douple and triple layers coated inserts respectively, Table (4.9) reveals temperature at failure minute which wear width reached into 0.4mm for each H.H.S insert. For triple layers coated inserts, the temperature at failure minute was reduced by 2-8% in comparing to that of uncoated insert.

Table (4.9): Temperature ℃ at failure minute through machining process

ExP No.	Temperature ℃ at failure minute																			
	Machining time (min) uncoated insert			Machining time (min) Triplex layer						Machining time (min) Monolayer				Machining time (min) Douple layer					
	1	2	3	1	2	3	4	5	6	1	2	3	4	1	2	3	4	5	6
1	69.	75	77.88	61	64.5	66.5	68	73.27	77.72	75.05	75.55	79.83		67.8	76.1	83.8	90.8	95.3	96
2	81	83	86.4	63.5	65.6	68.3	69.72	79.55		84.88	88.71			75.6	82	86.3	93.8	104.3	
3	89.9	100	104	81	85.38	89.9	91.4	97.85		90	105			78.5	89.3	96.9	116		
4	100	107	112	71.6	76.3	80.3	82.3	84.16		102	108.4			93	106.9	109	118.5		
5	115	126	135.2	101	109	118	123.5			129.	131.1			110	112.7	136. 2			
6	117	132 .		108	116	124	134.1			124.3	131.6			114.3	116.4	141. 5			
7	129	138		119	124	127	130.3	135		127.7	138.3			121	125.1	143			
8	135	149		125	126	130	133.8			137.7	146.5			113.7	119.3	155			
9	140	153		112	**125**	135	138.1			149.2				133.9	**159**				

Figures (4.53) it is easy to understand differences in heating generation for uncoated cutting insert and coated triple layers inserts with increase machining time, see appendixes D1-D8 .

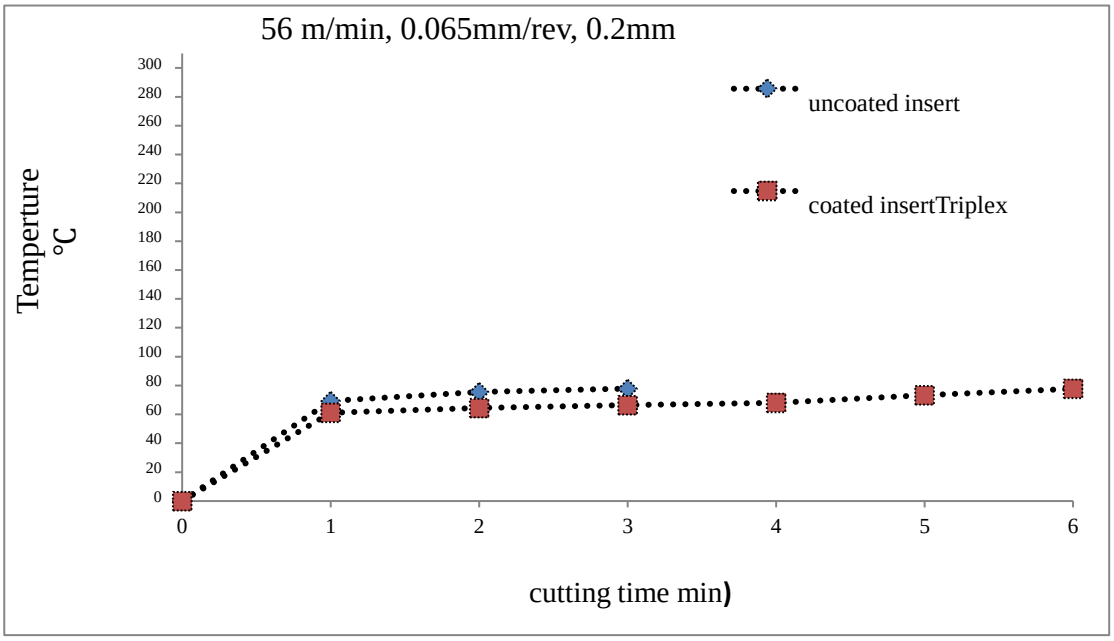

Figure (4.53): Temperature change ℃ for triple layer coated and uncoated inserts at the same machining conditions

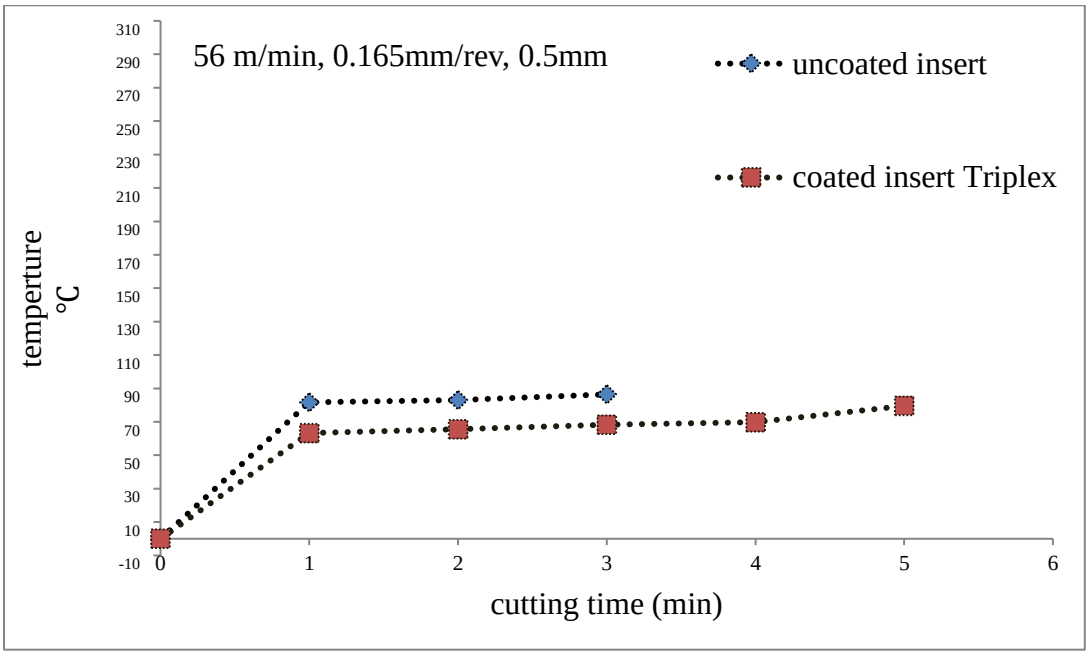

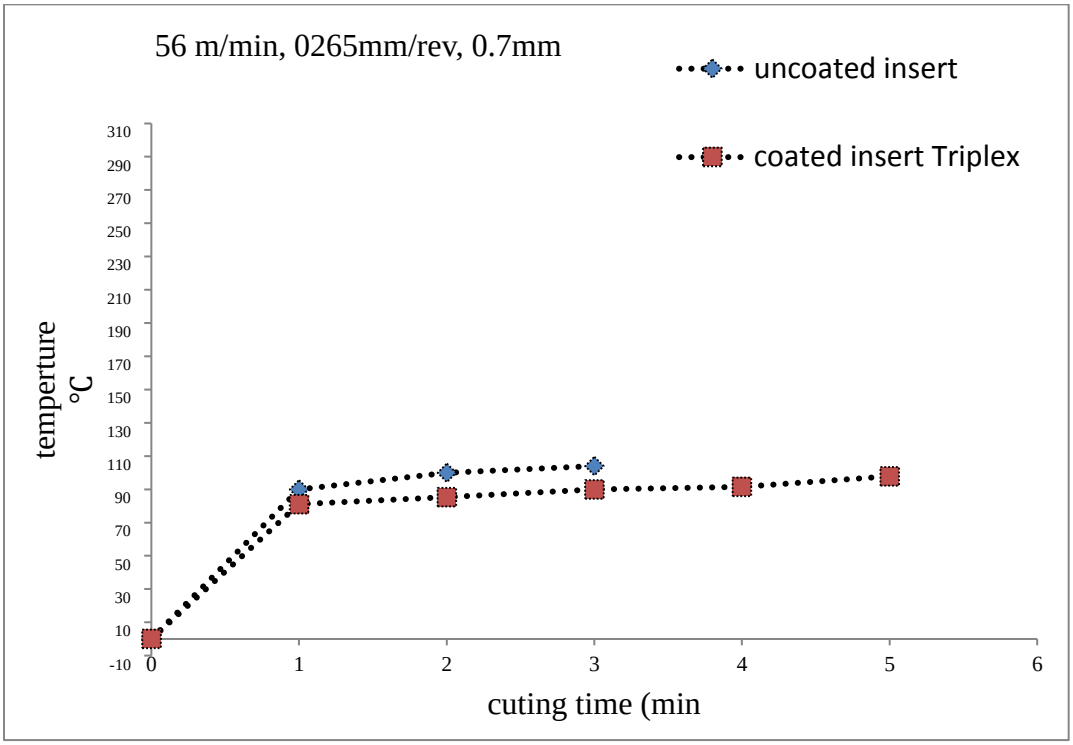

Continue Figure (4.53)

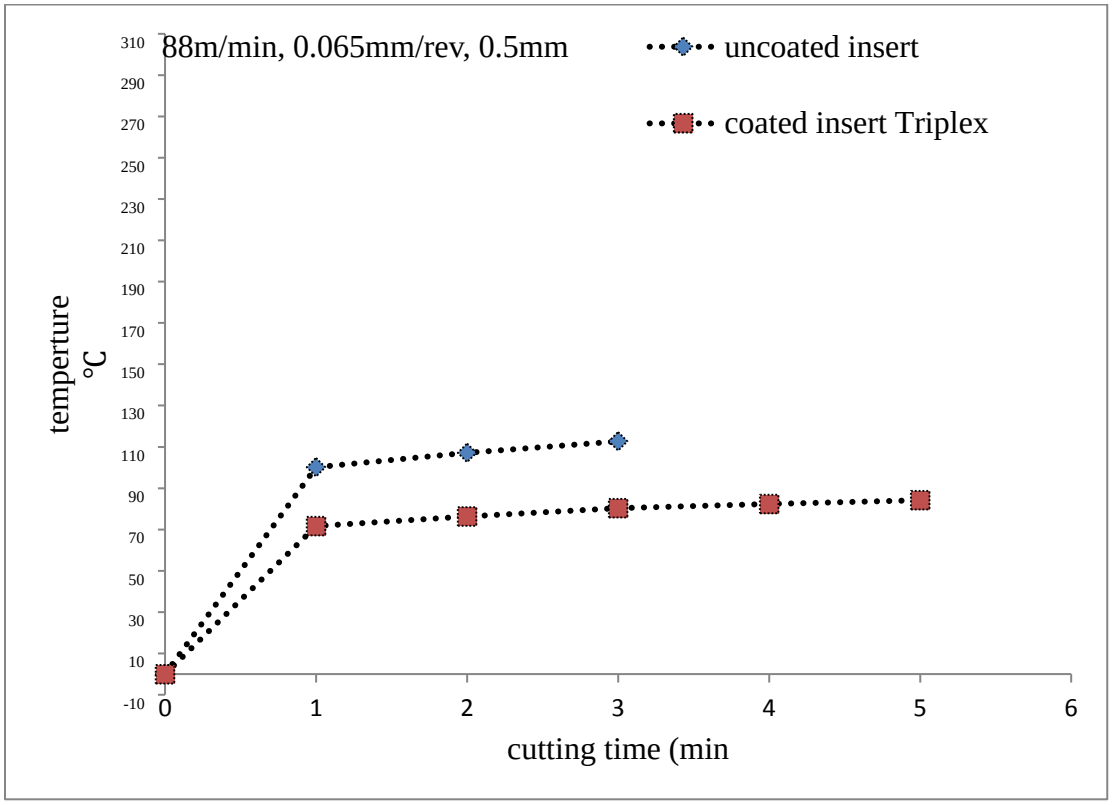

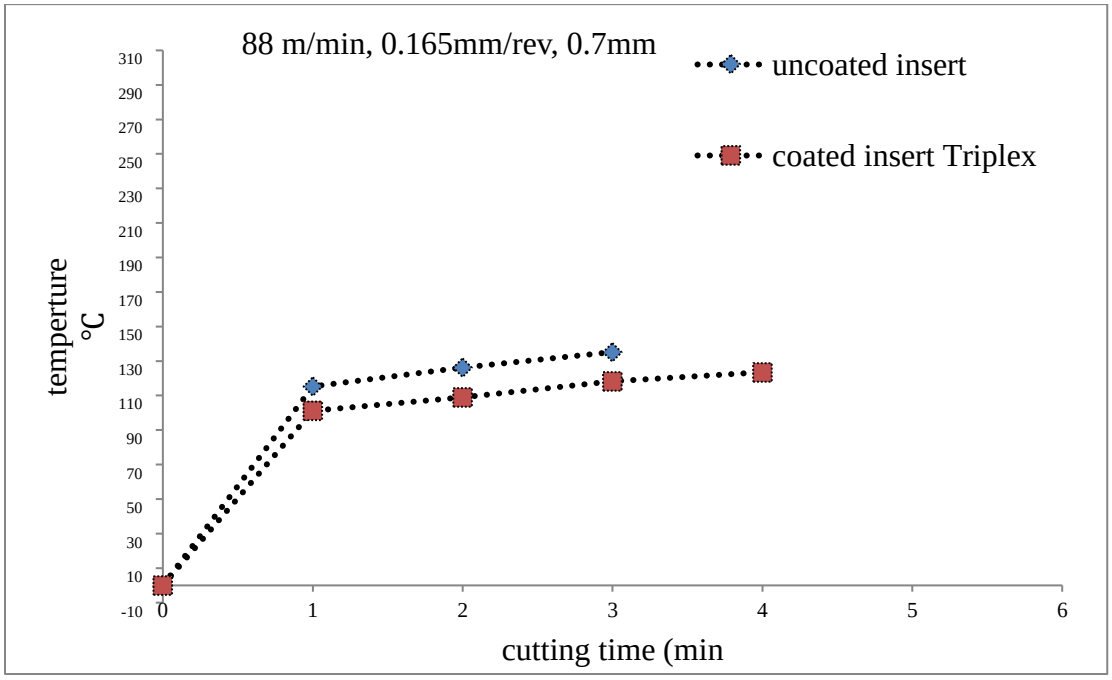

Continue Figure (4.53)

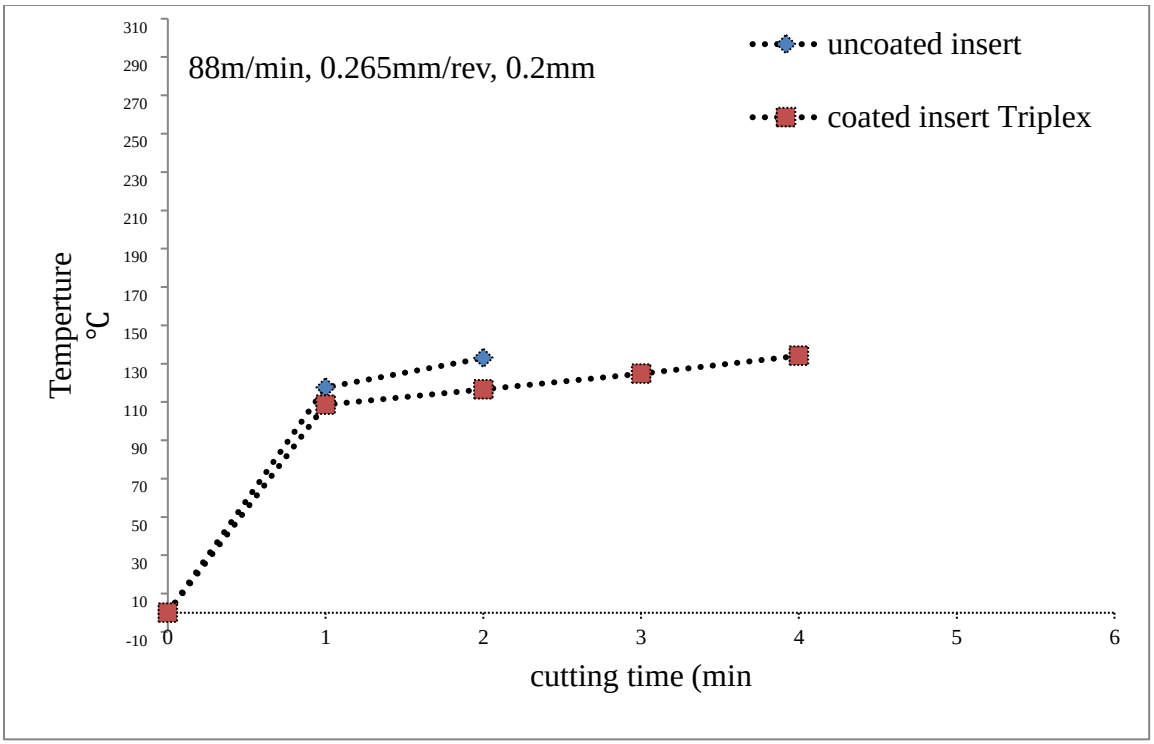

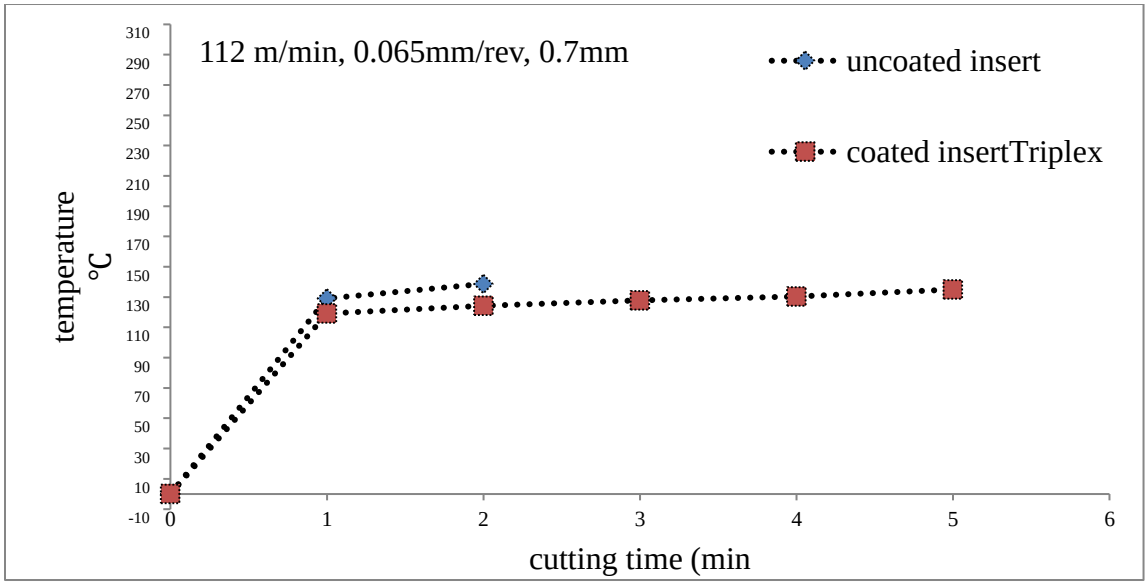

Continue Figure (4.53)

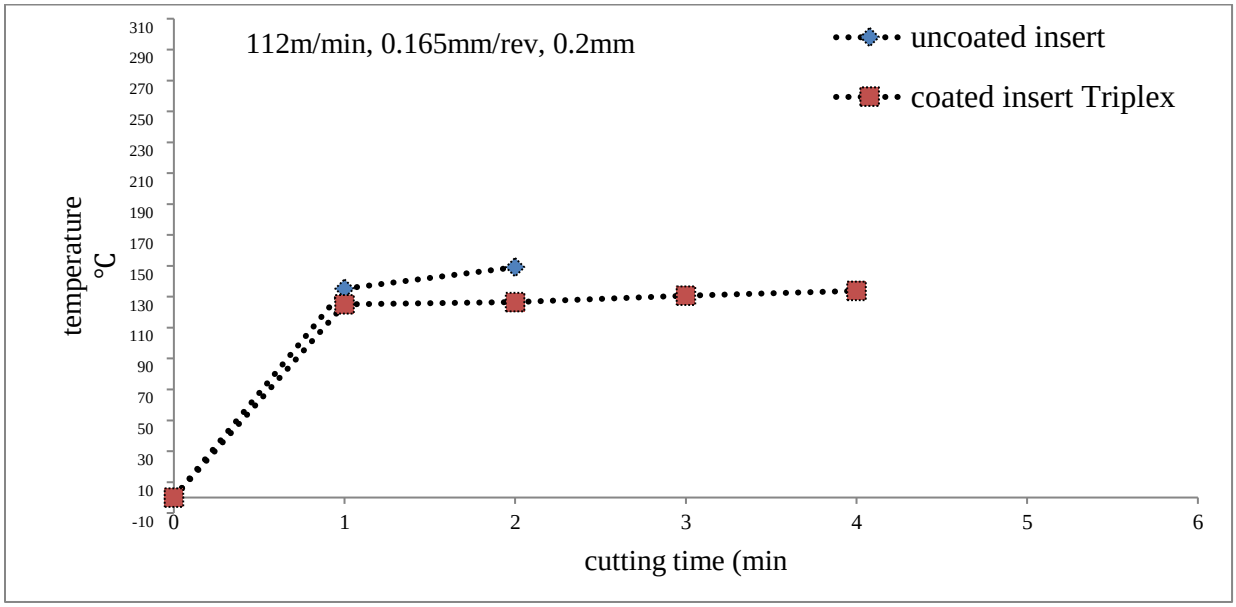

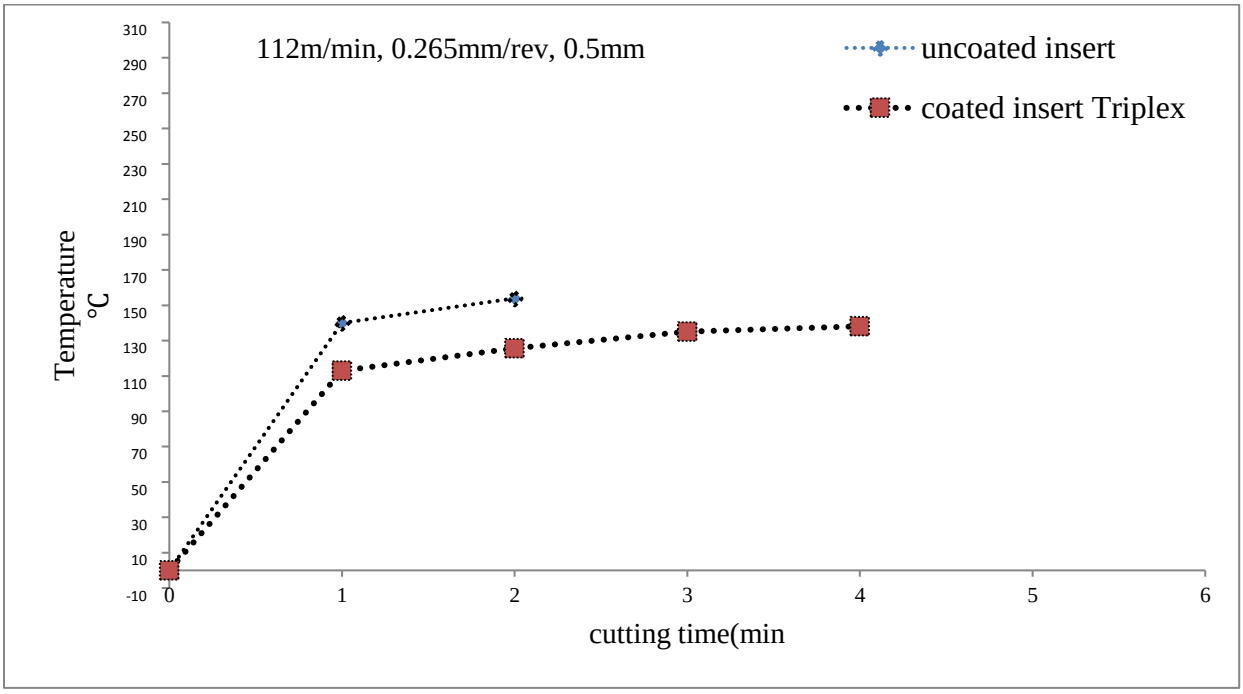

Continue Figure (4.53)

The temperature distributions during cutting process were recorded by IR camera to measure the temperature in F° at insert –machined surface contact. Figure (4.54) shows examples of the thermal images resulted at the failure minute (tool life finished).

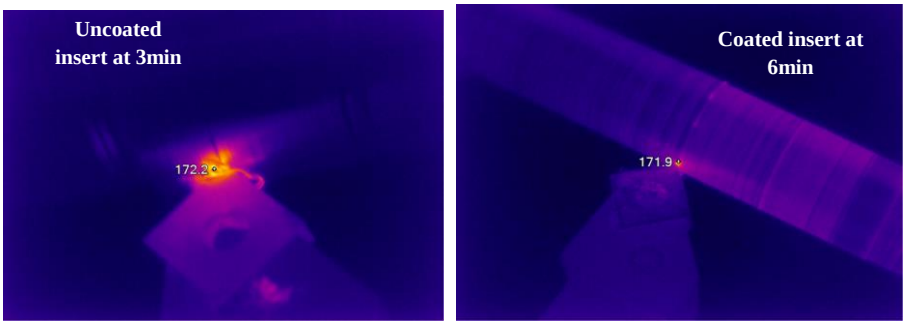

(a) 56 m/min, 0.065mm/rev, 0.2mm

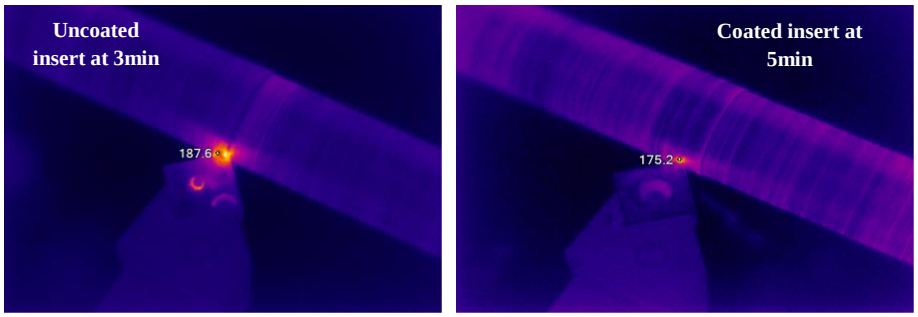

(b) 56 m/min, 0.165 mm/rev, 0.5mm

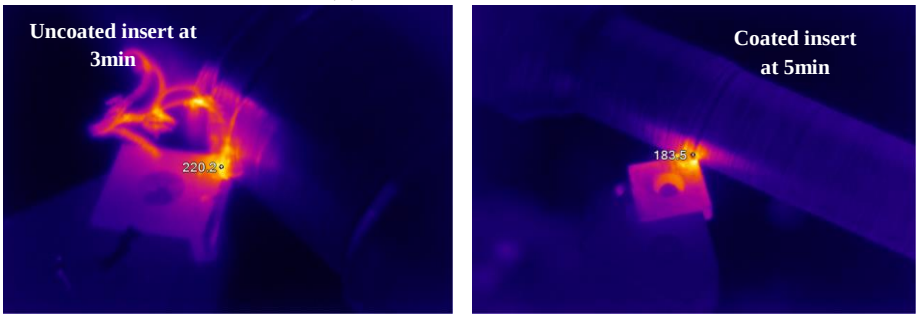

(c) 56m/min, 0.265mm/rev, 0.7mm

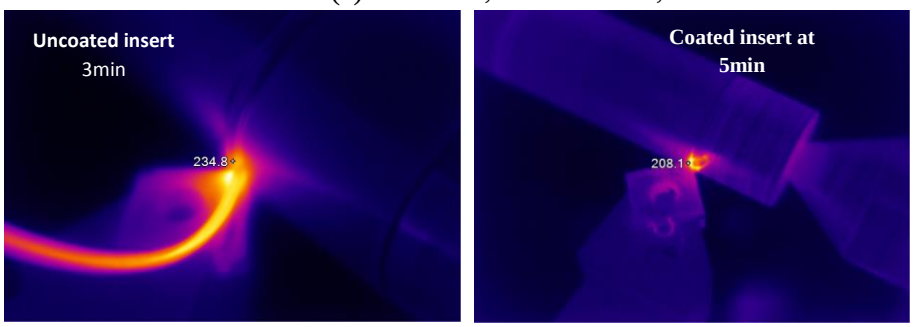

(d) 88m/min, 0.065mm/rev, 0.5mm

Figure (4.54): Recorded temperature in Fahrenheit degree at the contact point between the insert tip and work piece at failure minute at different machining conditions using different HSS inserts

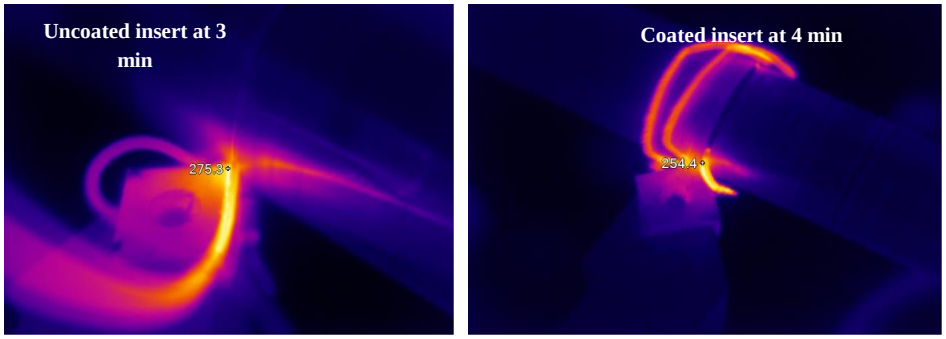

(e) 88m/min, 0.165mm/rev, 0.7mm

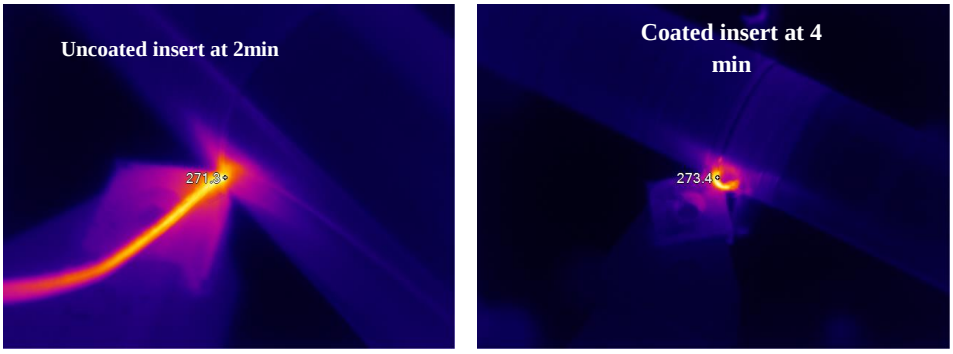

(f) 88m/min, 0.265mm/rev, 0.2mm

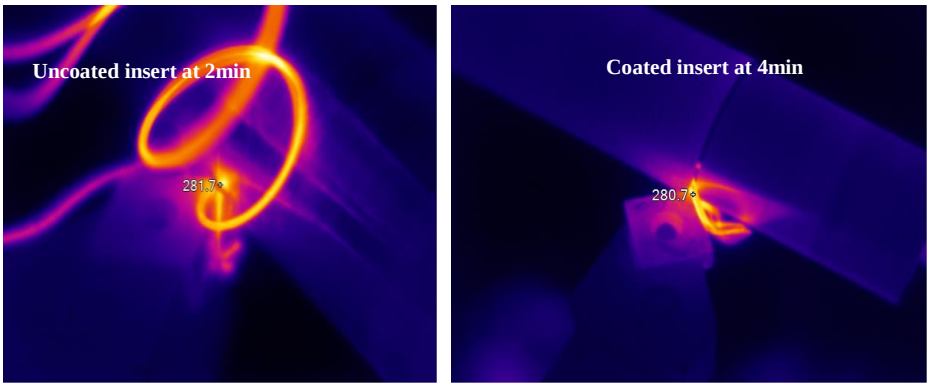

(g) 112m/min, 0.065mm/rev, 0.7mm

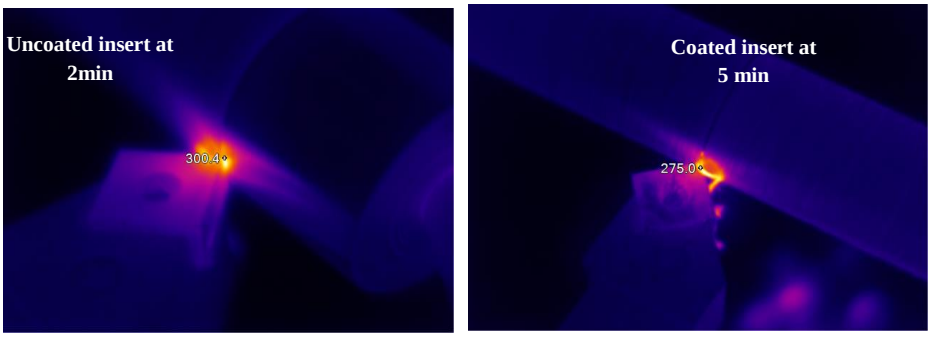

(h) 112m/min, 0.165mm/rev, 0.2mm

Continue Figure (4.54)

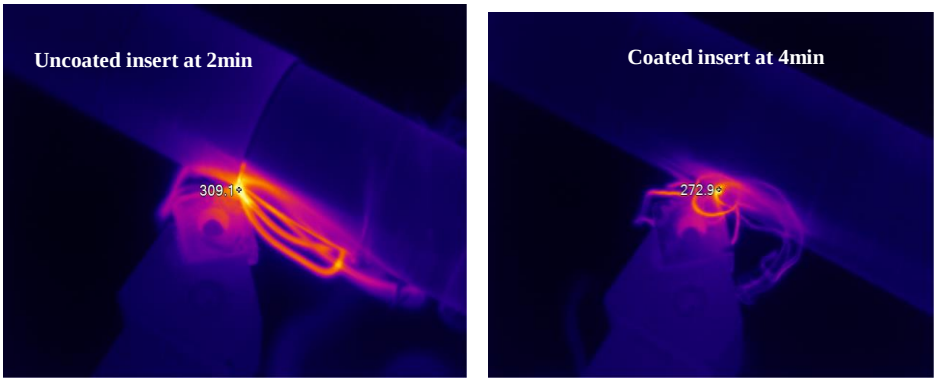

(i) 112m/min, 0.265mm/rev, 0.5mm

Continue Figure (4.54)

The monolayer inserts had higher temperature in comparing to uncoated due to rise coefficient of friction and lack layer adherence. Two layer had good results about temperature at failure minute comparing uncoated insert and less than coated insert three layer that related zirconia layer which has minimum thermal conductivity, low coefficient of friction that reduce temperature generation at contact region between tool and work piece. As shown appendix D1-D14.

Despite the fact that monolayer coated inserts have a lower thermal conductivity than uncoated inserts, monolayer coated inserts have a higher temperature at failure minute than uncoated inserts due to a higher coefficient of friction than uncoated, which is related to a lack of adhesion on HSS and poor layer deposition distribution.

Generating of the heat and temperature of the cutting insert at the contact region between work piece and insert is affected by v, ʃ, and t. When (v) increases, the temperature of each cutting insert increases due to plastic deformation for work piece and friction coefficient. Besides, the use of high (ʃ) led to a rise in the temperature compared with using lower value of (ʃ). The minimum temperature of the cutting insert for each type is achieved by (medium t) due to 0.5 mm of cutting

depth is more suitable for turning medium carbon steel with less temperature generation. As shown in Figure (4.55).

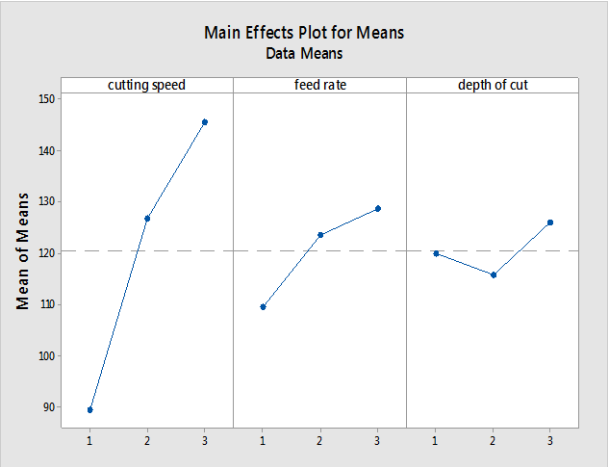

Temperature of uncoated

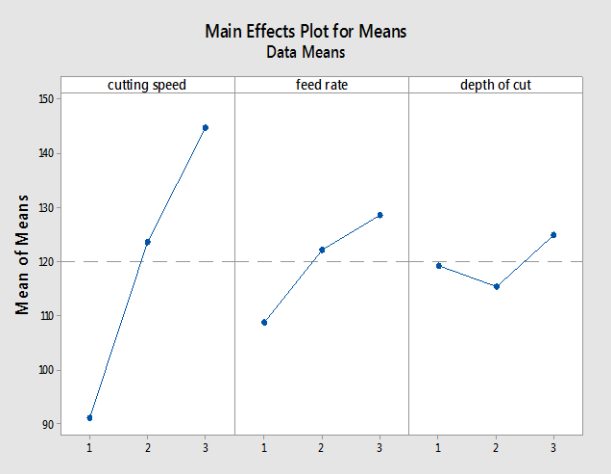

Temperature monolayer

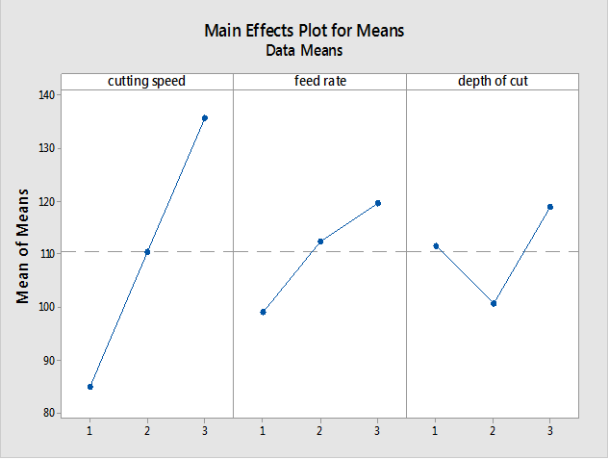

Temperature of triplex layers

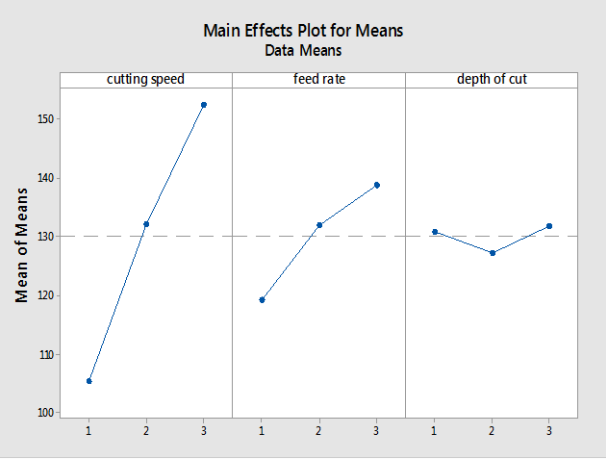

Temperature douple layers

Figure (4. 55): Main effect plot for temperature for each cutting insert

Table (4.10) abbreviates the variation of mechanical, physical and machining ``properties investigated in this study.

Table (4.10): Variation in mechanical, physical and machining properties of coated inserts comparing with uncoated HSS insert

Tested property	Enhancement (%)		
	Coated with triplex layer ($TiO_2/Al_2O_3/ZrO_2$)	Coated with douple layer (TiO_2/Al_2O_3)	Coated with monolayer (Al_2O_3)
Coefficient of friction	↓ 80%	↓ 58%	↑ 17%
Wear rate (gm/cm)	↓ 71%	↓ 57%	↓ 30%
Hardness HV	↑ 57%	↑ 34%	↑ 7%
Surface roughness for insert (nm)	↓ 63%	↓ 59%	↑ 29%
Thermal conductivity (W/m. K°)	↓ 36%	↓ 30%	↓ 28%
Tool life (min)	↑ (85-183)%	↑(40-75)%	↓(10-37)%
Temperature at first minute (℃)	↓ (11-13)%	↓ (4-16)%	↑ (9)%
Temperature at failure minute (℃)	↓ (2-8)%	----------	---------
Surface roughness of workpiece at first minute (µm)	↓ (30-96)%	↓ (22-76)%	↑(18-61)%

For more satisfied evaluation of the coating process, the tool life and the machining temperature of the coated HSS inserts were compared with those of carbide inserts.

All experiments for douple layers coated insert, showed an increase in tool life of by (3-32%) compared to the carbide inserts. While triplex layers coated HSS was increased by (30-53)% compared to carbide inserts.

Figure (4.56)represents examples for the method used for estimating the tool life according to the used machining conditions. All of the estimations are demonstrated in appendix E1-E3.

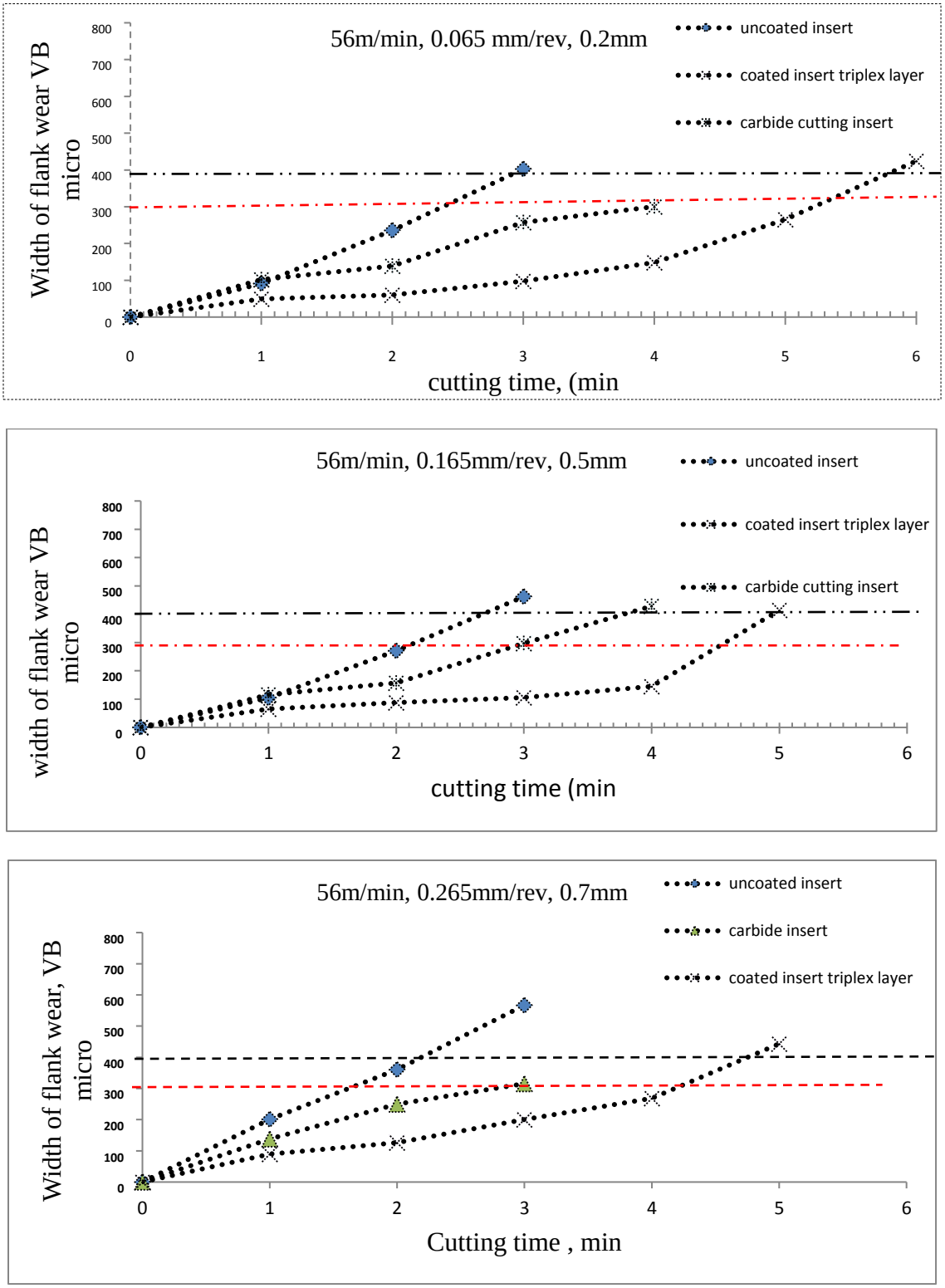

Figure (4.56): Estimation of the tool life for the coated HSS and carbide and uncoated HSS cutting inserts

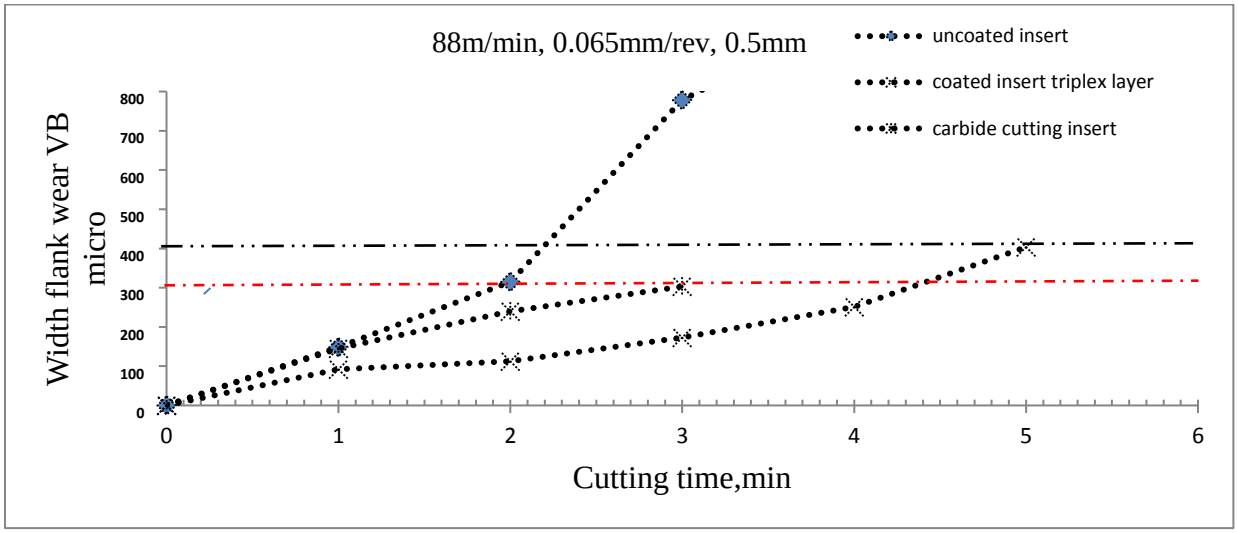
88m/min, 0.065mm/rev, 0.5mm
uncoated insert
coated insert triplex layer
carbide cutting insert
Width flank wear VB micro
800
700
600
500
400
300
200
100
0
0
1
2
3
4
5
6
Cutting time,min

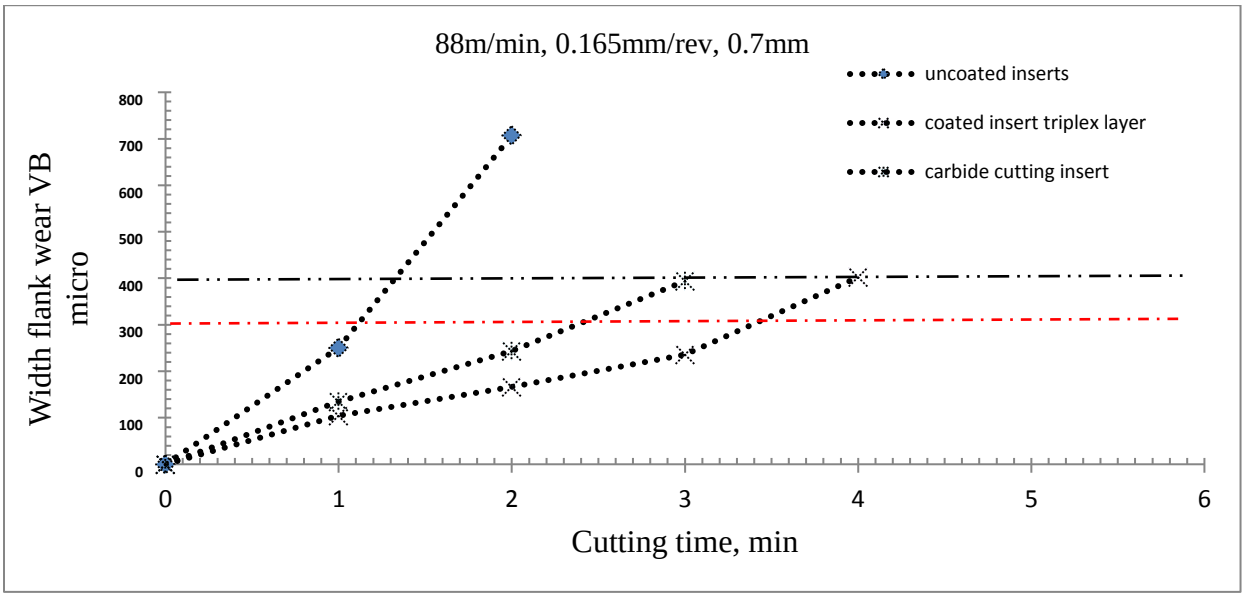
88m/min, 0.165mm/rev, 0.7mm
uncoated inserts
coated insert triplex layer
carbide cutting insert
Width flank wear VB micro
800
700
600
500
400
300
200
100
0
0
1
2
3
4
5
6
Cutting time, min

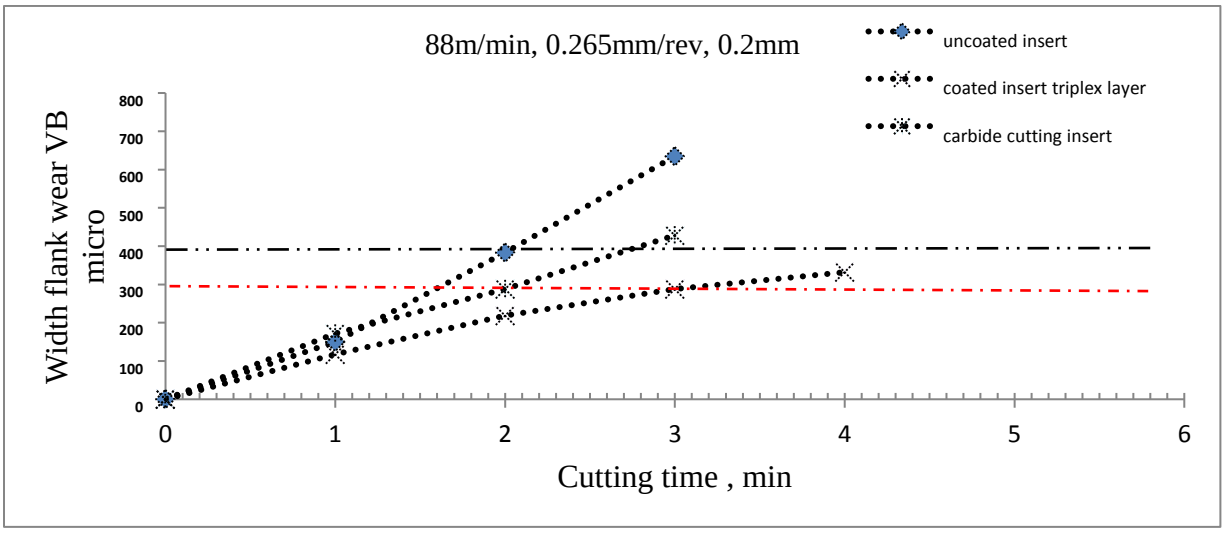
88m/min, 0.265mm/rev, 0.2mm
uncoated insert
coated insert triplex layer
carbide cutting insert
Width flank wear VB micro
800
700
600
500
400
300
200
100
0
0
1
2
3
4
5
6
Cutting time , min

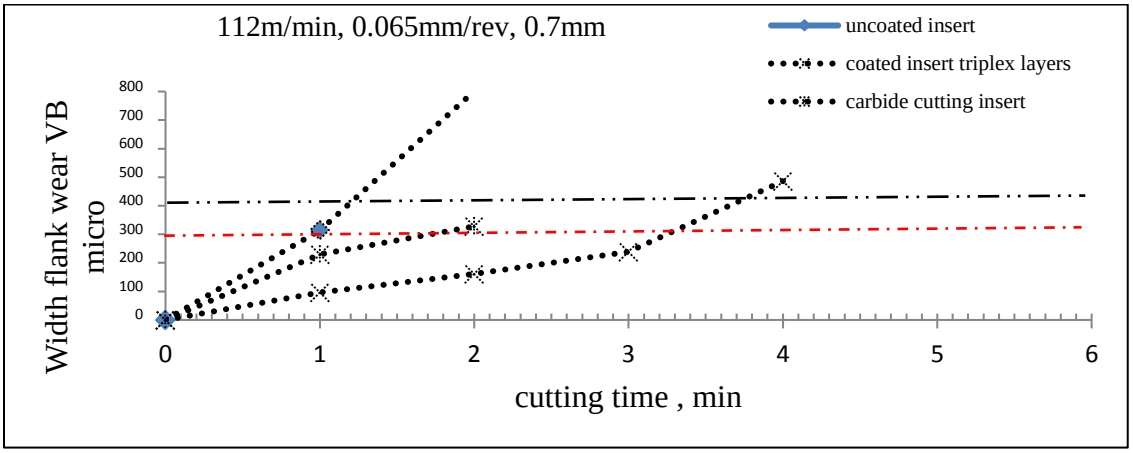

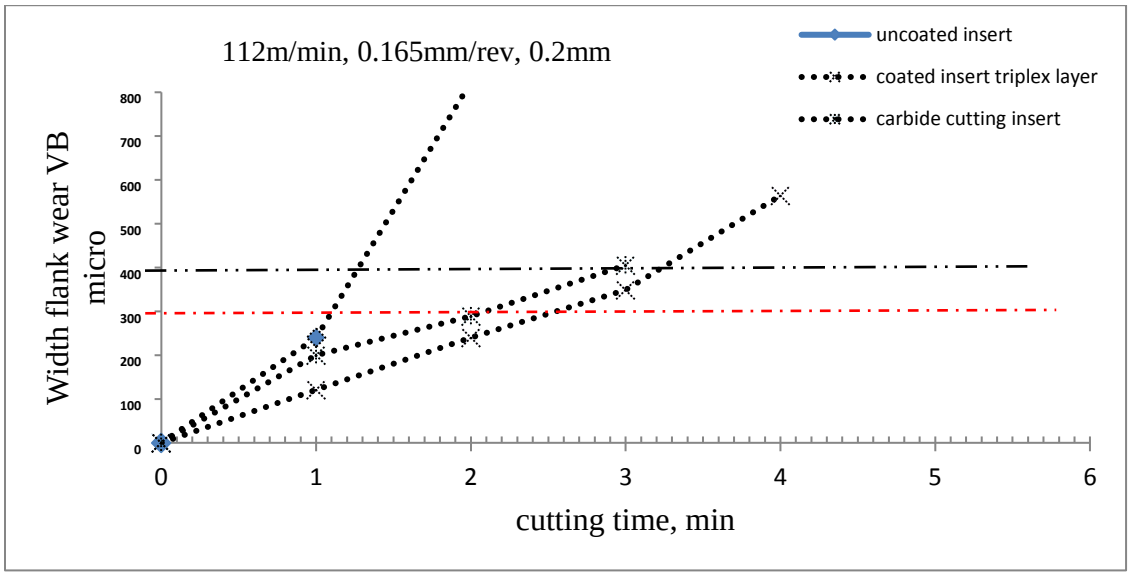

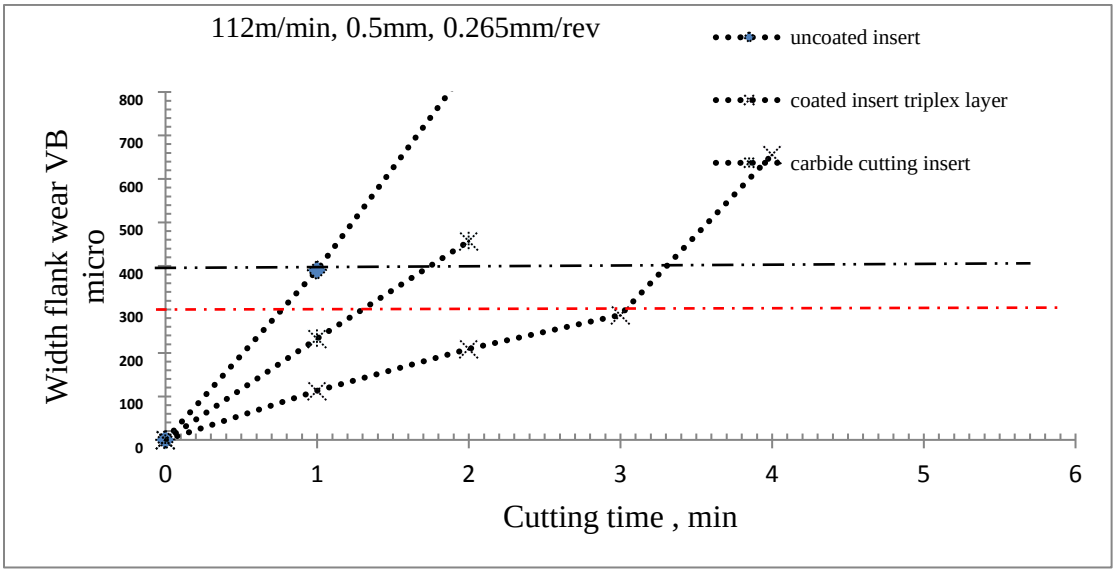

Continue Figure (4.56)

In comparison between carbide insert and coated HSS insert, three cutting velocity (56, 88, and 112 m/min) for each of which three feeds (0.065, 0.165 and 0.265 mm/rev) were used with the depth of cut (0.2, 0.5, and 0.7mm). The experiment is planned by considering three levels for each of the three input process parameters as shown in Table (4.11). The selected responses were the tool life and the cutting temperature.

At the same machining conditions, the carbide insert has a greater wear width at the region of contact with the work piece (ASTM A519- grade 1045) at the end of the machining minute, as shown Figures (4.57).

The cutting temperature of carbide inserts and coated HSS inserts were compared using three distinct experimental numbers (3, 4, and 9) under various conditions. Figure (4.58) shows that at the end of the machining minute, the carbide insert has a higher temperature in the region in contact with the work piece (failure minute). This is due to the thermal barrier coating on coated HSS inserts, which reduces the temperature generated at the region between work piece and insert-tip contact region during the turning process due to an increase in temperature distribution.

Table (4.11):Revealed into the tool life, and the wear width for cutting inserts: (uncoated HSS, coated HSS, and carbide insert)

Exp. No.	Width of flank wear (µm)																						Tool Life (min)			
	Uncoated HSS			Carbide insert					Coated Douple layers HSS							Coated Triple layers HSS							Uncoated	Carbide	Douple layer	Triple x Layer
	1 (min)	2	3	1 (min)	2	3	4	5	1 (min)	2	3	4	5	6		1 (min)	2	3	4	5	6					
1	91.03	235.7	402.2	101	139	257	300		48.83	53.03	108.8	201.1	381	555.2		48.96	59.9	97.63	148.1	265.2	424		2.9	4	5.1	5.8
2	104.9	271.4	462.1	115	157	297	428		74.75	106.5	206.2	299.2	646.9		-	65.57	87.43	105.6	145.3	414			2.7	3	4.4	5
3	201.1	360.4	567	138	250	315			96.31	161	239	486	----		-	89.92	126.7	200	268.5	443.3			2	2.8	3.8	4.7
4	148.1	315.1	778.3	145	240	303			92.37	130.8	281.9	390.4	751.3		-	91.84	112.2	173.2	250.8	403			2.2	3	4	5
5	250.2	707	-	134	243	393			179.8	280.1	471	--	-		-	104.3	166.1	236.2	402.4	-	-		1.3	2.3	2.4	4
6	150	382.9	634.8	171	288	428			136.6	297.3	444.9	-	-		-	117.1	218.6	288	331.9	490.4			2	2.1	2.8	4.5
7	313.9	800.9	-	230	327				125.3	234.5	437.6	-	-		-	96.31	161	239	486	-			1.1	2	2.7	3.2
8	239.4	823.1	-	200	289	405			150	267.3	444.9	-	-		-	121	240	348.5	564.1	-			1.2	2.2	2.8	3.4
9	390.4	859.7	-	233	457.				173.2	386.1	520.3					113.2	209.6	287.1	656	-			1	1.4	2	3.1

Figure (4.57) is evident which depicts FE-SEM of the machining zone that excess in width of wear of the uncoated HSS, triple layer coated HSS, and the carbide inserts at the failure minute.

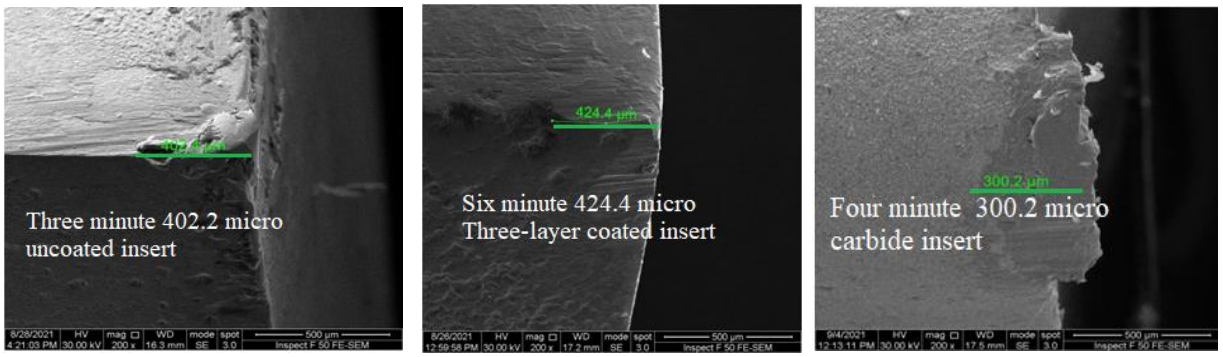

(a) 56m/min, 0.065 mm/rev, 0.2

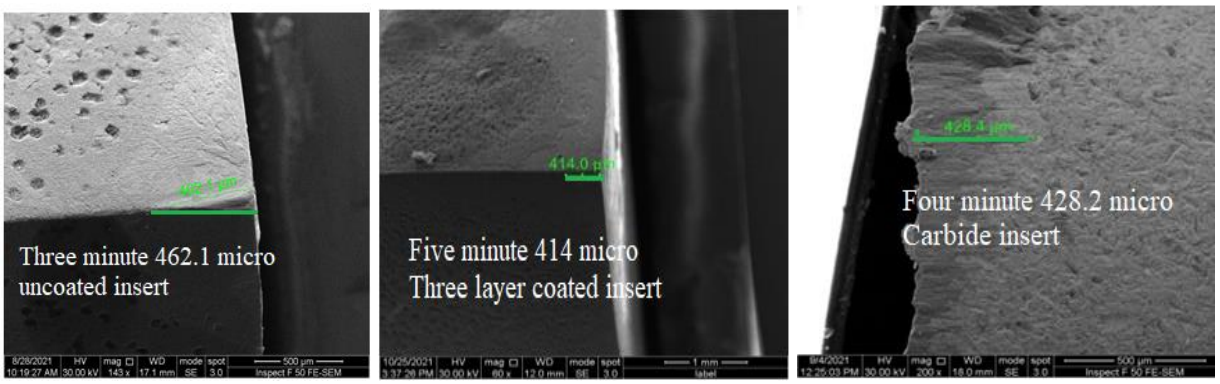

(b) 56m/min, 0.165 mm/rev,0.5mm

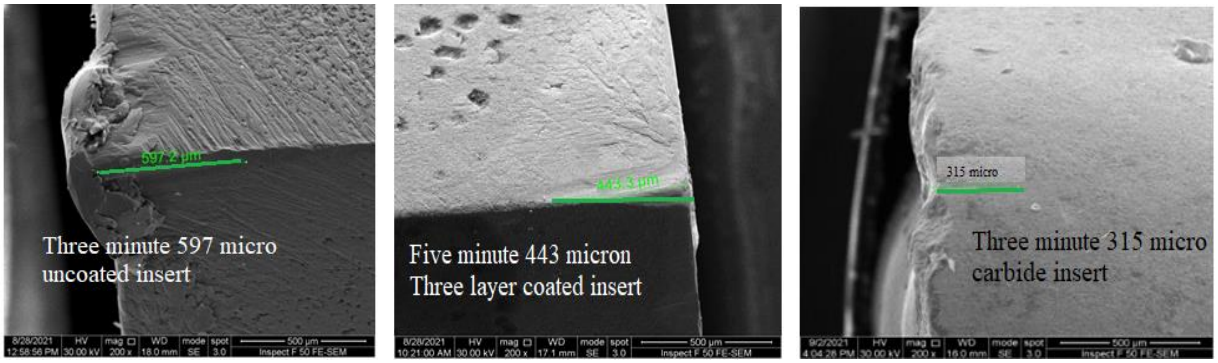

(c)56m/min, 0.265 mm/rev, 0.7mm

Figure (4.57): The evaluation of maximum flank wear at failure minute during machining using different HSS and carbide inserts

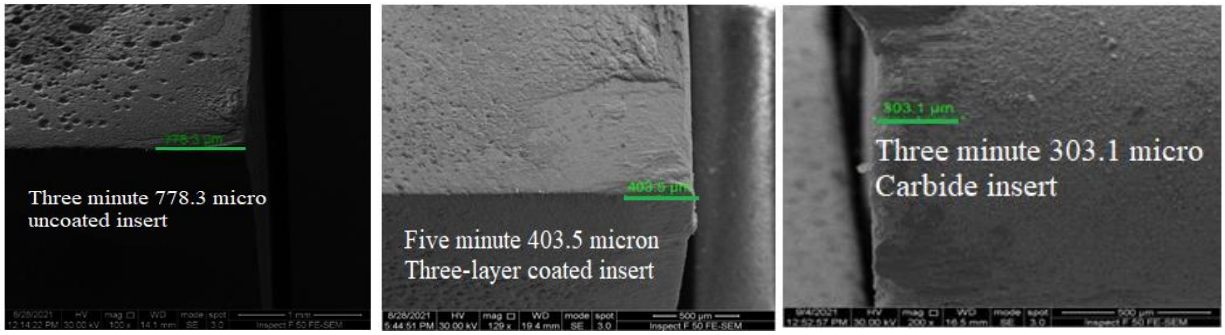

(d)88m/min, 0.065 mm/rev, 0.5m

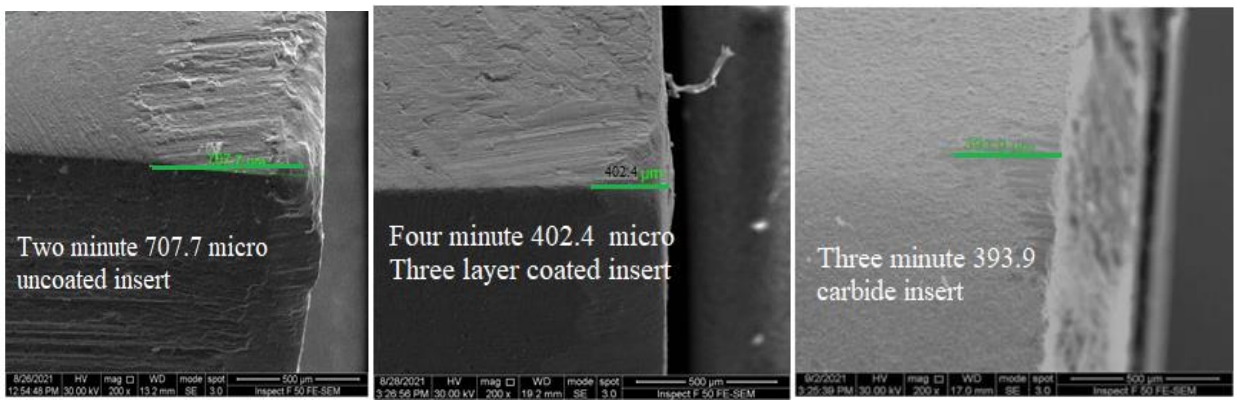

(e)88m/min, 0.165m/rev, 0.7mm

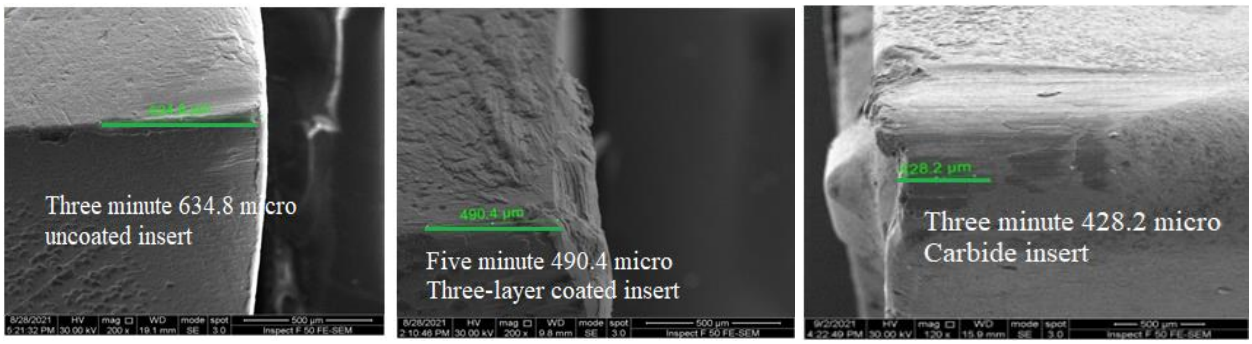

(f)88m/min, 0.265 mm/rev, 0.2mm

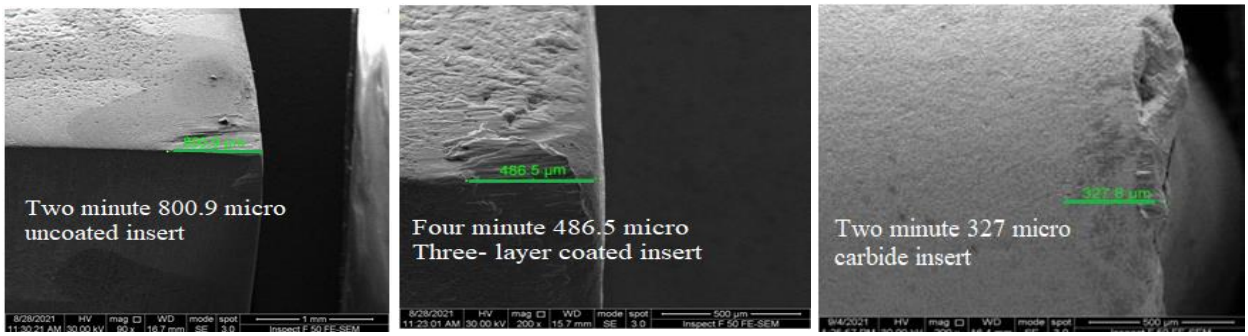

(g)112m/min, 0.065mm/rev, 0.7mm

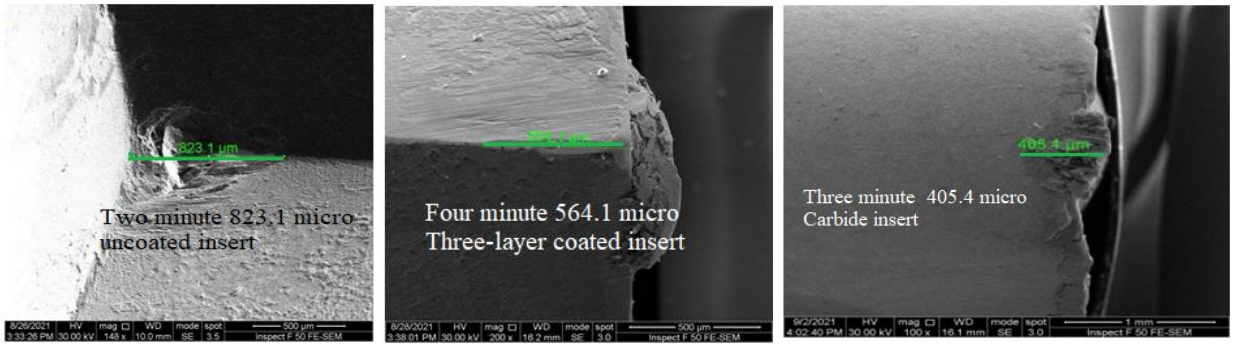

(h)112m/min, 0.165 mm/rev, 0.2mm

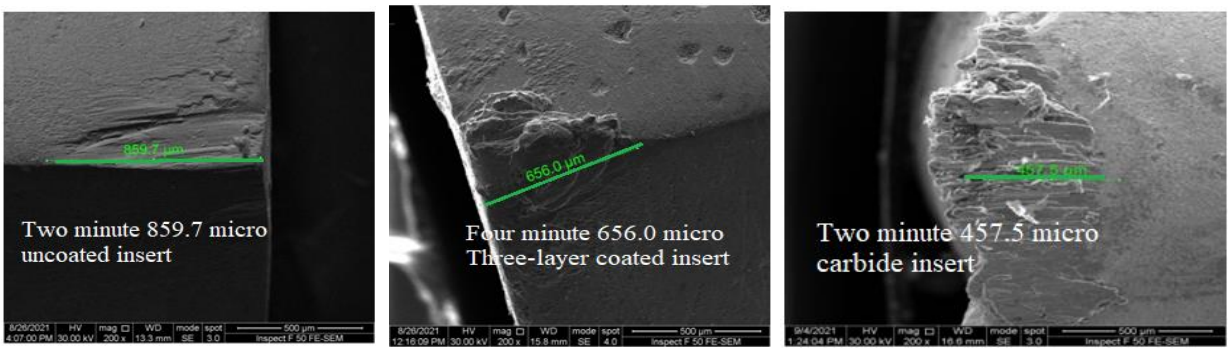

(k)112m/min, 0.265mm/rev, 0.5mm

Continue Figure (4.57)

At the same machining circumstances, the temperature at failure minute for triplex layers coated HSS was decreased by 4-14% comparing with carbide insert, as illustrated in Figure(4-58).

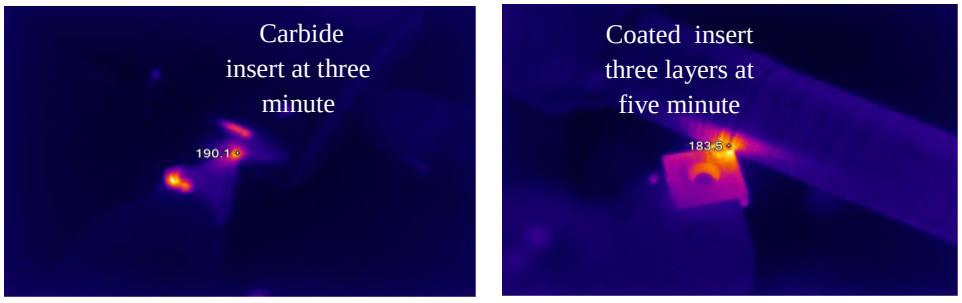

(a)-56m/min, 0.265mm/rev, 0.7mm

Figure (4.58): Recorded temperature (F°) at the contact point between the insert tip and work piece at different machining conditions forHSS coated aand carbide insert

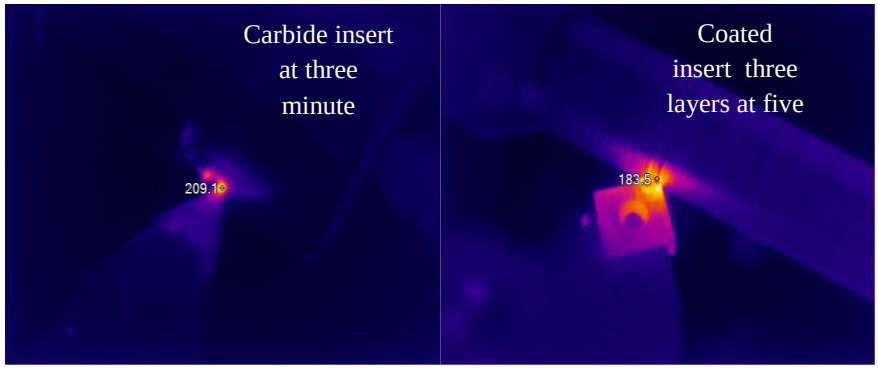

(b)-88m/min, 0.065 mm/rev, 0.5 mm

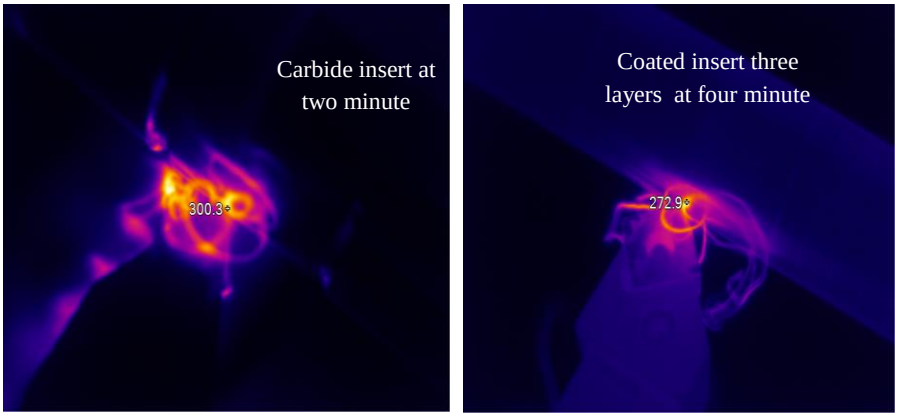

(c)-112m/min, 0.265mm/rev, 0.5mm

Continue Figure (4.58)

4.9. Modeling of the Result &Adequacy Checking of Model

An effective approach to determine the optimum parameters of a process for the multiple performance features, by the integration of the theory of grey relation with Taguchi technique was debated. Experiments were executed to find out the effect of process parameters (cutting velocity (ν), feed (ʃ) and depth of cut(t)) on the responses (tool life (F), temperature (T), and surface roughness (Ra)) of each cutting insert uncoated and coated with monolayer, two layers, and three layers. The results of the experiments are given in Table (4.12) for each cutting insert.

Table (4.12): Observed values for performance characteristics

EXP .NO.	The Responses														
	Machining conditions			Uncoated insert			Coated insert triple layers			Coated insert monolayer			Coated insert douple layers		
	(v) m/min	(ʃ) mm/rev	(t) mm	F(min)	T (℃)	Ra (µ)	F(min)	T (℃)	Ra (µ)	F (min)	T (℃)	Ra (µ)	F (min)	T (℃)	Ra (µ)
1	1	1	1	2.9	77.8	1.49	5.8	77.72	0.933	2.6	79.83	1.737	5.1	96	0.99
2	1	2	2	2.7	86.4	2.49	5	79.55	1.769	1.7	88.71	2.929	4.4	104.3	1.882
3	1	3	3	2.1	104	3.827	4.7	97.85	2.652	1.4	105.1	3.91	3.8	116	2.98
4	2	1	2	2.2	112	0.986	5	84.16	0.45	1.7	108.4	1.15	4	118.5	0.579
5	2	2	3	1.3	135.27	2.882	4	124.1	1.104	1.2	131.1	3.41	2.4	136.2	1.254
6	2	3	1	2	132.94	0.706	4.5	123	0.124	1.7	131.6	0.925	2.8	141.5	0.462
7	3	1	3	1.1	138.7	0.991	3.2	135	0.544	1.1	138.33	1.605	2.7	143.3	0.579
8	3	2	1	1.2	149.1	0.462	3.4	133.8	0.018	1.2	146.5	0.882	2.8	155.2	0.11
9	3	3	2	1	153.9	1.077	3.1	138.1	0.7	0.9	149.2	1.482	2	159	1.04

By using Data Fit ver. 9.1 software, regression models were developed for predicting the tool life ,surface roughness, and temperature for each cutting insert. Table (4.14) shows the predicted regression models for calculating the output (tool life, temperature , and surface roughness). The equations of output are developed with 95% confidence levels.

The coefficient of determination (R^2) is another measure that is familiarly utilized to explain adequacy of the predicted regression models. For the present resulted models, the values of the computed (R^2) for tool life, temperature, and surface roughness of the inserts, are shown in Table (4.13). Such values exhibit the quite adequacy of regression models.

Table (4.1): The designed models for predicting the tool life , temperature and surface roughness of the inserts with the coefficient of multiple determinations, R^2

Responses	Uncoated insert		Coated insert of triplex layer	
	Equations for Predicted regression model	R^2	Equations for Predicted regression model	R^2
Tool life (min)	**Tool life=-2.6013*10^{-2}v-1.83333ʃ-t+4.8223……..…(4.1)**	93.72	**Tool life = -3.3783*10^{-2} v-2.8333ʃ-1.1578t +8.1907…..(4.4)**	91.64
Temperature (℃)	**Temperature =1.0394v+103.766667ʃ+10.4149t+10.4474…….. (4.2)**	97.4	**Temperature = 0.8974v+103.45ʃ+10.9035t+11.6211…..(4.5)**	87.2
Surface roughness (µm)	**Surface roughness = -3.1533*10^{-2} v+3.5716ʃ+3.2621t+2.2359..(4.3)**	90.7	**Roughness =-2.5110*10^{-2} v+2.58166ʃ+2.1420t+1.6387…..(4.6)**	91.39

Responses	Coated insert monolayer		Coated insert of douple layer	
	Equations for Predicted regression model	R^2	Equations for Predicted regression model	R^2
Tool life (min)	**Tool life=-1.4695*10^{-2} v-2.3333ʃ-1.2105t+3.7039……(4.7)**	93.44	**Tool life =-3.4966*10^{-2} v-5.3333ʃ-1.1315t +7.7125.. (4.10)**	93.48
Temperature (℃)	**Temperature=0.9579 v+98.8999ʃ+9.1736 t+17.5167…..(4.8)**	97.3	**Temperature=0.8400 v +0.7631ʃ+ 0.7631t+41.8184…. (4.11)**	98.69
Surface roughness (µm)	**Roughness= $^{-}$2.7 680*10^{-2} v+3.0416ʃ+3.4810t+2.2390…..(4.9)**	86.83	**Roughness= -2.5217*10^{-2} v+3.89ʃ+2.1663t+1.5964….. (4.12)**	93.25

Adequacy of the developed models is then checked via employing the Analysis of Variance (ANOVA). Utilizing such method, one can notice that, as illustrated in Table (4.14), all the quadratic regression models are significant (0 < p-value < 0.05), except (t) on the uncoated insert's temperature responses, which have a less effect when compared to other machining conditions. Due to the narrow range levels for this condition, (ʃ) was added to the surface roughness of the uncoated insert. In addition, the (ʃ) & (t) have a less effect on the temperature of the coated insert with three layer due to the (v) greater effect when compared to other conditions. In coated inserts with two-layer, tool life response is unaffected by (t), whereas other machining variables have a greater impact. Finally, the (p-value of ʃ > 0.05) on the surface roughness of the coated insert with three layer because that factor has a limited range of levels, and so all models effectively represent the experimental data. In general, the feed is less influenced due to the narrow range for the value selected.

Table (4.14): The ANOVA for the fitted tool life for coated and uncoated cutting insert

Response	DF	Adj SS	Adj MS	F-value	P-value
Tool life of uncoated insert					
v(m/min)	1	3.2267	3.22667	87.21	0.000
ʃ (mm/rev)	1	0.2017	0.20167	5.45	0.067
t (mm)	1	0.4267	0.42667	11.53	0.019
Residual error	5	0.1850	0.03700		
Total	8	4.0400			
Temperature of uncoated insert					
vm/min)	2	5158.71	2579.36	329.03	0.003
ʃ(mm/rev)	2	658.20	329.10	41.98	0.023
t (mm)	2	110.80	55.40	7.07	0.124
Residual error	2	15.68	7.84		
Total	8	5943.39			
Surface roughness of uncoated insert					
vm/min)	1	4.6411	4.6411	27.29	0.003
ʃ(mm/rev)	1	0.7654	0.7654	4.50	0.087
t (mm	1	4.2370	4.2 70	24.91	0.004
Residual error	5	0.8504	0.1701		

Total	8	10.4939			
Tool Life of coated insert monolayer					
vm/min)	2	1.04667	0.52333	39.25	0.025
ʃ(mm/rev)	2	0.40667	0.20333	15.25	0.062
t (mm)	2	0.56000	0.28000	21.00	0.045
Residual error	2	0.02667	0.01333		
Total	8	2.04000			
Temperature of coated insert monolayer					
vm/min)	2	4353.73	2176.87	9588.31	0.000
ʃ(mm/rev)	2	609.45	304.73	1342.21	0.001
t (mm)	2	134.11	67.05	295.34	0.003
Residual error	2	0.45	0.23		
Total	8	5097.74			
Surface roughness of coated insert monolayer					
vm/min)	2	4.24744	2.12372	106.14	0.009
ʃ(mm/rev)	2	0.70325	0.35163	17.57	0.054
t (mm)	2	3.20555	1.60277	80.10	0.012
Residual error	2	0.04002	0.02001		
Total	2	8.19626			
Tool life for coated insert douple layer					
vm/min)	1	5.6067	5.6067	40.83	0.001
ʃ(mm/rev)	1	1.7067	1.7067	12.43	0.017
t (mm)	1	0.5400	0.5400	3.93	0.104
Residual error	5	0.6867	0.1373		
Total	8	8.5400			
Temperature of coated insert douple layer					
vm/min)	2	3342.13	1671.06	4284.78	0.000
ʃ(mm/rev)	2	590.53	295.26	757.09	0.001
t (mm)	2	34.93	17.46	44.78	0.022
Residual error	2	0.78	0.39		
Total	8	3968.36			
Surface roughness of coated insert douple layer					
vm/min)	1	2.8332	2.8332	23.12	0.005
ʃ(mm/rev)	1	0.9079	0.9079	7.41	0.042
t (mm)	1	1.7615	0.1225	14.38	0.013
Residual error	5	0.6127	0.1225		
Total	8	6.1153			
Tool life of coated insert triplex layer					
v (m/min)	2	5.78667	2.89333	217.00	0.005
ʃ(mm/rev)		0.60667	0.30333	22.75	0.042
t(mm)	2	0.56000	0.28000	21.00	0.045
Residual error	2	0.02667	0.01333		
Total	8	6.98000			
Temperature of coated insert triplex layer					
v (m/min)	2	3839.5	1919.77	32.61	0.030

ʃ(mm/rev)	2	662.3	331.16	5.63	0.151
t (mm)	2	512.6	256.30	4.35	0.187
Residual error	2	117.7	58.86		
Total	8	5132.2			
Surface roughness of coated insert triplex layer					
v (m/min)	**2**	3.38117	1.69058	43.28	0.023
ʃ(mm/rev)	**2**	0.40788	0.20394	5.22	0.161
t(mm)	**2**	1.74535	0.87267	22.34	0.043
Residual error	**2**	0.07813	0.03907		
Total	**8**	5.61252			

Figures (4.59) shows the 3D surface plot of output parameters tool life, , temperature, surface roughness for each uncoated and coated insert with three layers varying to the level of input parameters (ν) and (t). The tool life decreased with increased (ν and t) and temperature increased with increased (ν and t).While the surface roughness decreased with increased (ν) and decreased (t) for each coated with three-layer and uncoated inserts. According to ANOVA, these parameters had a greater impact on responses, hence they were chosen to demonstrate behavior.

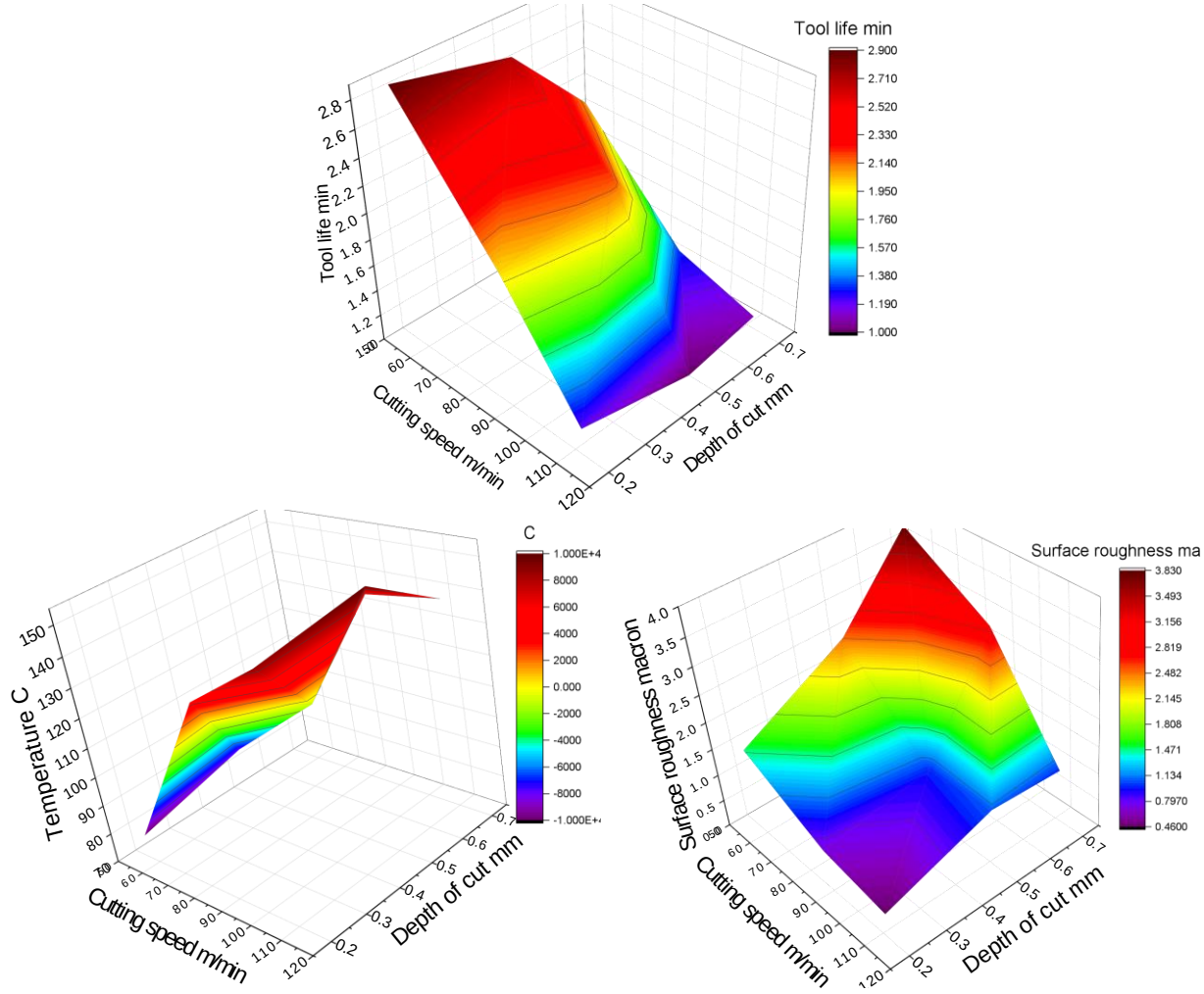

(a) uncoated insert

Figure (4.59): Effects of cutting speed and depth of cut on tool life, surface roughness, temperature for,(a):uncoated and (b):coated three layers inserts

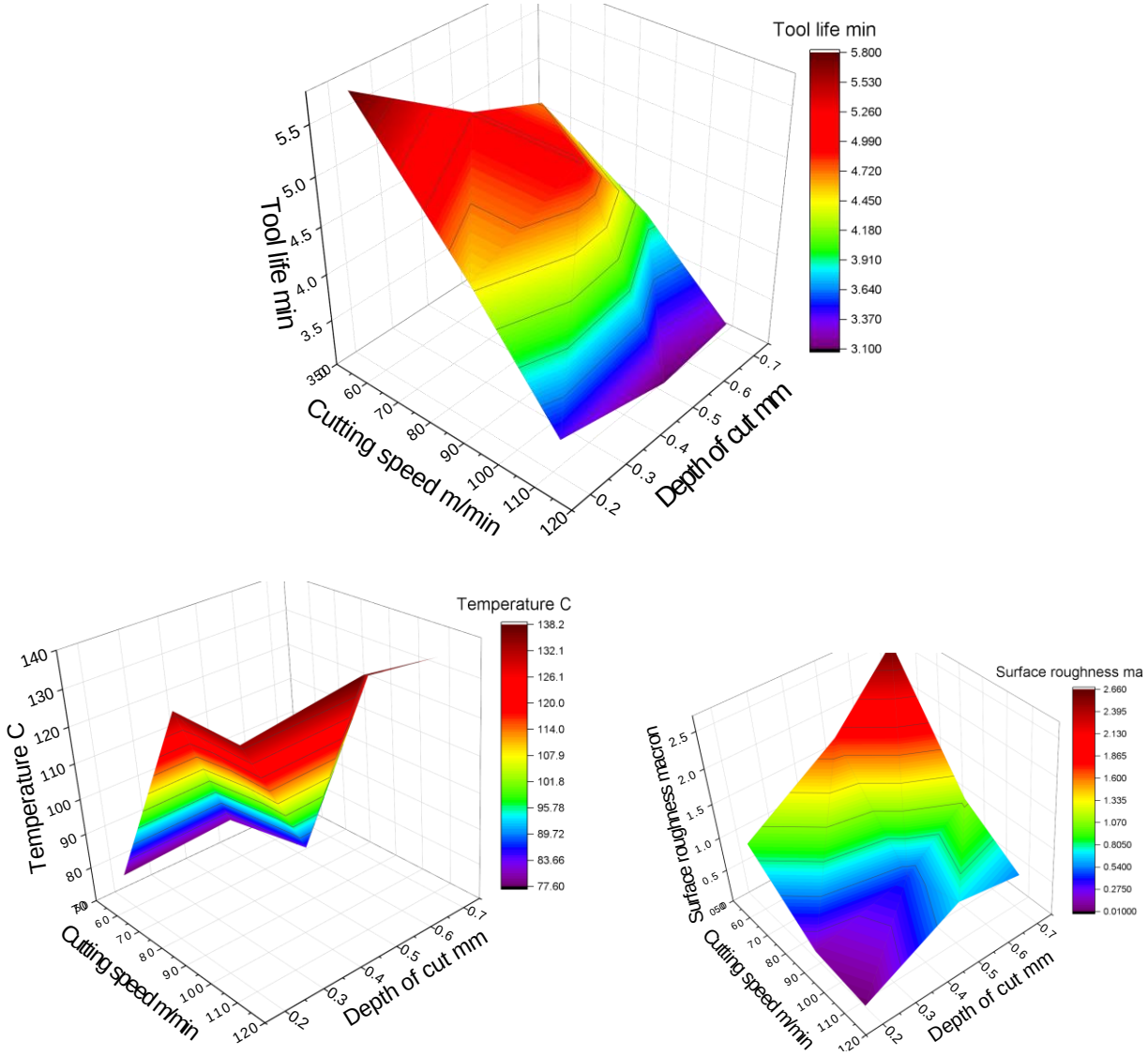

(b)Coated insert with three layers

Continue Figure (4.59)

4.9.1. Determination of optimal machining parameters in Gray Relation Analysis GRA

Here, the employment of Taguchi orthogonal array (OA) and (GRA) to determine the optimum values for the process parameters is explained in sequence. The optimum parameters of process with consideration of multiple performance features are determined and proved.

Pre-processing of data

In Gray relation analysis, pre-processing of data is needed because the range and a unit in the order of a single data may be unlike the others. Preprocessing of data is also inevitable if the scatter range of order is very big, or if the goal directions in the order are unlike. It is a transferring process of the initial order to a comparable order. For such intention, the results of experiments are normalized in the range (0-1). Based upon the data order features, there exist different techniques of pre-processing of data being used for the gray relation analysis. Response or output can be converted into the comparative series $x_i^{*}(k)$ according to equations 2.5, 2.6, for "the larger, the better", "the smaller, the better" characteristics.

Table (4.14) lists the normalized values for the tool life , temperature and surface roughness, where the tool life is for the larger the better while temperature and surface roughness are for the smaller the better. Then, the deviation sequence of the reference sequence $x_0^{*}(k)$ and the comparability sequence $x_i^{*}(k)$, for experiment numbers 1 to 9 can be calculated by application equation (2.7) the results are presented in below Table.

After data pre-processing is carried out, a grey relational coefficient can be calculated with the pre-processed sequence. It expresses the relationship between the ideal and actual normalized experimental results. The grey relational coefficient and grey relational grade are defined based on equations 2.8.

After obtaining the grey relational coefficient, the grey relational grade is computed by averaging the grey relational coefficient corresponding to each performance characteristic. The overall evaluation of the multiple characteristics is based on the grey relational grade. Table (4.15) shows the grey relational grade for each experiment using L_9 OA. The higher grey relational grade represents that the

corresponding experimental result is closer to the ideally normalized value. Experiment 9 has the best multiple performance characteristics among eight experiments because it has the highest grey relational grade. It can be seen that in the present study, the optimization of the complicated multiple performance characteristics of machining process has been converted into optimization of a grey relational grade.

Table (4.15): Normalized Deviation sequences, GRC and the rank of each experiment for uncoated and coated insert

Uncoated cutting insert								
Exp. No.	Tool life		Temperature		Surface roughness		Grey relational grade $\gamma i\ (k)= \frac{1}{3}(\xi i\ (1)+ \xi i\ (2) + \xi i\ (3))$	Rank
	Deviation Sequences	GRC ξi (1)	Deviation Sequences	GRC ξi (2)	Deviation Sequences	GRC ξi (3)		
1	0	1	0	1	0.305498	0.540661	0.846887	1
2	0.105263	0.818182	0.112076	0.806934	0.602675	0.373687	0.666268	2
3	0.421053	0.529412	0.343594	0.576867	1	0.264481	0.45692	7
4	0.368421	0.5625	0.448829	0.510684	0.155721	0.697809	0.590331	3
5	0.842105	0.36	0.754933	0.382903	0.719168	0.333333	0.358746	9
6	0.473684	0.5	0.724283	0.392743	0.072511	0.832187	0.574977	4
7	0.947368	0.333333	0.800053	0.369283	0.157207	0.695802	0.46614	6
8	0.894737	0.346154	0.936859	0.333333	0	1	0.559829	5
9	1	0.321429	1	0.319	0.182764	0.663014	0.434481	8
Coated cutting insert (monolayer)								
Exp. No.	Tool life		Temperature		Surface rough)ness		Grey relational grade $\gamma i\ (k)= \frac{1}{3}(\xi i\ (1)+ \xi i\ (2) + \xi i\ (3))$	Rank
	Deviation Sequences	GRC ξi (1)	Deviation Sequences	GRC ξi (2)	Deviation Sequences	GRC ξi (2)		
1	0	1	0	1	0.282365	0.596508	0.865503	1
2	0.529412	0.454545	0.128009	0.789648	0.676024	0.381758	0.541984	5
3	0.705882	0.384615	0.364279	0.568808	1	0.294501	0.415975	8
4	0.529412	0.454545	0.41185	0.538486	0.088507	0.825065	0.606032	2
5	0.823529	0.348837	0.73908	0.394007	0.834875	0.333333	0.358726	9
6	0.823529	0.454545	0.746288	0.391693	0.014201	0.9671	0.604446	3
7	0.882353	0.333333	0.843304	0.362988	0.238771	0.636135	0.444152	6
8	0.823529	0.348837	0.961078	0.333333	0	1	0.560724	4
9	1	0.306122	1	0.32457	0.198151	0.678112	0.436268	7
Coated cutting insert (douple layers)								

EXP. No.	Tool life		Temperature		Surface roughness		Grey relational grade $\gamma i\ (k)= \frac{1}{3}(\xi i\ (1)+ \xi i\ (2) + \xi i\ (3))$	Rank
	Deviation Sequences	GRC ξi (1)	Deviation Sequences	GRC ξi (2)	Deviation Sequences	GRC ξi(3)		
1	0	1	0	1	0.30662	0.501699	0.8339	1
2	0.225806	0.658537	0.131746	0.781003	0.617422	0.333333	0.590958	3
3	0.419355	0.509434	0.31746	0.596774	1	0.235889	0.447366	8
4	0.354839	1.227273	0.357143	0.568138	0.163415	0.653875	0.816428	2
5	0.870968	0.5	0.638095	0.424069	0.398606	0.436453	0.453507	7
6	0.741935	0.369863	0.722222	0.394141	0.122648	0.71567	0.493225	5
7	0.774194	0.36	0.750794	0.384915	0.163415	0.653875	0.466263	6
8	0.741935	0.369863	0.939683	0.333333	0	1	0.567732	4
9	1	0.303371	1	0.319654	0.324042	0.487885	0.370304	9
Coated cutting insert (triplex layers)								
Exp.No.	Tool life		Temperature		Surface roughness		Grey relational grade $\gamma i\ (k)= \frac{1}{3}(\xi i\ (1)+ \xi i\ (2) + \xi i(3))$	Rank
	Deviation Sequences	GRC ξi (1)	Deviation Sequences	GRC ξi (2)	Deviation Sequences	GRC ξi(3)		
1	0	1	0	1	0.34738	0.48897	0.829657	1
2	0.296296	0.6	0.030308	0.939941	0.34738	0.333333	0.624425	3
3	0.407407	0.521739	0.333389	0.587246	1	0.249466	0.452817	6
4	0.296296	0.6	0.106658	0.81642	0.164009	0.669598	0.695339	2
5	0.666667	0.4	0.768135	0.381765	0.412301	0.446342	0.409369	8
6	0.481481	0.48	0.749917	0.387446	0.040243	0.892002	0.586483	4
7	0.962963	0.315789	0.948658	0.333333	0.199696	0.624688	0.424604	7
8	0.888889	0.333333	0.928784	0.338055	0	1	0.557129	5
9	1	0.307692	1	0.321725	0.258922	0.562119	0.397179	9

Since the experimental design is orthogonal, it is then possible to separate out the effect of each process parameter on the grey relational grade at different levels. The mean of the grey relational grade for each level of the process parameters, namely cutting velocity, feed and depth of cut, can be computed. The results are shown in Table (4.16). As the larger GRG is suitable for optimum performance, the levels of the parameters for that are presented in the Table (4.16) for each cutting insert.

Table (4.16): Response table for the grey relational grade

Symbol	Machining Parameters	GRG Main Effect for uncoated insert					Levels for optimum performance
		Level 1	Level2	Level3	max-min	Rank	
A	Cutting speed (ν)	*0.656692	0.508018	0.486817	0.1699	2	
B	Feed rate (ʃ)	*0.634453	0.528281	0.488792	0.1457	3	
C	Depth of cut (t)	*0.660564	0.563693	0.427268	0.2333	1	A1B1C1
Total Mean Value GRG γm = 0.550509							
Symbol	Machining Parameters	GRG Main Effect for coated insert (monolayer)					
		Level1	Level2	Level 3	max-min	Rank	
A	Cutting speed (ν)	*0.60782	0.523068	0.480381	0.127439	3	Levels for optimum performance
B	Feed rate (ʃ)	0.638562	0.487144	0.485563	0.153002	2	
C	Depth of cut (t)	0.676891	0.528095	0.406284	0.270611	1	A1B1C1
Total Mean Value GRG γm =0.53709							
Symbol	Machining Parameters	GRG Main Effect for coated insert (two layers)					Levels for optimum performance
		Level1	Level2	Lvel3	max-min	Rank	
A	Cutting speed (ν)	*0.624074	0.58772	0.4681	0.155974	2	
B	Feed rate (ʃ)	*0.714518	0.537399	0.436965	0.277553	1	
C	Depth of cut (t)	*0.597796	0.592563	0.464699	0.133097	3	A1B1C1
Total Mean Value GRG γm=0.51882							
Symbol	Machining parameters	GRG Main Effect for coated insert (three layers)					Levels for optimum performance
		level 1	level 2	level 3	max-min	Rank	
A	cutting speed(ν)	*0.635633	0.56373	0.459637	0.1760	2	
B	feed (ʃ)	*0.649866	0.530308	0.478826	0.1710	3	A1B1C1
C	depth of cut (t)	*0.657756	0.572314	0.42893	0.2288	1	

	Total Mean Value GRG γm =0.553	
	*Optimal level of GRG for each parameters	

Figure (4.60) shows the grey relational grade obtained for different process parameters. The mean of the grey relational grade for each parameter is revealed by a horizontal line. Basically, the larger the grey relation grade is, the closer will be the cutting speed to the ideal value. Thus, the larger grey relational grade is desired for the optimum performance. Therefore, the optimal parameters setting for better tool life, lesser surface roughness and temperature is (A1B1C1), as presented in Table (4.17). Optimal level of the process parameters is the level with the highest grey relational grade for each cutting insert.

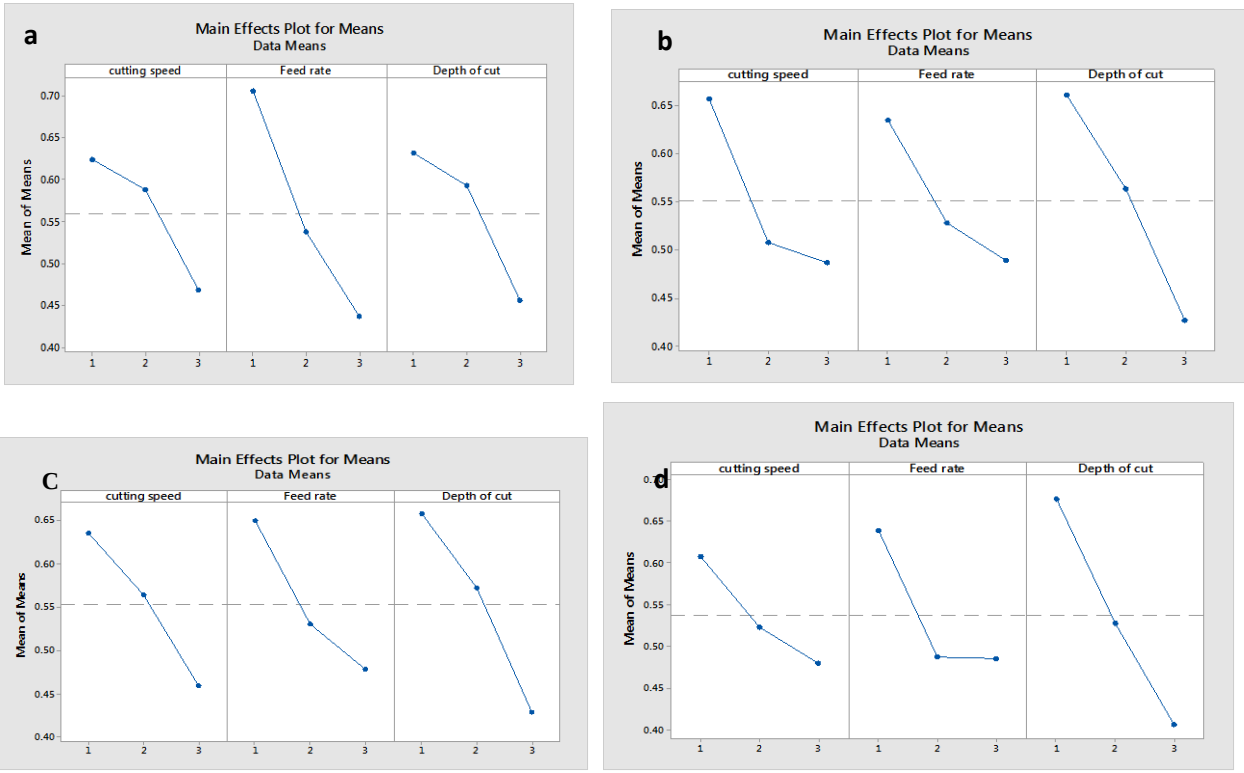

Figure (4.60): The effect of process parameters on the multi-performance characteristics cutting speed, feed rate, and depth of cut(a):uncoated insert,(b):coated insert triplex layer,(c): coated insert monolayer, (d): coated insert douple layers

Analysis of Variance for GRG

ANOVA for grey relational grade is presented in Table (4.17). Percentage contributions for each term affecting grey relational grade are shown in Figure (4.61).

This Figure clearly shows that the depth of cut is the dominant parameter that affects grey relational grade and hence contributes in improving the tool life and the minimum temperature and reducing the surface roughness of work piece for uncoated insert and coated insert with three layers.

Table(4.17): ANOVA of grey relational grade.

Uncoated insert						
Source	DF	Adj SS	Adj MS	F-value	P-value	Percentage contribution(ρ)
v(m/min)	2	0.051411	0.025705	29.51	0.033	30.308%
ʃ(mm/rev)	2	0.034049	0.017024	19.55	0.049	20.073%
t(mm)	2	0.082423	0.041211	47.32	0.021	48.591%
Residual error	2	0.001742	0.000871			1.026%
Total	8	0.169624				100%
Coated insert triplex layers						
v (m/min)	2	0.046980	0.023490	43.86	0.022	26.927%
ʃ (mm/rev)	2	0.046199	0.023100	43.13	0.023	26.479 %
t (mm)	2	0.080221	0.040110	74.89	0.013	45.979%
Residual error	2	0.001071	0.000536			0.613%
Total	8	0.174471				100%
Coated insert monolayer						
v(m/min)	2	0.025246	0.012623	20.66	0.046	13.79%
ʃ(mm/rev)	2	0.046339	0.023169	20.66	0.026	25.32%
t(mm)	2	0.110206	0.055103	90.19	0.011	60.21%
Residual error	2	0.001222	0.000611			0.66%
Total	8	0.183012				100%
Coated insert douple layers						
v(m/min)	3	0.03649	0.036492	7.62	0.040	16.96%
ʃ(mm/rev)	1	0.10819	0.108191	22.58	0.005	50.30%
t(mm)	1	0.04641	0.046415	9.69	0.026	21.58%
Residual error	5	0.02395	0.004791			11%
Total		0.21505				

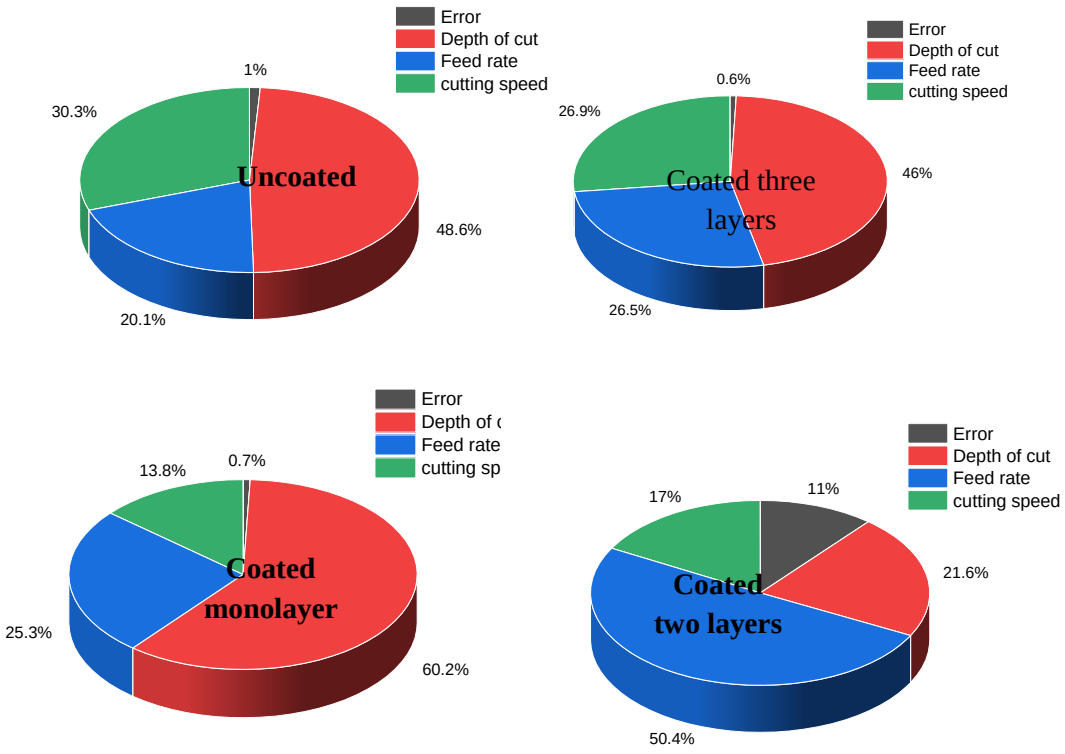

Figure (4.61): Percentage contributions of factors on the grey relational grade

Based on the above discussion, the optimal process parameters are cutting speed at level 1, feed rate at level 1, and depth of cut at level 1. It can be seen from Figures (4.60) and (4.61) that depth of cut is the most significant factor that affects the grey relational grade followed cutting speed and feed rate of uncoated insert and coated insert three layers. While in the coated insert monolayer layer, depth of cut is the most significant factor followed feed rate and cutting speed. In coated insert with two layer feed rate is the most significant factor that affects the GRG followed depth of cut and cutting speed.

For the best results, compare the responses (tool life, temperature, and surface roughness) of four cutting inserts (A1,B1,C1), show Table (4.17).

Confirmation test

Confirmation test has been carried out to verify the improvement of performance characteristics in machining coated and uncoated insert. The optimum parameters are selected for the confirmation test as presented in Table (4.18) shows the results of confirmation test carried out to validate GRA results. The estimated grey relational grade $\hat{\gamma}$ using the optimal level of the process parameters can be calculated using following equation [112, 113].

$$\hat{\gamma} = \gamma_m + \sum_{i=1}^{q}(\gamma_i - \gamma_m) \quad \ldots\ldots\ldots\ldots\ldots\ldots\ldots\ldots\ldots\ldots\ldots\ldots\ldots\ldots \quad (4.13)$$

Where γm is the total mean of the grey relational grade, γi is the mean of the grey relational grade at the optimal level, and q is the number of the process parameters that significantly affect multiple-performance characteristics.

The predicted tool life, temperature , surface roughness and grey relational grade for the optimal process parameters are obtained using equation (4.13) and also presented in Table (4.18), which shows the comparison of the experimental results using the initial (OA, A1B1C1) and optimal (grey theory prediction design, (A1B1C1), process parameters for uncoated and coated insert.

Based on Table 4.18, for example in uncoated insert, tool life is accelerated from 2.9to 2.98 min , temperature was decreased into 77.19 ℃ whereas the surface roughness was decreased into (1.02 µm).

The corresponding improvements in tool life temperature, surface roughness were 2.7 %, 0.8% and 31% respectively. In three layers coated HSS insert, the corresponding improvements in tool life ,temperature and surface roughness were 2%, 1.4% and 55% respectively. It is clearly shown that the multiple performance characteristics in the process are greatly improved through this study. Now, For the

best results, compare the responses (tool life, temperature, and surface roughness) of four cutting inserts (A1,B1,C1), show Table (4.16).

Table (4.18): Improvements In Grey Relational Grade with optimized process parameters.

Condition description	**Uncoated insert**		**Coated three layer**		**Coated two layer**		**Coated monolayer**	
	Predicted	Experimental	Predicted	Experimental	Predicted	Experimental	Predicted	Experimental
Tool life min	2.98	2.9	5.81	5.8	3.2	5.1	1.5	2.6
Temperature℃	77.19	77.8	76.61	77.72	112	96	86	79.83
Surface roughness µm	1.022	1.49	0.346	0.933	5	0.99	2	1.737
GRG	0.850647	0.550509	0.83635	0.553	0.89804	0.51882	0.84891	0.53709
Improvement in grey relational grade	=0.300138 =30%		= 0.283358 =28%		= 0.379 =37%		= 0.31182 =31%	

Now, compare the responses (tool life, temperature, and surface roughness) of four cutting inserts at the best experiment (A1,B1,C1). Tool life of three layer coated insert was increased by (100)%, temperature at first minute was decreased by(12)%, and surface roughness was deceased by (37)% comparing uncoated insert. While in comparing between two layer coated insert and uncoated insert. The life of coated inserts is extended by (75) %. The temperature dropped by (2) % in the first minute. In addition, the work piece's surface roughness was reduced by (34) %. Finally, When comparing these responses for all cutting inserts, the three layer coated insert is the best, with the longest tool life, lowest temperature, and lowest surface roughness, as shown in Table (4.19).

CHAPTER FIVE

Chapter Five

Conclusions and Recommendations

5.1. Conclusions and Recommendations

From the results of the present work, the following can be concluded:

1- The research found that the dip coating sol-gel procedure is an excellent way for depositing multi-layer of ceramic oxides on HSS tools.

2-To achieve the requisite film thickness, a total immersion period of thirty seconds was required, 5sec in titania precursor, 10 sec in alumina precursor, and 15 sec in zirconia in triplex coating. While in douple coating 5sec in titania precursor, 25 sec in alumina precursor. To achieve thin layer (douple) and (triplex) with thickness don't exceed (5-6) μm. A better adhering of HSS to the alumina+ zirconia coating was achieved through a layer of titania.

3- The highest surface roughness and coefficient of friction were recorded for the alumina monolayer coated insert. Monolayer also, has the shortest tool life and provides the highest work piece surface roughness.

4- The multilayer (triplex layers) coated HSS implant produced the best mechanical and physical performance. When comparing the triplex layer coated HSS insert to the uncoated cutting insert, the friction coefficient was reduced by 80%, the hardness was increased by 57%, the surface roughness was reduced by 63%, the thermal conductivity was reduced by 36%, and the wear rate was reduced by 71%.

5- In machining tests, the multi-layer (triplex layers) coating is proven to considerably minimize temperature ,flank wear, and surface roughness comparing

another cutting inserts. When coated (triplex layer) inserts compared to uncoated inserts, the life of coated inserts is extended by 85-183%. The temperature dropped by 11-13 % in the first minute. In addition, the work piece's surface roughness was reduced by 30-96%.

6- The results showed that the depth of cut is the dominant parameter that affects the grey relational grade for uncoated, triplex layers coated, and monolayer coated inserts and contributes 48%, 45%, and 60% respectively, in improving the responses, while the feed is the dominant parameter and contribution is 50% for douple layers coated insert in improving responses.

7- Under the same conditions of machining process and work piece, carbide cutting inserts was compared to coated (triplex layer) HSS inserts, tool life was extended by 30-53 %, and temperature at failure minute was reduced by (2-8)%.

5.2.Recommendations for Further Work

1- Studying the possibility of other cutting insert steel instead of high speed steel.

2-Trying to produce another coated cutting tool design(Single point turning tool) or drill to study the machining test for low carbon steel work piece.

References

[1] Bruna Aparecida Rezende, Anderson Junior dos Santos, and Marcelo Araujo Camara.(2019), " Characterization of ceramics coatings processed by sol-gel for cutting tools", Coatings, 9,557, pp. 1-12.

[2]Hassan Abdel –Gawad El-Hofy. (1976), Advanced Machining Processes, Alexandria University, Egypt.

[3] Bolton, W., & Higgins, R. A. (2006). Materials for engineers and technicians. Routledge.

[4] Yunqing Gu, Ke Xia, Denghao Wu, Jiegang Mou, and Shuihua Zheng. (2020), "Technical Characteristics and wear- resistant mechanism of nano coatings", Coatings, 10, 233, pp. 1-24.

[5] Krzak, J., Szczurek, A., Babiarczuk, B., Gąsiorek, J., & Borak, B. (2020). Sol–gel surface functionalization regardless of form and type of substrate. In Handbook of Nanomaterials for Manufacturing Applications (pp. 111-147). Elsevier.

[6] Mellor, B. G. (Ed.). (2006). Surface coatings for protection against wear. Woodhead Publishing.

[7] Hugh O. Pierson, Handbook Of Chemical Vapor Deposition(CVD) Principles, Technology, and Applications, Second Edition, (NOYES PUBLICATIONS Park Ridge, New Jersey, U.S.A. William Andrew Publishing, Llc Norwich, New York,1999), Consultant and Sandia National Laboratories (retired) Albuquerque, New Mexico.

[8] Bose, K. and Wood, R.J.K., (2005), 'High velocity solid particle erosion behavior of CVD boron carbide on tungsten carbide', Wear, 258, 366–376.

[9] K.F.Tam, F.T.Cheng, and H.C. Man. (2000), " Proceeding of the conference on laser –solid interactions for materials processing", MRS Spring Meeting, Materials research society.

[10] W.E.Ballard. (1963), Metal spraying and Flame Deposition of Ceramics and Plastics, 4th ed., Griffin, London, U.K.

References

[11] Uhlmann, E., Wiemann, E., Yang, S., Krumeich, J., & Layyous, A. (1995). New coating developments for high performance cutting tools. *Metal finishing*, *93*(5), 2-2.

[12] Amir Dehghanghadikolnei, Jamal Ansary, and Reza Choreishi. (2018), "Sol-Gel process applications: Amini –review", Proceeding of the Nature Research Society.

[13] ASM Handbook. (1994), Surface Engineering, Volume 5, ASM International committee.

[14] Mahdi KHADEM, Oleksiy V. PENKOV Hee-Kyung YANG1, Dae-Eun KIM, (2017), "Tribology of multilayer coatings for wear reduction", Friction, pp 248-262.

[15] Dong Jin Kim, Sung Hong Hahn, Sung Hoon Oh, and Eui Jung Kim. (2002), " Influence of calcination temperature on structural and optical properties of TiO_2 thin films prepared by sol-gel dip coating", Materials Letters, No. 57, pp. 355-360.

[16] Pakseresht, A. H. (Ed.). (2018). Production, Properties, and Applications of High Temperature Coatings. IGI Global.

[17] Davim, J. P. (Ed.). (2011). Machining of hard materials. Springer Science & Business Media.

[18] Smith, G. T. (2008). Cutting tool technology: industrial handbook. Springer Science & Business Media.

[19] Astakhov, V. P., & Davim, J. P. (2008). Tools (geometry and material) and tool wear. In *Machining* (pp. 29-57). Springer, London.

[20] Groover, M. P. (2020). Fundamentals of modern manufacturing: materials, processes, and systems. John Wiley & Sons.

[21] Trent, E. M., & Wright, P. K. (2000). Metal cutting. Butterworth-Heinemann.

[22] Valery Marinov, (2008), Manufacturing Process For Metal Products, Copyright Kendall Hunt Publishing Company.

References

[23] Shaojun, S., Xianping, Z., & Chengtong, S. (2018, October). Heat-treatment and properties of high-speed steel cutting tools. In IOP Conference Series: Materials Science and Engineering (Vol. 423, No. 1, p. 012031). IOP Publishing..

[24] Takigawa, H., Manto, H., Kawai, N., & Homma, K. (1981). Properties of high-speed steels produced by powder metallurgy. powder metallurgy, 24(4), 196-202.

[25] Shephard, R. G., Harrison, J. D. L., & Russell, L. E. (1973). The fabrication of high-speed tool steel by ultrafine powder metallurgy. Powder Metallurgy, 16(32), 200-219.

[26] Burakowski, T., & Wierzchon, T. (1998). Surface engineering of metals: principles, equipment, technologies. CRC press.

[27] Black, J. T., & Kohser, R. A. (2007). Material & processes in manufacturing tenth edition. University of Missouri–Rolla 1807.

[28] Mikell P. , Groover, (2012), Introduction To Manufacturing Process.

[29] Sonawane Gaurav, V. G. Sargade, (2011), "Comparative performance evaluation of uncoated and coated carbide inserts in dry end milling of stainless steel (SS 316L)", International Conference In Computational Intelligence (ICCIA).

[30] Childs, T. H., Maekawa, K., Obikawa, T., & Yamane, Y. (2000). Metal machining: theory and applications. Butterworth-Heinemann.

[31] Isha Tawade, Pradnya, Shingade, Tanu Thakur, (2014), Cutting tool wear measurement using image processing techniques ,Journal Of Harmonized Research In Engineering ,141- 146.

[32] Mohamed Shnfir, Oluwole A. Olufayo , Walid Jomaa and Victor Songmene. (2019), “Machinability Study of Hardened 1045 Steel When Milling with Ceramic Cutting Inserts”, Article, Materials.

[33] Rusdi Nur, MY Noordin, S Izman and D Kurniawan. (2015), “Machining parameters effect in dry turning of AISI 316L stainless steel using coated carbide tools”, Journal Process Mechanical Engineering.

References

[34] K. Salonitis , A. Kolios, (2013), Reliability assessment of cutting tools life based on advanced approximation methods, Procedia CIRP, Volume 8, 397-402.

[35] B. Fnides, S. Boutabba, M. Fnides, H. Aouici, M. A. Yallese, (2013), Cutting tools flank wear and productivity investigation in straight turning of X38crmov5-1 (50 HRc), International Journal of Applied Engineering and Technology , Vol. 3 (1) January-March, Pp.1-10.

[36] Gada, V. B., & Nookala, A. (2013). The impact of cutting conditions on cutting forces and chatter length for steel and aluminum.

[37] Tash M.et.al., (2006) Effect of metallurgical parameters on the machinability of heat-treated 356 and 319 aluminum alloys, Materials Science and Engineering A 434 pp: 207–217.

[38] Kadirgama K, Noor MM, Abou-El-Hossein KA, et al. (2010), "Effect of dry cutting on force and tool life when machining aerospace material", International Journal of Mechanical, Aerospace, Industrial, Mechatronic and Manufacturing Engineering 4: 1222–1226.

[39] Xie, L. (2004). Estimation of two-dimension tool wear based on finite element method (Doctoral dissertation, Zugl.: Karlsruhe, Univ., Diss., 2004).

[40] Khandey Umesh,(2000), Optimization of surface roughness, material removal rate and cutting tool flank wear in turning using extended taguchi approach, MSc. thesis, National Institute of technology Rourkela 769008, India, .

[41]Young Perry L., (2007), Estimating parameters resulting from various machining techniques for fluid flow applications, Proceedings of the Fifth International Conference on Nanochannels, Microchannels and Minichannels ICNMM.

[42] Childs, T. H., Maekawa, K., Obikawa, T., & Yamane, Y. (2000). Metal machining: theory and applications. Butterworth-Heinemann.

[43] Rajshekhar Lalbondre, Prasad Krishnab, Mohankumar G. , (2014), An experimental investigation on machinability studies of steels by face turning, 3rd international conference on materials processing and characterisation (ICMPC 2014), Procedia Materials Science 6 1386 – 1395..

References

[44] Bin Li, (2012), A Review of tool wear estimation using theoretical analysis and numerical simulation technologies, Int. Journal of Refractory Metals and Hard Materials 35, 143–151.

[45] Gaurav Bahuguna, Amit Kumar, Rajeev Singh. (2016), "Thin film coating through sol-gel Technique", Chemical sciences, Vol. 6 (7), pp. 65-72.

[46] Ch. Sateesh, Kumar, Saroj Kumar Patel. (2018), " Application of surface modification techniques during hard turning", Internatinal Journal of refractory metals and hard materials, PP. (112-127).

[47] Ran Ji, (2014),Development and characterization of nano-multilayer cralsin coating systems for cutting tools, PhD. Thesis of The University of Birmingham,.

[48] S.E. Cordes, (2012),PVD-alumina coatings on cemented carbide cutting tools: a study about the effect on friction and adhesion mechanism, Journal of Tribology in Industry, Vol. 34, No 1,24-28.

[49] K.Tuffy, G.Byrne, D. Dowling. (2004), " Determination of the optimum TiN coating thickness on WC inserts for machining carbon steels", J.Mater. Process Technol, pp. (1861-1866).

[50] C.S.Kumar, S.K.Patel. (2017), " Hard machining performances of PVD AlCrN coated Al_2O_3/TiCN ceramic inserts as a function of a thin film thickness", Ceram, pp.(13314-13329).

[51] SergeiN. Grigoriev, A.A. Vereschaka, A.S. Vereschaka, A.A.Kutin.(2012), "Cutting tools made of layered composite ceramics with nano-scale multilayered coatings", Sciverse Science Direct, pp.301-306.

[52] E.Uhlmann, J.A. Oyanedel Fuentes, R.Gerstenberger, H.Frank, (2013) "NAlTiN/a-Si_3N_4 and nc-AlCrN/a-Si_3N_4 nanocomposite coatings as protection layer for PCBN tools in hard machining", Surf. Coat. Technol, pp. 142-148.

[53] Srecko Paskvale."Properties of PVD hard coatings" University of Ljubljana faculty of Mathematics and Physics.

References

[54] Bose, K. and Wood, R.J.K.,(2005), 'High velocity solid particle erosion behavior of CVD boron carbide on tungsten carbide', Wear, 258, 366–376.

[55] N.B.Dahotre, Ed. (1998), Lasers in Surface Engineering, ASM International.

[56] K.F.Tam, F.T.Cheng, and H.C. Man. (2000), " Proceeding of the conference on laser –solid interactions for materials processing", MRS Spring Meeting, Materials research society.

[57] Streitberger, H. J., & Dossel, K. F. (Eds.). (2008). Automotive paints and coatings. John Wiley & Sons.

[58] W.E.Ballard. (1963), Metal spraying and Flame Deposition of Ceramics and Plastics, 4th ed., Griffin, London, U.K.

[59] Raliya, R., Saharan, V., Choudhary, K., Summarwar, S., Gulecha, K., Gupta, V., & Sain, P. M. (2019). Synthesis and Characterization. Nanoscale Engineering in Agricultural Management.

[60]Pertti Auerrkari. Espoo (1996), Mechanical and Physical Properties of Engineering Alumina Ceramics, VTT Manufacturing Technology.

[61] Xiaobo Chen and Samuel S. Mao. (2007), " Titanium Dioxide Nanomaterials: Synthesis, properties modification, and Application", American Chemical Society.

[62] Smallman, R. E., & Bishop, R. J. (1999). Modern physical metallurgy and materials engineering, Butterworth-Heinemann.

[63] James F.Shackelford and RobertH.Doremus, (2008), Ceramic and Glass Materials, New York.

[64] Ralf Riedel and Wei Chen, (2010), Ceramic Science and Technology, printed , in the Federal Republic of Germany.

[65] Ilhan Asiltürk and Süleyman Nes_eli, (2012),' Multi response optimisation of cnc turning parameters via taguchi method-based 131 response surface analysis', Measurement, Vol. 45, PP: 785–794,

References

[66] M. Nalbant , H. Gokkaya and G. Sur, (2007),'Application of Taguchi method in the optimization of cutting parameters for surface roughness in turning', Materials and Design, Vol.28, PP: 1379–1385, DOI:10.1016/j.matdes.2006.01.008

[67] Anoop Kumar Sood , R.K. Ohdar and S.S. Mahapatra, (2009),' Improving dimensional accuracy of fused deposition modelling processed part using grey taguchi method', Materials and Design, Vol. 30,PP: 4243– 4252, DOI:10.1016/j.matdes.2009.04.030.

[68] Rama Rao. S and Padmanabhan. G. (2012) "Application of taguchi methods and anova in optimization of process parameters for metal removal rate in electrochemical machining of al/5%sic composites", International Journal of Engineering Research and Applications (IJERA), Vol. 2, Issue 3, pp. 192-197, May-June.

[69] Md Zakir Hussain, Sabah Khan and Pranjal Sarmah, (2020),'Optimization of powder metallurgy processing parameters of al_2o_3/cu composite through taguchi method with grey relational analysis', journal of king saud university– engineering sciences,Vol. 32, PP:274–286, DOI:10.1016/j.jksues.2019.01.003.

[70] Anoop Kumar Sood , R.K. Ohdar and S.S. Mahapatra, (2009),' Improving dimensional accuracy of fused deposition modelling processed part using grey taguchi method', Materials and Design, Vol. 30,PP: 4243– 4252, DOI:10.1016/j.matdes.2009.04.030

[71] Saad Hameed Al-Shafai, (2018), " Multi objective optimization to improve surface integrity in WEDM of Al/WCP metal matrix composites using grey relational analysis, Journal of engineering and applied sciences, University of Babylon, pp. 10173-10181

[72] A. Noorul Haq, P. Marimuthu and R. Jeyapaul, (2008),' Multi response optimization of machining parameters of drilling al/sic metal matrix composite using grey relational analysis in the taguchi method', Advanced Manufacture Technology, Vol. 37,PP:250–255, DOI 10.1007/s00170-007-0981-4.

[73] D.Pakula, L.A.Dobrzanski,K. Golombek, M. Pancielejko, A.Kriz.,(2004) " Structure and properties of Si_3N_4 nitride ceramics with hard wear resistant coating", Materials processing technology, volume9, No. 60, pp. 388-393.

[74] L.A.Dobrzanski and J. Mikula. (2005), " Structure and properties of PVD and CVD coated Al_2O_3+TiC mixed oxide tool ceramics for dry on high speed cutting processes", Journal of Materials Processing Technology, pp. 822-831.

[75] M.A.EI Hakim, M.D. Abad, M.M.Abdelhameed, M.A.Shalaby, S.C Veldhuis. (2011), " Wear behavior of some cutting tool materials in hard turning of HSS", Tribology International, pp.1174-1181.

[76] SergeiN. Grigoriev, A.A. Vereschaka, A.S. Vereschaka, A.A.Kutin.(2012), "Cutting tools made of layered composite ceramics with nano-scale multilayered coatings", Sciverse Science Direct, pp.301-306.

[77] Natalia L. Cadena, Rodrigo Cue-Sampedro, Hector R. Siller, Ana M. Arizmendi-Morquecho, Carlos I.Rivera- Solorio. (2013), " Study of PVD ALCrN coating for reducing carbide cutting tool deterioration in the machining of titanium alloys", Journal Materials, pp. 2143-2154.

[78] Kawthar Y.AL-Dulaimi, Dr. Haydar A. H. Al-Ethari, BogdanWarcholinski, (2019), Taguchi DOE for investigating the effect of TiC coating layer on the performance of cemented carbide cutting tools, Al-Qadisiyah Journal for Engineering Science.

[79] Amin D. Thamir , Adawiya J. Haider , Faras Q. Mohammed , Khaled M. Chahrour. (2017), "Hybrid gas phase Ti-B-C-N coatings doped with Al", Journal of Alloys and Compounds, pp.368-375.

[80] Puneeth H V and Smitha B S, (2017)," Studies on Tool Life and Cutting forces for drilling operation using uncoated and coated HSS tool", International Research Journal of Engineering and Technology (IRJET), Volume 04.

[81] Meng Hu, Lulu Jing, Qinglong An, Weiwei Ming, Chunrong Bian, Ming Chen .(2017), " Tribological properties and milling performance of HSS-Co-E tools with fluorinated surfactants-based coatings agaist Ti-6Al-4V", Journal Wear, pp. 134-142

[82] Juan Carlos Campos Rabio, Bruna Aparecida Rezende, Luciano Machado Gomes Vieira, Manuel Houmard. (2017), "Drilling of aluminum/PE sandwich material with novel TiO_2-coated HSS drill deposited by sol- gel process", Ind Journal Adv Manuf Technol.

References

[83] Guangming Zheng, Rufeng Xu, Xiang Cheng, Guoyong Zhao, LiLi, Jun Zhao. (2018), " Effect of cutting parameters on wear behavior of coated tool and surface roughness in high –speed turning of 300M", Journal Measurement, pp.99-108

[84] Natalia Fernanda santos pereira, Juan Carlos Campos Rubio, Anderson Junior dos Santos. (2019), "Drilling of nodular cast iron with anovel SiO_2 coating deposited by sol-gel process in HSS drill", The International Journal of Advanced Manufacturing Technology.

[85] Al-Ethari, H., Al-Dulaimi, K. Y., Warcholinski, B., & Kuznetsova, T. A. (2019). Interrelation of surface temperature and tribological characteristics of a protective coating on a tool. Journal of Friction and Wear, 40(6), 603-608.

[86] M.S,Liborio, G.B.Praxedes, L.L.F.Lima, I.G.Nascimento, R.R.M. Sousa, M.Naeem. (2020), " Surface modification of M2 steel by combination of cathodic cage plasma deposition and magnetron sputtered MoS2-TiN multilayer coatings", Surface and Coating Technology.

[87] R.Manivannan, S. Sundararaj, R.Dheenasagar, K.Giridharan, P.R. Sivaraman, V.Udhayarani.(2020), " Influence of Al_2O_3, SiC and B_4C covalent multilayer PVD coating on surface properties of HSS", Materials Today: Proceedings.

[88] ASTM Handbook (1989), Iron and Metal Products, vol. 01.01.

[89] NileshT.Khot, Anil S.Morkane, Umesh V.Borkar, Sanke S.Maske, Prof. B.S.Kamble, (2018), Study the effect of eching time and concenteration on microstructure of SG 400/12 Grade ductile cast iron, Volume 4, Issue 9, Science and Technology

[90] T. Ramkumar, P. Narayanasamy, M. Selvakumar, and P. Balasundar, (2018),' Effect of B_4C Reinforcement on the Dry Sliding Wear Behaviour of 138 Ti-6Al-$_4$V/B_4C Sintered Composites Using Response Surface Methodology', Arch. Metall. Mater. Vol. 63, No.3, PP: 1179-1200, DOI: 10.24425/123791.

[91] ASTM Standards C633-79, American Society of Testing and Materials, Philadelphia, PA.

References

[92] Duanjie L.(2014), Nanovea, Scratch hardness measurement using mechanical tester.

[93] Hani Mahmood Hussien, (2013), " Studying the ultrasonic properties, DC conductivity, and coefficient of thermal conductivity of PVA-Egg shells composite, Advances in physical theories and applications.

[94] Aman Joshi, Rohit Rampal.2014 " Effect of cutting parameters on tool wear of coated carbide tool in hard turning of aisi 4340", Scientific Journal Impact Factor, Joshi, 3(11): Nov November.

[95] Tool-Life testing with single- point turning tools, ISO 3685:1993.

[96] Tadao Sugimoto, Xingping Zhou, and Atsushi Muramatsu. (2003), " Synthesis of uniform anatase TiO_2 nanoparticles by gel-sol method formation process and size control", Journal of Colloid and Interface Science pp. 43-52.

[97] Jung Won Lee, H.Y.Sohn, and Byong-Sun Chun. (1993), " Dip coating of alumina films by the sol-gel method", Material Research Society.

[98] S.Sakka. (1988), "Science of Sol –Gel Methods", Uchidarokakuho Publishing Co, Tokyo, Japan, pp.85-103.

[99] Natalia L. Cadena, Rodrigo Cue-Sampedro, and Santiago Di-Nardo. (2013), " Study of PVD AlCrN Coating for reducing carbide cutting tool deterioration in machining of titanium alloys", Journal Materials, Surface and coating technology.

[100] J. Valli and U.Makela. (1985), " TiN coating adhesion studies using the scratch test method", J.Vac.Scl. Technol, A,Vol. 3, No.6.

[101] Masalski, J., Gluszek, J., Zabrzeski, J., Nitsch, K., & Gluszek, P. (1999). "Improvement in corrosion resistance of the 316l stainless steel by means of Al2O3 coatings deposited by the sol-gel method". *Thin solid films*, *349*(1-2), 186-190.

[102] S.K.Tiwari, Manju Tripathi, and Raghuvir Singh. (2012), " Electrochemical behavior of zirconia based coatings on mild steel prepared by Sol-gel method", Corrosion Science, pp. (334-341).

[103] Prengel H.G.and et.al.(1998), " State of the art in hard coating for carbide cutting tools", Surface and Coating Technology, 102, 183-190.

[104] Jia, R., et al., Microstructure and wear resistance of WC and high chromium cast iron hardfacing layers, (2020),Coatings,. 10(9): p. 852.

[105] Dishwar, R.K., et al., Smelting process of chromite ore fines to produce crude Fe–Cr–Ni–N Alloy, (2020),Transactions of the Indian Institute of Metals, **73**(3): p. 537-542.

[106] Yan, H., X. Huang, and S. Xi, Using ethanol for preparation of nanosized TiO_2 by gaseous detonatio, (2014), Combustion, Explosion, and Shock Waves, **50**(2): p. 192-195.

[107] Ussain, D.H., A.M. Rheima, and S.H. Jaber, (2020), Cadmium ions pollution treatments in aqueous solution using electrochemically synthesized gamma aluminum oxide nanoparticles with DFT study, Egyptian Journal of Chemistry, 63(2): p. 417-424.

[108] Shi, F., et al., Fabrication of well-dispersive yttrium-stabilized cubic zirconia nanoparticles via vapor phase hydrolysis. (2012), Progress in Natural Science: Materials International, **22**(1): p. 15-20.

[109] Andi M. Limarga, Sujanto Widjaja, and Tick Hon Yip. (2005), " Mechanical properties and oxidation resistance of plasma-sprayed multilayered Al_2O_3/ZrO_2 thermal barrier coatings", Surface and Coatings Technology, pp. (93-102).

[110] Mia, M. and Dhar, N.R., (2018), Modeling of surface roughness using RSM, FL and SA in Dry hard turning, Arab. J. Sci. Eng., vol. 43, pp. 1125–1136.

[111] Zhang, S. and Liu, Z., (2008) An analytical model for transient temperature distributions in coated carbide cutting tools, Int. Commun. Heat Mass Transfer, vol. 35, pp. 1311–1315.

[112] Balasubramanian S. and Ganapathy S. (2011) "Grey relational analysis to determine optimum process parameters for wire electro discharge machining (WEDM)", International Journal of Engineering Science and Technology", 3 (1), 95-101.

[113] Al-Ethari, H., Abbas, S., & Zamel, E. K. (2021, February). Optimization of Manufacturing Titanium-Magnesium alloy for Biomaterial Applications using

References

Grey Relational Analyses. In *IOP Conference Series: Materials Science and Engineering* (Vol. 1094, No. 1, p. 012148). IOP Publishing.

TÜV AUSTRIA
EN ISO 9001:2015
EN ISO 14001:2015

Ministry of Industry and Minerals
State Company for Inspection and Engineering Rehabilitation (SIER)
Engineering Insp. & lab Department

Client : وزارة التعليم العالي والبحث العلمي / جامعة بابل – كلية الدراسات العليا
Order No: 121 / 2021
Tested Item: قطعة معدنية
Address: Iraq- Babylon
Date of Test: 23 / 3 / 2021
Type of Test: Chemical Composition

Test Report

Sample	C%	Si%	Mn%	P%	S%	Cr%	Mo%	Ni%	Al%	Cu%	W%	Co%	V%	Fe %
قطعة معدنية	1.03	0.271	0.308	0.0292	0.0129	4.03	5.3	0.136	0.0000 5	0.0927	6.8	0.32	1.99	Bal.

الملاحظات
- النتيجة تخص النموذج المفحوص فقط .
- تم الفحص بدرجة حرارة (24°C) ونسبة الرطوبة(% 20).

مدير قسم الفحص الهندسي و المختبرات
المراجعة
الفاحص

AUSTRIA
EN ISO 9001:2015
EN ISO 14001:2015

Ministry of Industry and Minerals
State Company for Inspection and Engineering Rehabilitation
(SIER)

121 ISO 17025:2005 ISO 9001: 2015 ISO14001: 2015

Client: وزارة التعليم العالي والبحث العلمي / جامعة بابل / كلية الدراسات العليا
الطالب / وزارة اسعد فيلي

Address:-Iraq- Baghdad

Order No:-121/ 2021

Date of Test: 23 / 6/ 2021

Tested Item:- مقاطع حديدية

CERTIFICATE

Sample	Type of Material	
Shaft (Ø= 51mm	ASTM A 1 60-84	المعدن يقارب النوعية
Metal piece HSS	ASTM A 600 M3 Class 1	المعدن يقارب النوعية

الملاحظات :

- المطابقة من حيث الخواص المفحوصة فقط .

مدير قسم البحث والتطوير
م. [illegible]

مسؤول شعبة المواصفات
م. ثمارة نوري عبد علي

اعداد
صفا عبد الحمن مجيد

TÜV AUSTRIA
EN ISO 9001:2015
EN ISO 14001:2015

Ministry of Industry and Minerals
State Company for Inspection and Engineering Rehabilitation (SIER)
Engineering Insp. & lab Department

Client: وزاره التعليم العالي والبحث العلمي/ جامعه بابل/ كليه الدراسات العليا / الطالبه - ورود اسعد مذب
Order No: 121/2021
Tested Item: مقاطع حديديه
Address: Baghdad- Iraq
Date of Test: 21/6/ 2021
Type of Test: Hardness

Test Report

Sample	Ultimate Stress (Rm) N/mm²	Yield strength (Re) N/ mm²	Stress ratio (tensile/yield (Rm/Re)	Elongation %	Elongation at max. force %	Bending Test	Hardness Test HRB	Hardne.. Test HRC
Shaft Ø=51mm	----	----	----	----	----	----	93	.....
Metal piece HSS	----	----		----	----	----	.....	65.7

ملاحظات
- النتيجة تخص النموذج المفحوص فقط .
- تم الفحص بدرجة حرارة (24 C) ونسبة الرطوبة(% 20).

مدير قسم الفحص الهندسي و المختبرات
م. حيدر [illegible] سلمان

المراجعة
م. حيدر [illegible] سلمان

الفاحص
[illegible] حسين

Head office: Baghdad -Iraq /Baghdad -Hilla Highway E-mail: mahedir@sier.gov.iq, lab.sier@sier.gov.iq
DG Office +9647810484016 Planning Dep Head: +9647706084844IP: 91.106.34.21 – SIER@engineering.com

TÜV AUSTRIA
EN ISO 9001:2015
EN ISO 14001:2015

Ministry of Industry and Minerals
State Company for Inspection and Engineering Rehabilitation (SIER)
Engineering Insp. & lab Department

Client : وزارة التعليم العالي والبحث العلمي – جامعة بابل – كلية الدراسات العليا
Order No : 121 / 2021
Tested Item: shaft
Address: Baghdad -Iraq
Date of Test: 1 / 6 / 2021
Type of Test: Chemical Composition

Test Report

Sample	C%	Si%	Mn%	P%	S%	Cr%	Mo%	Ni%	Al%	Cu%	Fe%
Shaft Ø40mm	0.132	0.187	0.586	0.0205	0.0428	0.0414	0.0062	0.0389	0.0039	0.0607	Bal.
✓ Shaft Ø50mm	0.505	0.304	0.610	0.030	0.0432	0.128	0.0097	0.135	0.0147	0.192	Bal.

الملاحظات :
- النتيجة تخص النموذج المفحوص فقط
- تم الفحص بدرجة حرارة (25°C) ونسبة الرطوبة (20 %)

مدير قسم الفحص الهندسي و المختبرات | المراجعة | الفاحص

Head office: Baghdad -Iraq 'Baghdad –Hilla Highway' E-mail: mahed@sier.gov.iq, lab.sier@sier.gov.iq
DG Office +964 7810484016 Planning Dep Head: +964 770 0848448 ... - SIER engineering Comp

DOCUMENT ID: [illegible] | Issue No: 01 | Issue Date 18/02/2020 | Revision NO 00 | Page NO 1 of 1

TÜV AUSTRIA
EN ISO 9001:2015
EN ISO 14001:2015

Ministry of Industry and Minerals
State Company for Inspection and Engineering Rehabilitation (SIER)
Engineering Insp. & lab Department

Client: جامعة بابل / كلية الهندسة
Order No: 121/2021
Tested Item: عينة شد
Address: babylon - Iraq
Date of Test: 31 / 8 / 2021
Type of Test: Tensile –Elongation -Yield - Impact

Test Report

Sample	Ultimate Stress (Rm) N/mm²	Yield strength (Re) N/ mm²	Stress ratio (tensile/yield) (Rm/Re)	Elongation %	Impact test (avg) at (-29°C) (J)	Hardness Test HRB	Hardness Test HRC
عينة شد	611	343	----	24	---	----	----

الملاحظات
- النتيجة تخص النموذج المفحوص فقط .
- تم الفحص بدرجة حرارة (24 C) ونسبة الرطوبة(% 20)
- تم اعتماد الطول القياسي 50mm

مدير قسم الفحص الهندسي و المختبرات | المراجعة | الفاحص

Head office : Baghdad –Iraq /Baghdad - Hilla Highway E-mail: mahed@sier.gov.iq, lab.sier@sier.gov.iq
Dr. Office : 9647810484016, Planning Dep Head : 9647706684841 IP : 9...106.34.21 SIER@engineering Comp

DOCUMENT ID F-IC-78 MC-01 | Issue No: 01 | Issued Date 18-12-2021 | Revision NO: 04 | Page NO: 1 OF 1

sier

NEW Tensile Properties of Metals (MHEAD) Metric

Specimen ID 1
Test Number 878
Report Number 219
Test Date 8/31/2021 10:08 PM

Test Results

Yieldforce (N)	42.200
Yieldstress (mpa)	343.88
tensileforce (N)	74.991
Tensilestress (mpa)	611.08

STRESS (N / mm) vs EXT (%)

900.0
800.0
700.0
600.0
500.0
400.0
300.0
200.0
100.0
0.0

-5.00 0.00 5.00 10.00 15.00 20.00

Testing Machine Smart Series

Preload Value (N) 100
Crosshead Speed (mm / min) or 30
Extension or Position Measured by XHD_100 (XHD100)

By: _____ Date: _____

Order
W
LO

Operator
T
R

Customer Name
sample
speed

TÜV AUSTRIA
EN ISO 9001:2015
EN ISO 14001:2015

Ministry of Industry and Minerals
State Company for Inspection and Engineering Rehabilitation (SIER)
Engineering Insp. & lab Department

Client: وزاره التعليم العالي والبحث العلمي/ جامعه بابل/ كليه الدراسات العليا / الطالبه - ورود اسعد مدب
Order No: 121/2021
Tested Item: مقاطع حديديه
Address: Baghdad- Iraq
Date of Test: 23/6/ 2021
Type of Test: Hardness

Test Report

Sample	Ultimate Stress (Rm) N/mm²	Yield strength (Re) N/ mm²	Stress ratio (tensile/yield (Rm/Re)	Elongation %	Elongation at max. force %	Bending Test	Hardness Test HRB	Hardness Test HRC
Shaft O=51mm	----	----	----	----	----	----	----	50
Metal piece WC	----	----	----	----	----	----	.....	60

الملاحظات
- النتيجة تخص النموذج المفحوص فقط
- تم الفحص بدرجة حراره (24°C) ونسبة الرطوبة(20 %)

و/مدير قسم الفحص الهندسي و المختبرات
م. احمد فاضل

المراجعة
م. احمد فاضل

الفاحص
م. بشير فؤاد

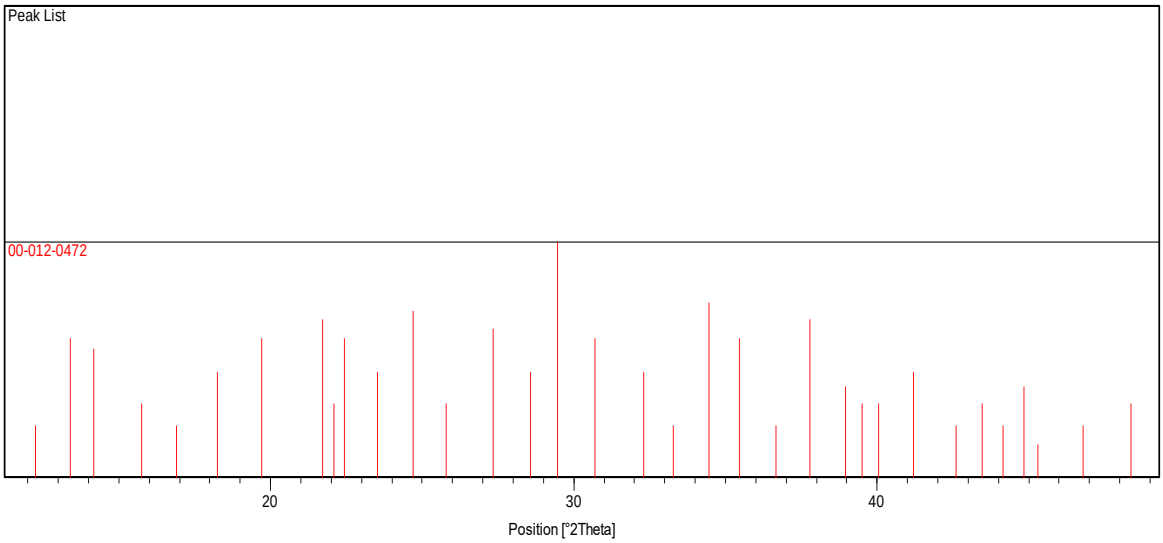

Figure (1): XRD for aluminum nitrate

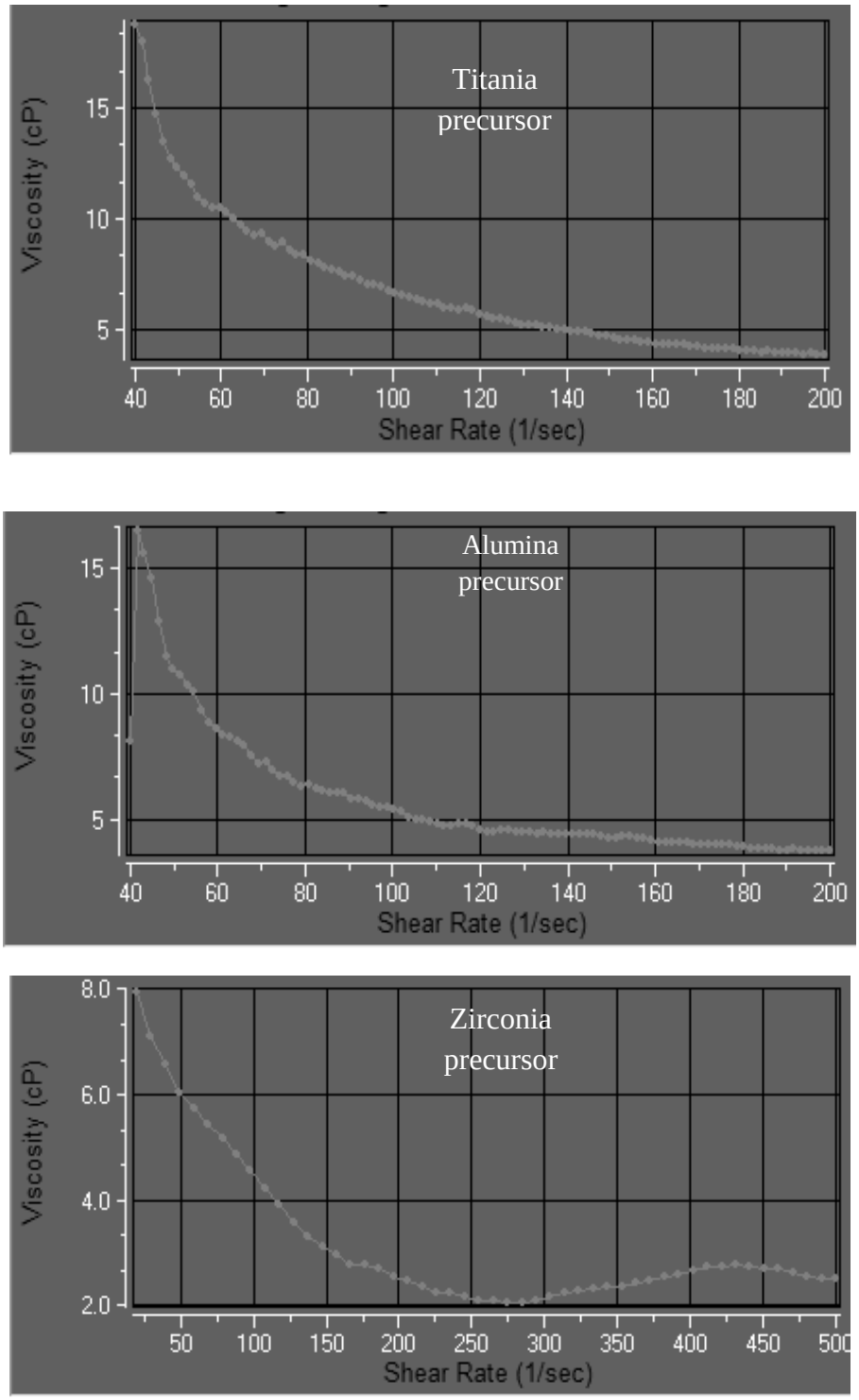

Figure (1) Viscosity measurement for each coating precursor

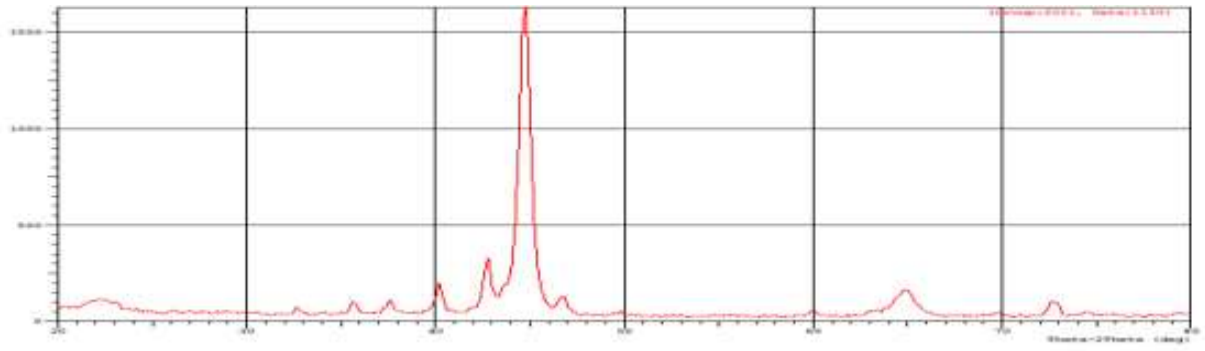

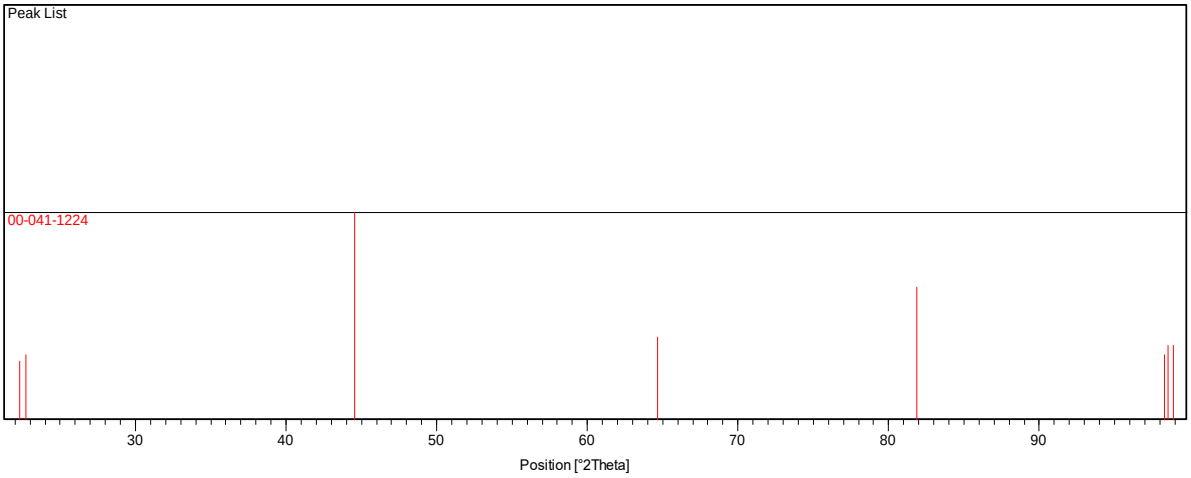

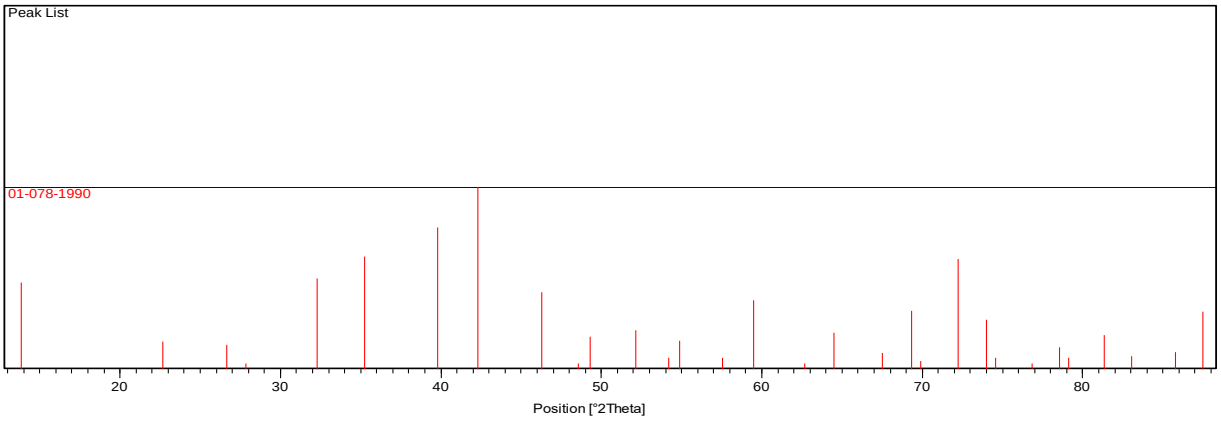

Figure (2): XRD for HSS

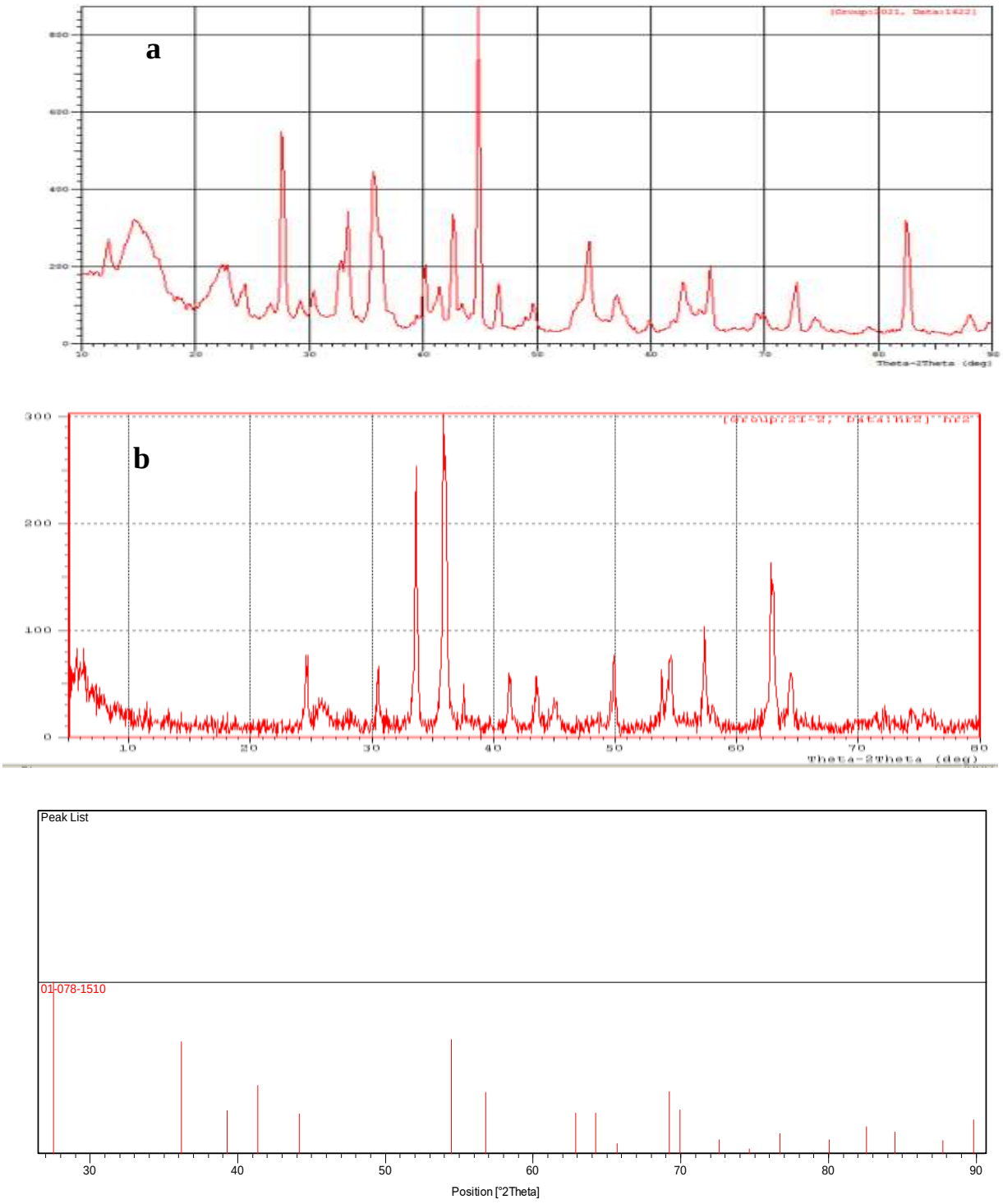

Figure (3): XRD of sample TiO_2 coating , (a): calcination temperature at 650°C for one hour,(b): calcination temperature at 500°C for two hour

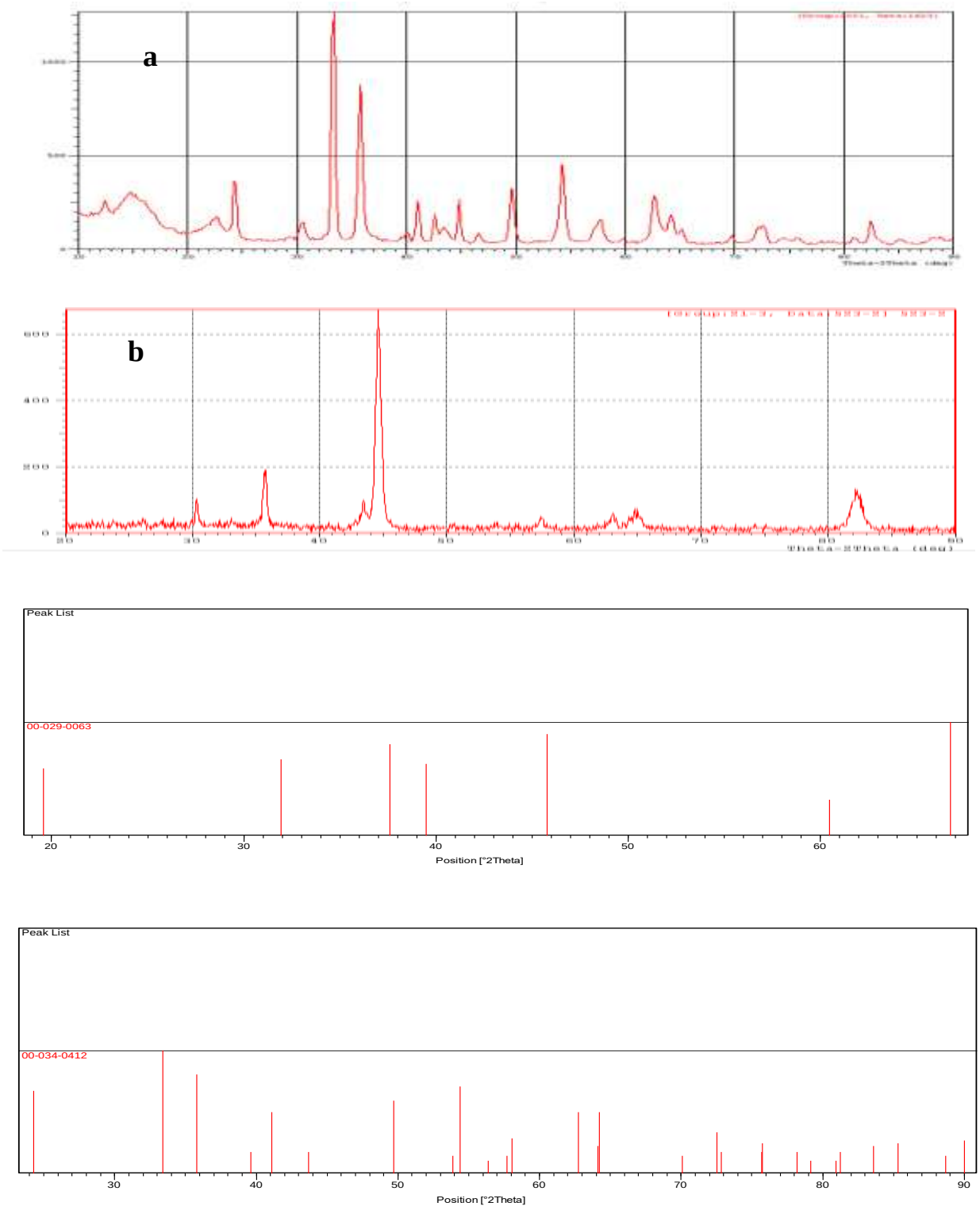

Figure(4): XRD of sample Al_2O_3, (a): calcination temperature at 650°C for one hour,(b): calcination temperature at 500°C for two hour

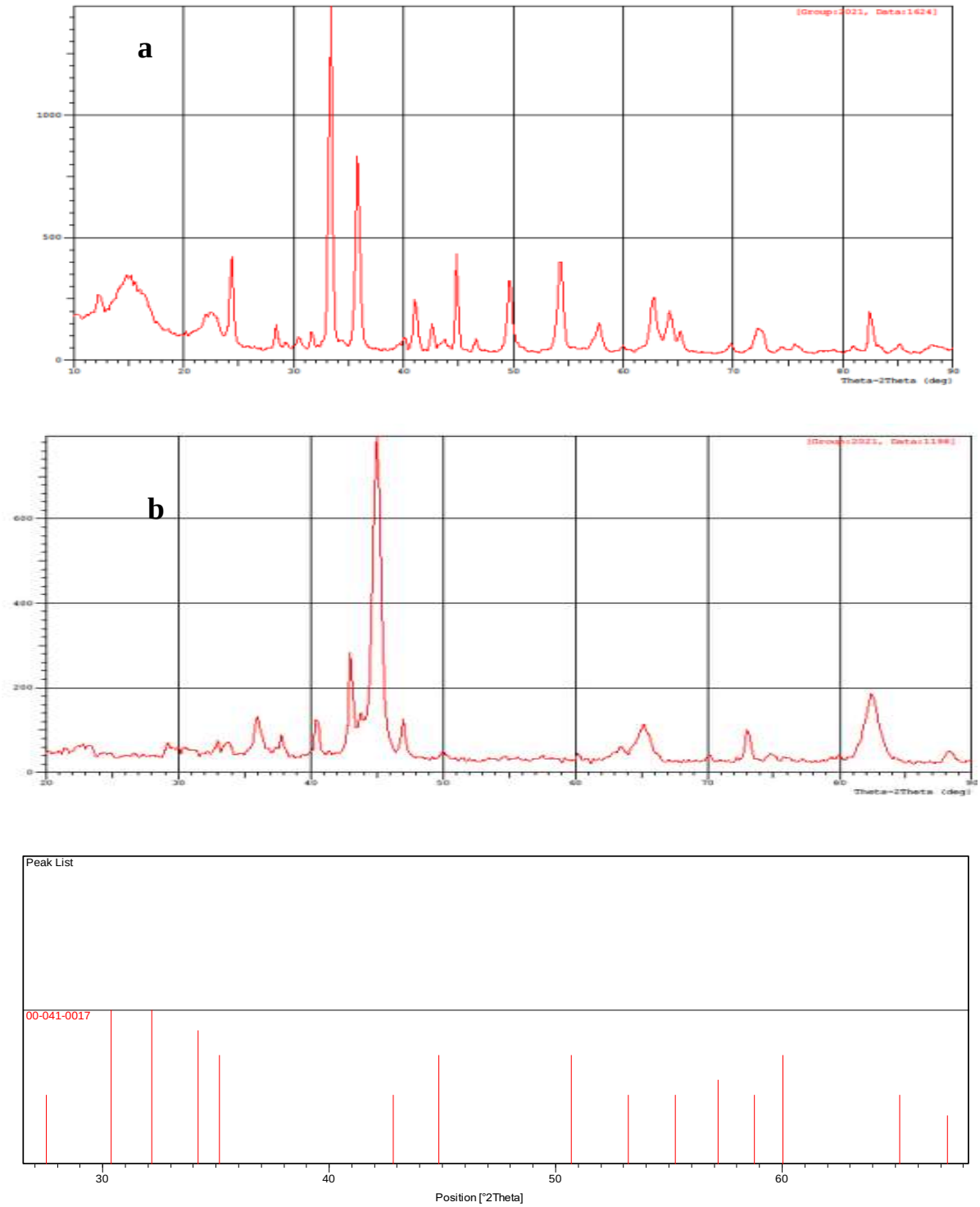

Figure(5):XRD of sample ZrO_2,(a):calcination temperature at 650℃ for one hour,(b):calcination temperature at 500℃ for two hour

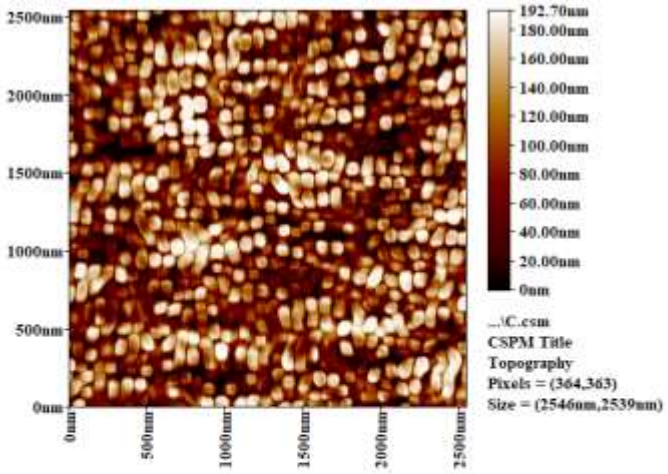

Monolayer Al2O3

CSPM Imager Surface Roughness Analysis

Image size:2546.30nm X 2539.30nm

Amplitude parameters:
Sa(Roughness Average) 48.4 [nm]
Sq(Root Mean Square) 55.9 [nm]
Ssk(Surface Skewness) 0.000215
Sku(Surface Kurtosis) 1.8
Sy(Peak-Peak) 194 [nm]
Sz(Ten Point Height) 193 [nm]

Hybrid Parameters:
Ssc(Mean Summit Curvature) -0.25 [1/nm]
Sdq(Root Mean Square Slope) 3.9 [1/nm]
Sdr(Surface Area Ratio) 468

Functional Parameters:
Sbi(Surface Bearing Index) 5.28
Sci(Core Fluid Retention Index) 1.5
Svi(Valley Fluid Retention Index) 0.0694
Spk(Reduced Summit Height) 20.9 [nm]
Sk(Core Roughness Depth) 168 [nm]
Svk(Reduced Valley Depth) 4.88 [nm]
Sdc 0-5(0-5% height intervals of Bearing Curve) 10.6 [nm]
Sdc 5-10(5-10% height intervals of Bearing Curve) 9.65 [nm]
Sdc 10-50(10-50% height intervals of Bearing Curve) 77.5 [nm]
Sdc 50-95(50-95% height intervals of Bearing Curve) 87.2 [nm]

Spatial Parameters:
Sds(Density of Summits) 246 [1/um2]

Fractal Dimension 2.56

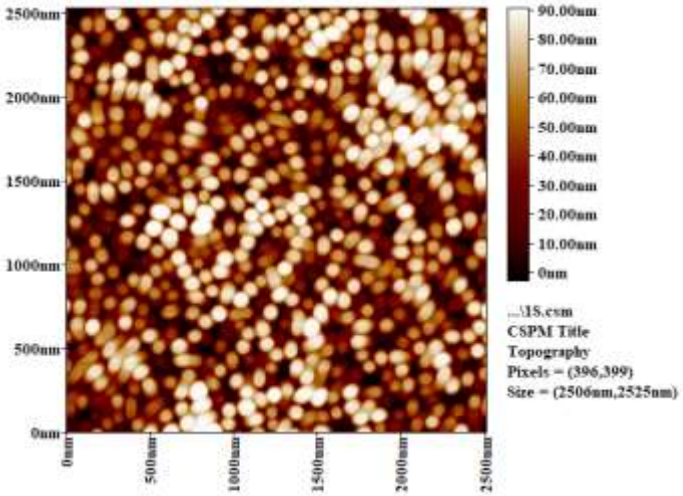

Monolayer TiO2

CSPM Imager Surface Roughness Analysis

Image size:2506.28nm X 2525.27nm

Amplitude parameters:
Sa(Roughness Average) 23.3 [nm]
Sq(Root Mean Square) 26.9 [nm]
Ssk(Surface Skewness) -0.103
Sku(Surface Kurtosis) 1.81
Sy(Peak-Peak) 93.1 [nm]
Sz(Ten Point Height) 93 [nm]

Hybrid Parameters
Ssc(Mean Summit Curvature) -0.0345[1/nm]
Sdq(Root Mean Square Slope) 1.41 [1/nm]
Sdr(Surface Area Ratio) 76.9

Functional Parameters
Sbi(Surface Bearing Index) 6.57
Sci(Core Fluid Retention Index) 1.42
Svi(Valley Fluid Retention Index) 0.0777
Spk(Reduced Summit Height) 0 [nm]
Sk(Core Roughness Depth) 84.8 [nm]
Svk(Reduced Valley Depth) 8.96 [nm]
Sdc 0-5(0-5% height intervals of Bearing Curve) 4.09 [nm]
Sdc 5-10(5-10% height intervals of Bearing Curve) 4.09 [nm]
Sdc 10-50(10-50% height intervals of Bearing Curve) 34.9 [nm]
Sdc 50-95(50-95% height intervals of Bearing Curve) 45 [nm]

Spatial Parameters
Sds(Density of Summits) 127 [1/um2]

Fractal Dimension 2.54

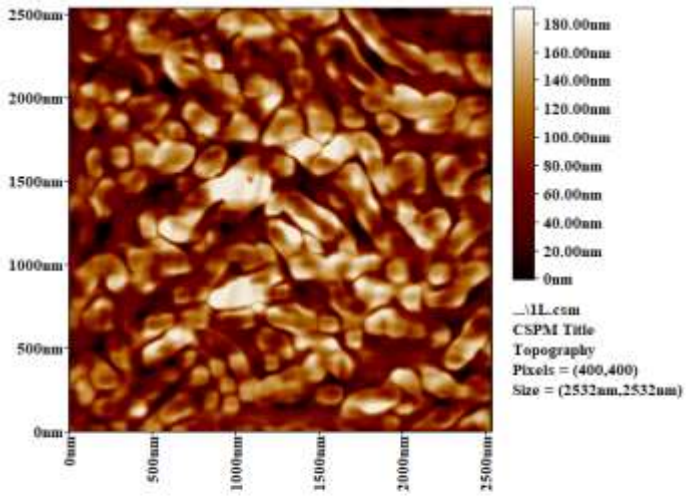

CSPM Imager Surface Roughness Analysis

Image size:2531.60nm X 2531.60nm

Amplitude parameters
Sa(Roughness Average) 37.6 [nm]
Sq(Root Mean Square) 44.9 [nm]
Ssk(Surface Skewness) 0.0851
Sku(Surface Kurtosis) 2.17
Sy(Peak-Peak) 183 [nm]
Sz(Ten Point Height) 183 [nm]

Hybrid Parameters
Ssc(Mean Summit Curvature) -0.185[1/nm]
Sdq(Root Mean Square Slope) 1.94 [1/nm]
Sdr(Surface Area Ratio) 138

Functional Parameters
Sbi(Surface Bearing Index) 2.07
Sci(Core Fluid Retention Index) 1.57
Svi(Valley Fluid Retention Index) 0.0688
Spk(Reduced Summit Height) 24.1 [nm]
Sk(Core Roughness Depth) 137 [nm]
Svk(Reduced Valley Depth) 23.5 [nm]
Sdc 0-5(0-5% height intervals of Bearing Curve) 21.7 [nm]
Sdc 5-10(5-10% height intervals of Bearing Curve) 13.4 [nm]
Sdc 10-50(10-50% height intervals of Bearing Curve) 60.9 [nm]
Sdc 50-95(50-95% height intervals of Bearing Curve) 72 [nm]

Spatial Parameters
Sds(Density of Summits) 135 [1/um2]

Fractal Dimension 2.5

Uncoated insert

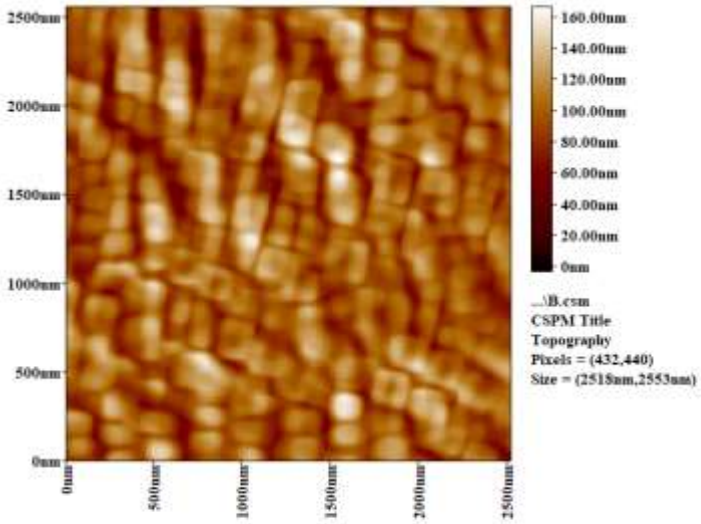

CSPM Imager Surface Roughness Analysis

Image size:2518.32nm X 2553.29nm

Amplitude parameters
Sa(Roughness Average) 15.4 [nm]
Sq(Root Mean Square) 19.1 [nm]
Ssk(Surface Skewness) 0.0775
Sku(Surface Kurtosis) 2.89
Sy(Peak-Peak) 136 [nm]
Sz(Ten Point Height) 132 [nm]

Hybrid Parameters
Ssc(Mean Summit Curvature) -0.0487[1/nm]
Sdq(Root Mean Square Slope) 0.613 [1/nm]
Sdr(Surface Area Ratio) 16.6

Functional Parameters
Sbi(Surface Bearing Index) 0.565
Sci(Core Fluid Retention Index) 1.59
Svi(Valley Fluid Retention Index) 0.106
Spk(Reduced Summit Height) 18.5 [nm]
Sk(Core Roughness Depth) 50.6 [nm]
Svk(Reduced Valley Depth) 16.3 [nm]
Sdc 0-5(0-5% height intervals of Bearing Curve) 33.9 [nm]
Sdc 5-10(5-10% height intervals of Bearing Curve) 7.15 [nm]
Sdc 10-50(10-50% height intervals of Bearing Curve) 25 [nm]
Sdc 50-95(50-95% height intervals of Bearing Curve) 31 [nm]

Spatial Parameters
Sds(Density of Summits) 122 [1/um2]

Fractal Dimension 2.59

Coated douple layers

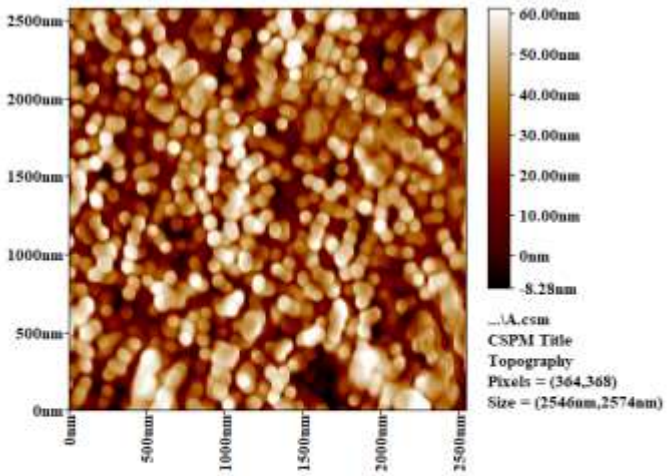

CSPM Imager Surface Roughness Analysis

Image size:2546.30nm X 2574.26nm

Amplitude parameters:
Sa(Roughness Average) 14 [nm]
Sq(Root Mean Square) 16.6 [nm]
Ssk(Surface Skewness) -0.265
Sku(Surface Kurtosis) 2.21
Sy(Peak-Peak) 69.4 [nm]
Sz(Ten Point Height) 69.3 [nm]

Hybrid Parameters:
Ssc(Mean Summit Curvature) -0.0668[1/nm]
Sdq(Root Mean Square Slope) 0.856 [1/nm]
Sdr(Surface Area Ratio) 28.3

Functional Parameters:
Sbi(Surface Bearing Index) 2.76
Sci(Core Fluid Retention Index) 1.37
Svi(Valley Fluid Retention Index) 0.116
Spk(Reduced Summit Height) 4.58 [nm]
Sk(Core Roughness Depth) 46.9 [nm]
Svk(Reduced Valley Depth) 16.5 [nm]
Sdc 0-5(0-5% height intervals of Bearing Curve) 6.03 [nm]
Sdc 5-10(5-10% height intervals of Bearing Curve) 3.39 [nm]
Sdc 10-50(10-50% height intervals of Bearing Curve) 19.4 [nm]
Sdc 50-95(50-95% height intervals of Bearing Curve) 32.3 [nm]

Spatial Parameters:
Sds(Density of Summits) 152 [1/um2]

Fractal Dimension 2.35

Coated triplex layers

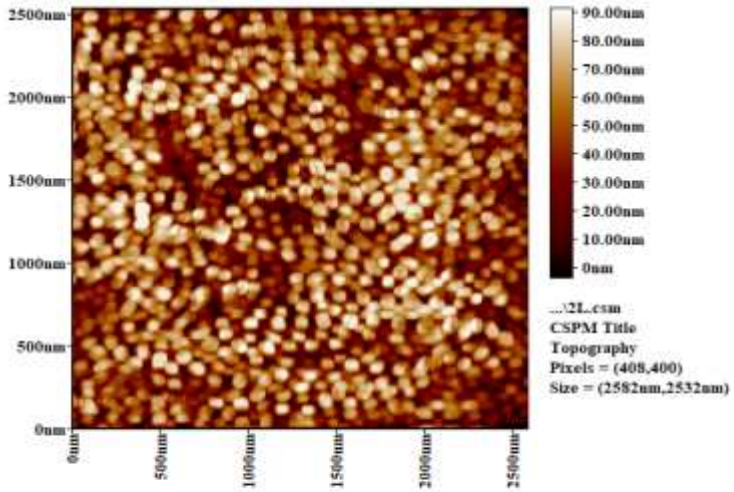

CSPM Imager Surface Roughness Analysis

Image size:2582.23nm X 2531.60nm

Amplitude parameters:
Sa(Roughness Average) 18.7 [nm]
Sq(Root Mean Square) 22.3 [nm]
Ssk(Surface Skewness) -0.221
Sku(Surface Kurtosis) 2.2
Sy(Peak-Peak) 93.7 [nm]
Sz(Ten Point Height) 51.2 [nm]

Hybrid Parameters:
Ssc(Mean Summit Curvature) -1.#J [1/nm]
Sdq(Root Mean Square Slope) 1.56 [1/nm]
Sdr(Surface Area Ratio) 83.2

Functional Parameters:
Sbi(Surface Bearing Index) 2.56
Sci(Core Fluid Retention Index) 1.42
Svi(Valley Fluid Retention Index) 0.106
Spk(Reduced Summit Height) 8.38 [nm]
Sk(Core Roughness Depth) 64.4 [nm]
Svk(Reduced Valley Depth) 17.1 [nm]
Sdc 0-5(0-5% height intervals of Bearing Curve) 8.69 [nm]
Sdc 5-10(5-10% height intervals of Bearing Curve) 5.31 [nm]
Sdc 10-50(10-50% height intervals of Bearing Curve) 26.8 [nm]
Sdc 50-95(50-95% height intervals of Bearing Curve) 40.3 [nm]

Spatial Parameters:
Sds(Density of Summits) 0 [1/um2]

Fractal Dimension 2.56

Monolayer
ZrO2

Figure (6): AFM for each cutting insert

Appendix

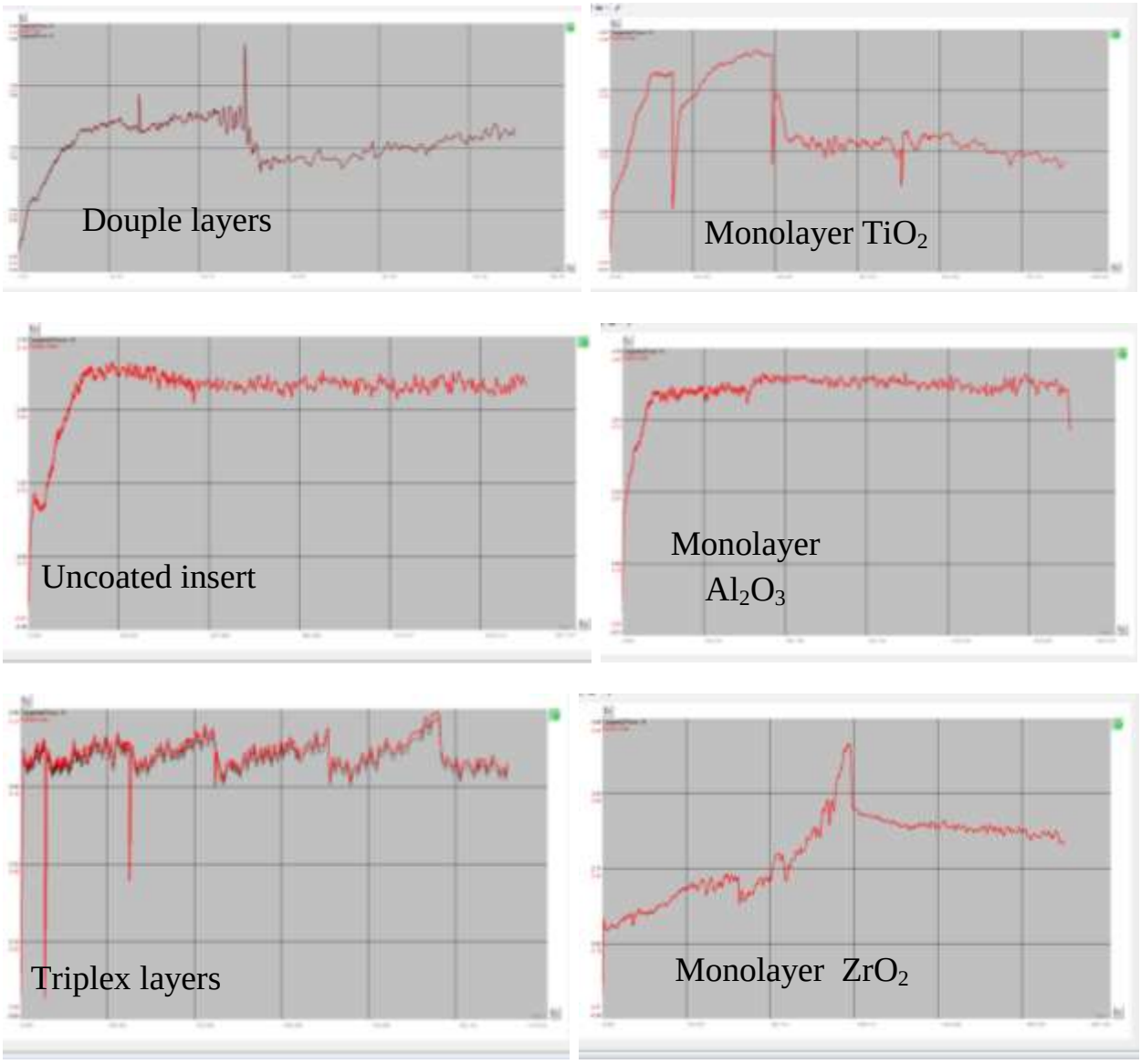

Figure (7): Coefficient of friction for each cutting insert

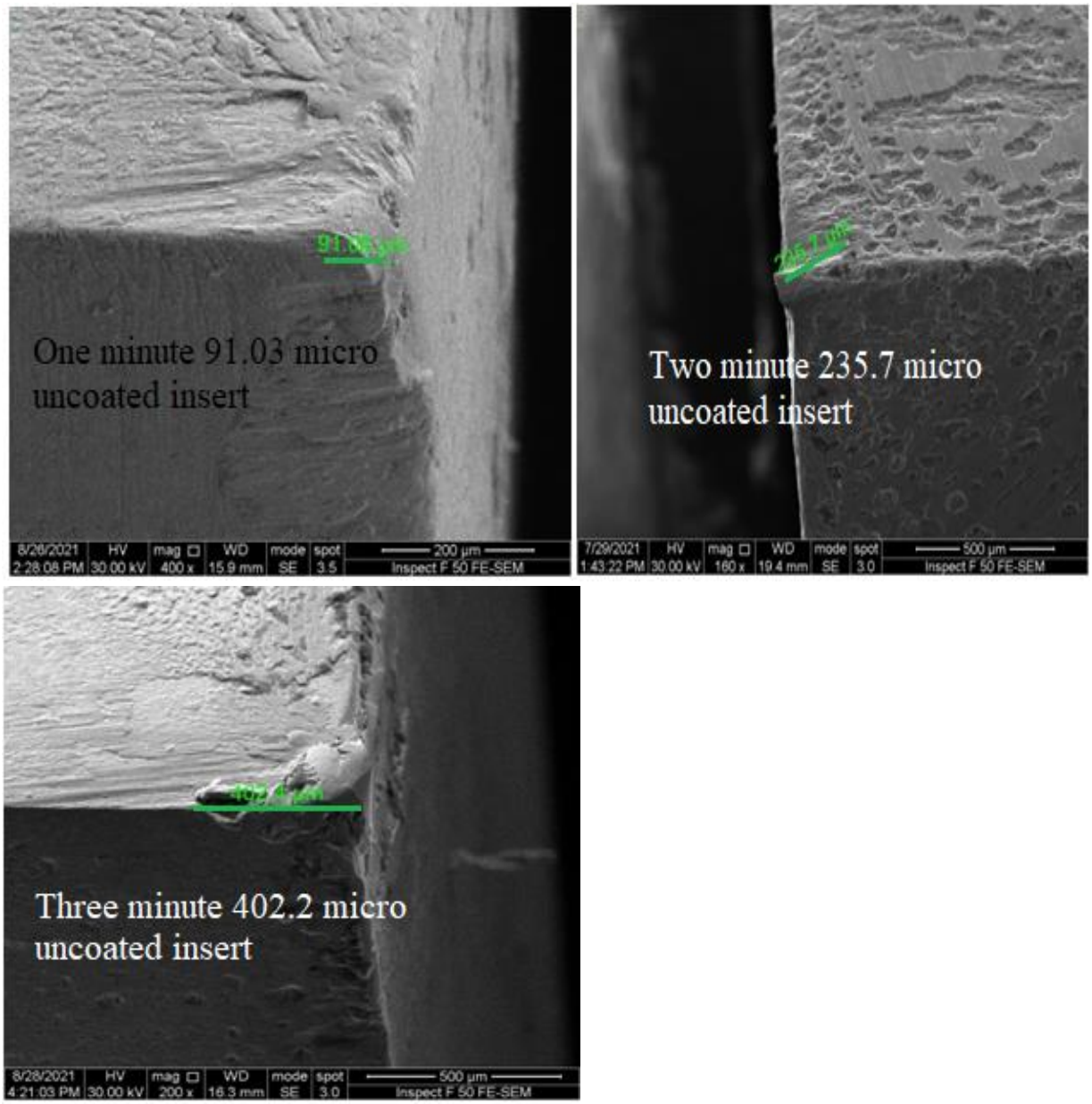

56 m/min, 0.065 mm/rev, 0.2mm

Figure (8): Wear width of uncoated cutting insert for each minute

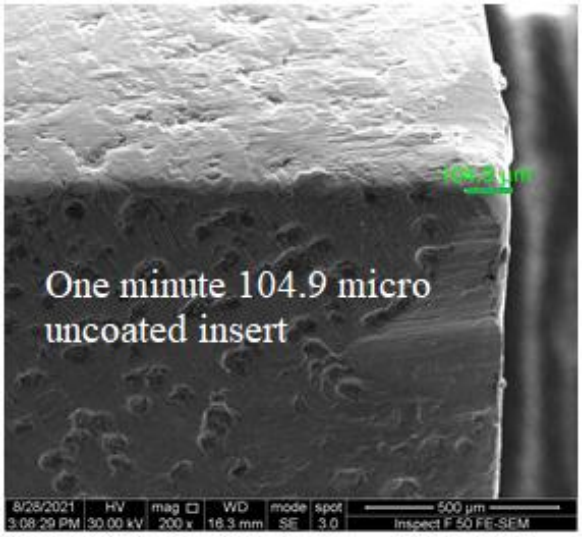

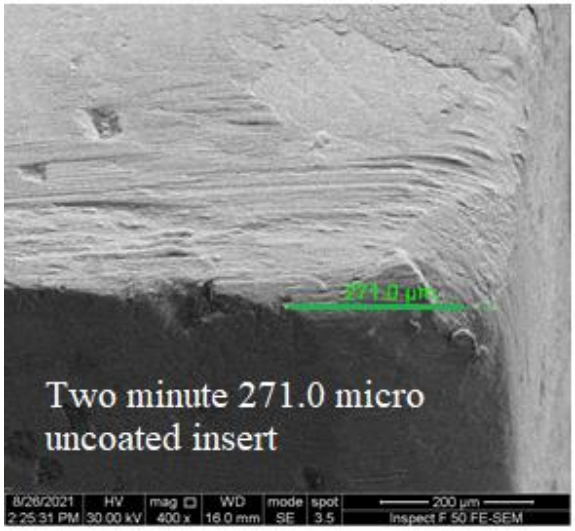

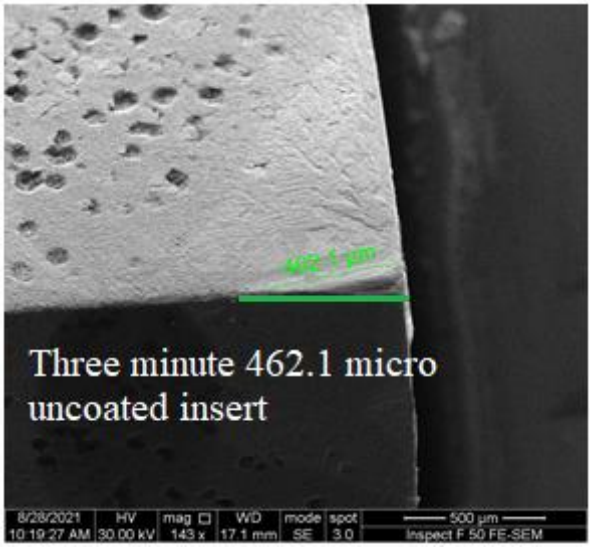

56 m/min, 0.165mm/rev, 0.5mm

Continue Figure (8)

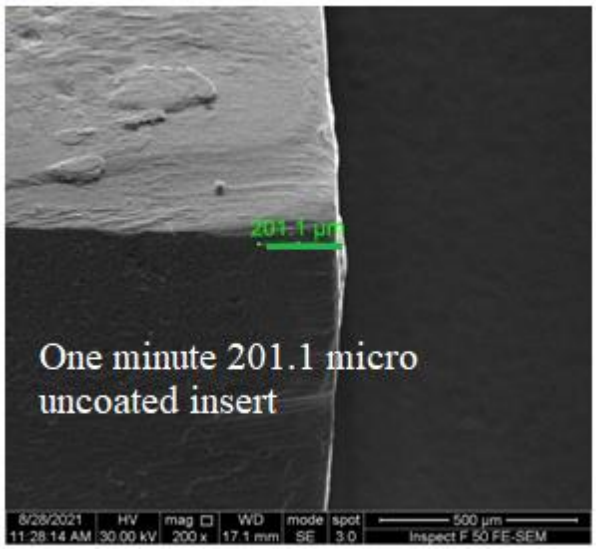

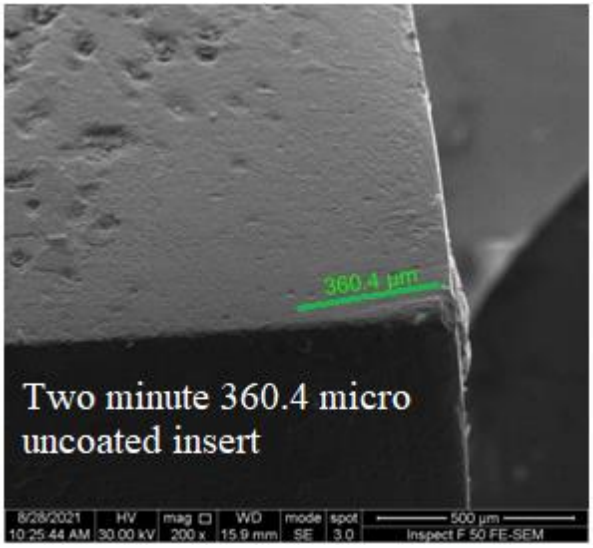

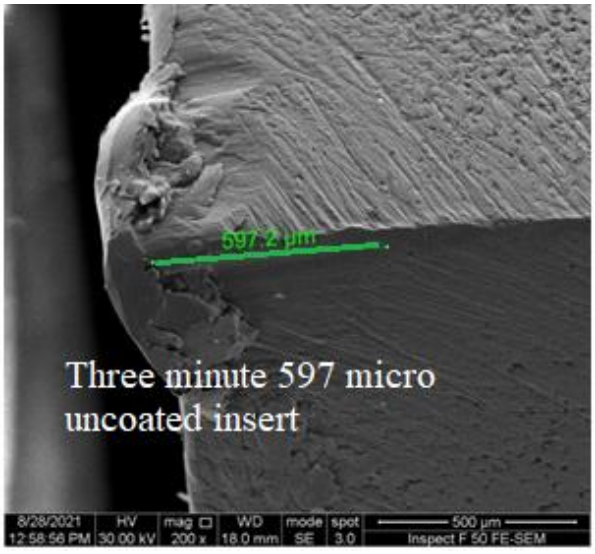

56m/min, 0.265mm/rev, 0.7mm

Continue Figure (8)

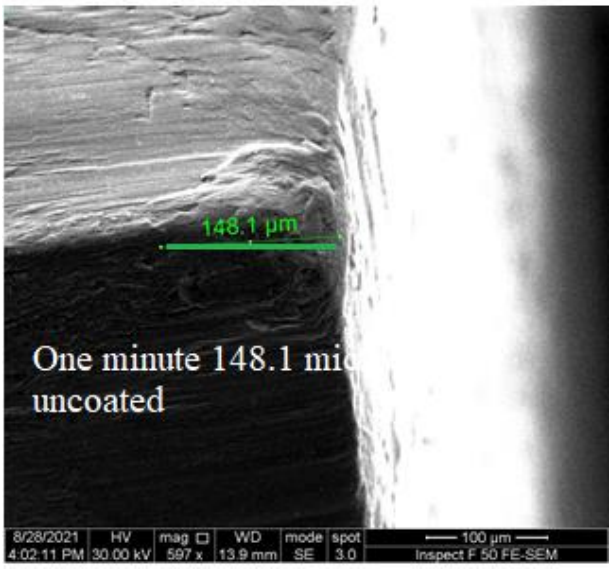

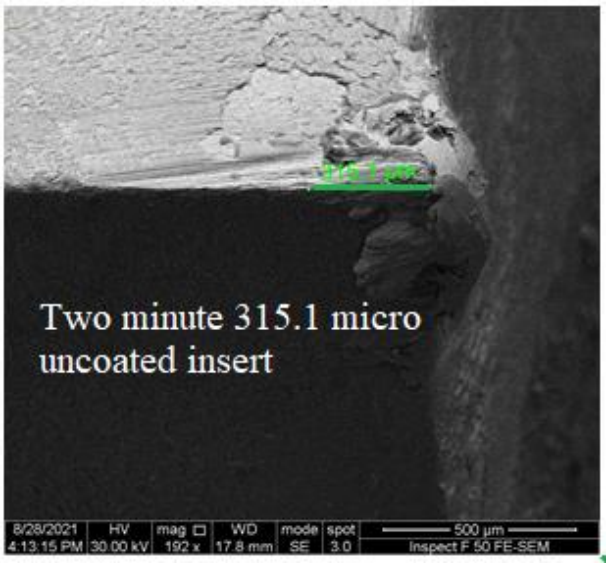

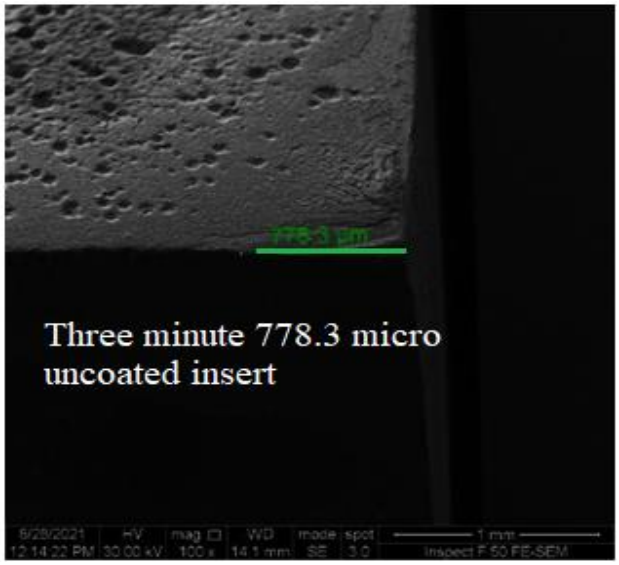

88 m/min, 0.065mm/rev, 0.5mm

Continue Figure (8)

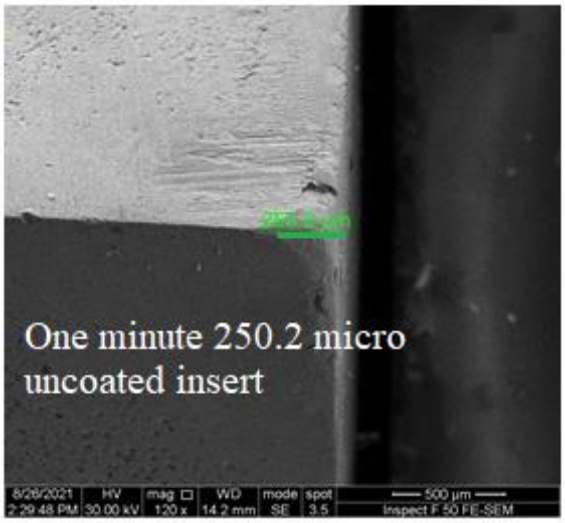

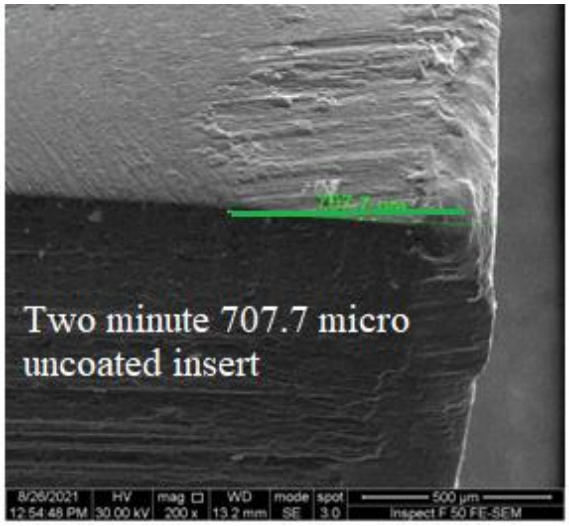

88 m/min, 0.165mm/rev, 0.7mm

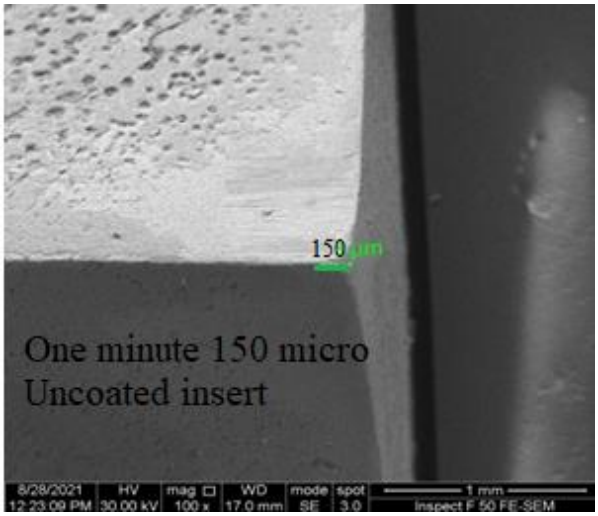

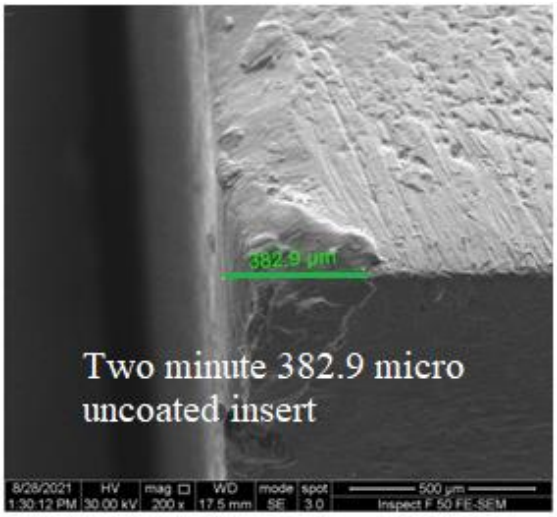

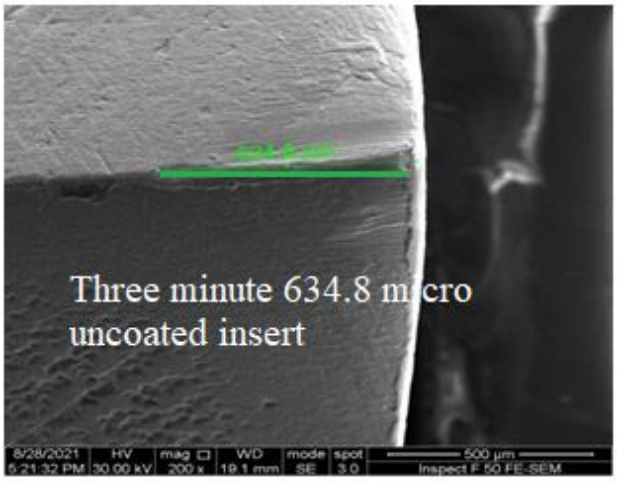

88 m/min, 0.265mm/rev, 0.2mm

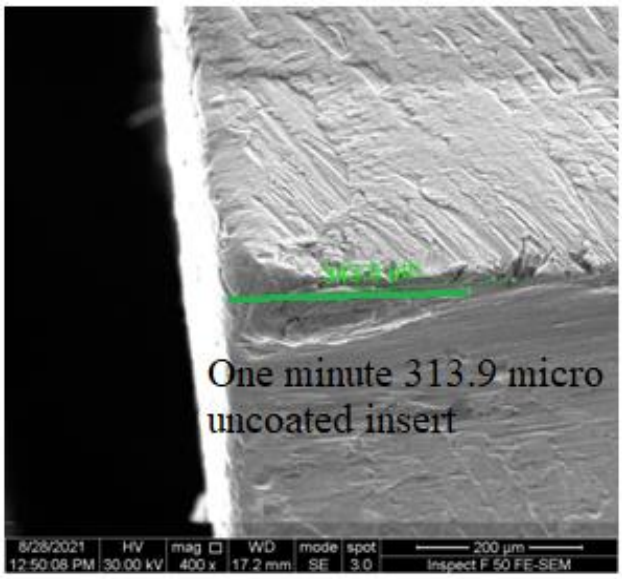

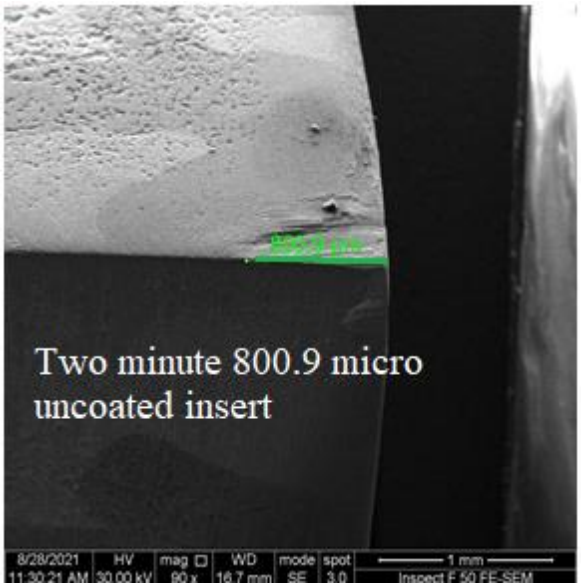

112 m/min, 0.065mm/rev, 0.7mm

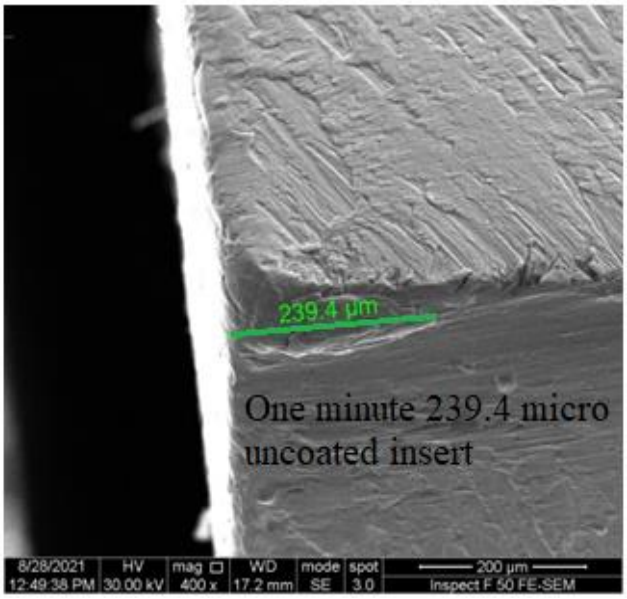

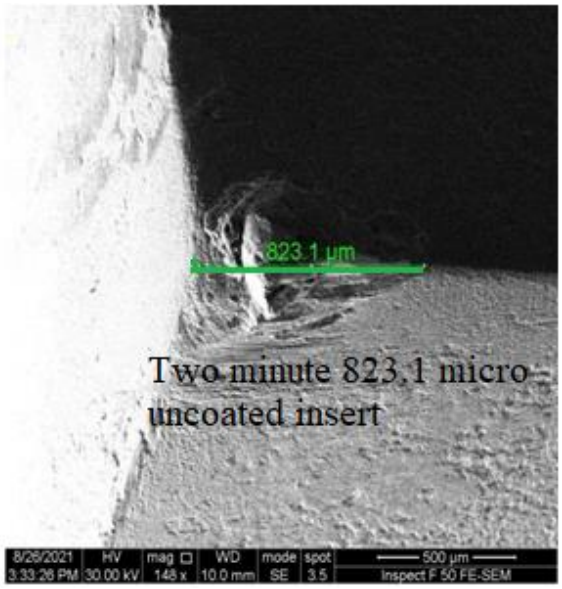

112m/min, 0.165mm/rev, 0.2mm

Continue Figure (8)

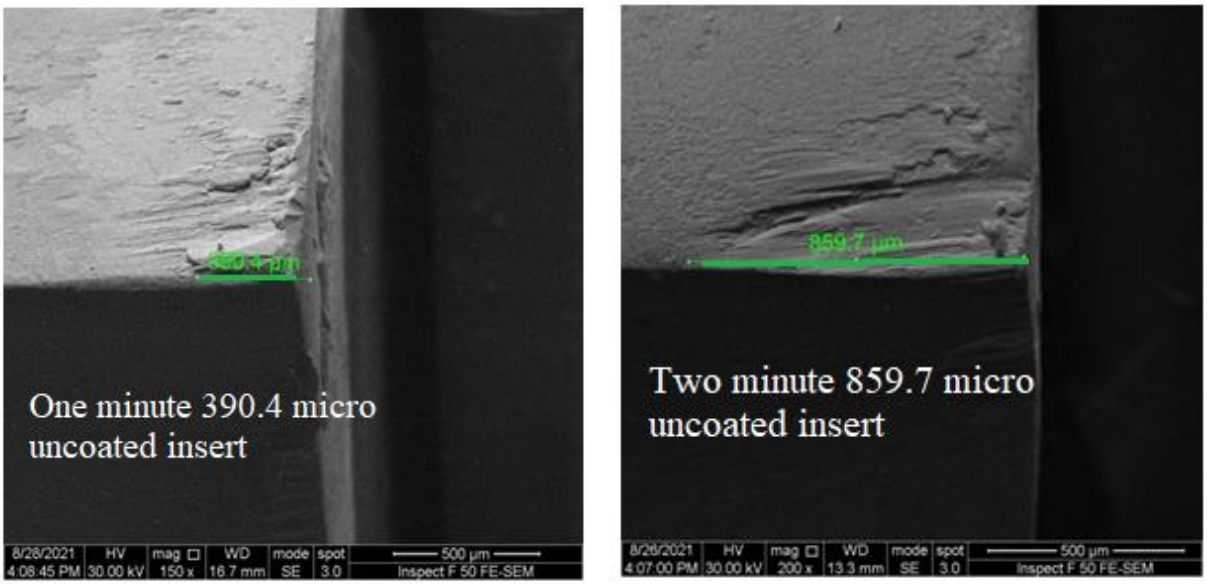

112 m/min, 0.5mm, 0.265mm/rev

Continue Figure (8)

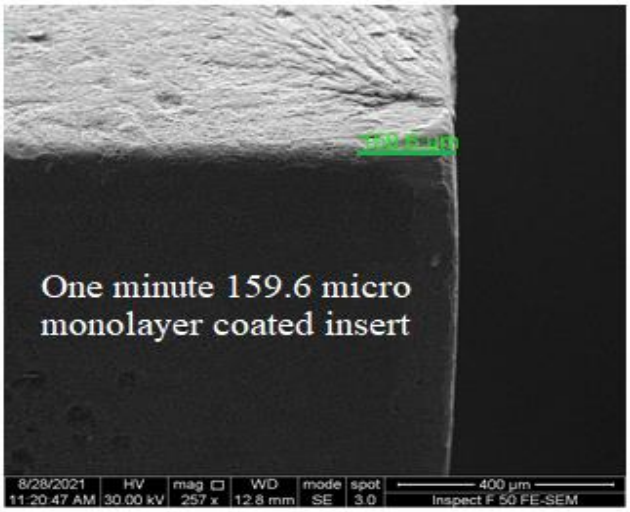

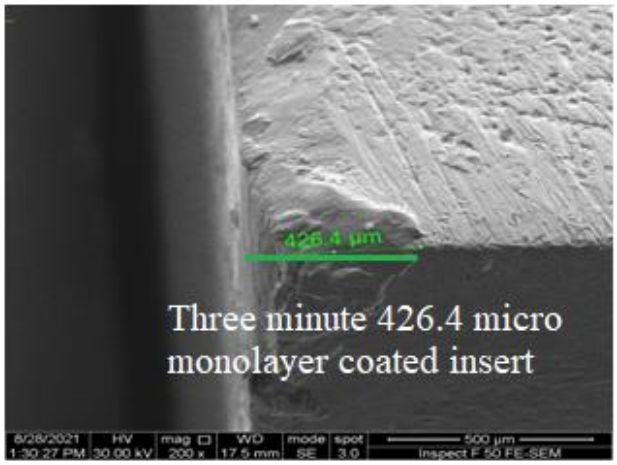

56m/min, 0.065 mm/rev, 0.2mm

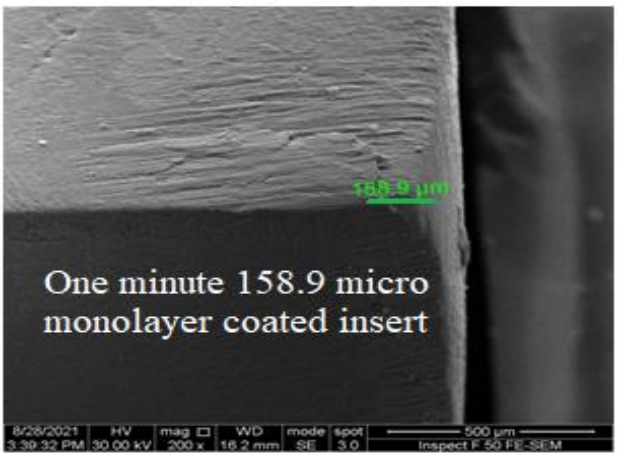

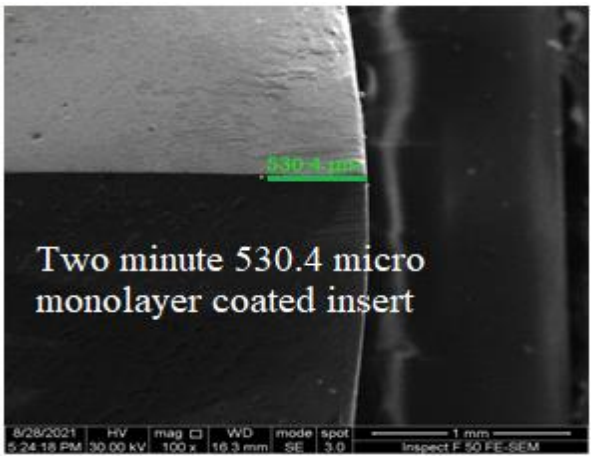

56 m/min, 0.165mm/rev, 0.5mm

Figure (9): Wear width for monolayer coated cutting insert for each minute

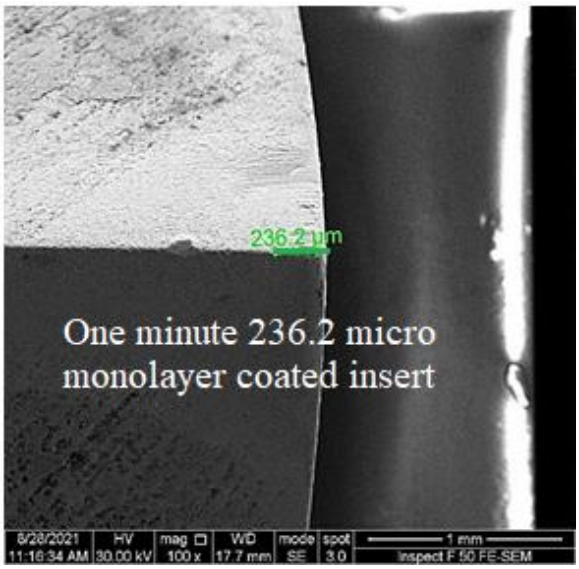

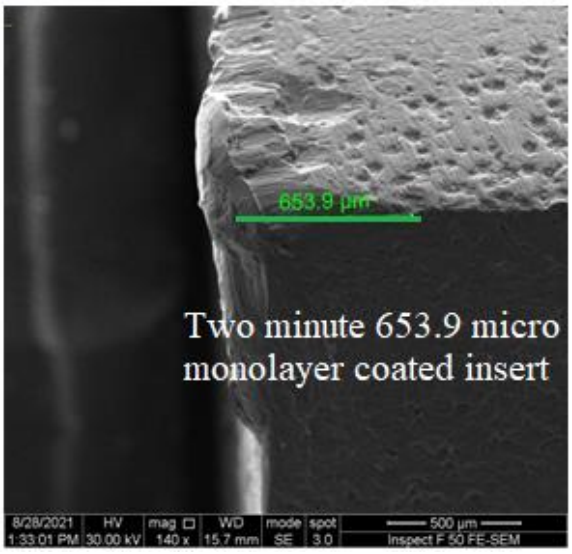

56 m/min, 0.265mm/rev, 0.7mm

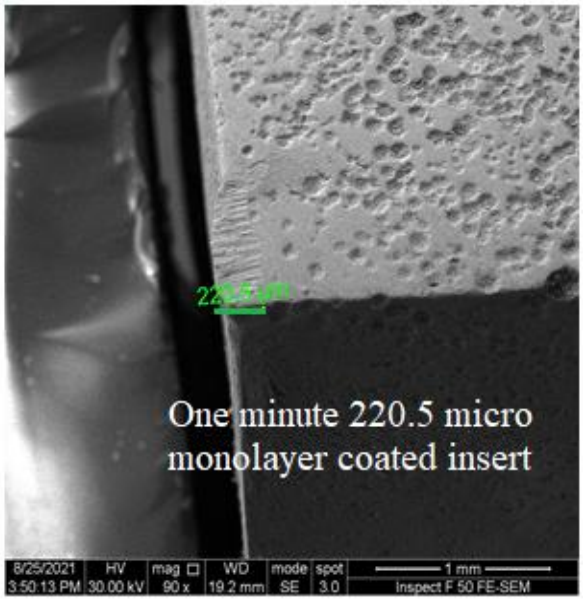

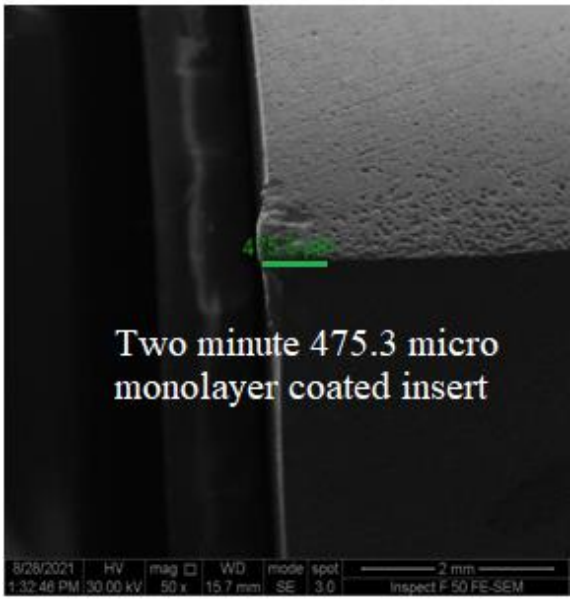

88 m/min, 0.065mm/rev, 0.5mm

Continue Figure (9)

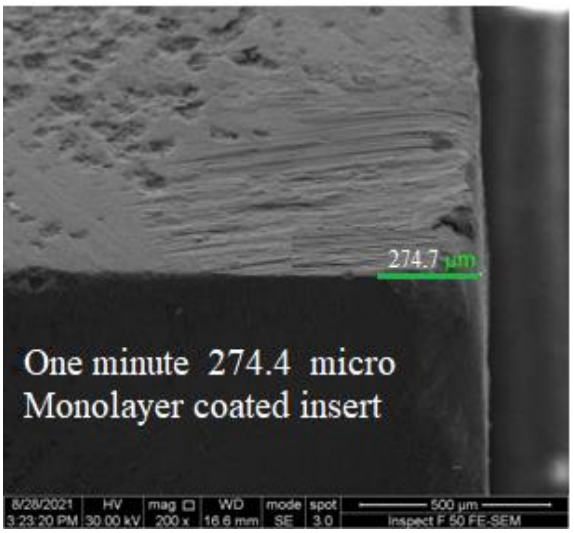

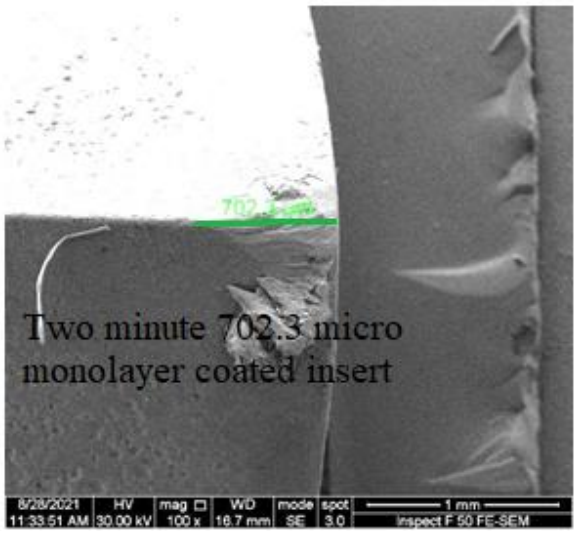

88 m/min, 0.165mm/rev, 0.7mm

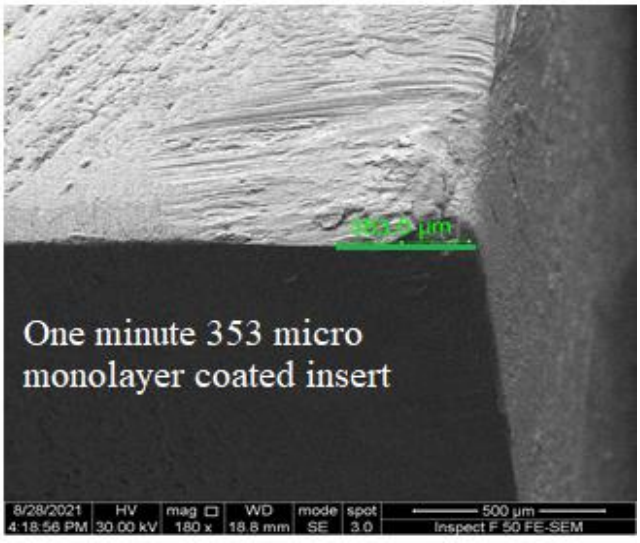

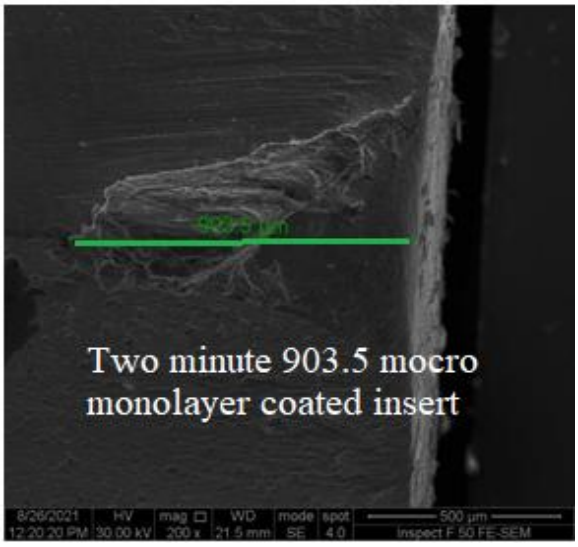

112m/min, 0.065mm/rev, 0.7mm

Continue Figure (9)

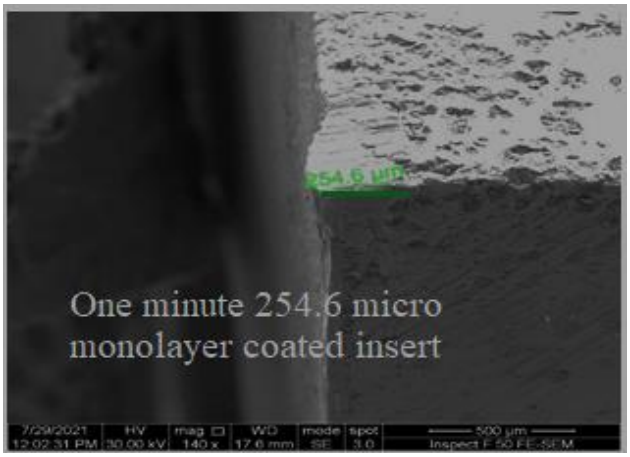

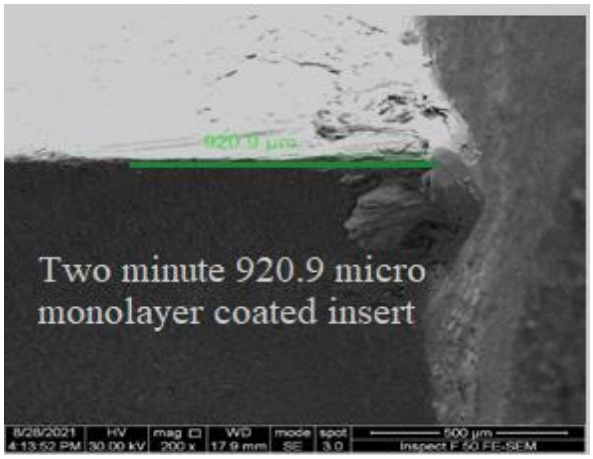

112m/min, 0.165mm/rev, 0.2mm

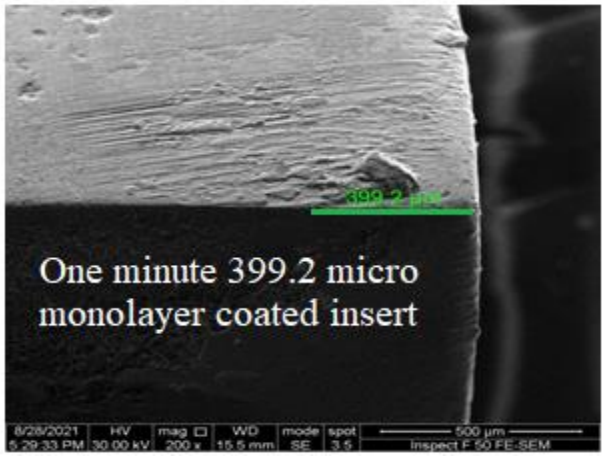

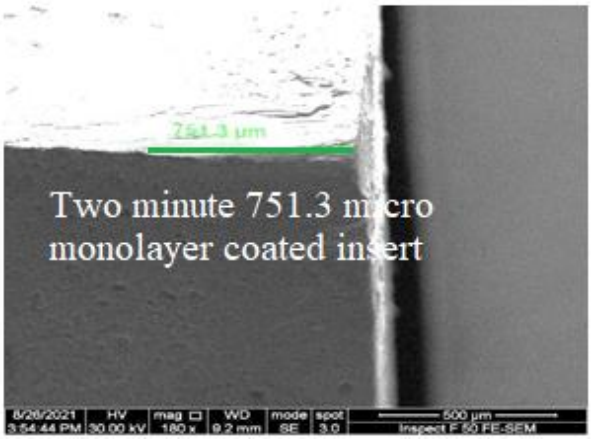

112m/min, 0.5mm, 0.265mm/rev

Continue Figure (9)

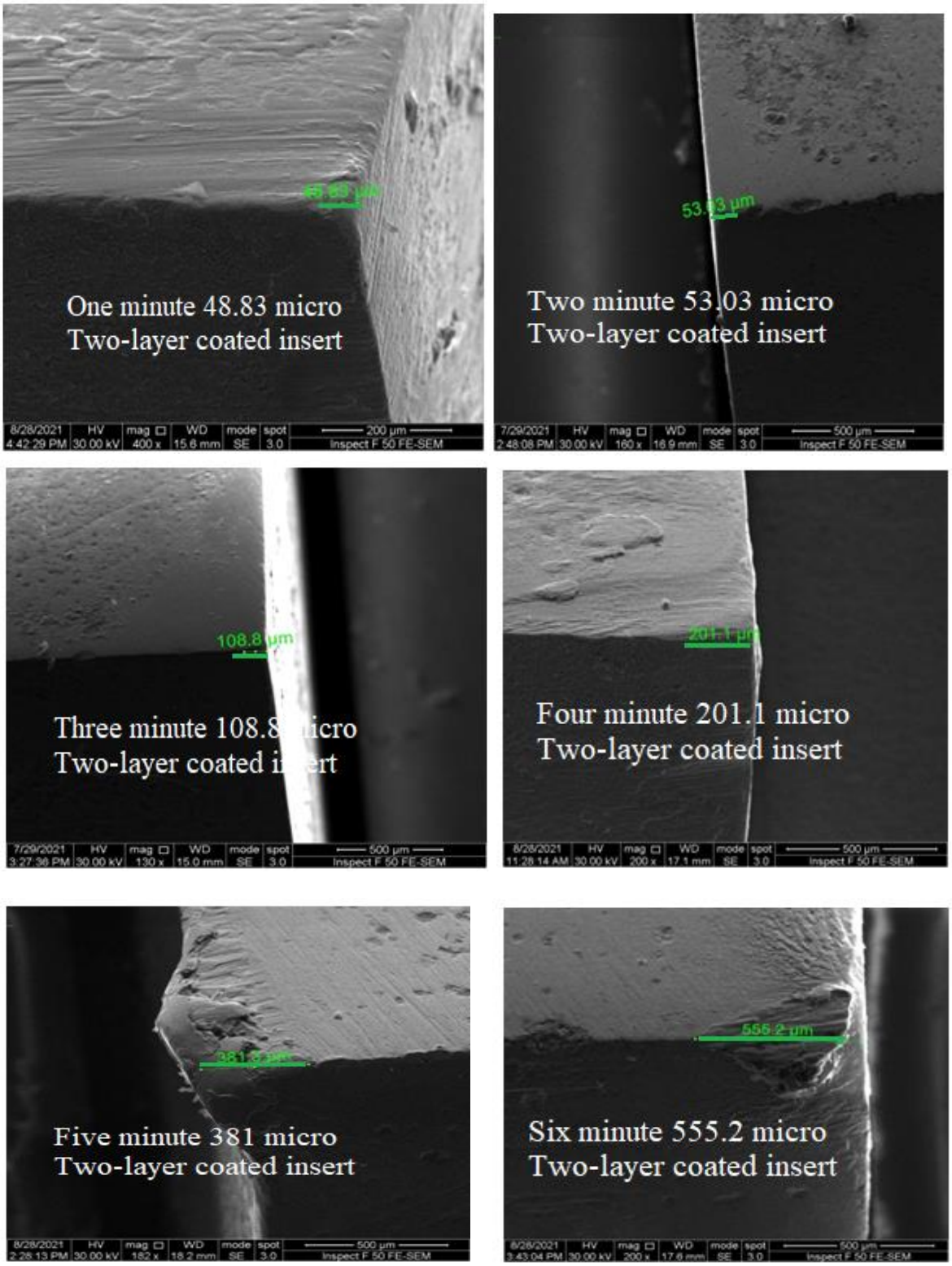

56 m/min, 0.065 mm/rev, 0.2mm

Figure (10): Wear width of Douple layer coated cutting insert for each minute

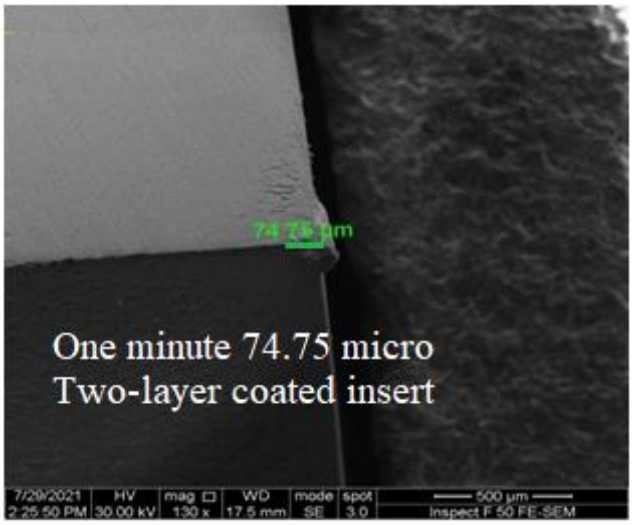

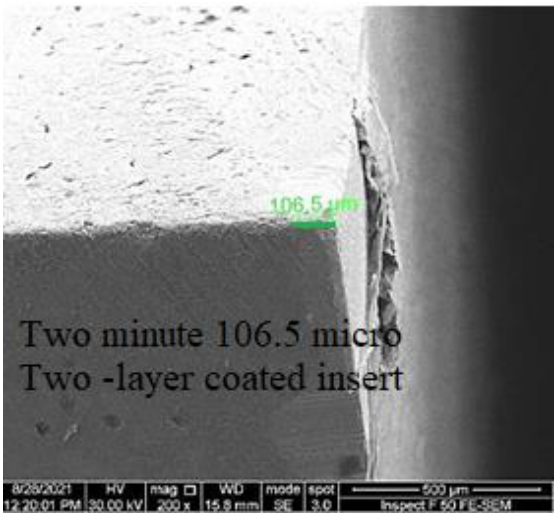

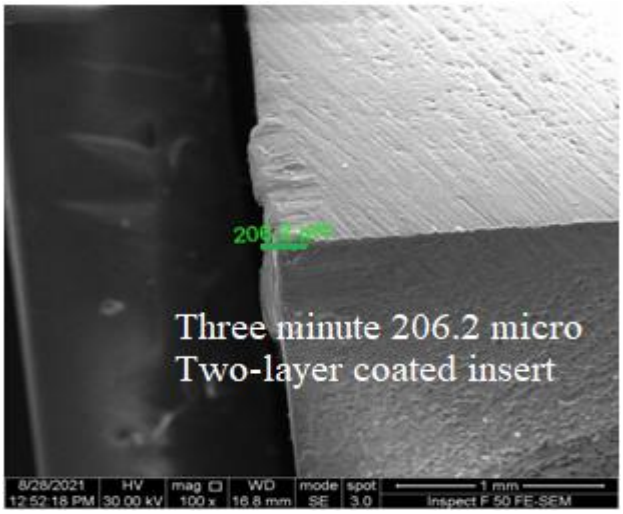

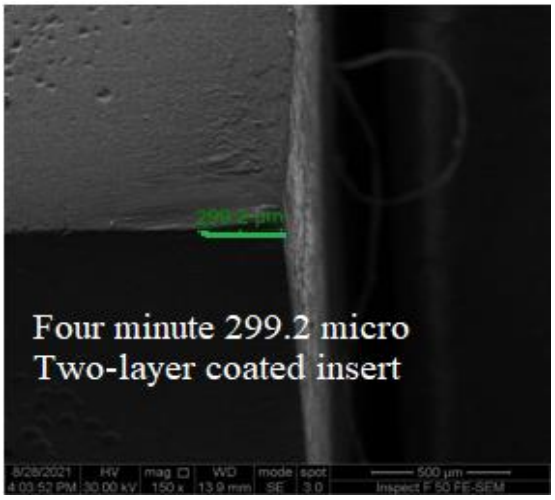

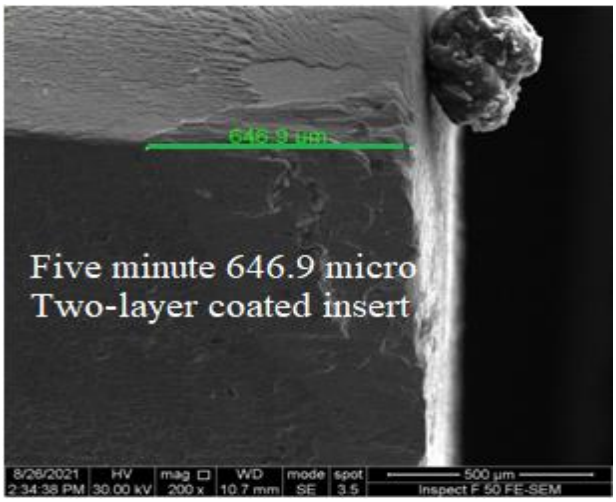

56 m/min, 0.165mm/rev, 0.5mm

Continue Figure (10)

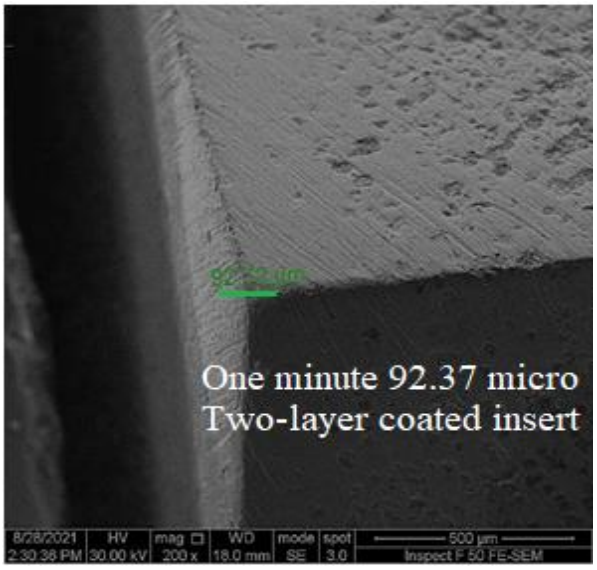

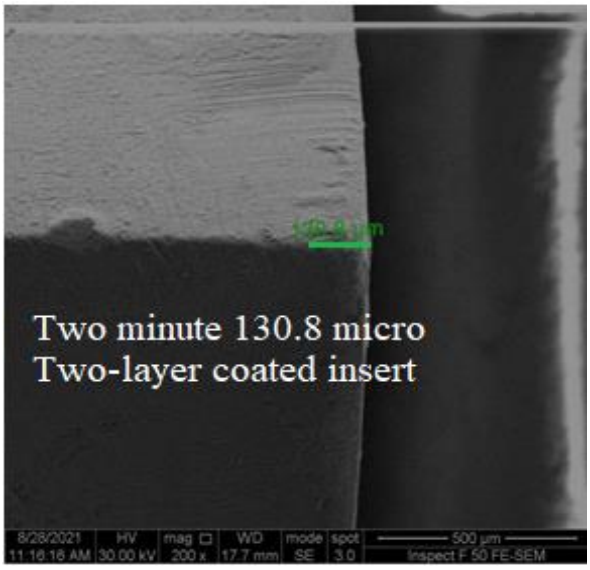

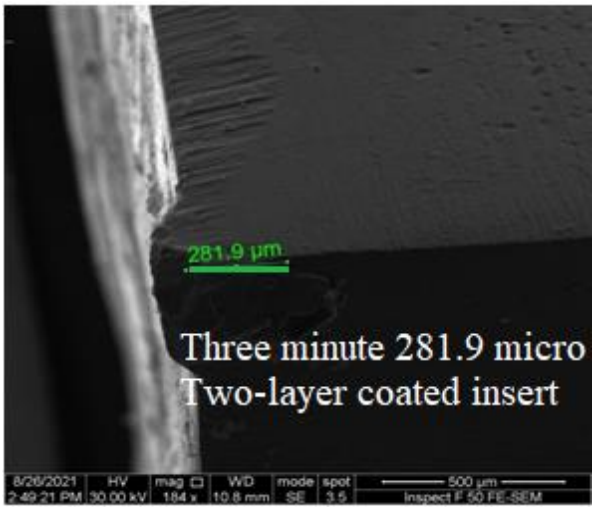

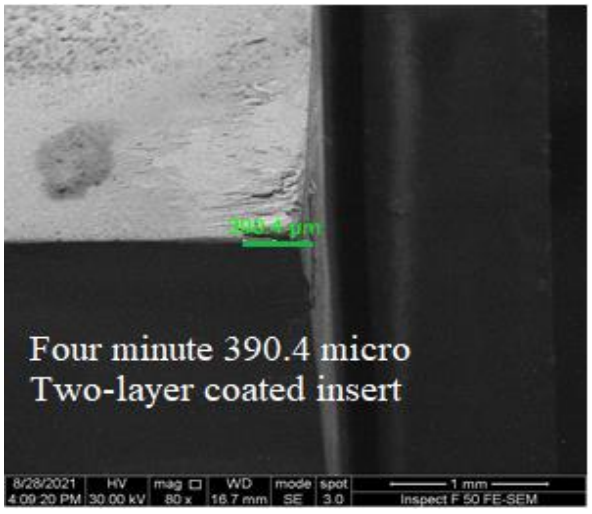

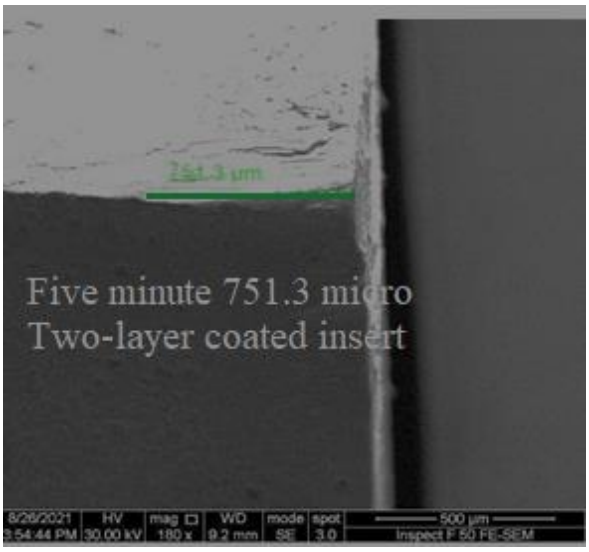

88 m/min, 0.065mm/rev, 0.5mm

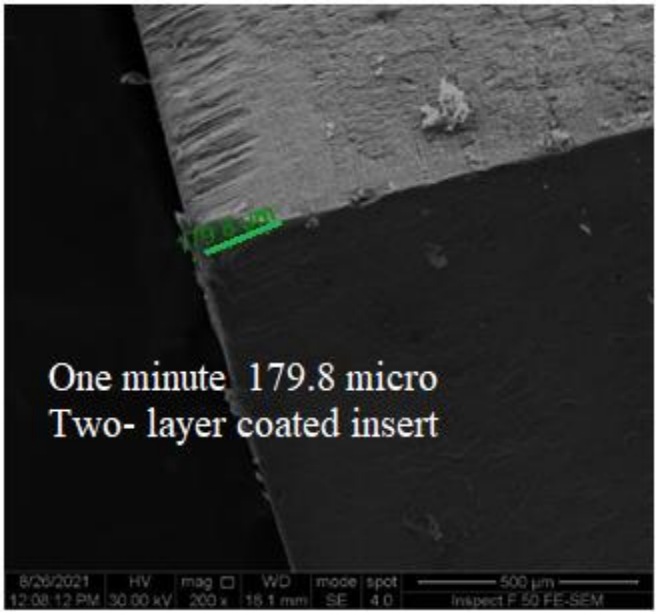

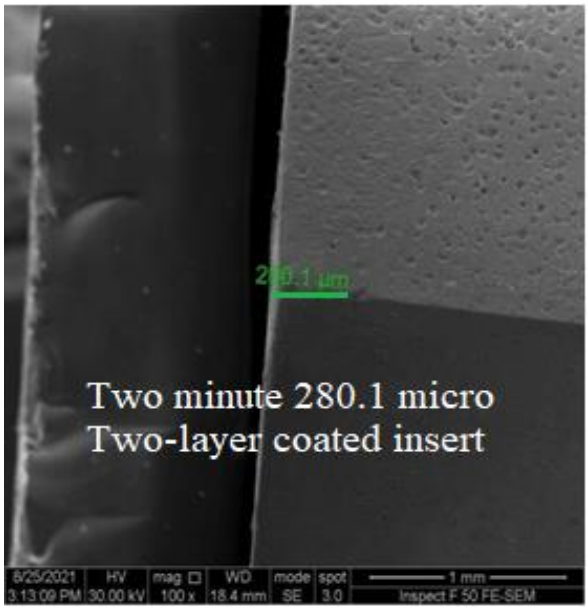

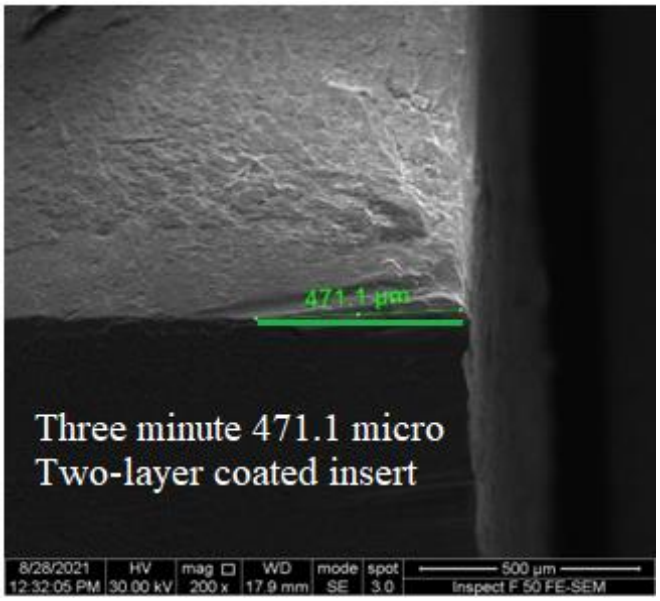

88 m/min, 0.165mm/rev, 0.7mm

Continue Figure (10)

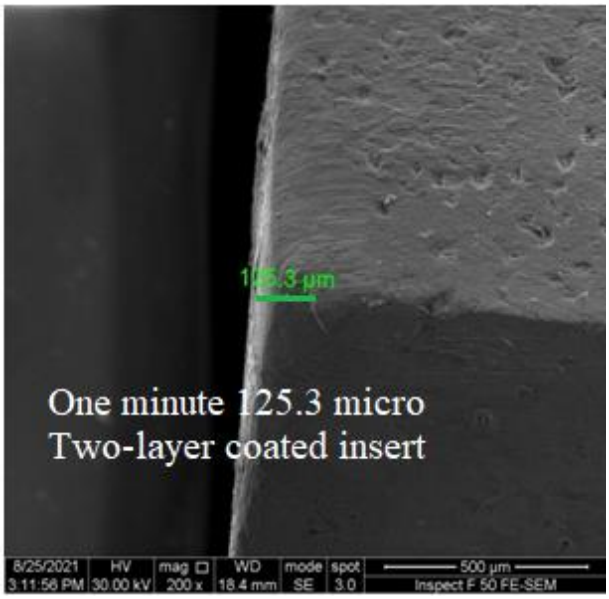

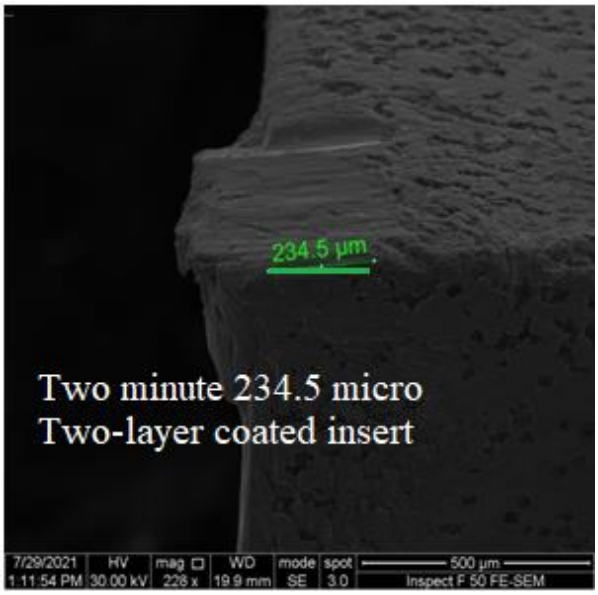

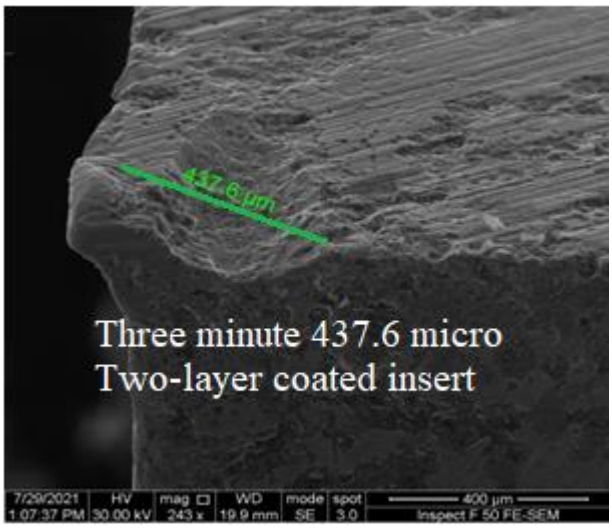

112, 0.065mm/rev, 0.7mm

Continue Figure (10)

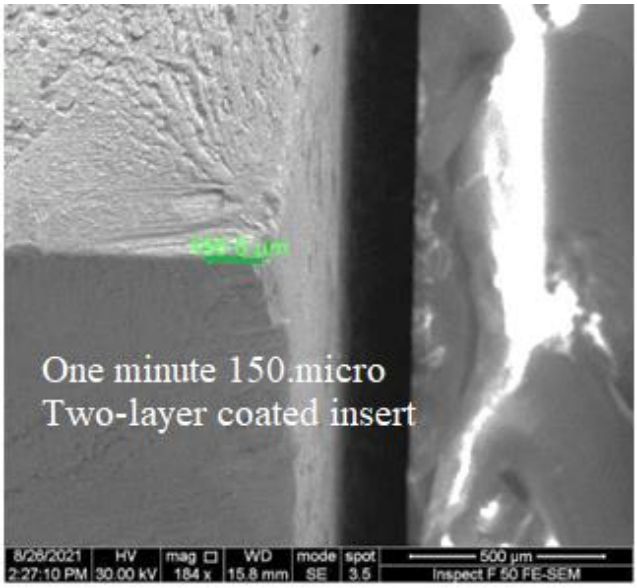

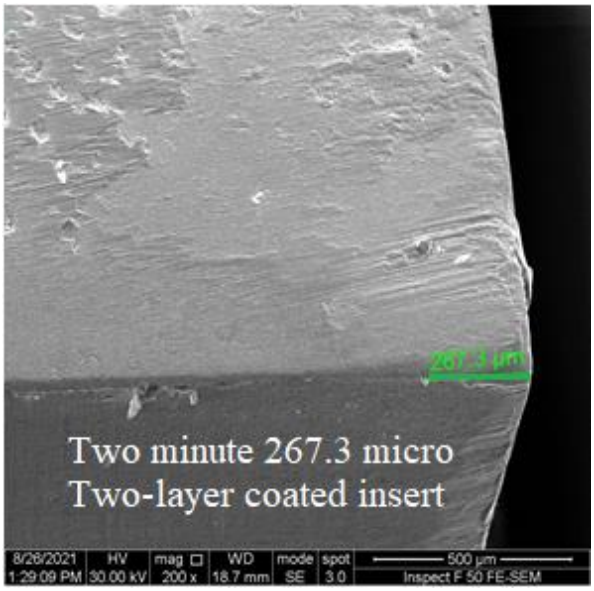

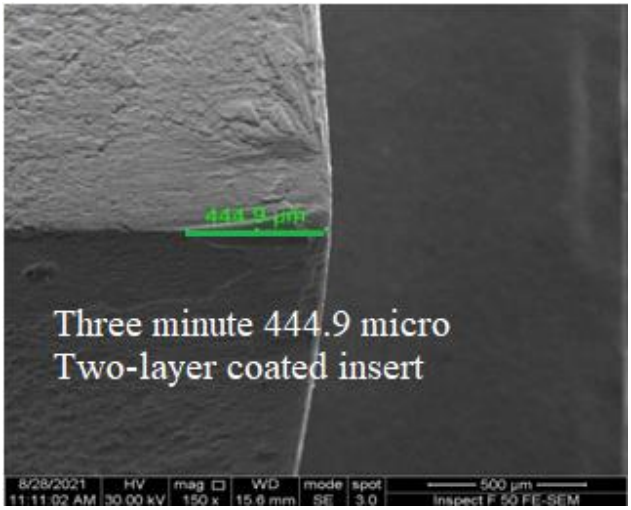

112, 0.165mm/rev, 0.2mm

Continue Figure (10)

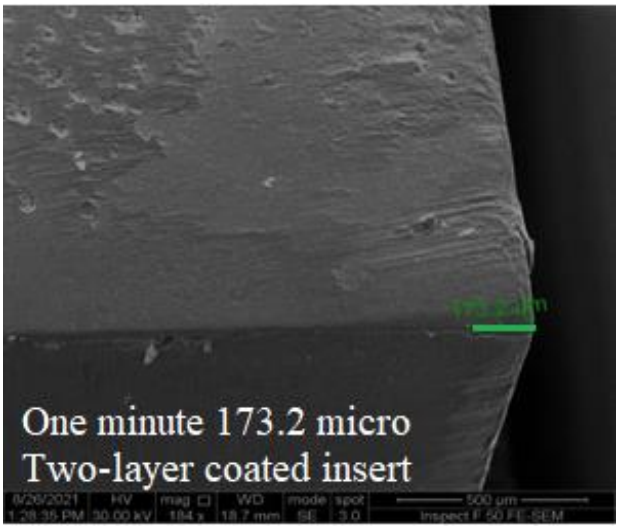

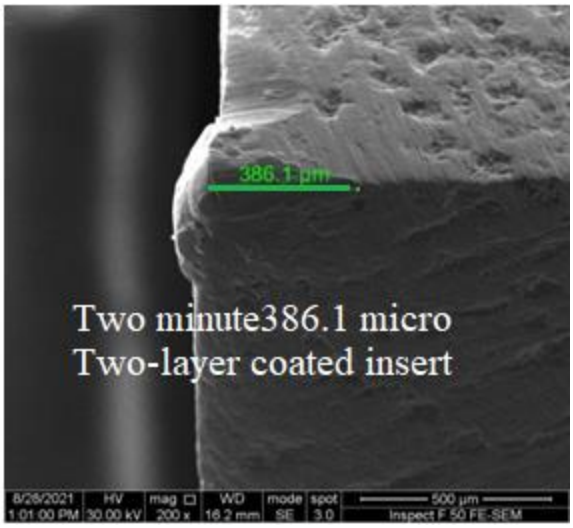

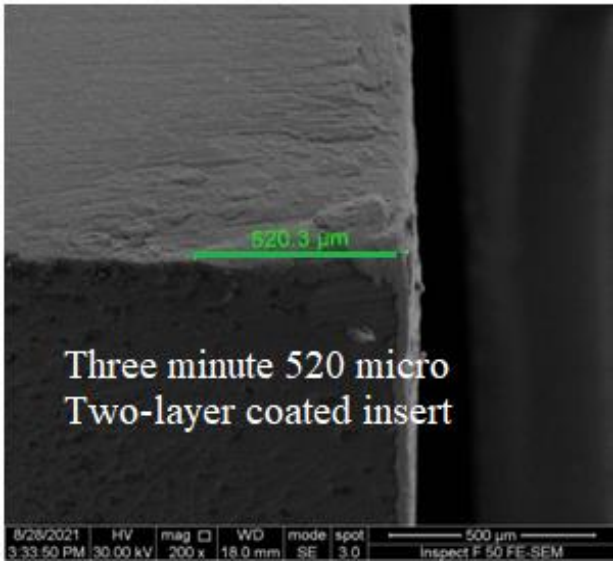

112 m/min, 0.5mm, 0.265mm/rev

Continue Figure (10)

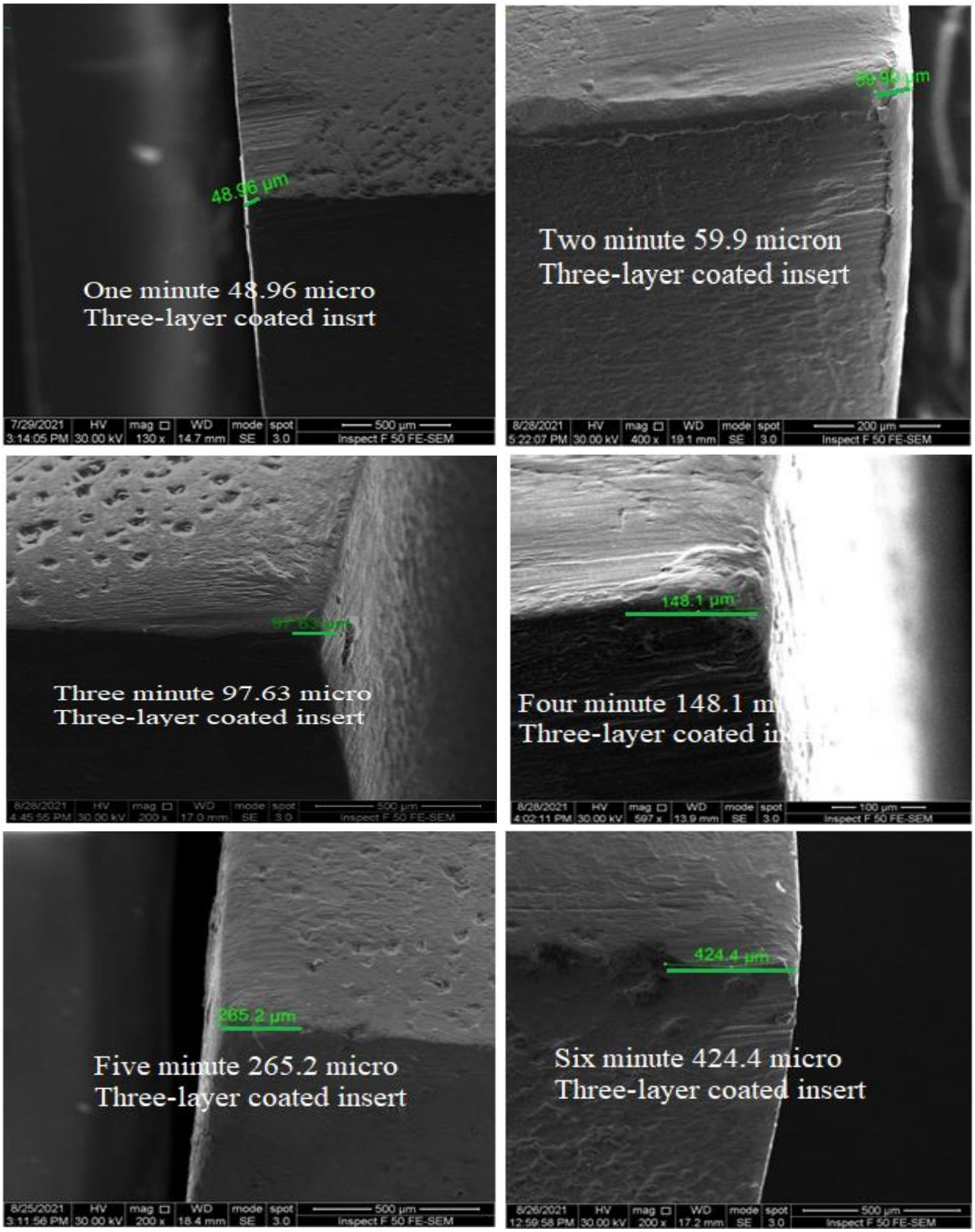

56m/min, 0.065 mm/rev, 0.2mm

Figure (11): Wear width for Triplex layer coated cutting insert for each minute

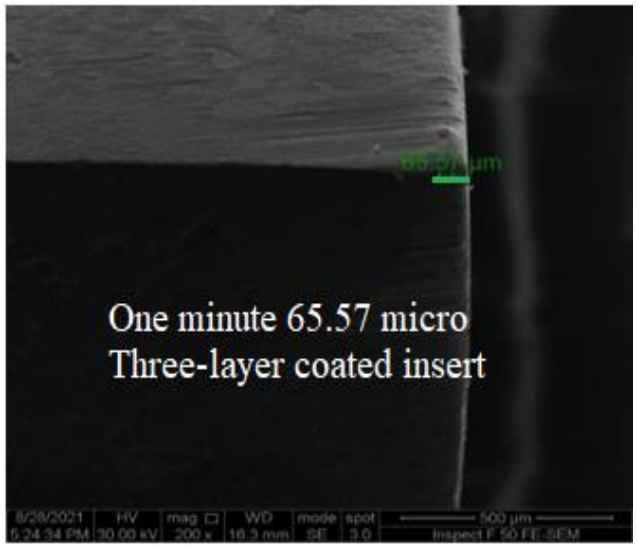

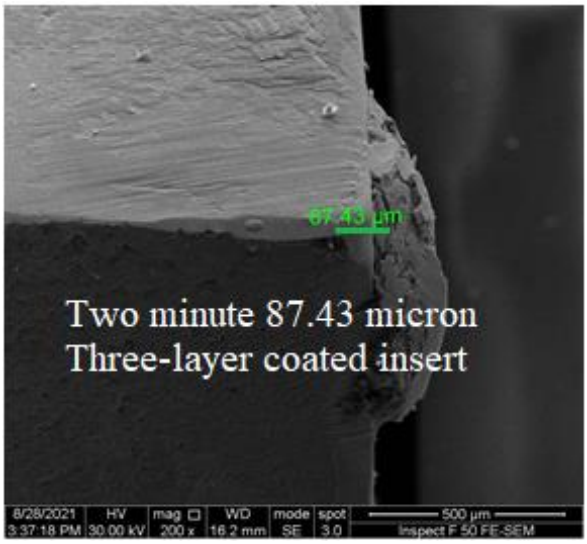

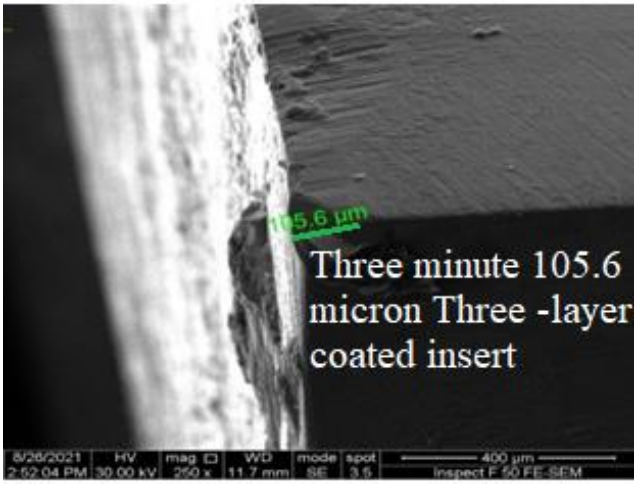

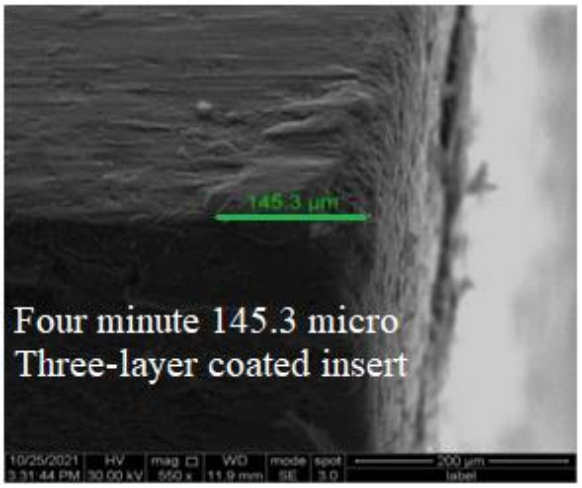

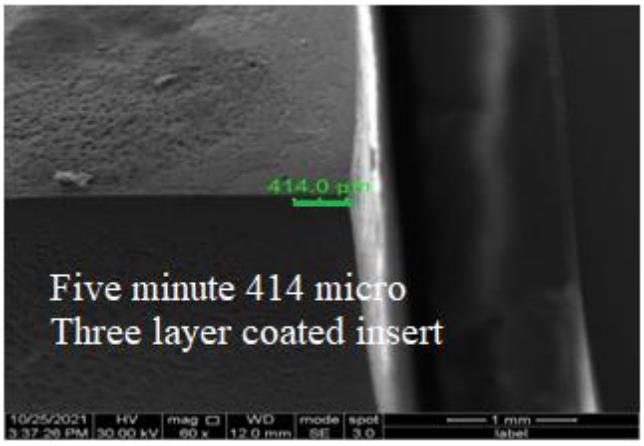

56 m/min, 0.165mm/rev, 0.5mm

Continue Figure (11)

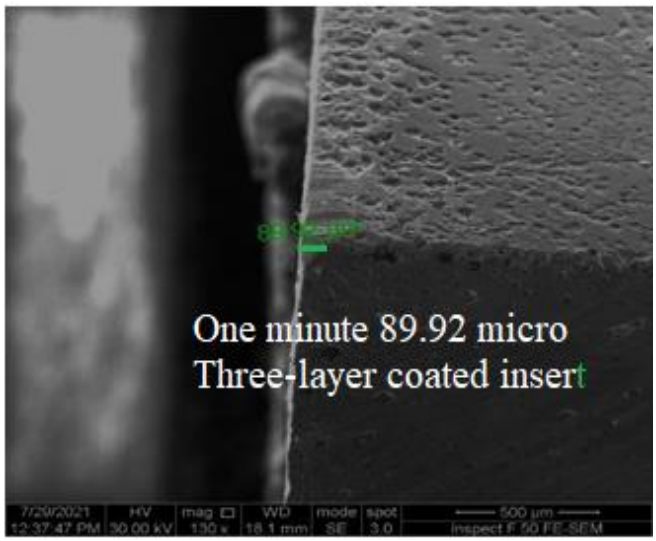

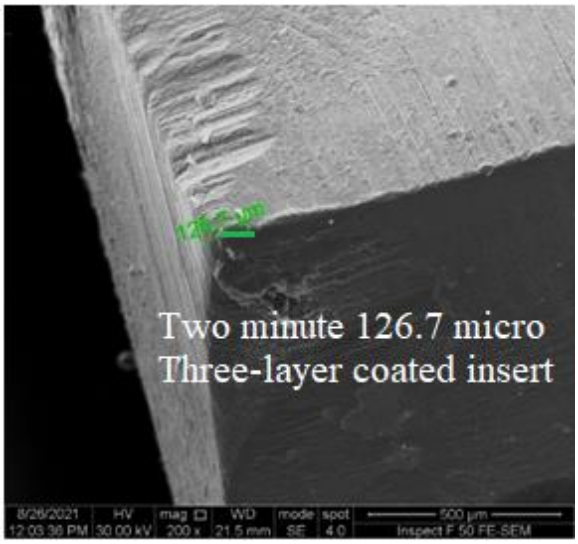

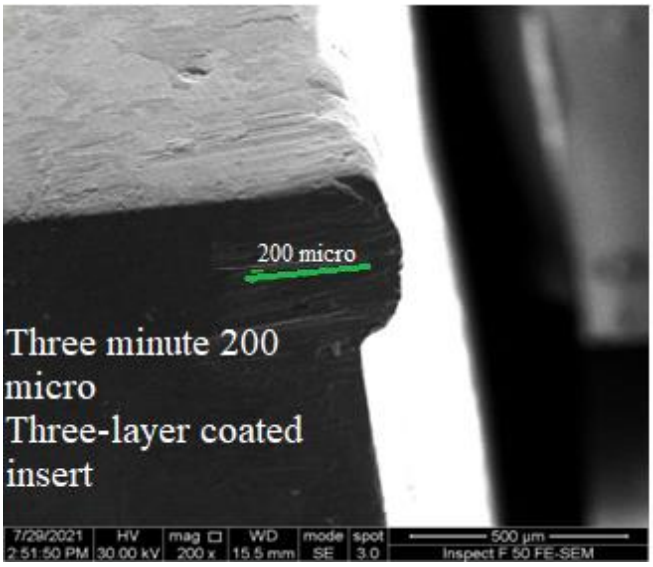

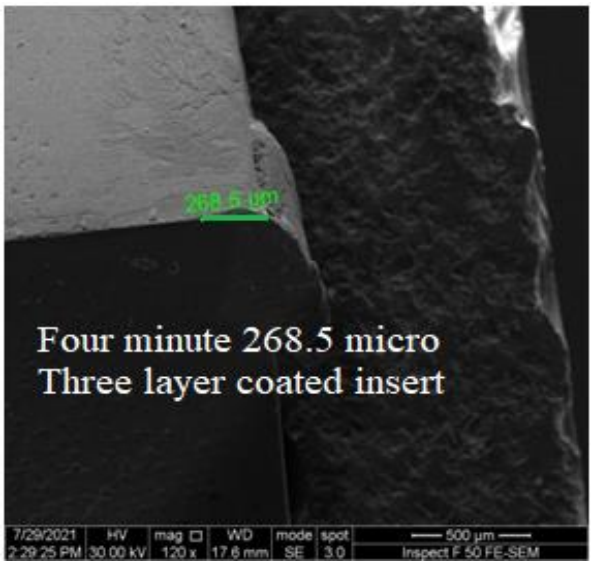

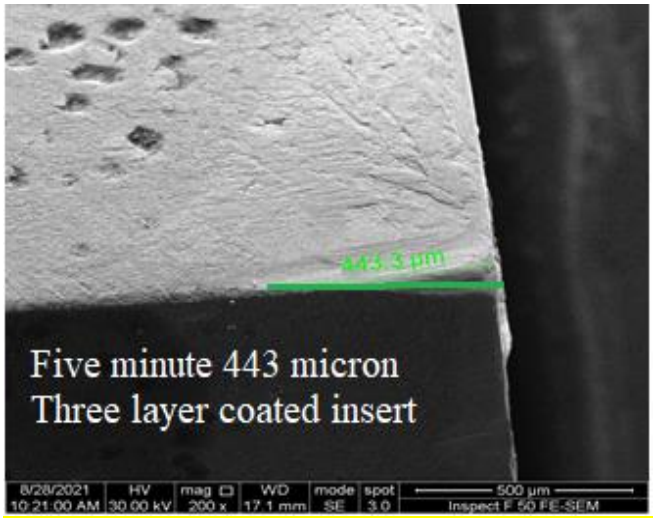

56 m/min, 0.265mm/rev, 0.7mm

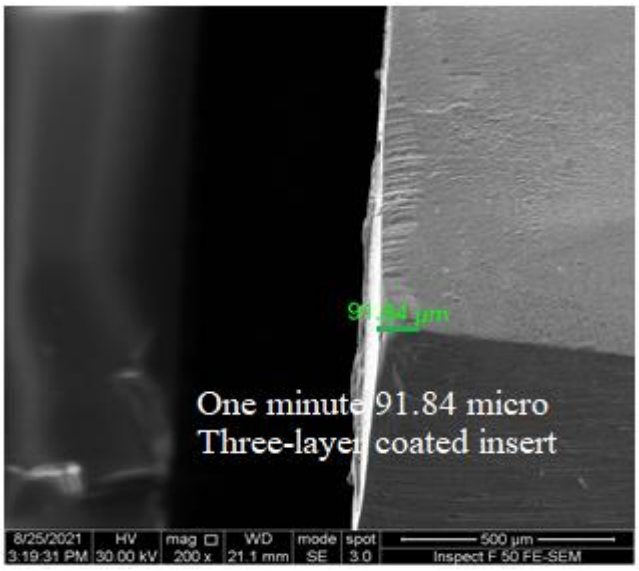

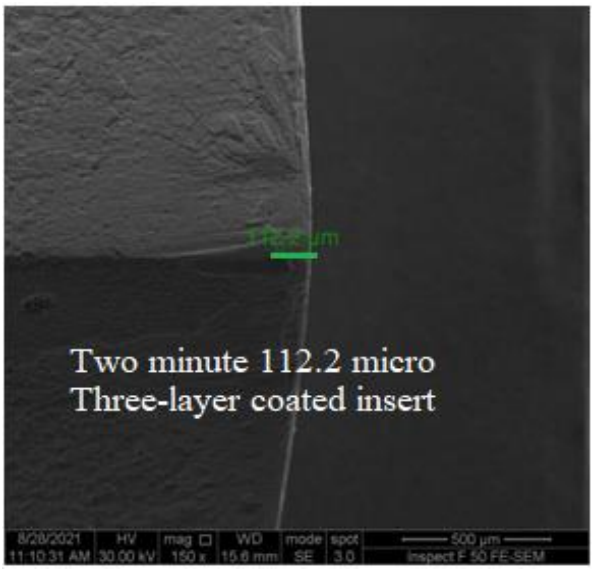

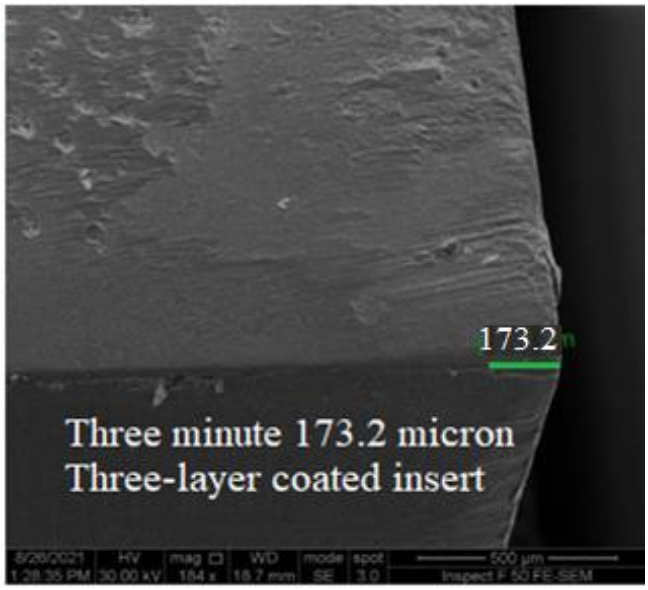

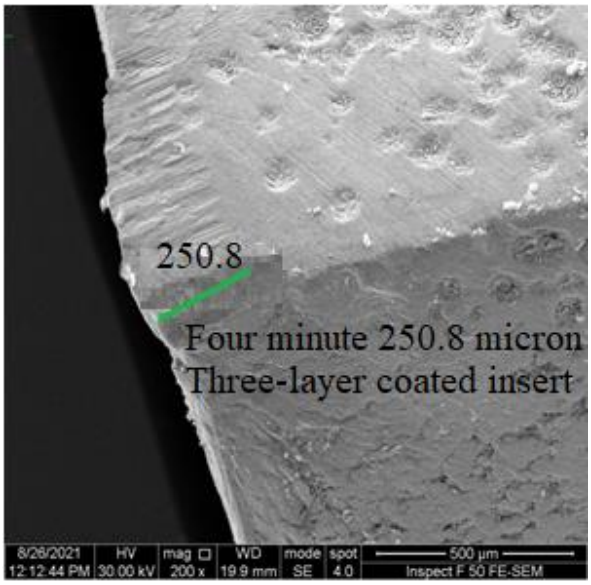

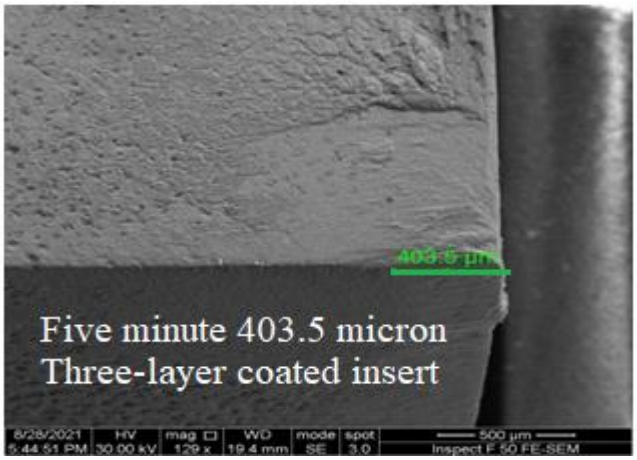

88 m/min, 0.065mm/rev, 0.5mm

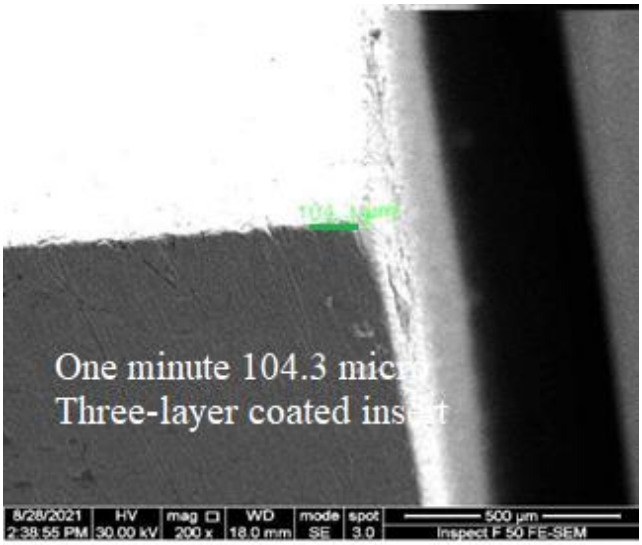

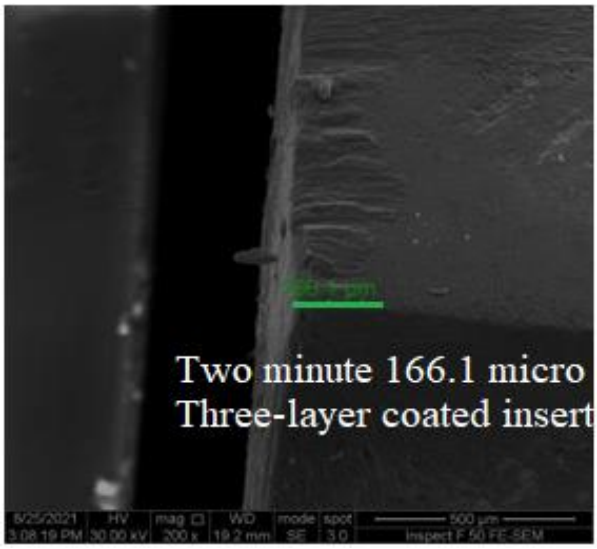

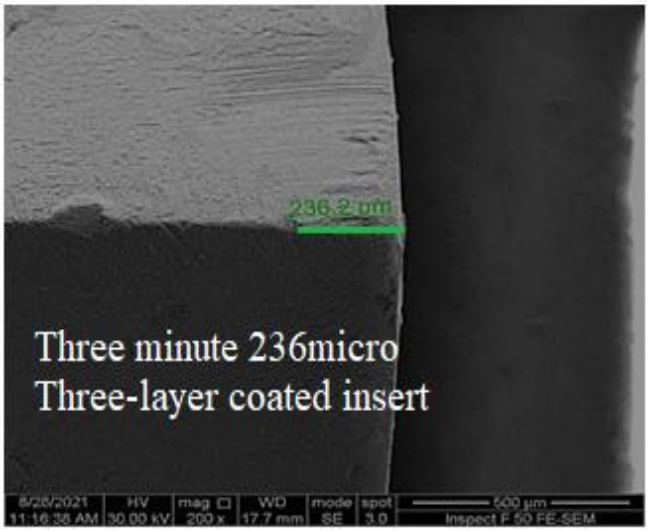

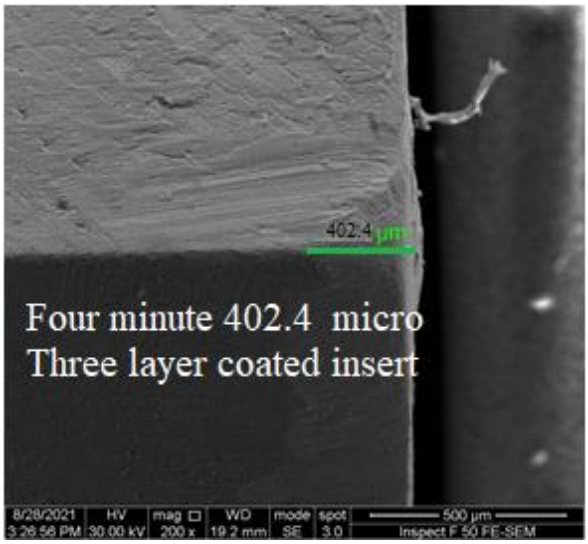

88m/min, 0.065mm/rev, 0.5mm

Continue Figure (11)

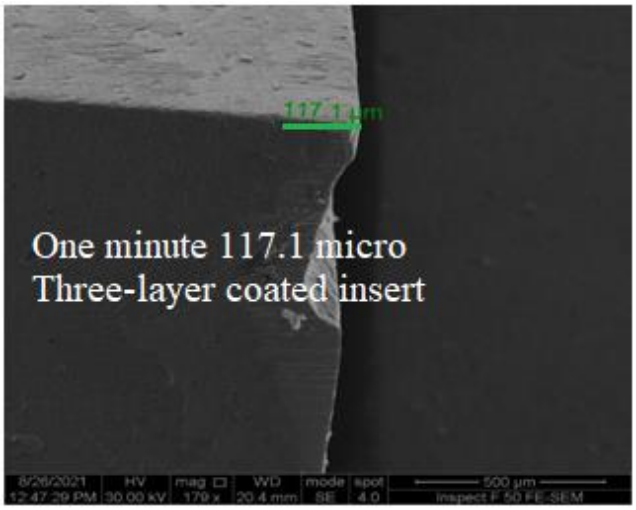

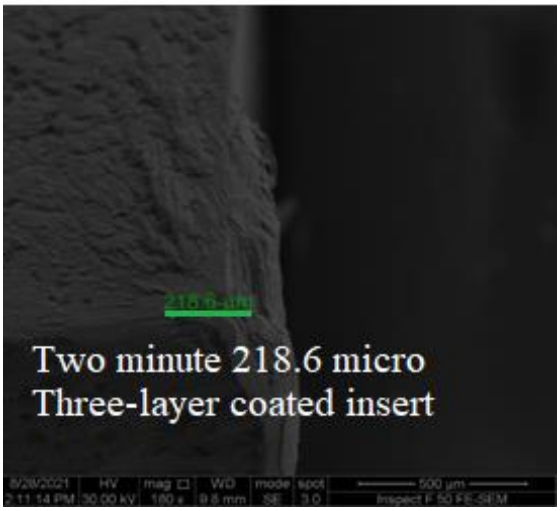

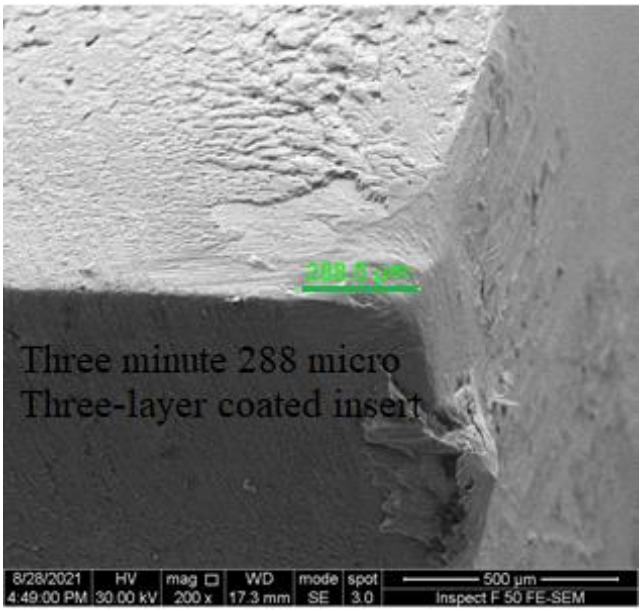

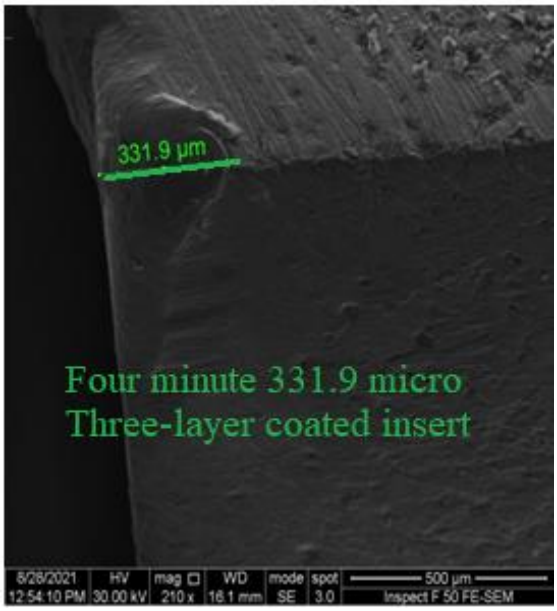

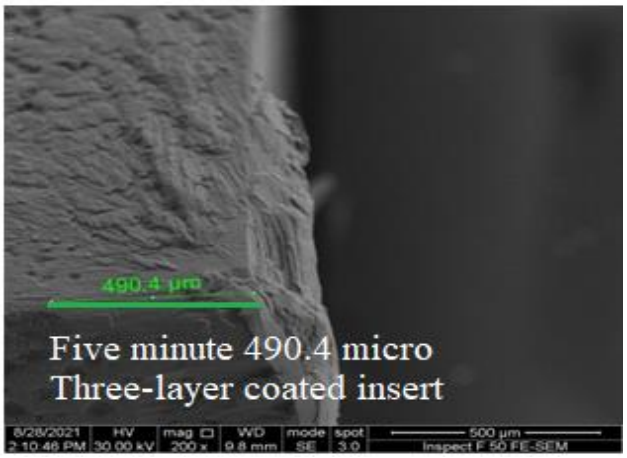

88m/min, 0.165mm/rev, 0.7mm

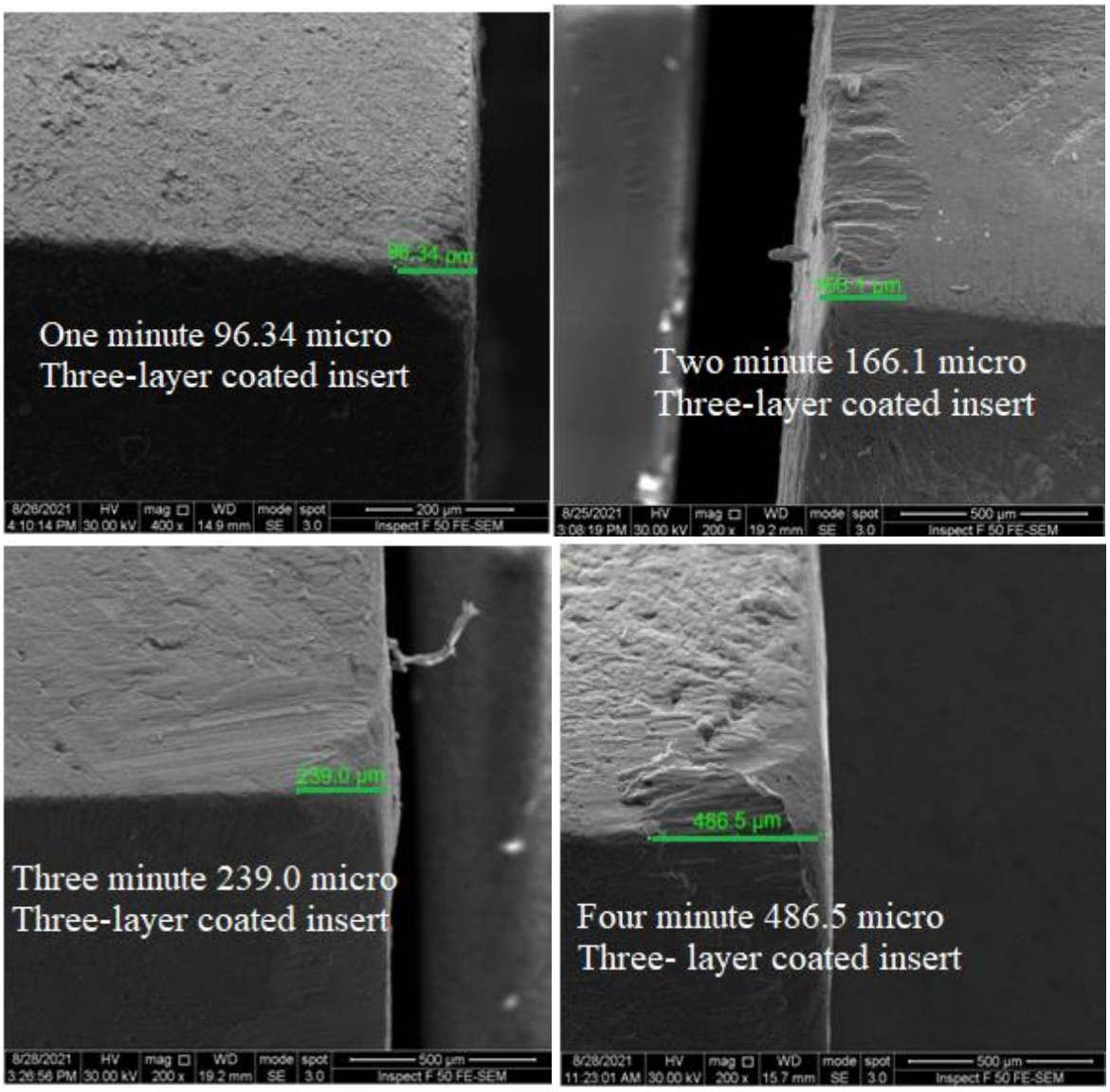

112 m/min, 0.065mm/rev, 0.7mm

Continue Figure (11)

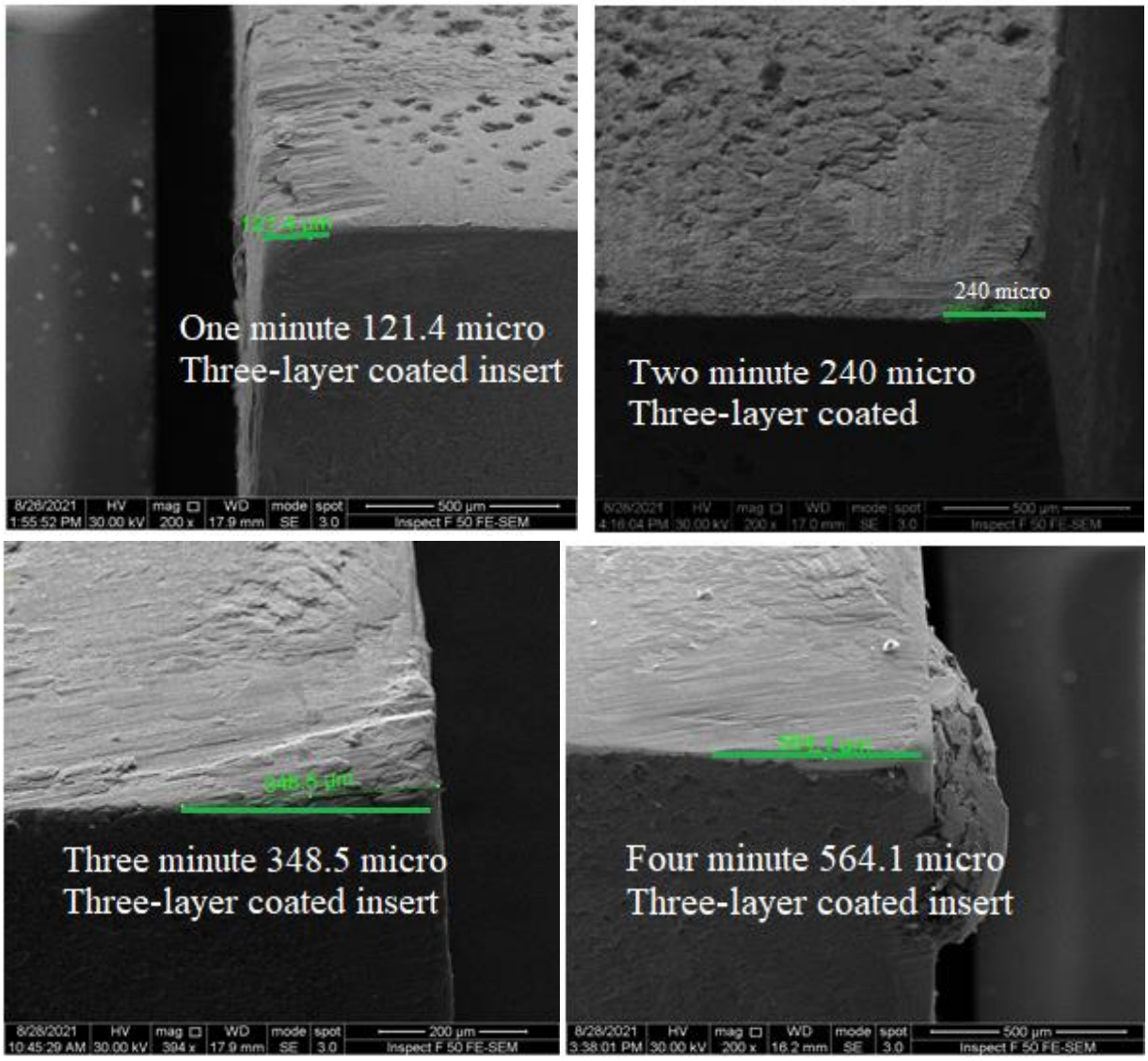

112 m/min, 0.165mm/rev, 0.2mm

Continue Figure (11)

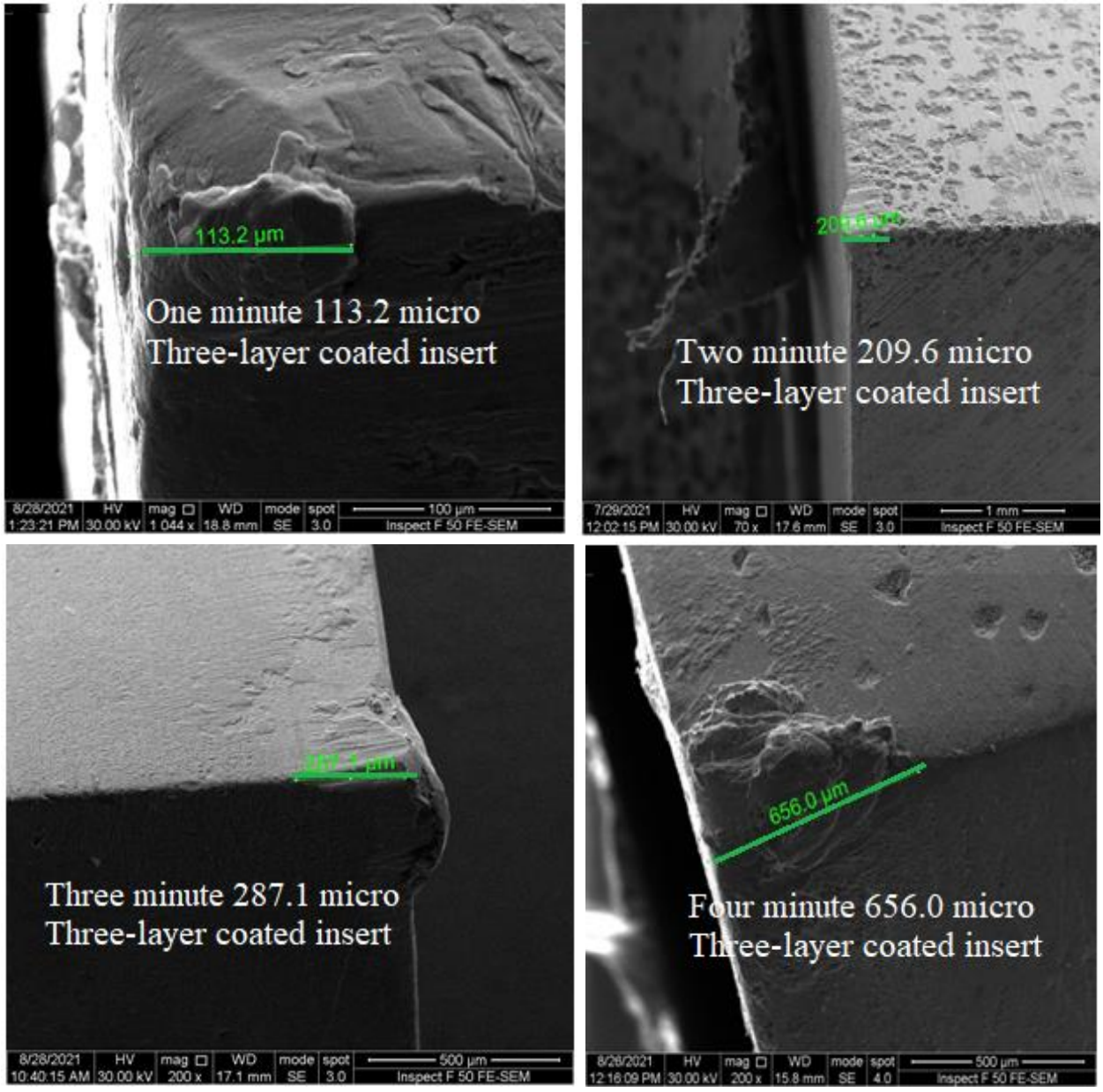

112m/min, 0.5mm, 0.265mm/rev

Continue Figure (11)

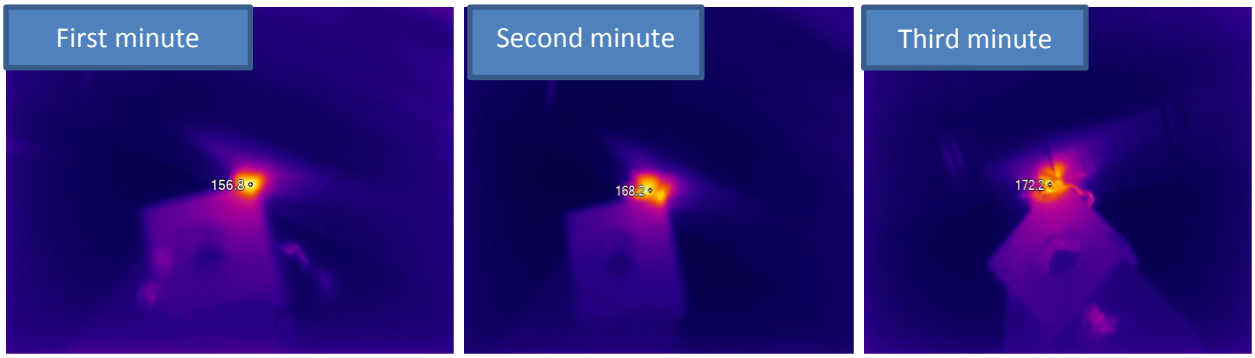

56 m/min, 0.065 mm/rev, 0.2mm

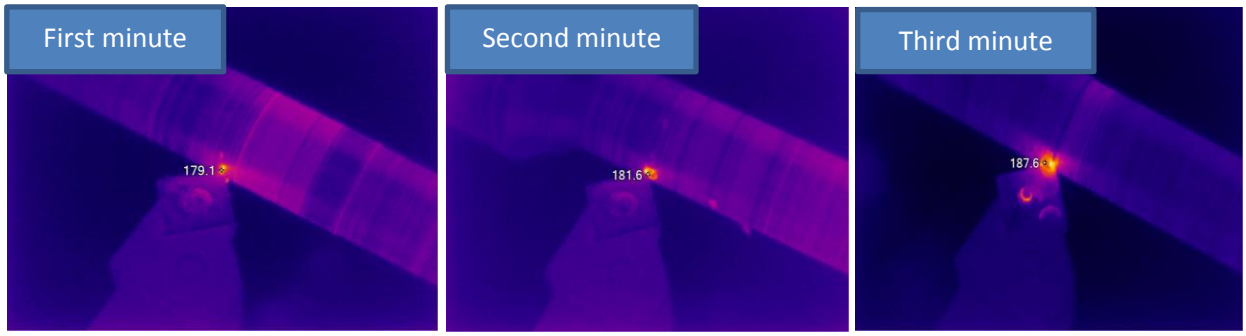

56 m/min, 0.165mm/rev, 0.5mm

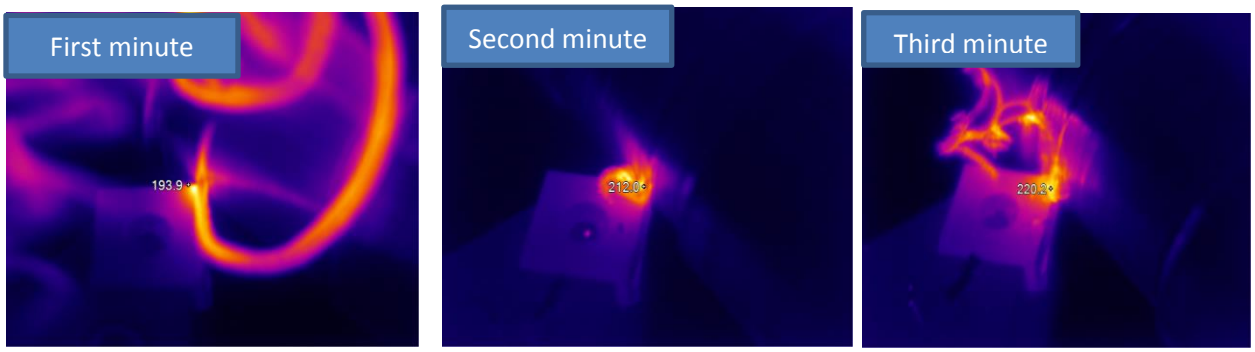

56m/min, 0.265mm/rev, 0.7mm

Figure (12): Temperature Fº for uncoated cutting insert for each minute

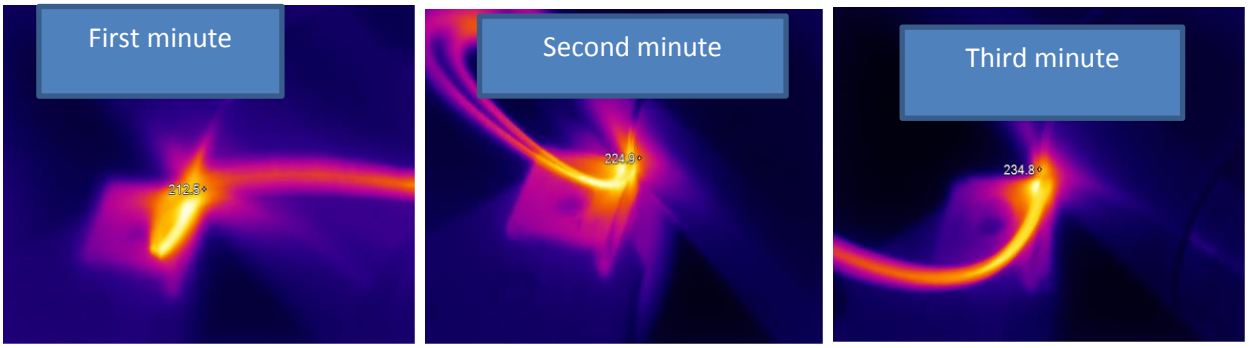

88m/min, 0.065mm/rev, 0.5mm

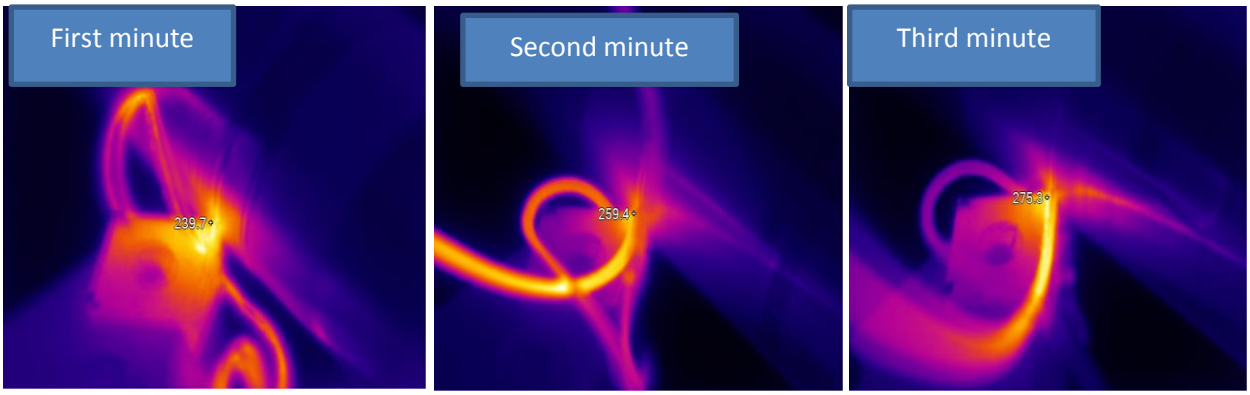

88m/min, 0.065mm/rev, 0.5mm

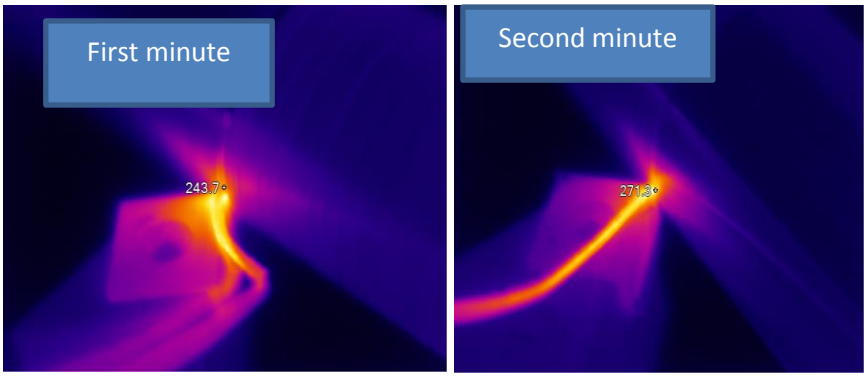

88m/min, 0.165mm/rev, 0.7mm

Continue Figure (12)

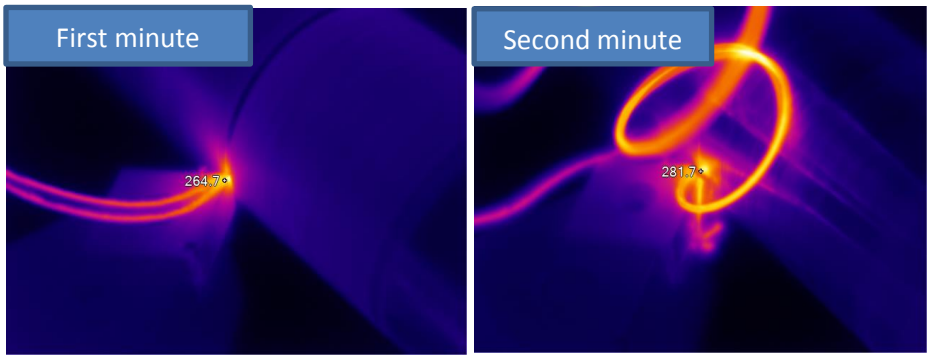

112 m/min, 0.065mm/rev, 0.7mm

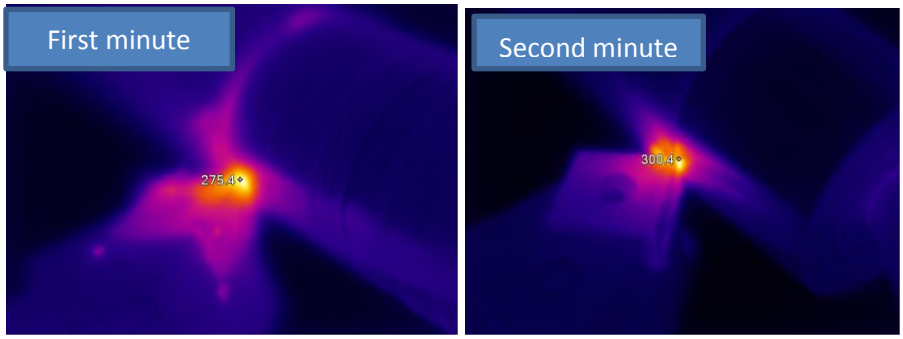

112 m/min, 0.165mm/rev, 0.2mm

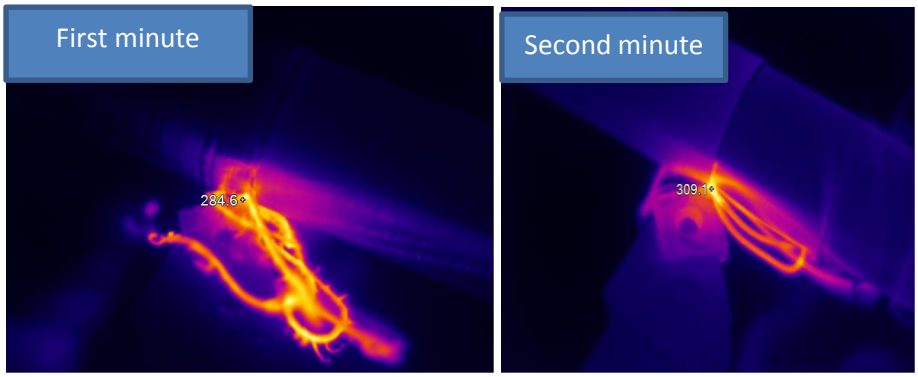

112m/min, 0.5mm, 0.265mm/rev

Continue Figure (12)

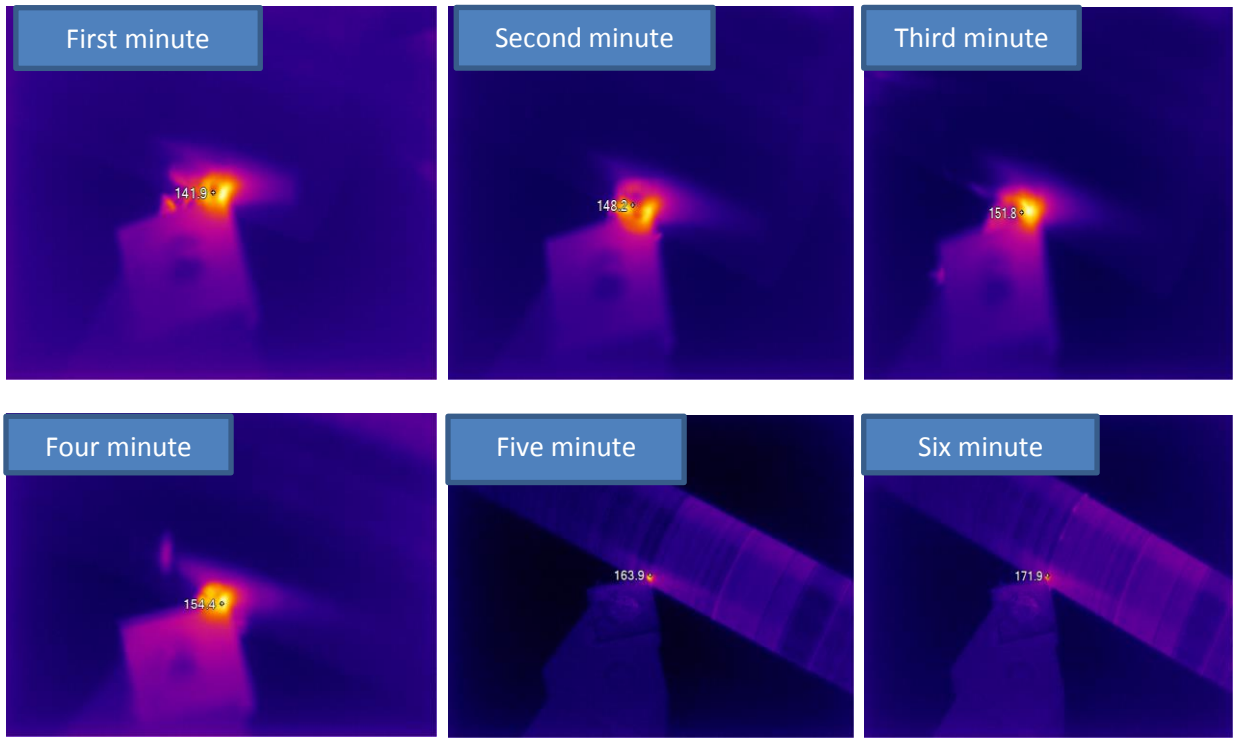

56 m/min, 0.065 mm/rev, 0.2mm

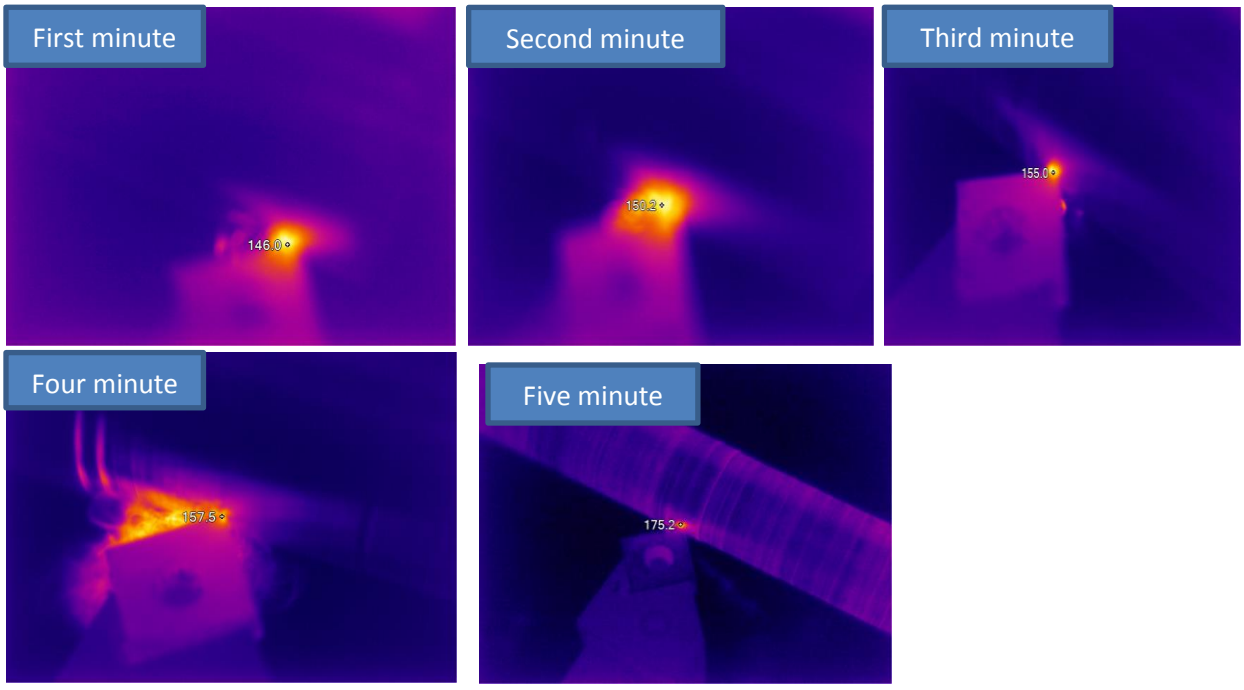

56m/min, 0.165mm/rev, 0.5mm

Figure (13): Temperature Fº for Triplex layers coated cutting insert for each minute

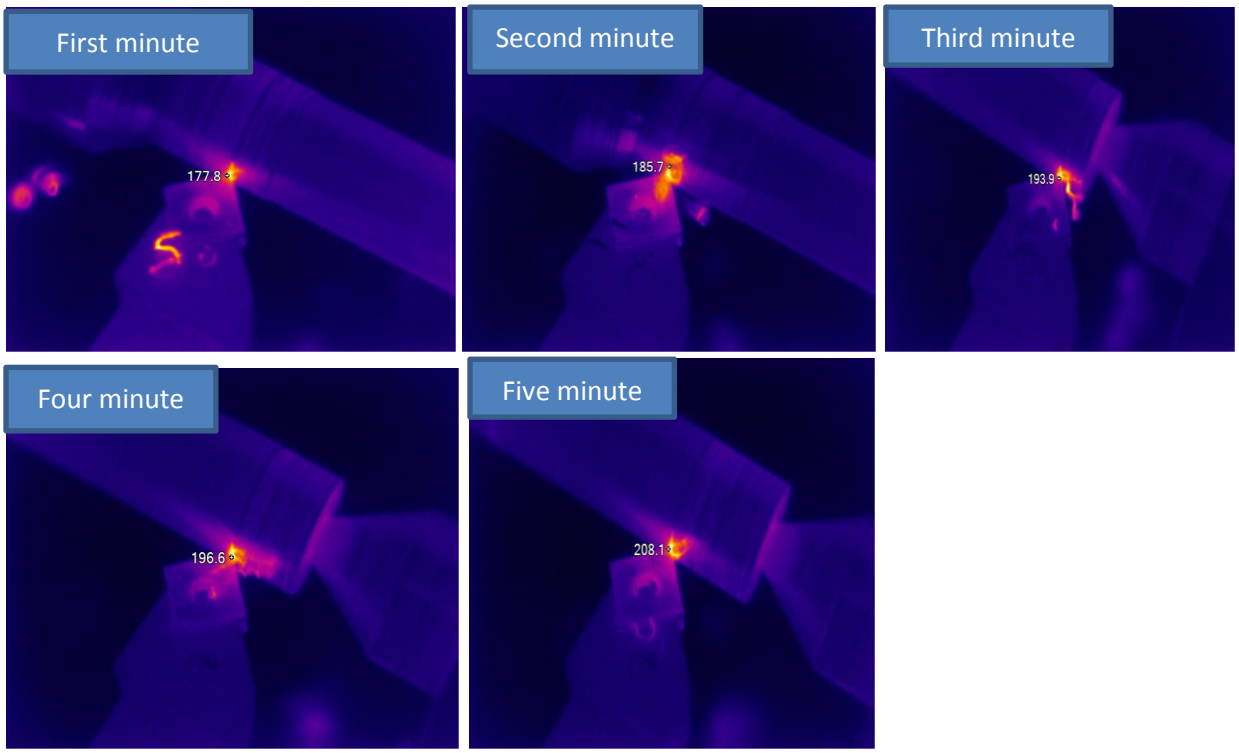

56 m/min, 0.265mm/rev, 0.7mm

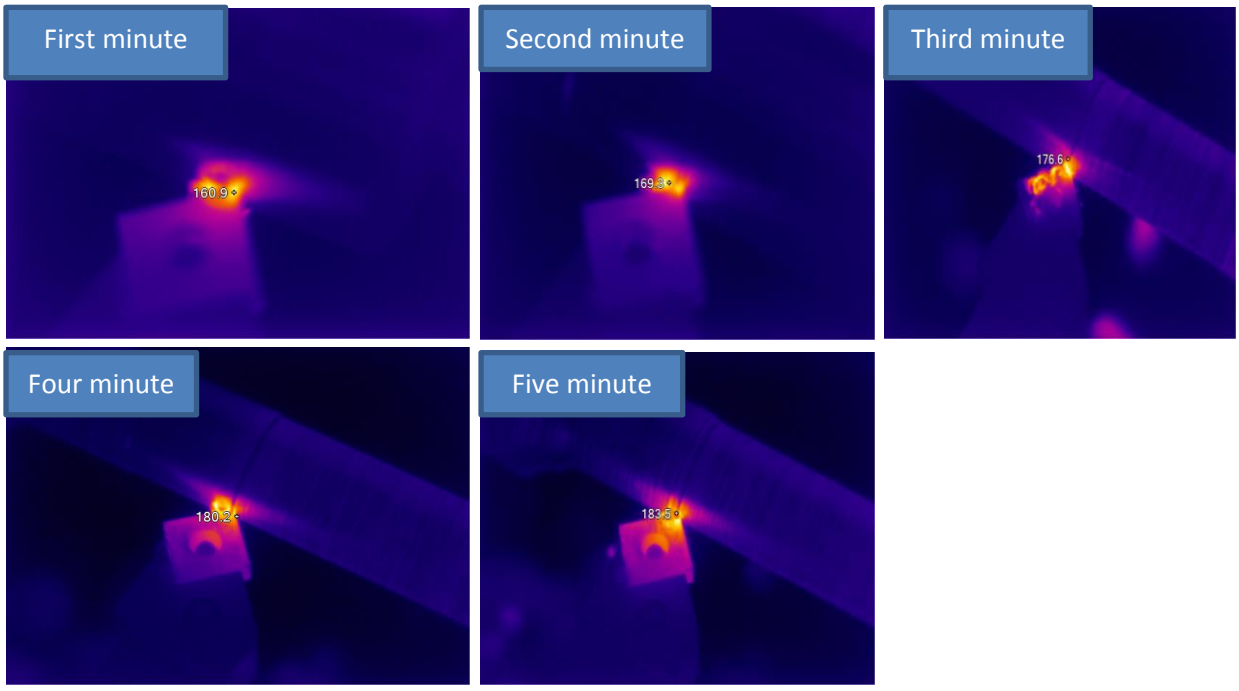

88 m/min, 0.065mm/rev, 0.5mm

Continue Figure (13)

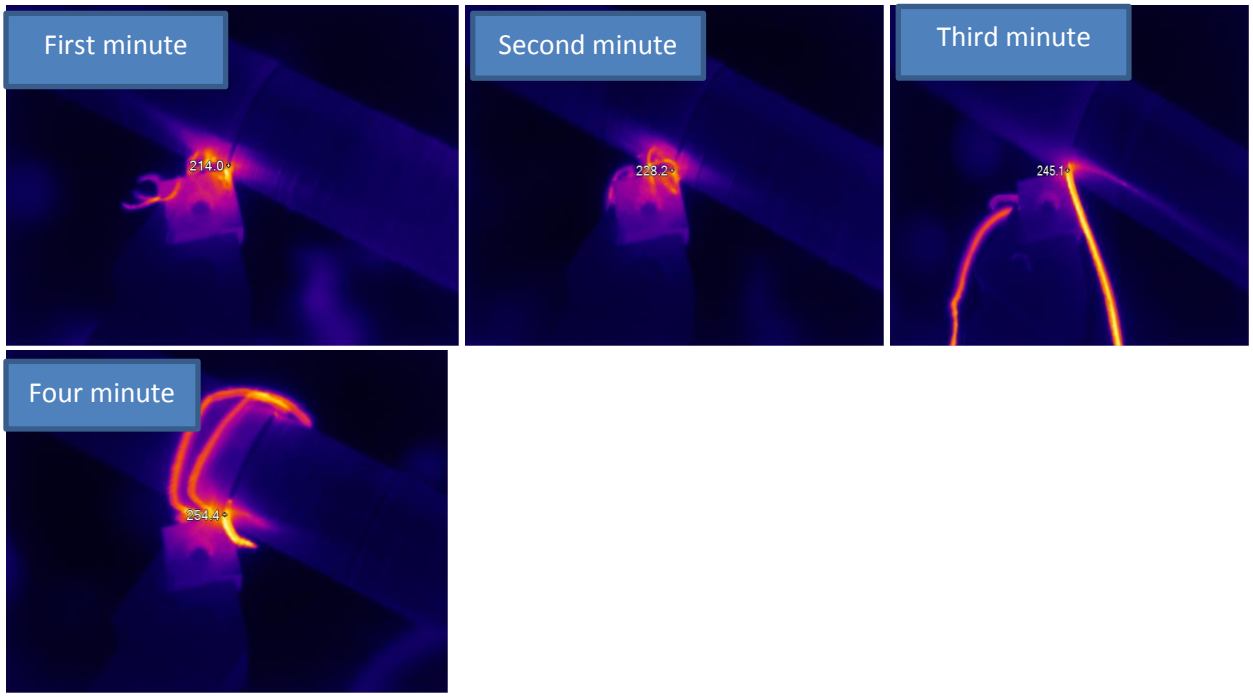

88m/min, 0.165mm/rev, 0.7mm

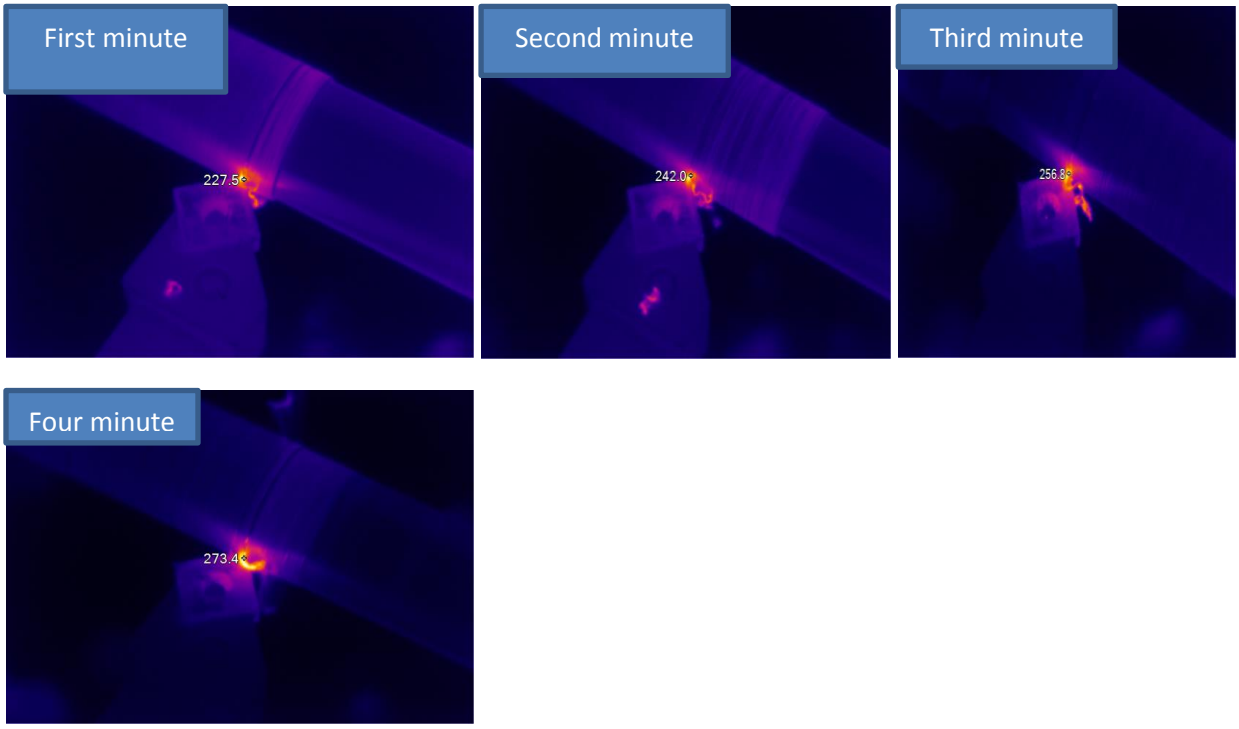

88m/min, 0.165mm/rev, 0.7mm

Continue Figure (13)

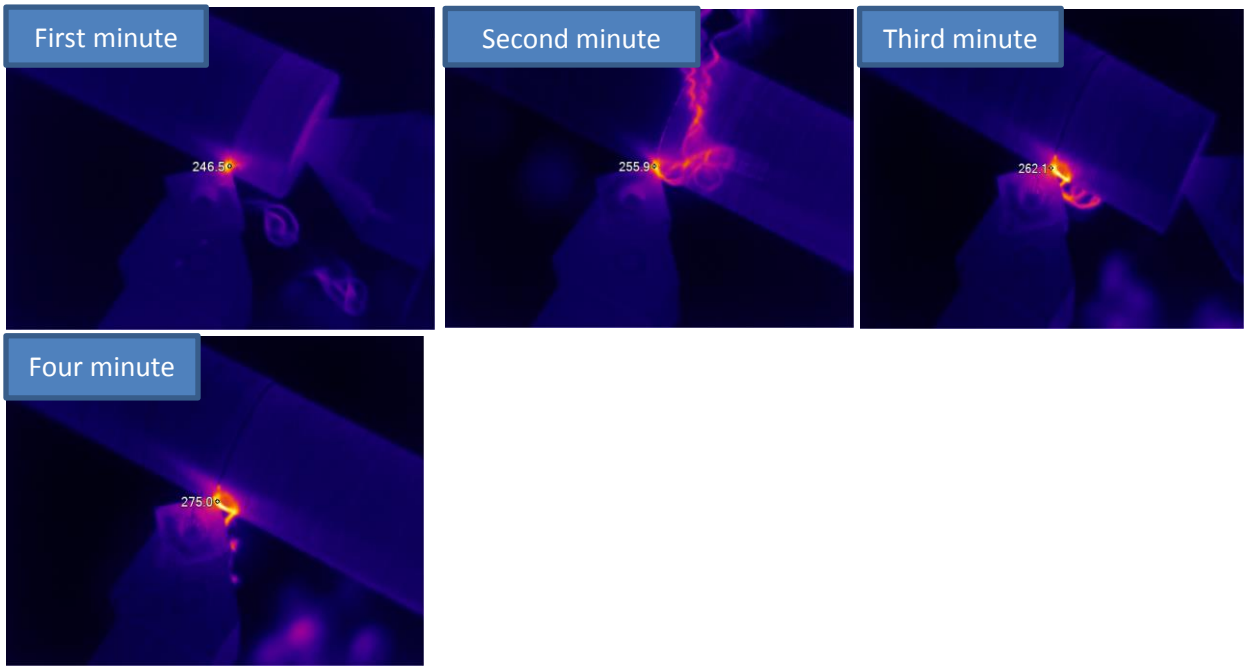

112m/min, 0.065mm/rev, 0.7mm

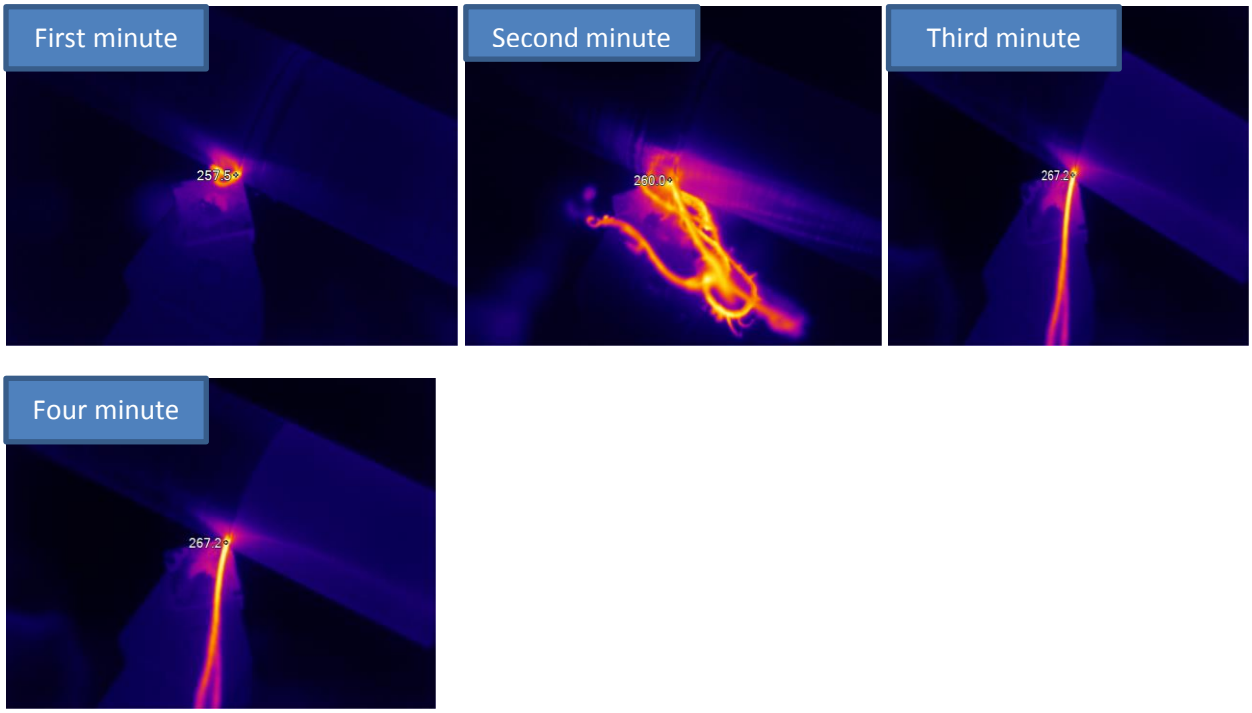

112m/min, 0.165mm/rev, 0.2mm

Continue Figure (13)

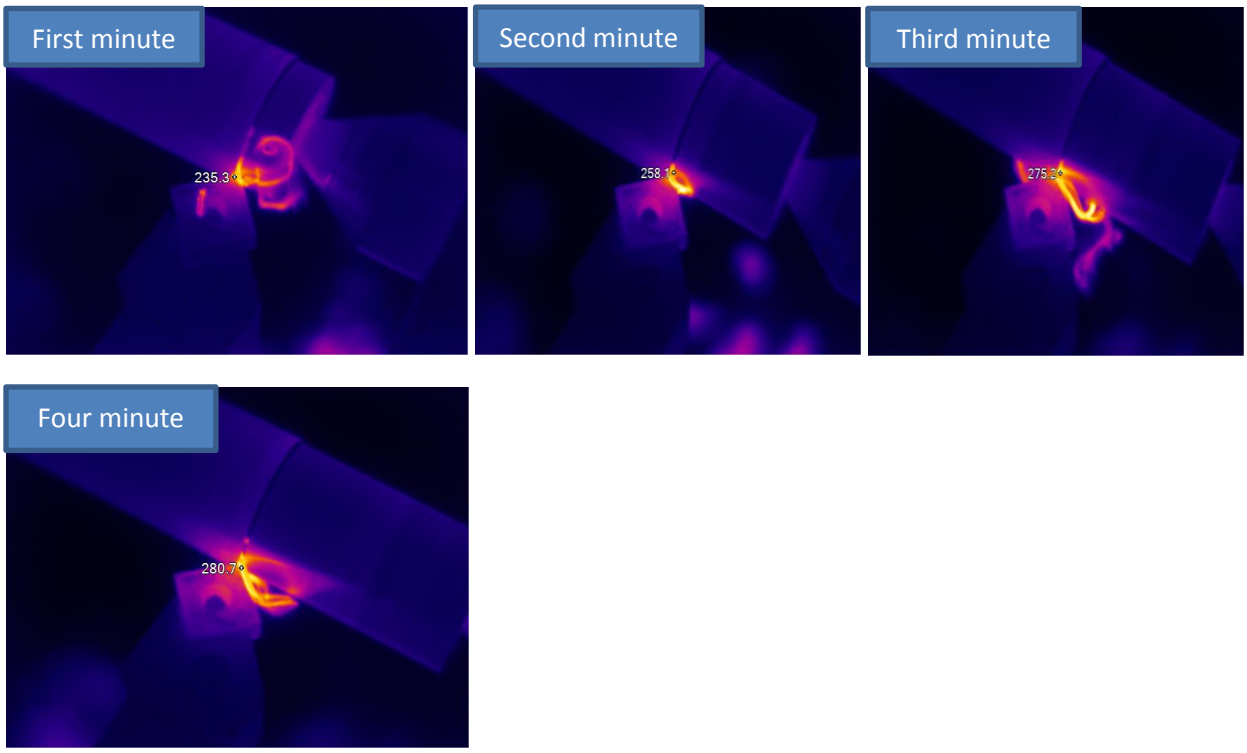

112m/min, 0.5mm, 0.265mm/rev

Continue Figure (13)

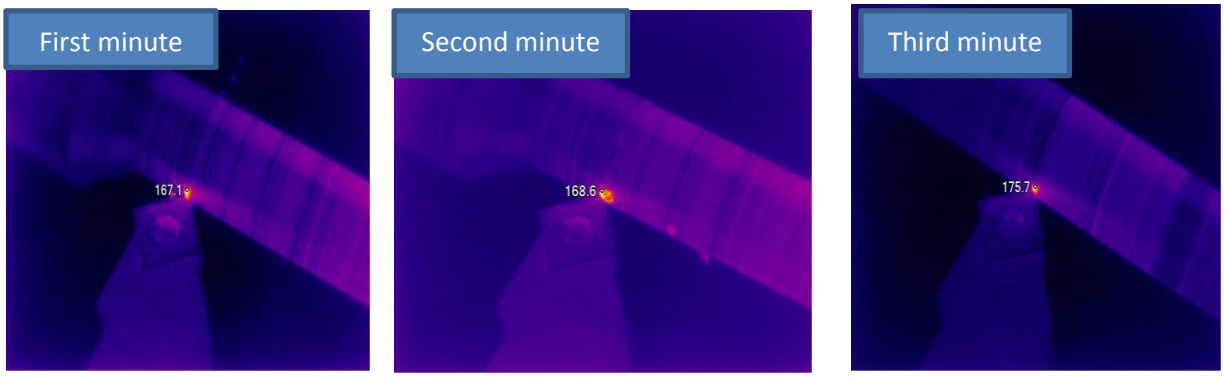

56 m/min, 0.065 mm/rev, 0.2mm

Figure (14): Temperature Fº for monolayer coated cutting insert for each minute

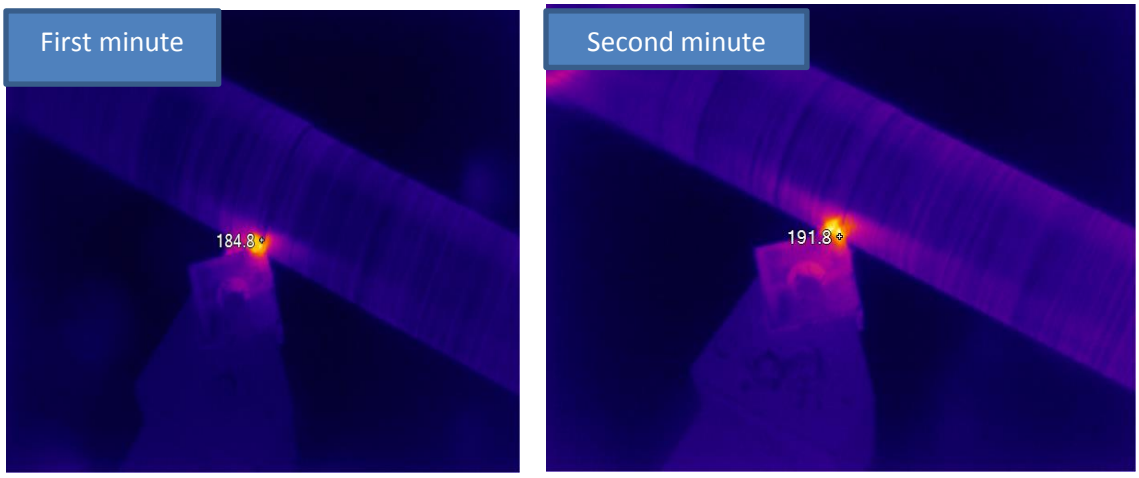

5 6m/min, 0.165mm/rev, 0.5mm

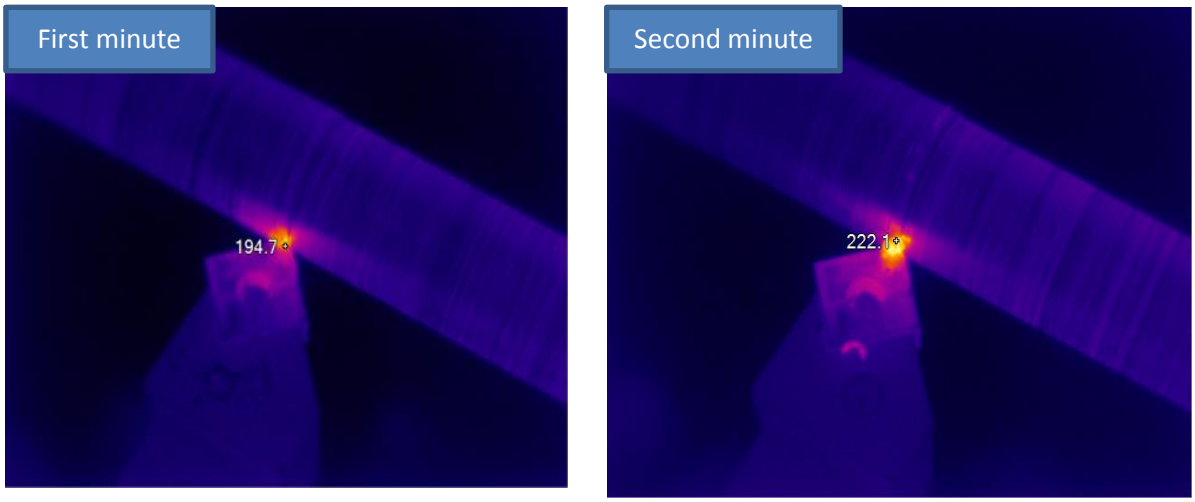

56m/min, 0.265mm/rev, 0.7mm

Continue Figure (14)

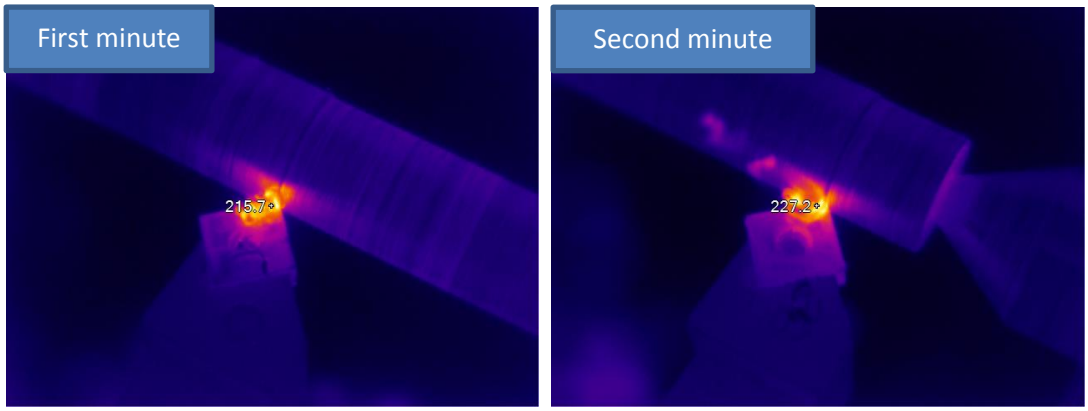

88m/min, 0.065mm/rev, 0.5mm

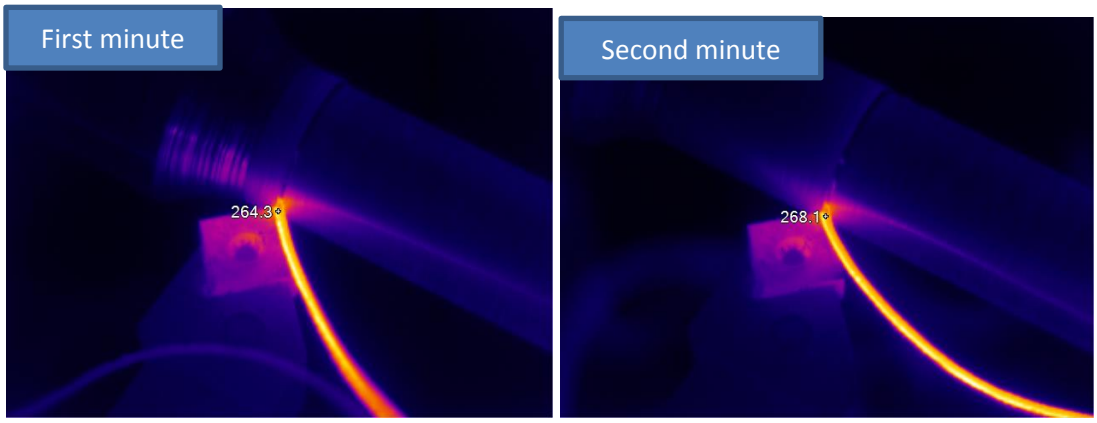

88m/min, 0.165mm/rev, 0.7mm

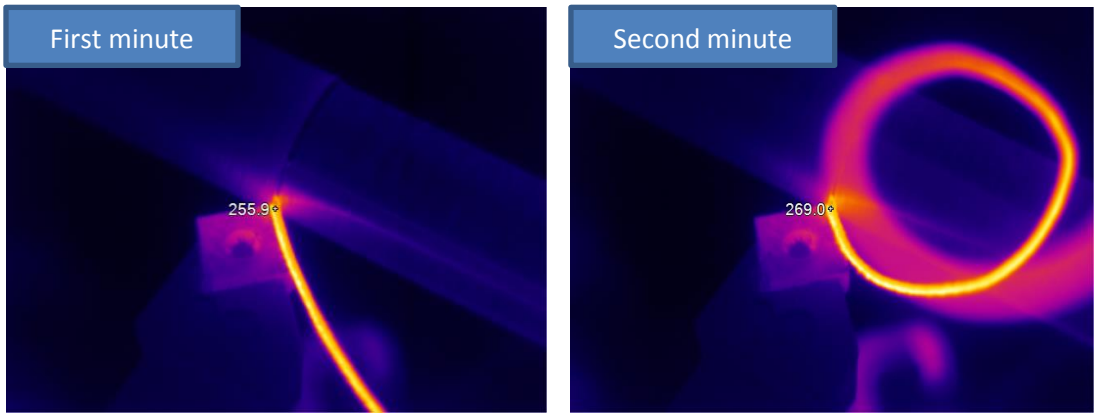

88m/min, 0.265mm/rev, 0.2mm

Continue Figure (14)

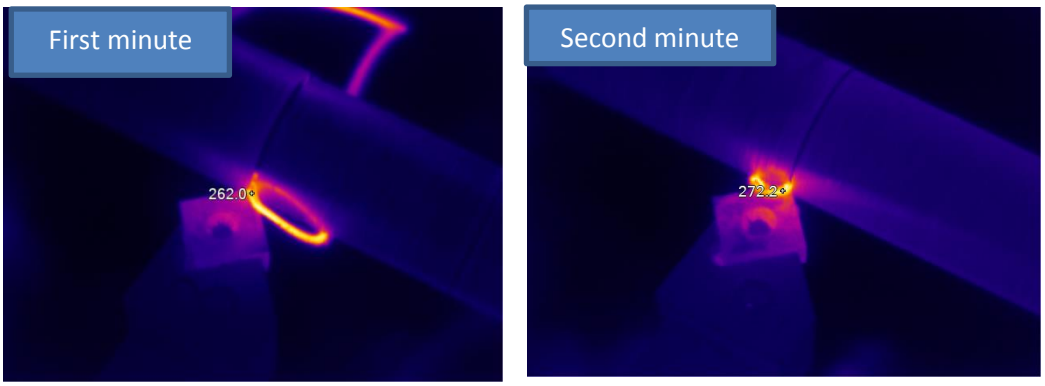

112m/min, 0.065mm/rev, 0.7mm

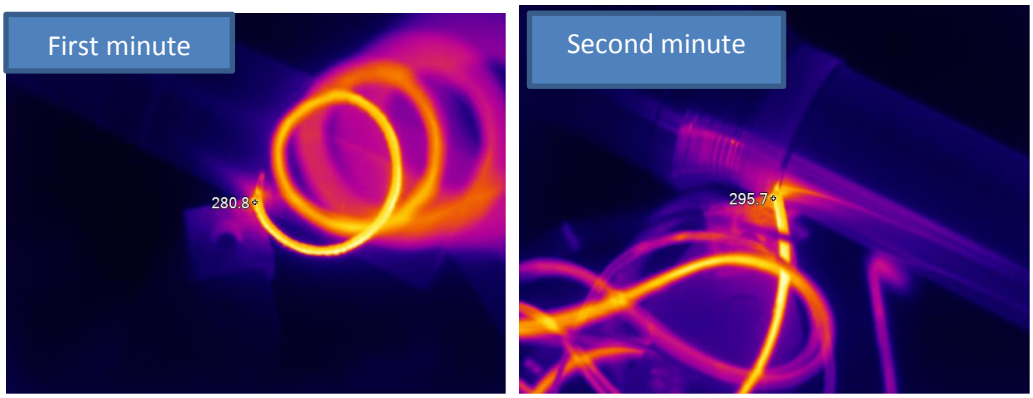

112m/min, 0.165mm/rev, 0.2mm

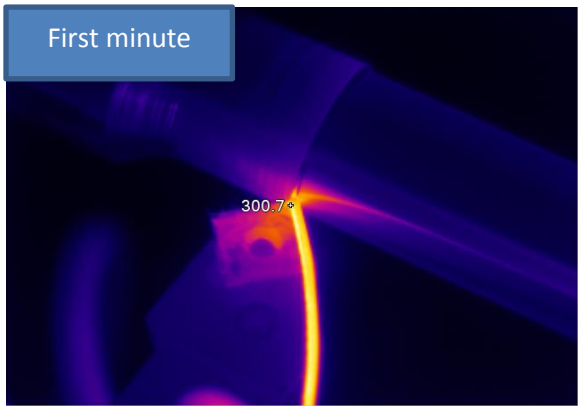

112m/min, 0.5mm, 0.265mm/rev

Continue Figure (14)

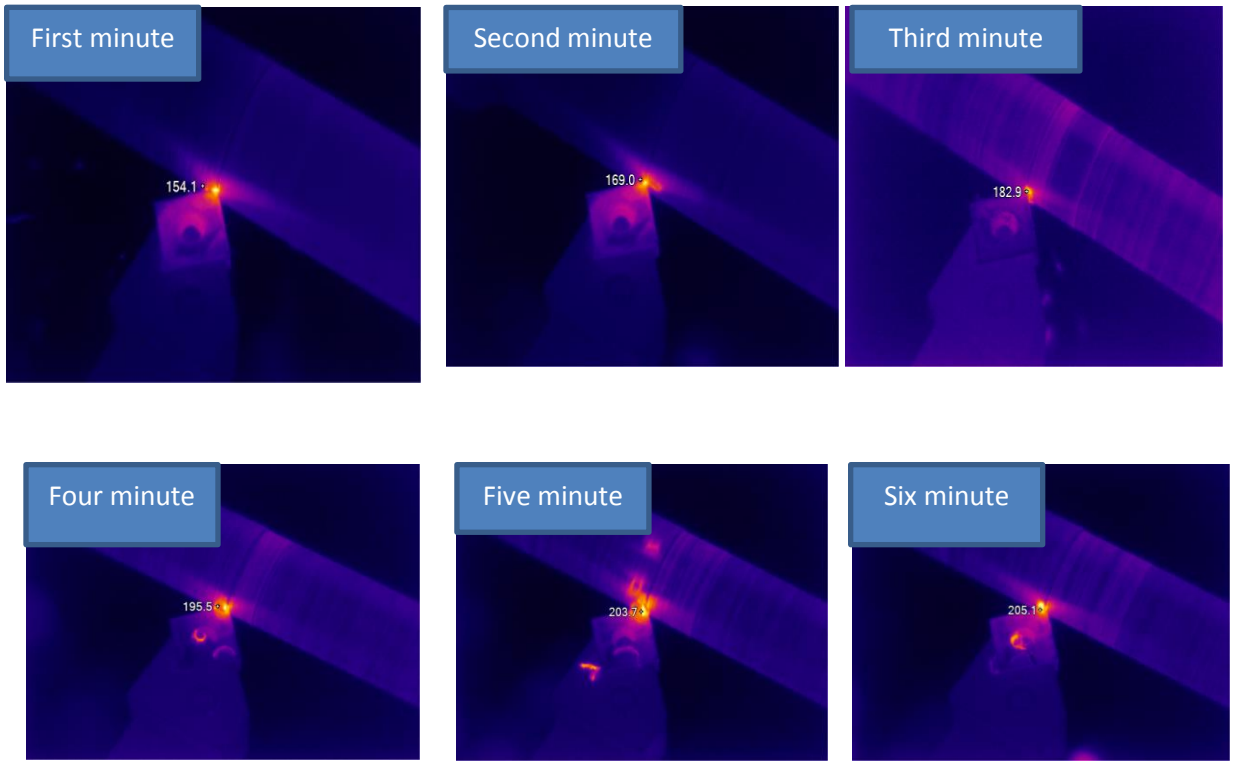

56m/min, 0.065 mm/rev, 0.2mm

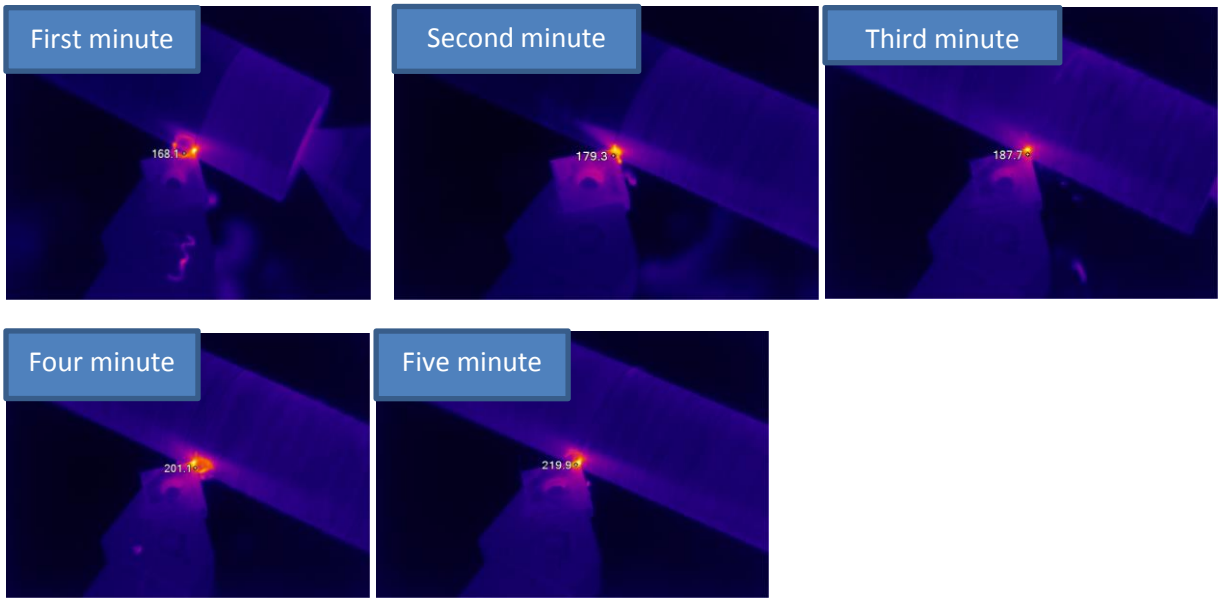

56m/min, 0.165mm/rev, 0.5mm

Figure (15): Temperature Fº for Douple layers coated cutting insert for each minute

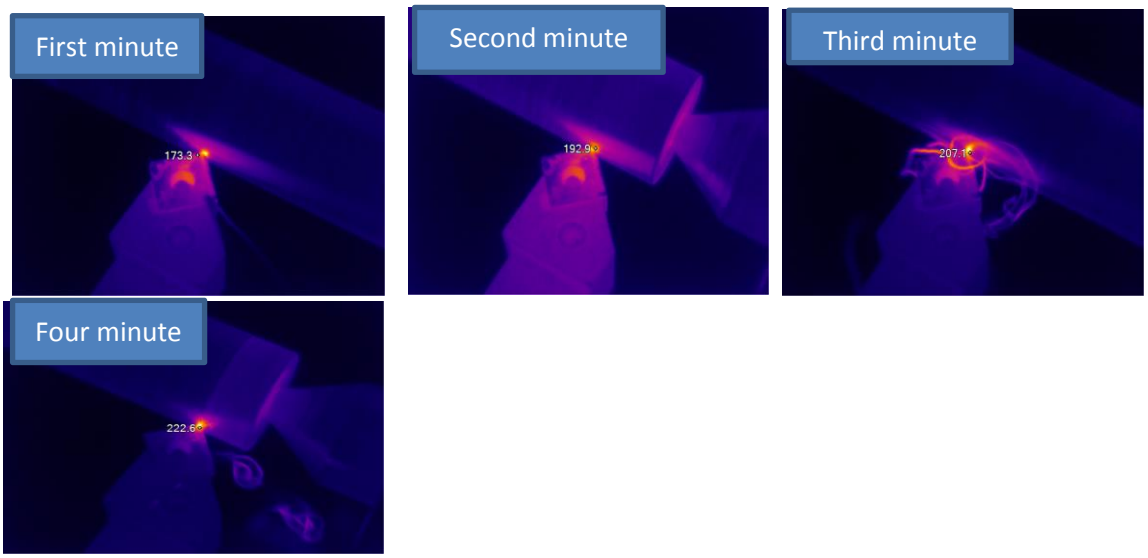

56m/min, 0.265mm/rev, 0.7mm

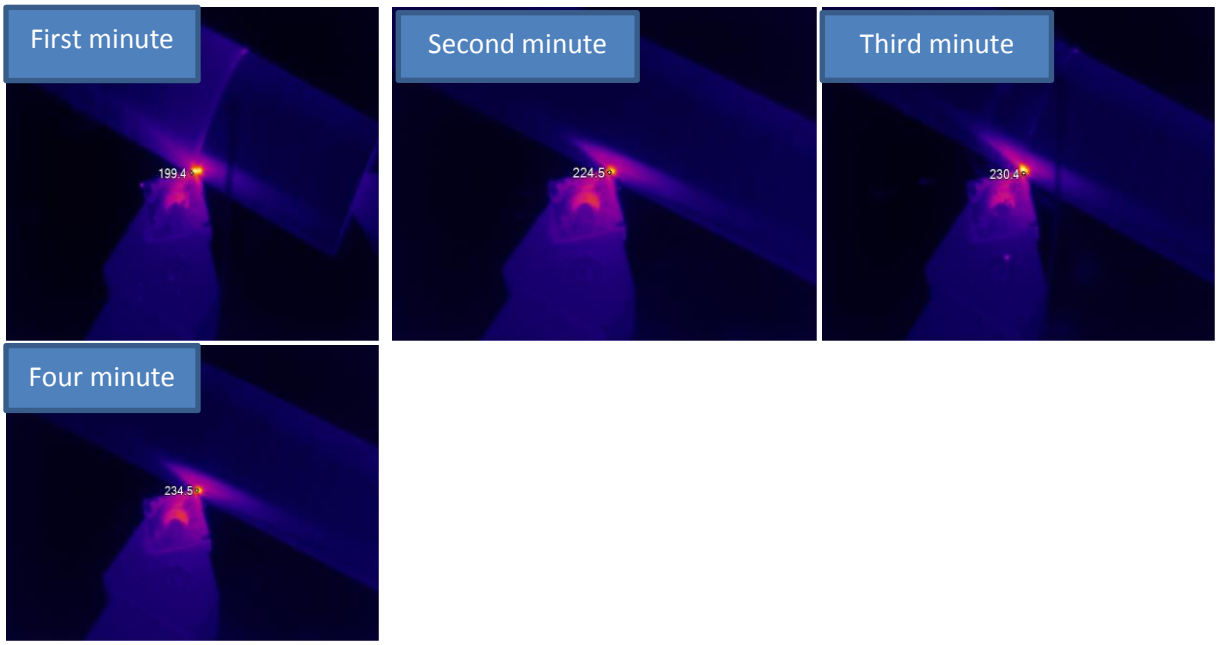

88m/min, 0.065mm/rev, 0.5mm

Continue Figure (15)

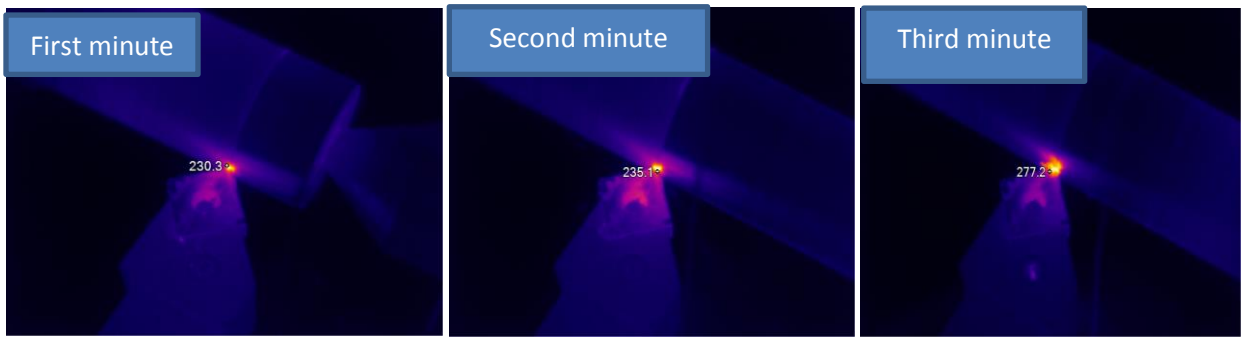

88m/min, 0.165mm/rev, 0.7mm

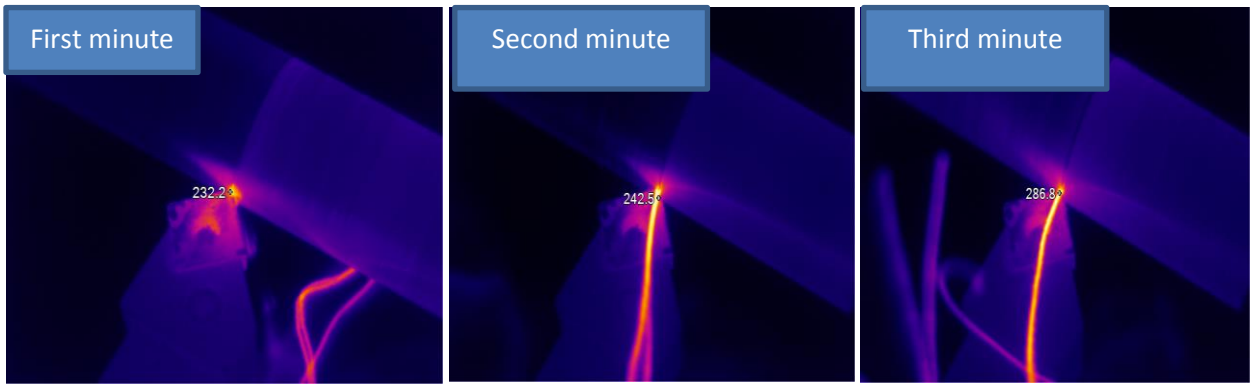

88m/min, 0.265mm/rev, 0.2mm

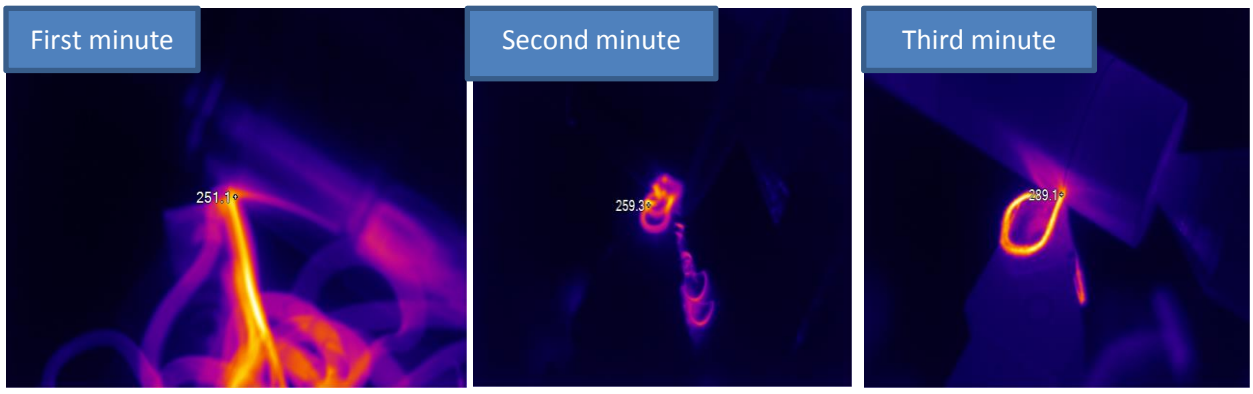

112m/min, 0.065mm/rev, 0.7mm

Continue Figure (15)

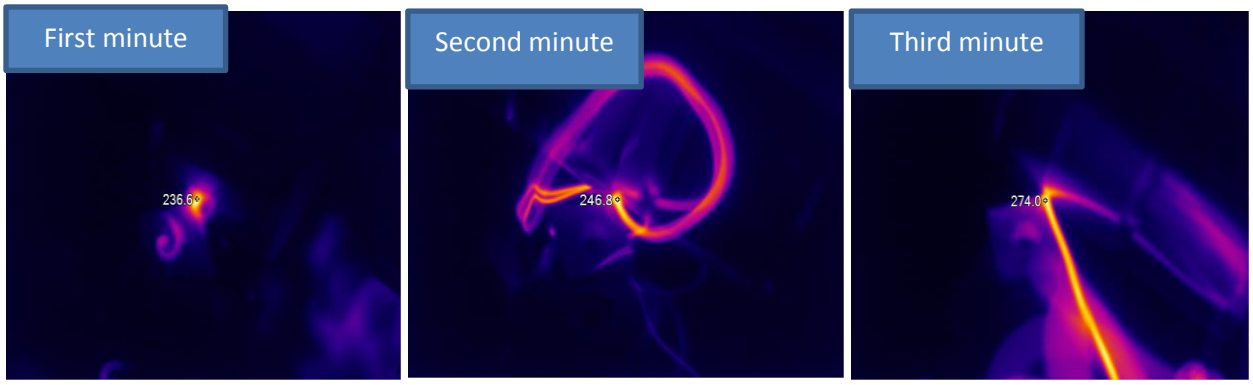

112m/min, 0.165mm/rev, 0.2mm

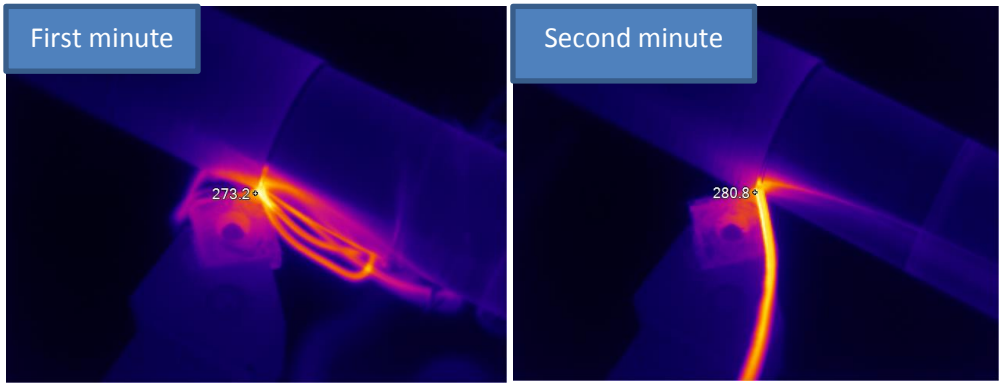

112m/min, 0.5mm, 0.265mm/rev

Continue Figure (15)

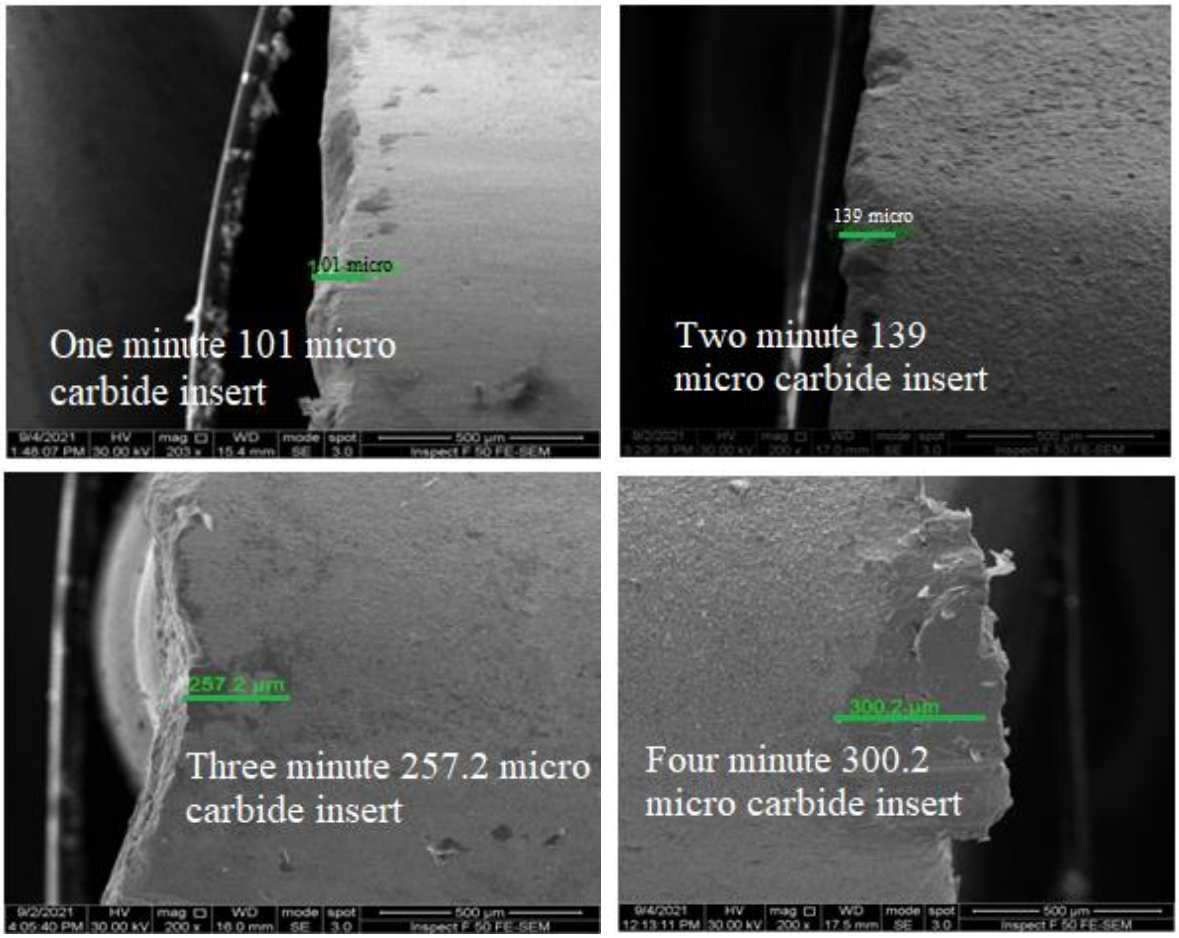

56 m/min, 0.065 mm/rev, 0.2mm

Figure (16): Wear width for carbide cutting insert for each minute

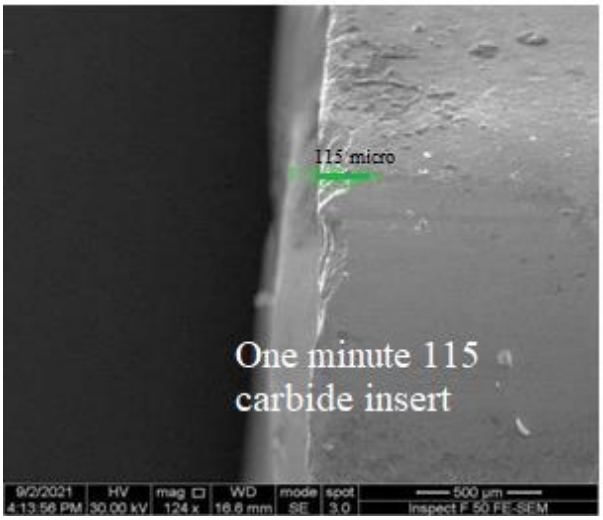

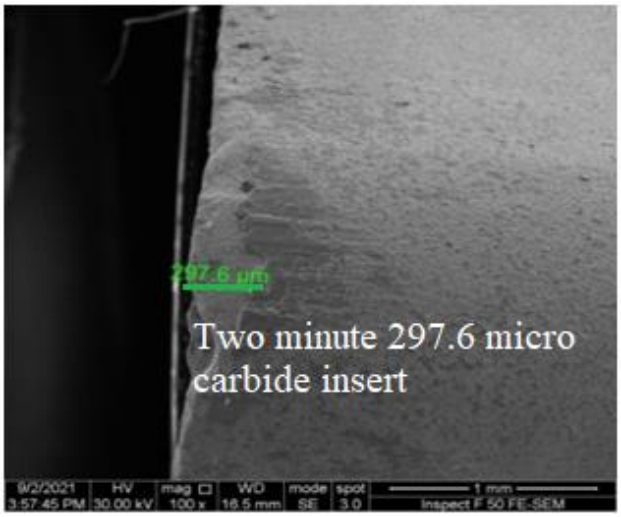

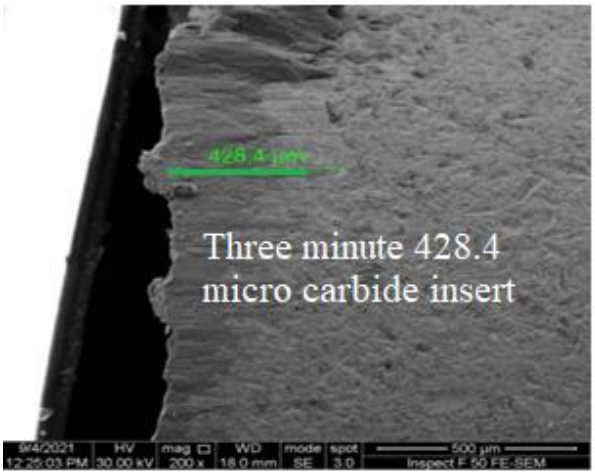

56m/min, 0.165mm/rev, 0.5mm

Continue Figure (16)

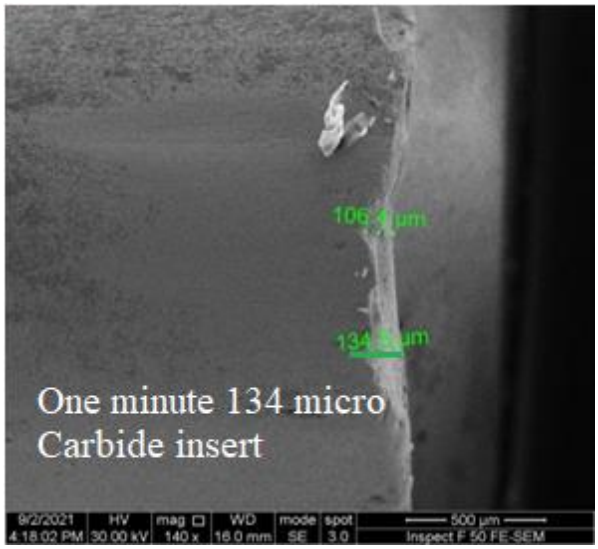

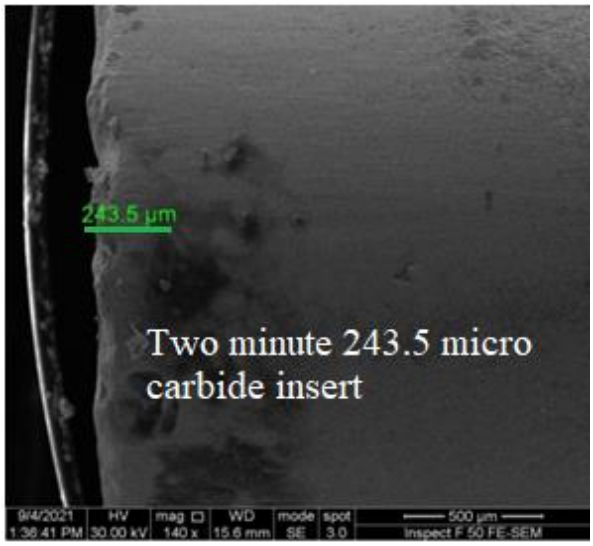

88m/min, 0.1 65mm/rev, 0.7 mm

Continue Figure (16)

الخلاصة

المعروف أن الطلاء يحسن أداء أدوات القطع في تطبيقات التشغيل المختلفة ، وان تطوير أداة القطع لتشغيل مواد صعبة القطع تبقى مشكلة بالنسبة لجودة الانتاج وكلفه العملية. يقدم البحث الحالي استخدام الطلاء متعدد الطبقات لأدوات عدد القطع من فولاذ السرعات العالية, وهو أقل تكلفة من الطلاء التجاري. تم دراسة الخصائص الحرارية والترايبولوجية لأداة عدة قطع (فولاذ السرعات العالية) لعده غير مطلية واخرى مطلية بطبقات متعددة من اكاسيد سيراميكية. تم استخدام الخراطة الجافة لتشغيل قطعة من فولاذ متوسط الكاربون لتأكيد أداء الطلاء الجديد في عمليات التشغيل التقليدية, والذي يتكون من التيتانيا و الالومينا و الزركونيا المنتج بواسطة تقنية السول- الجل والمرسب على سطح اداة العدة بطريقه الغمر. اذ تم تحديد الظروف المناسبة لتحضير و ترسيب الطلاء والمتضمنة PH, لزوجة المحلول، زمن التعتيق ، زمن الغمر عدد مرات الغمر والتجفيف، درجة حرارة الحرق والتلبيد و تأثيرها على كل من خشونة السطح والتجانس للطلاء وسمك الطلاء النهائي ولالتصاقيه. تم تحضير كل طبقة من طبقات الطلاءات الثلاث بعملية السول جل. حيث تم تحضير التيتانيا من و Titanium tetra-isopropoxide (TTIP) واذابتها في isopropanol IP كمذيب وحامض الهيدروكلوريك كمحفز لتخليق الهيدروكسيد وفق النسب المولارية المعتمدة . تم الخلط عند درجه حراره الغرفة وتحت سرعة دورانية 100ملم/ثانيه . تم غمر اللقمة لمده 5 ثواني عند سرعة دورانية ثابتة بلغت 100ملمتر/ثانيه, بعد اخراج اللقمة من محلول الطلاء جففت عند 335 درجه مئوية لمده ساعة واحدة. بعد ذلك نغمر اللقم المطلية بالتيتانيا في محلول طلاء هيدروكسيد الالمنيوم المحضر بطريقة السول- جل والمتضمن مزج كل من ايزوبروبوكساید مع ماء مؤين, وحامض النتريك. كما اضيف المشتت بنسبة مولارية معينه مع سرعة دورانية بلغت 100سنتمتر/دقيقه استمر التدوير لمده 2 ساعه عند درجه حراره 85 درجة مئوية. تم الغمر بمحلول هيدروكسيد الالمنيوم لمدة 10 ثانيه للحصول على السمك المطلوب مع سرعة 3 سنتمتر/دقيقه, اللقم المطلية جففت عند 335 درجة مئوية لمده ساعه للتخلص من المذيبات والمشتتات المضافة, بمعدل زياده بدرجه الحرارة 6 درجه بالدقيقة. اخيرا تم تحضير اوكسيد الزركونيوم من خاماته مع اضافه مشتت ومحفز Zirconium 70 percent n-propoxide (Zr(OC3H7)4), glacial acetic acid, ethylene glycol, and glycerol بعد تحضير هيدروكسيد الزركونيوم نغمر العدة المطلية بالتيتانيا والالومينا في المحلول لمدة 15 ثانيه لإكمال الحصول على سمك لا يتجاوز 6-5مايكرون. اخراج العدة بعد فترة غمر وسرعة تدوير ثابتة لتجفف لمده ساعه بدرجه 290 مئوية.

PH لمحاليل الطلاء الثلاث كانت(6.46, 5.83, 4.8 7) لكل من محلول التيتانيا ,الالومينا, الزركونيا على التوالي. اللزوجة لكل محلول تيتانيا, الومينا, زركونيا (8.74-8.11-7.9) ، كذلك مرات الغمر والتجفيف لنفس زمن الغمر (2-2-3) كانت انسب شيء لتقليل ظهور الشقوق انسب زمن غمر كان في محلول التيتانيا 5 ثانيه , 10 ثانيه في محلول الالومينا, 15 ثانيه في محلول الزركونيا واخيرا افضل زمن للتعتيق لا يتجاوز (48,12,6) لكل من محلول تيتانيا, الومينا و زركونيا من اجل الحصول على السمك المطلوب في العملية

التشغيلية والذي يتناسب مع درجه تقبل العدة للسمك الطلاء. للحصول على طبقه طلاء ذات كثافة والتصاقية جيدتين وتوزيع متجانس. تلبد العينة للطبقات الثلاث بدرجة 500 درجه مئوية ولمده 2 ساعه.

تم تحديد مواصفة العدة المطلية من خلال قوة الالتصاق, التجانس, خشونة السطح للطلاء السيراميك و سمك طبقات الطلاء الكلي حيث كانت أفضل التصاقية عند سمك لا يتجاوز 6-5مايكرون مع التصاقيه 93.60, 86.59 ميكا باسكال للطبقات الثلاثية والثنائية على التوالي. كما تم حساب كل من معدل البلى، معامل الاحتكاك، خشونة السطح للعدة المطلية، ومتوسط الحجم الحبيبي والموصلية الحرارية لأداة القطع المطلية وغير المطلية وتم التوصل الى انخفاض في معامل الاحتكاك ومعدل البلى بمقدار 80 %، 71% على التوالي كما ارتفعت الصلادة للعدة المطلية بمقدار 57% في حين انخفضت خشونة السطح للعدة المطلية بمقدار 63%. تم تقييس معامل التمدد الحراري لسبيكة العدة و لطبقة التيتانيا من اجل معرفه معامل التمدد الحراري لهما وتأكيد درجه تقاربه بينهما حيث هذا التقارب يفسر لنا جودة الطلاء المتعدد الطبقات بوجود التيتانيا. تم اعتماد ثلاث ظروف للقطع: سرعه القطع، تغذيه، عمق قطع، كما تم اعتماد ثلاث مستويات او قيم لكل ظرف للتشغيل وصممت التجارب لكل عدة من العدد المطلية وغير المطلية بالاعتماد على طريقة التحليل الرياضي (تاكوشي). التغذية,(0.065,0.165, 0.265) ملم/دوره. عمق القطع (0.2,0.5,0.7)ملم. سرع القطع المعتمدة (112 ,88 ,56 متر /دقيقه). تم إجراء اختبارات التشغيل بالخراطة على قطعة من الفولاذ متوسط الكاربون. حيث تم قياس التغير في درجة الحرارة باستخدام كاميرا حرارية عند منطقة التماس بين المشغولة وأداة القطع، كما تم قياس خشونة السطح في الدقيقة الأولى لعملية القطع للمشغولة، وتحديد عرض البلى لكل دقيقة عمل لأداة القطع الذي من خلاله تم تحديد عمر عدة القطع. لوحظ أن الطلاء متعدد الطبقات يقلل بدرجة كبيرة من درجة الحرارة عند منطقه التماس بين المشغولة وأداة القطع حيث انخفضت درجة الحرارة 11-13 %. اما خشونة السطح لقطعة الفولاذ الكربوني فقد انخفضت بمقدار 96-30% مع العدة المطلية وفيما يخص عمر العدة المطلية فقد تحسن بنسبه85-183%. بأعتماد تحليل ANOVA كانت اعلى قيمه لمعامل GRG الذي يمثل المخرجات مجتمعه عند ظروف القطع, 0.065ملم/دوره,56 متر/دقيقه و 0.2 ملم. قورنت نتائج التشغيل للعدة المطلية مع نتائج التشغيل باعتماد عدة قطع كاربيدية على نفس المشغولة وفي نفس ظروف عملية القطع أشارت مخرجات عملية التشغيل للعدة المطلية تفوقها على عدة القطع الكاربيدية اما عن عمر العدة فقد فاقت العدة المطلية العدة الكاربيدية بنسبة 30-53%.

وزاره التعليم العالي والبحث العلمي

جامعه بابل

كليه هندسه المواد

قسم هندسه المعادن

تحسين سطوح عدد القطع من صلب السرعات العالية بالطلاءات$TiO_2/Al_2O_3/ZrO_2$متعددة الطبقات بأستخدام طريقة السول-جل

رساله

مقدمه الى قسم هندسه المعادن في كليه هندسه المواد/جامعه بابل

كجزء من متطلبات نيل درجه الدكتوراه فلسفه في هندسه المواد/المعادن

من قبل

ورود اسعد مدب عباس

بإشراف

أ.د . حيدر عبد الحسن العذاري

أ.م. د. شيماء جابر كريم

2022م

1443